

Electronic Thesis and Dissertation Repository

---

4-10-2014 12:00 AM

## Development of Probabilistic Corrosion Growth Models with Applications in Integrity Management of Pipelines

Shenwei Zhang  
*The University of Western Ontario*

Supervisor  
Wenxing Zhou  
*The University of Western Ontario*

Graduate Program in Civil and Environmental Engineering  
A thesis submitted in partial fulfillment of the requirements for the degree in Doctor of Philosophy  
© Shenwei Zhang 2014

Follow this and additional works at: <https://ir.lib.uwo.ca/etd>



Part of the [Structural Engineering Commons](#)

---

### Recommended Citation

Zhang, Shenwei, "Development of Probabilistic Corrosion Growth Models with Applications in Integrity Management of Pipelines" (2014). *Electronic Thesis and Dissertation Repository*. 1951.  
<https://ir.lib.uwo.ca/etd/1951>

This Dissertation/Thesis is brought to you for free and open access by Scholarship@Western. It has been accepted for inclusion in Electronic Thesis and Dissertation Repository by an authorized administrator of Scholarship@Western. For more information, please contact [wlsadmin@uwo.ca](mailto:wlsadmin@uwo.ca).

**Development of Probabilistic Corrosion Growth Models with Applications in  
Integrity Management of Pipelines**

(Thesis format: Integrated Article)

by

Shenwei Zhang

Graduate Program in Engineering Science  
Department of Civil and Environmental Engineering

A thesis submitted in partial fulfillment  
of the requirements for the degree of  
Doctor of Philosophy

The School of Graduate and Postdoctoral Studies  
The University of Western Ontario  
London, Ontario, Canada

© Shenwei Zhang 2014

## Abstract

Metal-loss corrosion is a major threat to the structural integrity and safe operation of underground oil and gas pipelines worldwide. The reliability-based corrosion management program has been increasingly used in the pipeline industry, which typically includes three tasks, namely periodic high-resolution inline inspections (ILIs) to detect and size corrosion defects on a given pipeline, engineering critical assessment of corrosion defects reported by the inspection tool and mitigation of defects. This study addresses the engineering challenges involved in the reliability-based corrosion management program.

First, the stochastic process is applied to characterize the growth of the depth (i.e. in the through pipe wall thickness direction) of metal-loss corrosion defects on energy pipelines based on the imperfect inline inspection (ILI) data. Three stochastic processes, namely gamma process (GP) including both homogeneous and non-homogeneous gamma process (HGP and NHGP), inverse Gaussian process (IGP), and Geometric Brownian motion (GBM) are explored in this study. The growth models are formulated in the hierarchical Bayesian framework and Markov Chain Monte Carlo (MCMC) simulation techniques are employed to carry out the Bayesian updating and numerically evaluate the posterior distributions of the uncertain parameters in the growth model using inspection data obtained from multiple ILI runs. The application of the proposed models are illustrated using an example involving real ILI data for 62 external corrosion defects collected from an in-service natural gas pipeline in Alberta. The ILI data obtained from the inspections prior to the field measurement are used to carry out the Bayesian updating and evaluate the model parameters. The predictive quality of the growth models are validated by comparing the predicted defect depths at the time of field-measurement with the corresponding field-measured depths. The analysis results suggest that each of the four models considered predicts the growth of the defect depth reasonably well. The prediction is poor for the defects that are associated with large measurement errors.

Second, a simulation-based methodology is presented to evaluate the time-dependent system reliability of pressurized energy pipelines containing multiple active metal-loss

corrosion defects, whereby the HGP-, NHGP-, IGP- and GBM-based models are used to characterize the growth of the depth of individual corrosion defect, and the Poisson square wave process (PSWP) is employed to model the internal pressure of the pipeline. The methodology further incorporates the inspection data in the reliability analysis by using the hierarchical Bayesian method and Markov Chain Monte Carlo (MCMC) simulation to update the growth model for the defect depth based on data collected from multiple ILIs. The impact of the internal pressure model, the uncertainty and correlation of the model parameters, and the growth models on the probabilities of small leak, large leak and rupture are investigated through two examples.

Finally, a probabilistic investigation is carried out to determine the optimal inspection interval for the newly-built onshore underground natural gas pipelines with respect to external metal-loss corrosion by considering the generation of corrosion defects over time and time-dependent growth of individual defects. The non-homogeneous Poisson process is used to model the generation of new defects and the homogeneous gamma process is used to model the growth of individual defects. A realistic maintenance strategy that is consistent with the industry practice and accounts for the probability of detection (PoD) and sizing errors of the inspection tool is incorporated in the methodology. Both the direct and indirect costs of failure are considered. A simulation-based approach is used to numerically evaluate the expected cost rate at a given inspection interval. The minimum expected cost rule is employed to determine the optimal inspection interval. An example gas pipeline is used to illustrate the investigation. The impact of the cost of failure, PoD, the excavation and repair criteria, the growth rate of the defect depth, the instantaneous generation rate of the generation model and defect generation model on the optimal inspection interval is investigated through parametric analyses. The proposed algorithms will assist engineers in making the optimal maintenance decision for corroding natural gas pipelines and facilitate the reliability-based corrosion management.

**Key words:** Pipeline, metal-loss corrosion, stochastic process, hierarchical Bayesian, measurement error, Markov Chain Monte Carlo simulation, system reliability, optimal inspection interval

## Co-Authorship Statement

A portion of version of Chapter 2, co-authored by **Shenwei Zhang** and Wenxing Zhou, has been published in *International Journal of Pressure Vessels and Piping*, 111-112: 120-130; the other portion of version of Chapter 2, co-authored by **Shenwei Zhang**, Wenxing Zhou, Mohammad Al-Amin, Shahani Kariyawasam and Hong Wang, has been published in *Journal of Pressure Vessel Technology*, DOI: 10.1115/1.4026798.

A version of Chapter 3, co-authored by **Shenwei Zhang**, Wenxing Zhou and Hao Qin, has been published in *Corrosion Science*, 2013, 73: 309-320.

A version of Chapter 4, co-authored by **Shenwei Zhang** and Wenxing Zhou, has been published in *Structure and Infrastructure Engineering*, DOI:10.1080/15732479.2013.875045.

A portion of version of Chapter 5, co-authored by **Shenwei Zhang** and Wenxing Zhou, has been published in *International Journal of Pressure Vessels and Piping*, 111-112: 120-130.

A version of Chapter 6, co-authored by **Shenwei Zhang** and Wenxing Zhou, has been submitted to *Engineering Structures* for possible publication (revision submitted in February 2014).

## **Acknowledgements**

It is my pleasure to take this opportunity to thank those who helped me through my graduate studies. First, I cannot express enough appreciation to my supervisor Dr. Wenxing Zhou. You have made your support in a number of ways, not only for my work, but also for my life. I cannot be more grateful!

I extend a special note of appreciation to Dr. Hanping Hong, who has encouraged me with his knowledge, patience, enthusiastic support, and guidance throughout my study. I also would like to extend my gratitude to Dr. Shahani Kariyawasam working with TransCanada for providing me with valuable and critical comments and suggestions on my research.

I am grateful to my committee members - Dr. Michael Bartlett, Dr. Hanping Hong, Dr. Xianbin Wang, and Dr. Xianxun Yuan for their insight, advice and critical assessment of my dissertation. The research reported in this dissertation was, in part, jointly supported by the Natural Sciences and Engineering Research Council (NSERC) of Canada and TransCanada Pipelines Limited through the Collaborative Research and Development Program. This research is also, in part, supported by the Alexander Graham Bell Canada Graduate Scholarships (CGS) provided by NSERC. These financial supports are very much appreciated.

I also would like to thank wonderful fellow graduate students of our research group for providing me with technical knowledge, lively discussions and friendship along the road.

I am truly grateful to my parents for their love, support and encouragement they have provided throughout my life, to my wife, Guoxiang Liu, for her support, to my kids, Jenny Zhang and Jerry Zhang for bringing immeasurable happiness to my life.

Lastly, thanks to all people I know for accompanying me through this long journey at the University of Western Ontario. I appreciate everyone I met here and cherish my memories with each of you.

# Table of Contents

Abstract .....	ii
Co-Authorship Statement.....	iv
Acknowledgements.....	v
Table of Contents .....	vi
List of Tables .....	x
List of Figures .....	xi
List of Appendices .....	xiv
List of Symbols.....	xv
Chapter 1 Introduction .....	1
1.1 Background.....	1
1.2 Objective and Research Significance.....	4
1.3 Scope of the Study .....	5
1.4 Thesis Format.....	6
References.....	6
Chapter 2 Gamma Process-based Corrosion Growth Modeling Based on Imperfect Inspection Data .....	10
2.1 Introduction.....	10
2.2 Gamma Process.....	11
2.3 ILI Data and Uncertainties.....	12
2.4 Growth Modeling for Multiple Defects .....	14
2.5 Bayesian Updating of Growth Model.....	16
2.5.1 Overview of Bayesian Updating.....	16
2.5.2 Prior Distribution .....	20
2.5.3 Likelihood Functions of the ILI Data .....	21
2.5.4 Likelihood Functions of Model Parameters.....	21
2.5.5 Posterior Distribution.....	22
2.5.6 Hierarchical Representation of the Growth Model.....	23
2.5.7 MCMC Simulation-based Bayesian Updating Procedures .....	24
2.6 Model Validation .....	24

2.6.1 General.....	24
2.6.2 NHGP-based Growth Model.....	27
2.6.3 HGP-based Corrosion Growth Model .....	38
2.6.4 Comparison of the NHGP- and HGP-based Corrosion Growth Models .....	46
2.7 Conclusions.....	54
Reference .....	56
Chapter 3 Inverse Gaussian Process-based Corrosion Growth Modeling Based on Imperfect Inspection Data.....	59
3.1 Introduction.....	59
3.2 Inverse Gaussian Process .....	60
3.3 Growth Modeling for Multiple Defects .....	62
3.4 Bayesian Updating of the Growth Model .....	63
3.4.1 Likelihood Function.....	63
3.4.2 Prior and Posterior Distributions .....	65
3.4.3 Hierarchical Representation of the Growth Model.....	67
3.5 Example .....	68
3.5.1 Illustration and Validation of Growth Model .....	68
3.5.2 Parametric Analysis .....	76
3.5.3 Comparisons with the GP-based and Conventional Growth Models .....	88
3.6 Conclusions.....	89
Reference .....	91
Chapter 4 Geometric Brownian Motion-based Corrosion Growth Modeling Based on Imperfect Inspection Data.....	93
4.1 Introduction.....	93
4.2 Brownian Motion-based Degradation Model .....	95
4.2.1 Standard Brownian Motion.....	95
4.2.2 Usual Form of Brownian Motion-based Degradation Model .....	96
4.2.3 Geometric Brownian Motion-based Growth Rate Model.....	97
4.3 Bayesian Updating of the Growth Model .....	101
4.3.1 Likelihood Function.....	101
4.3.2 Prior and Posterior Distributions .....	102



4.4 Prediction .....	104
4.4.1 Predictive Analysis-based Approach .....	105
4.4.2 Mean Value-based Approach.....	106
4.4.3 Extrapolation-based Approach.....	106
4.5 Example .....	107
4.5.1 Model Validation .....	107
4.5.2 Comparison with Other Growth Models.....	117
4.6 Conclusions.....	119
References.....	120
Chapter 5 System Reliability of Corroding Pipelines Considering Stochastic Process-based Models for Defect Growth and Internal Pressure .....	124
5.1 Introduction.....	124
5.2 Time-dependent Corrosion Growth Models .....	125
5.2.1 Gamma Process-based Model.....	126
5.2.2 Inverse Gaussian Process-based Model .....	127
5.2.3 Geometric Brownian Motion-based Model .....	127
5.3 Time-dependent Internal Pressure Model.....	127
5.4 Time-dependent Reliability Evaluation of Pipeline Segment with Multiple Defects.....	129
5.4.1 Limit state Functions for a Single Corrosion Defect .....	129
5.4.2 Methodology for System Reliability Analysis.....	130
5.5 Example .....	133
5.5.1 General.....	133
5.5.2 Time-dependent Reliability Analysis Using the HGP-based Growth Model....	134
5.5.3 Impact of Growth Models on the Time-dependent Reliability .....	142
5.6 Conclusions.....	147
References.....	149
Chapter 6 Cost-based Optimal Inspection Interval for Corroding Natural Gas Pipelines Based on Stochastic Degradation Models.....	154
6.1 Introduction.....	154
6.2 Degradation Models.....	156
6.2.1 Generation of New Defect .....	156

6.2.2 Growth of Defect .....	158
6.2.3 Simulation Procedures for Generating New Defects .....	159
6.3 Uncertainties Associated with the ILI Tool .....	160
6.3.1 Probability of Detection .....	160
6.3.2 Measurement Error .....	160
6.4 Optimal Condition-based Maintenance Decisions.....	161
6.4.1 Limit State Function for Failure Due to Corrosion.....	161
6.4.2 Maintenance and Replacement Policy .....	163
6.4.3 Evaluation of the Expected Cost Rate .....	164
6.5 Example .....	168
6.5.1 General .....	168
6.5.2 Results of Parametric Analysis .....	171
6.6 Conclusions.....	188
References.....	189
Chapter 7 Summary, Conclusions and Recommendations for Future Study.....	192
7.1 General.....	192
7.2 Development of Probabilistic Models for the Growth of Metal-loss Corrosion .....	192
7.3 Time-dependent System Reliability Analysis of a Corroding Pipeline .....	194
7.4 Optimal Maintenance Decisions on Corroding Energy Pipelines .....	195
7.5 Recommendations for Future Study .....	196
Appendix A Full Conditional Posterior Distributions of Model Parameters (GP-based Model).....	198
Appendix B Procedure of the MCMC Simulation.....	200
Appendix C Full Conditional Posterior Distributions of Model Parameters (IGP-based Model).....	202
Appendix D Full Conditional Posterior Distributions of Model Parameters (GBM-based Model).....	210
Appendix E Copyright Permission .....	213
Curriculum Vitae .....	223

## **List of Tables**

Table 2.1 Summary of sensitivity scenarios for the NHGP-based model.....	30
Table 2.2 Summary of sensitivity scenarios for the HGP-based model .....	38
Table 3.1 Comparison of four scenarios for the growth model .....	77
Table 4.1 Summary of the six scenarios for model prediction .....	108
Table 5.1 Probabilistic characteristic of the random variables .....	138
Table 5.2 Summary of the growth models.....	143
Table 6.1 Probabilistic characteristic of the random variables .....	169
Table 6.2 Summary of unit costs .....	170
Table 6.3 Details of the parametric analysis .....	171

## List of Figures

Figure 1.1 Overview of the research topics in the thesis .....	6
Figure 2.1 Illustration of the measurement errors associated with the ILI data .....	13
Figure 2.2 Schematic of the MCMC simulation method.....	18
Figure 2.3 Hierarchical structure of the growth model.....	24
Figure 2.4 General information of the ILI-reported and field-measured data .....	26
Figure 2.5 Comparison of the predicted and field-measured depths .....	28
Figure 2.6 Comparison of the predicted and field-measured depths for different scenarios .....	31
Figure 2.7 Predicted growth paths of ten defects using NHGP-based models .....	37
Figure 2.8 Comparison of the predicted and field-measured depths for different scenarios .....	39
Figure 2.9 Predicted growth paths of ten defects using HGP-based model.....	45
Figure 2.10 Comparison of the growth paths of a given defect corresponding to NHGP- and HGP-based models.....	52
Figure 2.11 Time-dependent PDF curves of defect depth of Defect #3 at years 2000-2009 .....	53
Figure 2.12 PDF curves of defect depths of Defects #1-10 at year 2009 .....	53
Figure 3.1 PDF function of the inverse Gaussian distribution.....	61
Figure 3.2 Flowchart of the MCMC simulation-based Bayesian updating procedures....	67
Figure 3.3 DAG of the growth model.....	68
Figure 3.4 Comparison of the predicted depths in 2010 with the corresponding field- measured depths.....	69
Figure 3.5 Predicted growth path of a given defect .....	75
Figure 3.6 Time-dependent PDF of the defect depth.....	76
Figure 3.7 Comparison of the mean predicted depth with the field-measured depths corresponding to Scenarios I, II, III and IV .....	78
Figure 3.8 Comparison of the mean predicted growth paths corresponding to Scenarios I, II, III and IV .....	84

Figure 3.9 Impact of the prior distributions of $\alpha$ and $\xi$ on the predictive quality of the growth model .....	87
Figure 3.10 Comparison of the predictions of the IGP-, GP-based and conventional models.....	89
Figure 4.1 Illustration of realizations of the Brownian motion .....	97
Figure 4.2 Illustration of notations.....	99
Figure 4.3 DAG representation of the growth model .....	103
Figure 4.4 Illustration of the Bayesian updating of the growth model .....	104
Figure 4.5 Comparison of the predicted and field-measured depths in 2010 for Scenario I .....	108
Figure 4.6 Predicted growth paths for Defects #2, #4, #5, #7, #15, #18, #19, #49, #60 and #61.....	114
Figure 4.7 Comparison of the predictions corresponding to Scenarios I through VI.....	116
Figure 4.8 The prior and posterior distributions $\beta$ of $\sigma^2$ .....	117
Figure 4.9 Comparison with the HGP- and IGP-based and conventional growth models .....	118
Figure 5.1 Poisson square wave process model.....	129
Figure 5.2 Simulated time-dependent internal pressure based on PSWP model.....	129
Figure 5.3 Apparent growth paths indicated by the ILI-reported depths.....	135
Figure 5.4 Defect lengths of 25 defects reported by the ILI in 2011 .....	136
Figure 5.5 Comparison of probabilities of small leak (large leak) associated with different internal pressure models .....	140
Figure 5.6 Comparison of probabilities of large leak associated with three scenarios for growth model .....	142
Figure 5.7 Comparison of the predicted and actual depths in 2010 for the 10 defects on Segment 2.....	144
Figure 5.8 Time-dependent failure probabilities based on different growth models.....	146
Figure 6.1 Illustration of the NHPP .....	157
Figure 6.2 Illustration of the extension of the B31G Modified model for defects more than 80% through wall thickness .....	163

Figure 6.3 Comparison of the expected cost rates associated with different maintenance actions based on the baseline case .....	172
Figure 6.4 Expected cost rate vs the inspection interval $T_I$ in term of $C_F = 30, 60$ and $200$ .....	174
Figure 6.5 Expected cost rate vs the inspection interval $T_I$ in term of PoD.....	177
Figure 6.6 Expected cost rate vs the inspection interval $T_I$ in term of the safety factors	179
Figure 6.7 Expected cost rate vs the inspection interval $T_I$ in term of mean of growth rate .....	181
Figure 6.8 Expected cost rate vs the inspection interval $T_I$ in term of $\lambda_0$ .....	182
Figure 6.9 Expected cost rate vs the inspection interval $T_I$ in term of the defect generation model.....	184
Figure 6.10 Annual failure probability vs the inspection interval $T_I$ .....	187
Figure 6.11 Comparison of the expectation of the HPP and NHPP .....	188

## List of Appendices

Appendix A Full Conditional Posterior Distributions of Model Parameters (GP-based Model).....	198
Appendix B Procedure of the MCMC Simulation.....	200
Appendix C Full Conditional Posterior Distributions of Model Parameters (IGP-based Model).....	202
Appendix D Full Conditional Posterior Distributions of Model Parameters (GBM-based Model).....	210
Appendix E Copyright Permission .....	213

## List of Symbols

$\mathbf{a}$	= vector of the constant biases associated with ILI tools
$a_j$	= constant bias associated with the $j^{\text{th}}$ inspection tool
$\mathbf{b}$	= vector of the non-constant biases associated with ILI tools
$b_j$	= non-constant bias associated with the $j^{\text{th}}$ inspection tool
$c_{1d}, c_{2d}$	= constant and non-constant biases of defect depth
$c_{1l}, c_{2l}$	= constant and non-constant biases of defect length
$d_i(t)$	= predicted depth up to the $t^{\text{th}}$ year of the forecasting period
$f(X)$	= probability density function of random variable $X$
$g_1$	= limit state function for the corrosion defect penetrating the pipe wall
$g_2$	= limit state function for plastic collapse under internal pressure at the defect
$g_3$	= limit state function for the unstable axial extension of the through-wall
iid	= independent and identically distributed
$p$	= internal pressure of the pipeline
$p_1 - p_5$ ( $q_1 - q_5$ )	= distribution parameters of the prior distributions of model parameters
$r_b$	= burst pressure resistance of the pipe at the defect
$r_i$	= depth growth rate of the $i^{\text{th}}$ in the linear model
$r_{ij}$	= the average growth rate of the $i^{\text{th}}$ defect between the $j^{\text{th}}$ and $(j+1)^{\text{th}}$ inspections
$r_i(k)$	= growth rate of the $k^{\text{th}}$ -step prediction
$r_{rp}$	= pressure resistance of the pipeline at the location of the through-wall defect
$t$	= time elapsed since the installation of pipeline
$t_0$	= corrosion initiation time
$\mathbf{t}_0$	= vector of the corrosion initiation time
$t_{i0}$	= corrosion initiation time of defect $i$
$t_j$	= elapsed time from the installation date up to the $j^{\text{th}}$ inspection
$wt$	= wall thickness
$x_a$	= field-measured depth



$x_{ai}$	= field-measured depth of the $i^{\text{th}}$ defect
$x_{ij}$	= actual depth of the $i^{\text{th}}$ defect at the time of the $j^{\text{th}}$ inspection
$x_i(k)$	= defect depth of the $k^{\text{th}}$ -step prediction
$\mathbf{x}_i$	= vector of the actual depth of the $i^{\text{th}}$ defect
$x_p$	= predicted depth at the time of field measurement
$x_{pi}$	= predicted depth of the $i^{\text{th}}$ defect at the time of field measurement
$y_{ij}$	= ILI-reported depth of the $i^{\text{th}}$ defect obtained from the $j^{\text{th}}$ inspection
$\mathbf{y}_i$	= vector of the ILI-reported depth of the $i^{\text{th}}$ defect
$C_{EV}$	= cost of excavation
$C_F$	= failure cost
$C_{IN}$	= cost of inspection
$C_{RC}$	= cost of re-coating
$C_{RS}$	= cost of re-sleeving
CDF	= cumulative distribution function
COV[·]	= coefficient of variation
$D$	= outside diameter of the pipeline
$\mathbf{D}$	= vector of observation data
DAG	= directed acyclic graph
$E[\cdot]$	= expectation
$F(X)$	= cumulative distribution function of random variable $X$
GP	= gamma process
GBM	= geometric Brownian motion
HGP	= homogenous gamma process
HPP	= homogeneous Poisson process
$I_{(0,\infty)}(\cdot)$	= indicator function
IGP	= inverse Gaussian process
ILI	= in-line inspection
$L_i$	= length of corrosion defect $i$
$L(\cdot)$	= likelihood function
M	= Folias factor or bulging factor
MC	= Markov chain

MCMC	= Markov chain Monte Carlo
MFL	= Magnetic Flux Leakage
MSEP	= mean squared error of prediction
NHGP	= non-homogeneous gamma process
NHPP	= non-homogeneous Poisson process
$P_{ll}$	= probability of large leak
$P_{rp}$	= probability of rupture xvi
$P_{sl}$	= probability of small leak
PDF	= probability density function
PoD	= probability of detection
PSWP	= Poisson square wave process
Var[·]	= variance
SMYS	= specified minimum yield stress
SMTS	= specified minimum tensile strength
$T$	= total forecasting period
$T_I$	= inspection interval
$Y_t$	= response variable at time $t$
$\alpha$	= parameter of the mean growth path of the GP- and IGP-based models
$\alpha_i$	= growth rate of the $i$ th defect in the IGP-based model
$\beta$	= rate parameter of the gamma process
$\boldsymbol{\beta}$	= vector of the rate parameters of the gamma process
$\beta_i$	= rate parameter of the gamma process associated with the $i^{\text{th}}$ defect
$\gamma$	= discount rate
$\chi(\cdot)$	= incomplete gamma function
$\varepsilon_d$	= random scattering of defect depth
$\varepsilon_l$	= random scattering of defect length
$\varepsilon_{ij}$	= random scattering error associated with the actual depth of the $i^{\text{th}}$ defect reported by the $j^{\text{th}}$ inspection
$\eta_{i,j-1}$	= random change in the logarithms of the average growth rates for defect $i$ between the time intervals $\Delta t_{j-1}$ and $\Delta t_j$

$\kappa$	= exponential of the mean growth path of the gamma process
$\theta$	= shape parameter of the inverse Gaussian distribution
$\theta$	= uncertain parameters
$\lambda$	= Poisson rate
$\lambda(t)$	= instantaneous of the generation rate of corrosion defect
$\mu$	= mean parameter of the inverse Gaussian distribution
$\mu_i(t)$	= mean of the predicted depth at time $t$
$\eta_E$	= safety factors associated with the internal pressure-related excavation criteria
$\eta_R$	= safety factors associated with the internal pressure-related repair criteria
$\xi$	= scale parameter of the inverse Gaussian process
$\xi_b$	= model error associated with the burst capacity model
$\xi_E$	= safety factors associated with the wall thickness- related excavation criteria
$\xi_R$	= safety factors associated with the wall thickness-related repair criteria
$\pi(\cdot)$	= prior distribution
$\rho_{jk}$	= correlation coefficient of the random scattering errors associated with the $j^{\text{th}}$ and $k^{\text{th}}$ inspections
$\sigma_i(t)$	= standard deviation of the predicted depth at time $t$
$\sigma_j$	= random scattering error associated with the ILI tool used at the $j^{\text{th}}$ inspection
$\omega$	= vector of the distribution parameters of the prior distribution
$A(t)$	= shape parameter of the gamma process
$\Gamma(\cdot)$	= gamma function
$\Delta d_{it}(1)$	= growth of defect depth within the $t^{\text{th}}$ year of the forecasting period
$\Delta x_{ij}$	= growth of depth of the $i^{\text{th}}$ defect between the $(j-1)^{\text{th}}$ and $j^{\text{th}}$ inspections
$\Delta t$	= time increment
$\Delta \mathbf{x}_i$	= vector of the growth of depth of the $i^{\text{th}}$ defect
$\Delta \mathbf{x}$	= matrix of the growth of depth of all defects

$\Delta A_{ij}$	= shape parameter of the gamma distribution of $\Delta x_{ij}$
$\Delta A_{it}$	= shape parameter of the gamma distribution of $\Delta d_{it}(1)$
$\Theta(t)$	= mean function of the inverse Gaussian process
$\Lambda(t)$	= expected number of defects generated over $[0, t]$
$\Sigma_{Ei}$	= covariance matrix of the random scattering error
$\Phi(\cdot)$	= CDF of the standard normal distribution

## Chapter 1 Introduction

### 1.1 Background

Pipeline systems are the most efficient and economic means to transport large quantities of hydrocarbons (e.g. crude oil and natural gas) over long distances. Metal-loss corrosion is a major threat to the structural integrity and safe operation of underground oil and gas pipelines worldwide (Cosham et al. 2007; Nessim et al. 2009). The reliability-based corrosion management program has been increasingly used in the pipeline industry because it provides a reasonable framework to account for the various uncertainties (e.g. measurement error, and randomness associated with the corrosion growth and material properties) that impact the development of suitable maintenance strategies. The reliability-based pipeline corrosion management typically includes three tasks, namely periodic high-resolution inline inspections (ILIs) to detect and size corrosion defects on a given pipeline, engineering critical assessment of the corrosion defects reported by the inspection tool and mitigation of defects.

The corrosion growth modeling plays an important role in the pipeline corrosion management in that it is critical to the determination of the re-inspection interval and development of a staged defect mitigation plan that meets the safety and resource constraints. Overly conservative growth models will lead to unnecessary inspections and mitigations, which can translate into significant cost penalties for the pipeline operators. On the other hand, growth models that significantly underestimate the defect growth may lead to critical defects being missed by the mitigation actions and failure of the pipeline due to such defects.

The corrosion growth process is inherently random, and includes both temporal and spatial variability. The temporal variability means that the growth path of a given defect varies with time; the spatial variability means that the growth paths of different defects are different but may potentially be correlated, for example, if the defects are closely spaced. The probabilistic corrosion growth models reported in the literature can be classified as random variable-based models and stochastic process-based models, e.g.

(Amirat et al. 2006; Little et al. 2004a, 2004b; Maes et al. 2009; Qin and Cui 2003; Teixeira et al. 2008; van Noordwijk et al. 2007). Because the growth rate in the former models is time-independent random variable, they cannot capture the temporal variability of the corrosion growth process whereas the latter models can overcome this drawback. Two stochastic processes, namely the Markov chain and gamma process, have been widely employed in the literature to model the growth of corrosion defects on pipelines (Hong 1999a, 1999b; Timashev et al. 2008; Valor et al. 2007; Maes et al. 2009; Caleyó et al. 2009; Zhou et al. 2012). The homogeneous and non-homogenous Markov chains were used (Hong 1999a, 1999b) to model the growth of pitting corrosion in the context of selecting the optimal inspection interval for pipelines. The homogeneous gamma process was employed (Zhou et al. 2012) to characterize the growth of defect depth for the purpose of evaluating the time-dependent system reliability of pipeline containing multiple active corrosion defects. The probabilistic characteristics of the parameters of the corrosion growth models can be evaluated or updated using the inspection data. For example, Maes et al. (2009) and Zhang et al. (2012) used a hierarchical Bayesian approach to update the gamma process-based growth models for corrosion defects on pipelines based on the ILI data.

Periodic inline inspections (ILI) using high-resolution tool, e.g. the magnetic flux leakage (MFL) tool, are routinely used to maintain the safe operation of pipeline systems with respect to metal-loss corrosion. The ILI data obtained from multiple ILI runs provide valuable information about the growth of corrosion defects on the pipelines. Therefore, it is of high practical value to develop the probabilistic model for the growth of corrosion defects on the pipelines based on ILI data collected from multiple ILIs (Kariyawasam and Peterson 2010).

Studies on the reliability of corroding pipelines have been extensively reported in the literature (e.g. Ahammed 1998; Pandey 1998; Hong 1999; Caleyó et al. 2002; Amirat et al. 2006; Teixeira et al. 2008; Zhou 2010; Zhou et al 2012; Valor et al. 2013). The majority of these investigations employed random variable-based growth models for the depth (i.e. in the through pipe wall thickness direction) and/or length (i.e. in the longitudinal direction of the pipe) of the corrosion defect. The Markov chain and gamma

process-based models have also been used to characterize the growth of corrosion defects for evaluating the time-dependent failure probabilities. Furthermore, the internal pressure of the pipeline is typically assumed to be either a (time-independent) random variable or a deterministic quantity while in reality the internal pressure varies with time and should be characterized as a stochastic process. A simple stochastic process, the Ferry-Borges process, was employed in (Zhou 2010) to model the internal pressure for evaluating the system reliability of corroding pipelines. However, the Ferry-Borges process is somewhat simplistic in comparison to the reality; therefore, more realistic and sophisticated models for the internal pressure are desirable for the reliability analysis. Note that sophisticated stochastic process-based load models have been employed in the reliability analysis of building structures (Madsen 2006; Melchers 1999; El-Reedy 2009), e.g. the Poisson Square Wave Process (PSWP) for modelling the sustained live loads. The reliability analyses of corroding pipelines incorporating the Bayesian-based growth models and the PSWP-based internal pressure model, to the best knowledge of the author, has not been reported in the literature.

The selection of optimal maintenance schedules for corroding pipelines has been investigated using the reliability- or cost-based criterion (e.g. Rodriguez and Provan 1989; Morrison and Worthingham 1992; Hong 1999b; Gomes et al. 2013). Provan and Rodriguez (1989) developed a Markov chain-based model for the growth of corrosion defects in the context of determining the optimal inspection time. They considered the imperfection of inspection tools in detecting the defect, i.e. the probability of detection (PoD), but ignored the imperfection of inspection tools in sizing the defect, i.e. the measurement errors. Morrison and Worthingham (1992) employed the same corrosion growth model to determine the optimal inspection time but ignored both PoD and measurement errors associated with the inspection tools. Hong (1999b) investigated the optimal inspection and maintenance schedule for corroding pipelines based on the reliability constraint. The Markov chain was employed to model the growth of corrosion defects; the PoD and measurement errors associated with the inspection tool were incorporated in the failure probability evaluation, and the Poisson process was used to model the generation of new defects. Recently, Gomes et al. (2013) used a simulation-based approach to investigate the optimal inspection interval for buried pressurized

pipelines subjected to external corrosion based on the minimum expected cost rule. A single pipeline segment that contains at most one corrosion defect at a given time was considered in the analysis, which is somewhat unrealistic. A time-independent power-law model that incorporates uncertain power law parameters but a deterministic corrosion initiation time was assumed to characterize the growth of the defect depth. Although PoD of the inspection tool was incorporated in the analysis, the measurement errors of the tool were ignored. The generation of new corrosion defects was also ignored. Furthermore, determination of the optimal inspection interval for corroding piping system on nuclear power plant has been reported by Cheng and Pandey (2012), where the degradation of the system was modeled as a homogeneous gamma process and the optimal inspection interval was selected based on the minimum expected cost rule. Perfect inspection was implicitly assumed in their study. Therefore, a realistic probabilistic model that incorporates all the potential uncertainties is desirable for the pipeline industry to properly evaluate the optimal maintenance interval.

## **1.2 Objective and Research Significance**

The study reported in this thesis was carried out under a research project jointly funded by the Natural Sciences and Engineering Research Council (NSERC) of Canada and TransCanada Ltd. through a Collaborative Research and Development (CRD) program. It is also, in part, supported by the Alexander Graham Bell Canada Graduate Scholarships (CGS) provided by NSERC. The objectives of this study include: 1) development of probabilistic models to characterize the growth of the depths of individual metal-loss corrosion defects on energy pipelines based on imperfect data collected from multiple ILIs; 2) development of methodologies to evaluate the time-dependent system reliability of corroding pipelines by incorporating the corrosion growth models developed based on the ILI data, and 3) development of a methodology to determine the optimal maintenance interval for energy pipelines under the threat of corrosion considering different uncertainties. It is anticipated that the research outcome will assist pipeline integrity engineers in developing optimal re-inspection intervals and defect mitigation plans that satisfy both the safety and resource constraints. This is beneficial to not only the Canadian pipeline industry but also the communities near the



pipeline facilities throughout Canada. Furthermore, the models and methodology developed in this study are also applicable to other infrastructure systems such as nuclear piping and pavement.

### **1.3 Scope of the Study**

This study consists of five main topics that are presented in Chapters 2 through 6, respectively. Chapters 2, 3 and 4 present three stochastic processes-based models, namely gamma process-, inverse Gaussian process- and geometric Brownian motion-based models, to characterize the growth of the depths of corrosion defects on energy pipelines based on imperfect inspection data obtained from multiple ILIs. Each of the three models is formulated in a hierarchical Bayesian framework to consider the uncertainties from different sources, and employ the Markov Chain Monte Carlo (MCMC) simulation techniques to estimate the model parameters. These models account for a general form of the measurement errors, including the bias and random scattering error, associated with the ILI tools as well as the potential correlation between the random scattering errors among different ILI tools. The growth models are validated by a set of real ILI data collected from an in-service pipeline segment. A simulation-based methodology to evaluate the time-dependent system reliability of corroding pipelines containing multiple active corrosion defects is presented in Chapter 5. This methodology incorporates the developed growth models and a time-dependent internal pressure model, namely the Poisson Square Wave process-based model. A comparative study of the time-dependent reliabilities based on the growth models described in Chapters 2 through 4 is also included in Chapter 5. Chapter 6 presents a probabilistic methodology to determine the optimal maintenance interval for newly-built onshore pipelines with respect to external metal-loss corrosion. This methodology incorporates the stochastic process-based models for the generation and growth of corrosion defects, and a realistic maintenance strategy representative of the industry practice. The methodology incorporates the probability of detection (PoD) and measurement errors associated with the inspection tool, and considers both direct and indirect costs of failure. The relationship of those topics described above is illustrated in Figure 1.1.

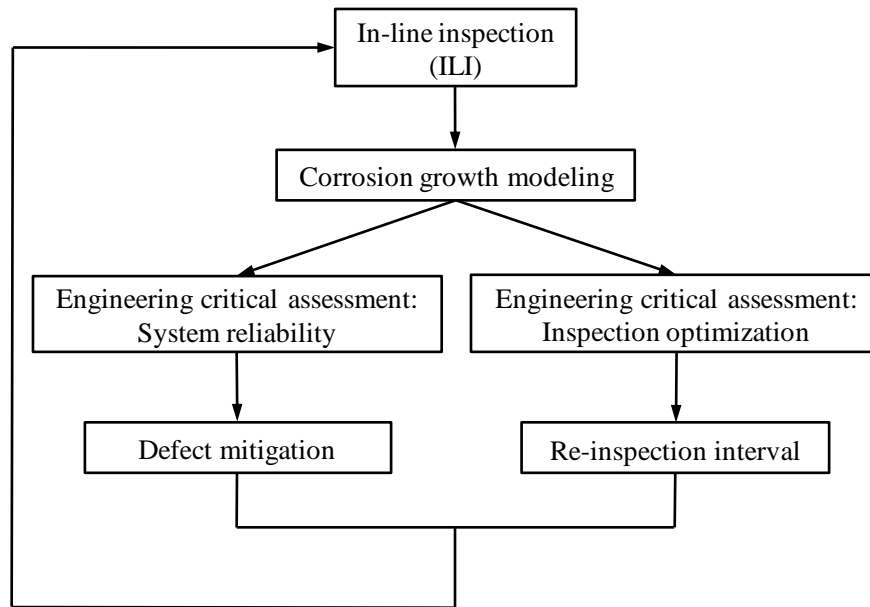


Figure 1.1 Overview of the research topics in the thesis

## 1.4 Thesis Format

This thesis is prepared in an Integrated-Article Format as specified by the School of Graduate and Postdoctoral Studies at Western University, London, Ontario, Canada. A total of seven chapters are included in the thesis. Chapter 1 presents a brief introduction of the background, objective and scope of this study. Chapters 2 through 6 form the main body of the thesis, each of which addresses an individual topic and forms the core of the published papers and submitted manuscripts listed in my Curriculum Vitae. The main conclusions and further recommendations for the research reported in this thesis are given in Chapter 7.

## References

- Amirat A, Mohamed-Chateaneuf A and Chaoui K. (2006). Reliability assessment of underground pipelines under the combined effect of active corrosion and residual stress. *International Journal of Pressure Vessels and Piping*, 83:107-117.
- Caleyo, F., Velázquez, J. C., Valor, A. and Hallen, J. M. (2009). Markov chain modelling of pitting corrosion in underground pipelines. *Corrosion Science*, 51(9): 2197-2207.

- Cheng, T. and Pandey, M. D. (2012). An accurate analysis of maintenance cost of structures experiencing stochastic degradation. *Structure and Infrastructure Engineering*, 8(4): 329-339.
- Cosham A., Hopkins, P. and Macdonald, K. A. (2007). Best practice for the assessment of defects in pipelines–corrosion. *Engineering Failure Analysis*, 14: 1245–65.
- Gomes, W. J. S., Beck, A. T. and Haukaas, T. (2013). Optimal inspection planning for onshore pipelines subjected to external corrosion. *Reliability Engineering and System Safety*, 118: 18-27.
- Hong, H. P. (1999a). Application of stochastic process to pitting corrosion. *Corrosion*, 55(1): 10-16.
- Hong, H. P. (1999b). Inspection and maintenance planning for pipelines under external corrosion considering generation of new defects. *Structural Safety*, 21: 203-22.
- Kariyawasam, S. and Peterson, W. (2010). Effective Improvements to Reliability Based Corrosion Management. *Proceedings of 8th International Pipeline Conference*, ASME, Calgary, Alberta, Canada, 603-615.
- Little, J., Goldstein, M. and Jonathan, P. (2004a). Spatio-temporal modelling of corrosion in an industrial furnace. *Applied Stochastic Models in Business and Industry*, 20: 219-38.
- Little, J., Goldstein, M., Jonathan, P. and den Heijer, K. (2004b). Efficient Bayesian sampling inspection processes based on transformed spatio-temporal data. *Statistical Modeling*, 4: 299-313.
- Maes, M. A. Faber, M. H. and Dann, M. R. (2009). Hierarchical modeling of pipeline defect growth subject to ILI uncertainty, *Proceedings of the ASME 28th international conference on Ocean, Offshore and Arctic Engineering*, OMAE2009-79470, Honolulu, Hawaii, USA.
- Morrison, T. B. and Worthingham, R. G. (1992). Reliability of high pressure line pipe under external corrosion. *ASME, OMAE*, V-B, 401-408.

- Nessim, M. A., Zhou, W., Zhou, J., Rothwell, B., and McLamb, M. (2009). Target reliability levels for design and assessment of onshore natural gas pipelines. *Journal of Pressure Vessel Technology ASME*, 131(6): 061701(1-12).
- Rodriguez III, E. S. and Provan, J. W. (1989). Part II: development of general failure control system for estimating the reliability of deteriorating structures. *Corrosion Science*, 45(3):193-206.
- Qin, S. and Cui, W. (2003). Effect of corrosion models on the time-dependent reliability of steel plated elements. *Marine Structures*, 16: 15–34.
- Teixeira, A. P., Guedes Soares, C., Netto, T. A. and Estefen, S. F. (2008). Reliability of pipelines with corrosion defects. *International Journal of Pressure Vessels and Piping*, 85: 228-237.
- Timashev, S. A., Malyukova, M. G., Poluian, L. V. and Bushinskaya, A. V. (2008). Markov description of corrosion defects growth and its application to reliability based inspection and maintenance of pipelines. *Proceedings of IPC 2008*, IPC2008-64546, ASME, Calgary.
- Valor, A., Caleyó, F., Alfonso, L., Rivas, D. and Hallen, J. M. (2007). Stochastic modeling of pitting corrosion: A new model for initiation and growth of multiple corrosion pits. *Corrosion Science*, 49: 559-579.
- Valor, A., Caleyó, F., Hallen, J. M. and Velázquez, J. C. (2013). Reliability assessment of buried pipelines based on different corrosion rate models, *Corrosion Science*, 66: 78-87.
- van Noordwijk, J. M., van der Weide, J. A. M., Kallen, M. J. and Pandy, M. D. (2007). Gamma process and peaks-over-threshold distribution for time-dependent reliability, *Reliability Engineering and System Safety*, 92: 1651-1658.
- Zhou, W., Hong, H. P. and Zhang, S. (2012). Impact of dependent stochastic defect growth on system reliability of corroding pipelines. *International Journal of Pressure Vessels and Piping*, 96-97: 68-77.

Zhang, S., Zhou, W., Al-Amin, M., Kariyawasam, S. and Wang, H. (2012). Time-dependent corrosion growth modeling using multiple ILI data, Proceedings of 9th International Pipeline Conference, IPC2012-90502, ASME, Calgary.

## **Chapter 2 Gamma Process-based Corrosion Growth Modeling Based on Imperfect Inspection Data**

### **2.1 Introduction**

A gamma process is a non-decreasing stochastic process that consists of a series of independent and gamma-distributed increments with the same scale parameter. The gamma process has been widely employed to characterize the degradation of engineering structures, such as creep, fatigue, corrosion and crack growth (van Noortwijk 2009). The advantages of using the gamma process to model the degradation of structures are twofold: the mathematical tractability and the monotonic increasing nature. The gamma process can be further classified as the homogeneous (or stationary) or non-homogeneous (or non-stationary) gamma process (van Noortwijk 2009), as described in detail in Section 2.2.

The use of the gamma process to characterize the deterioration of engineering structures (e.g. berm breakwaters, steel pressure vessels, dikes, pipelines, nuclear power plant facilities) in the context of optimal maintenance decision or time-dependent reliability analysis have been reported extensively in the literature (e.g. van Noortwijk and van Gelder 1996; Kallen and van Noortwijk 2005; van Noortwijk et al. 2007; Zhou et al. 2012; Yuan et al. 2008; Cheng and Pandey 2012; Cheng et al. 2012). For example, van Noortwijk and van Gelder (1996) adopted the gamma process to characterize the rock displacement for the purpose of determining the optimal maintenance plan for berm breakwaters. The gamma process was employed to model the deterioration of steel pressure vessels to determine the optimal maintenance intervals (Kallen and van Noortwijk 2005), and model the crest-level decline of dikes to evaluate the time-dependent reliability of dikes subjected to sea waves (van Noortwijk et al. 2007). The gamma process was also used to characterize the growth of the defect depth for evaluating the time-dependent system reliability of pipeline containing multiple active corrosion defects (Zhou et al. 2012), and to characterize the degradation of nuclear power plant facilities due to corrosion (Yuan et al. 2008; Cheng and Pandey 2012; Cheng et al. 2012). If inspection data are available, the Bayesian methodology can be used to update

the probabilistic characteristics of the parameters in the corrosion growth model. For example, a hierarchical Bayesian approach (Maes et al. 2009; Zhang et al. 2012) was used to update the gamma process-based growth models for corrosion defects on pipelines based on the ILI data.

This chapter describes a gamma process-based model to characterize the growth of depths of corrosion defects on energy pipelines. The growth model included in this study differs from the gamma process-based growth models reported in the literature (Maes et al. 2009) on two aspects. First, the model presented in this study considers the initiation time of the corrosion defect. Second, a general form of measurement error including the biases, random scattering error associated with the ILI tools as well as the correlation between the random scattering errors associated with different ILI tools is considered in this model. In contrast, only the random scattering error associated with the ILI data is considered in the model reported by Maes et al. (2009). The hierarchical Bayesian method and Markov Chain Monte Carlo (MCMC) simulation are used to update the growth model for the defect depth based on data collected from multiple ILIs.

The remainder of the chapter is organized as follows. Sections 2.2 and 2.3 describe the gamma process and the uncertainties involved in the ILI data, respectively. Section 2.4 presents the formulation of the corrosion growth model. Section 2.5 gives a description of the hierarchical Bayesian method for updating the model parameters. An example to illustrate above-described methodologies is shown in Section 2.6 followed by the conclusions in Section 2.7. Appendix A includes the derivations of the full conditional posterior distributions used in the MCMC simulation.

## 2.2 Gamma Process

Consider  $\{X(t); t \geq 0\}$  as a gamma process (GP) over time  $t$ . The probability density function (PDF) of  $X(t)$  is given by (van Noortwijk 2009; Yuan et al. 2008)

$$f_{X(t)}(x(t)|A(t), \beta) = \beta^{A(t)} x(t)^{A(t)-1} e^{-x(t)\beta} / \Gamma(A(t)) I_{(0, \infty)}(x(t)) \quad (2.1)$$

where  $A(t)$  denotes the time-dependent shape parameter and  $\beta$  is the so-called rate parameter or inverse of the scale parameter (Ang and Tang 1975; Jonhson 2000);  $\Gamma(s)$  is the gamma function and given by  $\Gamma(s) = \int_0^{\infty} z^{s-1} e^{-z} dz$  for  $s > 0$ , and  $I_{(0, \infty)}(x(t))$  is an indicator function, which equals unity if  $x(t) > 0$  and zero otherwise.

It follow from Eq. (2.1) that the mean, variance and coefficient of variation (COV) of  $X(t)$ , denoted by  $E[X(t)]$ ,  $\text{Var}[X(t)]$  and  $\text{COV}[X(t)]$ , respectively, are

$$E[X(t)] = \frac{A(t)}{\beta} \quad (2.2a)$$

$$\text{Var}[X(t)] = \frac{A(t)}{\beta^2} \quad (2.2b)$$

$$\text{COV}[X(t)] = \frac{1}{\sqrt{A(t)}} \quad (2.2c)$$

The GP defined by Eq. (2.1) has the following properties (van Noortwijk 2009):

- (1)  $X(0) = 0$  with probability one;
- (2)  $X(\tau) - X(t)$  follows a gamma distribution with a shape parameter of  $A(\tau) - A(t)$  and a scale parameter of  $\beta$  for all  $\tau > t \geq 0$ , and
- (3)  $X(t)$  has independent gamma-distributed increments.

Equation (2.2) indicates that the mean and variance of  $X(t)$  increase as time increases whereas the COV of  $X(t)$  decreases as time increases because  $A(t)$  must be a monotonically increasing function of time  $t$ . Note that Eq. (2.1) is a homogeneous gamma process if the shape parameter  $A(t)$  is a linear function of  $t$  for any  $t \geq 0$ , and a non-homogeneous gamma process otherwise (Wang 2008).

### 2.3 ILI Data and Uncertainties

The periodic ILI data provide valuable information for the corrosion growth modeling and structural integrity management for energy pipelines. The ILI data are subjected to measurement errors as a result of the uncertainties associated with the ILI tool and sizing



algorithm (Kariyawasam and Peterson 2010). It is commonly assumed in the literature that the measured defect depth follows a normal distribution with a mean value equal to the actual depth and a standard deviation characterizing the random scattering error (Maes et al. 2009; Yuan et al. 2009). This assumption however ignores the potential bias in the ILI data. A comparison of the ILI-reported and field-measured depths that are considered error-free (see Fig. 2.1) for a set of defects collected from an in-service pipelines indicates that the ILI data can deviate markedly from the field measurements, and involve both the biases and random scattering error (Al-Amin et al. 2012). Therefore, the measurement errors must be properly incorporated in the model updating. Furthermore, inspection tools with similar technologies and/or sizing algorithms are usually employed in different ILIs on a given pipeline; as a result, certain degree of correlation is likely to exist between the measurement errors associated with the data from multiple ILIs for the same pipeline.

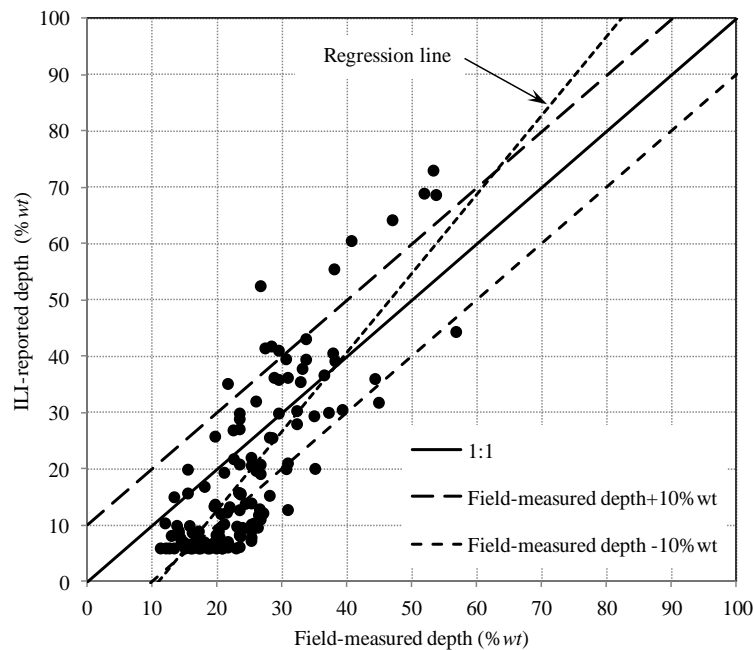


Figure 2.1 Illustration of the measurement errors associated with the ILI data

Consider that  $m$  active corrosion defects on a given pipeline have been subjected to  $n$  inspections over a period of time. The measured depth (i.e. in the through pipe wall

thickness direction) of the  $i^{\text{th}}$  defect at the  $j^{\text{th}}$  inspection,  $y_{ij}$ , ( $i = 1, 2, \dots, m; j = 1, 2, \dots, n$ ) is related to the actual depth,  $x_{ij}$ , as follows (Fuller 1987; Jeach 1985):

$$y_{ij} = a_j + b_j x_{ij} + \varepsilon_{ij} \quad (2.3)$$

where  $a_j$  and  $b_j$  denote the constant and non-constant biases associated with the ILI tool used in the  $j^{\text{th}}$  inspection, and  $\varepsilon_{ij}$  denotes the random scattering error associated with the ILI-reported depth of the  $i^{\text{th}}$  defect at the  $j^{\text{th}}$  inspection, and is assumed to follow a zero-mean normal distribution (Al-Amin et al. 2012). It is further assumed that for a given inspection  $\varepsilon_{ij}$  associated with different defects are independent, i.e. the random scattering errors are spatially independent, whereas for a given defect  $\varepsilon_{ij}$  associated with different inspections are correlated (Al-Amin et al. 2012). Let  $\mathbf{E}_i = (E_{i1}, E_{i2}, \dots, E_{in})'$  denote the vector of random scattering errors associated with defect  $i$  for inspections  $j = 1, 2, \dots, n$ , with “'” representing transposition. The PDF of  $\mathbf{E}_i$  is then given by

$$f_{\mathbf{E}_i}(\boldsymbol{\varepsilon}_i | \boldsymbol{\Sigma}_{\mathbf{E}_i}) = (2\pi)^{-\frac{n}{2}} |\boldsymbol{\Sigma}_{\mathbf{E}_i}|^{-\frac{1}{2}} \exp\left(-\frac{1}{2} \boldsymbol{\varepsilon}_i' \boldsymbol{\Sigma}_{\mathbf{E}_i}^{-1} \boldsymbol{\varepsilon}_i\right) \quad (2.4)$$

with  $|\boldsymbol{\Sigma}_{\mathbf{E}_i}|$  denoting the determinant of the variance matrix of  $\mathbf{E}_i$ .  $\boldsymbol{\Sigma}_{\mathbf{E}_i}$  is an  $n$  by  $n$  matrix with the element equal to  $\rho_{jk} \sigma_j \sigma_k$  ( $j = 1, 2, \dots, n; k = 1, 2, \dots, n$ ), where  $\rho_{jk}$  denotes the correlation coefficient between the random scattering errors associated with the  $j^{\text{th}}$  and  $k^{\text{th}}$  inspections, and  $\sigma_j$  and  $\sigma_k$  denote the standard deviations of the random scattering errors associated with the tools used at the  $j^{\text{th}}$  and  $k^{\text{th}}$  inspections, respectively. A Bayesian method has been developed to evaluate  $a_j$ ,  $b_j$ ,  $\sigma_j$  and  $\rho_{jk}$  ( $j = 1, 2, \dots, n; k = 1, 2, \dots, n$ ) involved in Eqs. (2.3) and (2.4) based on the ILI-reported depths for a set of static defects (i.e. defects that have been repaired prior to the ILI and ceased growing), details of which can be found in Al-Amin et al. (2012). In this study,  $a_j$ ,  $b_j$ ,  $\sigma_j$  and  $\rho_{jk}$  were assumed to be known and deterministic quantities.

## 2.4 Growth Modeling for Multiple Defects

The depth of a given corrosion defect on a pipeline at time  $t$  (years) ( $t = 0$  representing the time of installation of the pipeline),  $x(t)$ , was assumed to be characterized by a gamma

process given by Eq. (2.1), where  $A(t)$ , in general, can be assumed to be a power-law function of time, i.e.  $A(t) = \alpha(t - t_0)^\kappa$  ( $t > t_0$ ) with  $t_0$  denoting the defect initiation time (i.e. time elapsed from the installation of the pipeline up to the point at which the defect starts growing), and  $\kappa > 1$ ,  $\kappa < 1$  and  $\kappa = 1$  implying that the mean growth is an accelerating, decelerating and linear trajectory over time, respectively. It follows from Section 2.2 that Eq. (2.1) characterizes a homogeneous gamma process (HGP) if  $\kappa = 1$ , and a non-homogeneous gamma process (NHGP) if  $\kappa \neq 1$ . The value of  $\alpha/\beta$  represents the mean of the growth rate of defect depth (i.e. the increment of depth within one year) for the HGP, and the mean of the growth of defect depth at the first unit increment of time since  $t_0$  for the NHGP. In the present study,  $\alpha$  and  $\kappa$  were assumed to be common for all the corrosion defects on a given segment of pipeline whereas  $\beta$  and  $t_0$  were assumed to be defect specific. Both the NHGP and HGP were considered in this study.

It follows from the above that the growth of the depth of defect  $i$  ( $i = 1, 2, \dots, m$ ) between the  $(j-1)^{\text{th}}$  and  $j^{\text{th}}$  inspections ( $j = 2, 3, \dots, n$ ),  $\Delta x_{ij}$ , is gamma distributed with the PDF given by

$$f_{\Delta x_{ij}}(\Delta x_{ij} | \Delta A_{ij}, \beta_i) = \beta_i^{\Delta A_{ij}} \Delta x_{ij}^{\Delta A_{ij}-1} e^{-\Delta x_{ij} \beta_i} / \Gamma(\Delta A_{ij}) \quad (2.5)$$

where  $\beta_i$  and  $t_{i0}$  are the defect-specific rate parameter and initiation time associated with defect  $i$ , respectively, and  $\Delta A_{ij}$  is the time-dependent shape parameter associated with  $\Delta x_{ij}$  and given by

$$\Delta A_{ij} = \alpha(t_{ij} - t_{i0})^\kappa \quad (j = 1) \quad (2.6a)$$

$$\Delta A_{ij} = \alpha(t_{ij} - t_{i0})^\kappa - \alpha(t_{i,j-1} - t_{i0})^\kappa \quad (j = 2, 3, \dots, n) \quad (2.6b)$$

with  $t_{ij}$  ( $j = 1, 2, \dots, n$ ) denoting the time of the  $j^{\text{th}}$  inspection (e.g. time elapsed from the installation of pipeline up to the point when the  $j^{\text{th}}$  inspection was carried out) for the  $i^{\text{th}}$  defect. Note that Eq. (2.6) is simplified as  $\Delta A_{ij} = \alpha(t_{ij} - t_{i,j-1})$  ( $j = 1, 2, \dots, n$ ) for the HGP-based model (i.e.  $\kappa = 1$ ).

The actual depth of defect  $i$  at the time of the  $j^{\text{th}}$  inspection,  $x_{ij}$ , can be expressed as the sum of the depth at time  $t_{i,j-1}$  and the incremental depth between  $t_{i,j-1}$  and  $t_{ij}$ ; that is

$$x_{ij} = x_{i,j-1} + \Delta x_{ij} \quad (2.7)$$

It is assumed that the defect depth at  $t = t_0$  (i.e.  $x_{i0}$ ) equals zero.

In this study, it is assumed that  $\alpha$ ,  $\kappa$ ,  $\beta_i$  and  $t_{i0}$  in Eqs. (2.5) and (2.6) are all uncertain parameters and employed the Bayesian updating to evaluate the probability distributions of these parameters based on data obtained from multiple ILIs, which is described in the following section.

## 2.5 Bayesian Updating of Growth Model

### 2.5.1 Overview of Bayesian Updating

The Bayesian updating or inference is a method of evaluating the probability distributions of uncertain parameters of a given model by combining the previous knowledge of these parameters as reflected in the prior distribution with the new information contained in the observed data (Gelman 2004). The mechanism for combining the information is Bayes' theorem. The new information in the observed data is incorporated in the Bayesian updating through the so-called likelihood function, and the probability distribution obtained from the updating is known as the posterior distribution.

The prior distribution represents the preliminary belief on the parameters without considering the information implied in the data, and is typically specified based on information obtained from previous studies and/or experts' opinions. Various types of prior distributions, such as the informative and non-informative distributions, can be specified in the Bayesian inference. The former reflects specific prior information about a variable, whereas the latter does not contain any specific prior information about the variable. Note that the Bayesian inference is completely objective rather than subjective if a non-informative prior distribution is specified. Both the informative and non-informative prior distributions can be selected as conjugate prior distributions. The

conjugate prior indicates a particular distribution that is conjugate to the likelihood function and leads to a posterior distribution belonging to the same family as the prior. Furthermore, the assignment of the conjugate prior distribution can improve the computational efficiency of the MCMC simulation. The likelihood function characterizes how likely a particular set of parameter values are given the observed data. It is constructed using the marginal PDF of the observed data.

The Markov Chain Monte Carlo (MCMC) simulation techniques were commonly used to numerically evaluate the joint posterior distribution of model parameters. The MCMC simulation is a technique to sequentially generate random samples from a distribution (i.e. the target distribution) by constructing a Markov chain that converges to the target distribution. At each step random samples are drawn from distributions that depend on the random samples drawn in the previous step. After an initial sequence of iterations (i.e. the so-called burn-in period (Gelman 2004)), the random samples drawn from the subsequent iterations converge to the target distribution, which is the joint posterior distribution in the context of Bayesian updating. If the number of iterations is large enough, the samples drawn after the burn-in period can then be used to evaluate the probabilistic characteristics (e.g. mean and standard deviation) of the posterior distribution. Let  $\theta$  denote the model parameter of interest. The aforementioned MCMC simulation-based numerical method to evaluate the posterior distribution of  $\theta$  based on an  $n$  sequences of Markov chain of  $\theta$  is illustrated in Figure 2.2, where  $\theta^{(0)}$  denotes the initial value of  $\theta$  specified in the MCMC simulation,  $\theta^{(k)}$  denotes the random sample of  $\theta$  generated in the  $k^{\text{th}}$  iteration, and  $p(\theta)$  represents the posterior distribution of  $\theta$ .

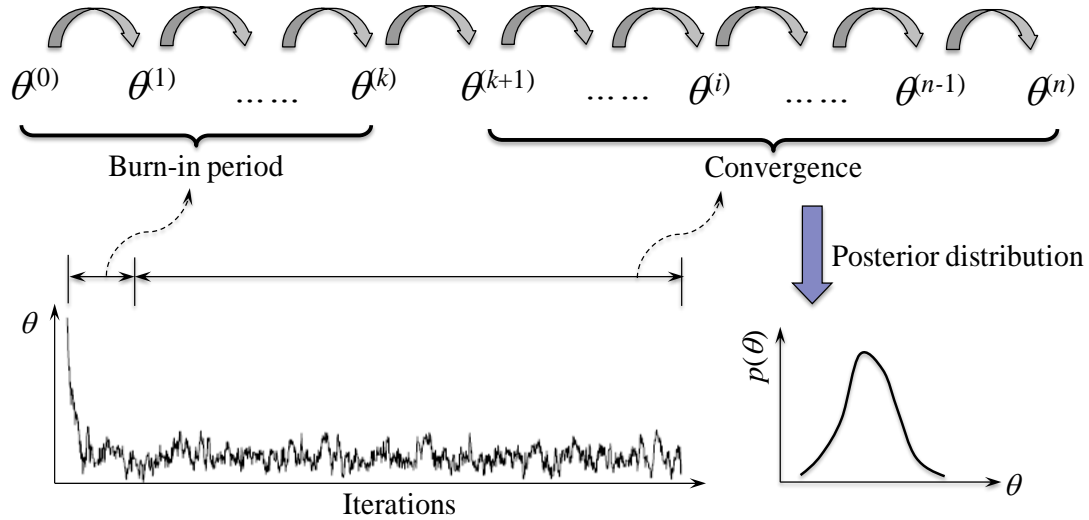


Figure 2.2 Schematic of the MCMC simulation method

The commonly used sampling algorithms in the MCMC simulation include, but are not limited to, the Metropolis-Hasting (M-H) algorithm (Gelman 2004), Gibbs sampler (Gelman 2004) and slice sampling approach (Neal 2003). The M-H algorithm is the most general Markov chain-based simulation technique and is suitable for any distribution types including multivariate distributions. The M-H algorithm typically involves two distributions, namely the proposal (or jumping) distribution (Chib and Greenberg 1995) and the target distribution. The former is employed to generate the random seeds of the candidate samples of model parameter of interest (denoted by  $\theta$ ), whereas the latter represents the full conditional posterior distribution derived from the Bayesian theorem. Given the value of  $\theta$ ,  $\theta^{(i)}$ , at a given iteration  $i$ , the value of  $\theta$  in the next iteration,  $\theta^{(i+1)}$ , equals either  $\theta^{(*)}$  or  $\theta^{(i)}$  with  $\theta^{(*)}$  denoting the random seed generated from the proposal distribution.  $\theta^{(*)}$  is accepted as  $\theta^{(i+1)}$  based on the acceptance function given by  $\phi = \min\left(1, \frac{p(\theta^{(*)})J(\theta^{(i)}|\theta^{(*)})}{p(\theta^{(i)})J(\theta^{(*)}|\theta^{(i)})}\right)$ , where  $p(\bullet)$  denotes the PDF of the target distribution (i.e. the full conditional posterior distribution), and  $J(\bullet|\theta^{(i)})$  denotes the PDF of the proposal distribution conditional on the current value  $\theta^{(i)}$ . The above-mentioned updating of  $\theta$  (i.e. from  $\theta^{(i)}$  to  $\theta^{(i+1)}$ ) can be achieved through the following four steps: 1) generate a candidate value of  $\theta$ ,  $\theta^{(*)}$ , from  $J(\bullet|\theta^{(i)})$ ; 2) calculate the acceptance rate  $\phi$ ; 3) draw a random number  $u$  from the uniform distribution between 0 and 1, and 4) set  $\theta^{(i+1)} = \theta^{(*)}$  if

$u \leq \phi$ , and  $\theta^{(i+1)} = \theta^{(i)}$  otherwise. Note that the proposal function is typically selected as a uniform or normal distribution, and the efficiency of the M-H algorithm is very sensitive to the specification of the proposal function (Lynch 2007).

The Gibbs sampler (Gelfand and Smith 1990; Gelman 2004) is a special case of the M-H algorithm and is applicable to the conjugate posterior distribution, i.e. the full conditional posterior distribution of a parameter has a closed form of a typical distribution, which can be used to generate the random samples directly. Denote  $\theta = (\theta_1, \dots, \theta_{j-1}, \theta_{j+1}, \dots, \theta_n)$  as the  $n$  model parameters of interest and assume that  $\theta_j$  ( $j = 1, 2, \dots, n$ ) have conjugate posterior distributions. The full conditional posterior distribution of  $\theta_j$  can be written as  $p(\theta_j | \theta_{(-j)})$  with  $\theta_{(-j)} = (\theta_1, \dots, \theta_{j-1}, \theta_{j+1}, \dots, \theta_n)$ . At a given iteration  $i$ , the sample of  $\theta_j^{(i)}$  ( $j = 1, 2, \dots, n$ ) can be drawn directly from  $p(\theta_j | \theta_1^{(i)}, \theta_2^{(i)}, \dots, \theta_{j-1}^{(i)}, \theta_{j+1}^{(i-1)}, \dots, \theta_n^{(i-1)})$ . The main advantage of the Gibbs sampler is its high computational efficiency in the convergence of the MCMC simulation in that the full conditional distribution is used as the proposal distribution and the candidate sample will always be accepted, i.e. the acceptance rate equals one (as opposed to the acceptance rate being less than one for the M-H algorithm).

The slice sampling approach is a generic sampling approach and applicable to a wide variety of distributions including the univariate and multivariate distributions. The simple form of univariate slice sampling is an alternative to the Gibbs sampler (Neal 2003). A key element involved in the slice sampling is that an adaptive uniform proposal distribution is used to replace the proposal function in the M-H algorithm and Gibbs sampler. Suppose that the model parameter  $\theta$  has a target distribution  $p(\theta)$ . By introducing an auxiliary variable  $u$  with a conditional PDF denoted by  $f(u|\theta)$ , the joint PDF of  $\theta$  and  $u$  can be written as  $f(u, \theta) = f(u|\theta)p(\theta)$ , which implies that  $f(\theta) = p(\theta)$  given that  $f(\theta) = \int f(u, \theta)du = \int f(u|\theta)p(\theta)du = p(\theta)$  (Neal 2003). A usual choice for  $f(u|\theta)$  is the uniform distribution between zero and  $p(\theta)$  to ensure the computational efficiency of the simulation. Given above, the current value  $\theta^{(i)}$  can be updated to  $\theta^{(i+1)}$  through the following three steps: 1) generate a random number  $u$  from the uniform distribution between zero and  $p(\theta^{(i)})$  and define a horizontal slice:  $S = \{ \theta: u \leq p(\theta) \}$ .

Note that  $\theta^{(i)}$  is always within  $S$ ; 2) find an interval,  $I = [L, R]$ , around  $\theta^{(i)}$  containing a substantial portion of the slice with  $L$  and  $R$  denoting the left and right bounds of  $I$ , and 3) draw a new point  $\theta^{(i+1)}$  from the portion of the slice within this interval (i.e.  $S \cap I$ ); in other words,  $\theta^{(i+1)}$  is generated from the truncated  $p(\theta)$  to satisfy the condition  $p(\theta^{(i+1)}) \geq u$ . Details of the slice sampling can be found in the literature (e.g. Neal 2003; Jasa and Xiang 2009).

Note that the full conditional posterior distributions of model parameters are not always conjugate. Therefore, a hybrid of the above-described algorithms (e.g. the M-H algorithm and Gibbs sampler) is often employed in the MCMC simulation to carry out the Bayesian updating. The likelihood functions, prior and posterior distributions as well as the MCMC simulation-based Bayesian updating procedures for the GP-based (i.e. the NHGP- and HGP-based) growth models are described in the following sections.

### 2.5.2 Prior Distribution

For  $m$  active corrosion defects, the NHGP-based corrosion growth model described in Section 2.4 includes  $2m + 2$  basic parameters, namely two common parameters (i.e.  $\alpha$  and  $\kappa$ ),  $m$  defect-specific rate parameters  $\beta_i$  and initiation times  $t_{i0}$  ( $i = 1, 2, \dots, m$ ). In this study, the gamma distribution was selected as the prior distributions of  $\alpha$ ,  $\kappa$  and  $\beta_i$ , ( $i = 1, 2, \dots, m$ ), which is mainly based on the consideration that the gamma distribution ensures  $\alpha$ ,  $\kappa$  and  $\beta_i$  to be positive quantities and can be conveniently made as a non-informative distribution. Furthermore, the assignment of the gamma distribution as the prior distribution of  $\beta_i$  can lead to a conjugate posterior distribution of  $\beta_i$  conditional on  $\alpha$ ,  $\kappa$  and  $t_{i0}$ , which improves the computational efficiency in the MCMC simulation (Gelman 2004). The prior distribution of  $t_{i0}$  was chosen to be a uniform distribution with a lower bound of zero and an upper bound equal to the time interval between the installation of the pipeline and the first detection of defect  $i$ . It was further assumed that  $\beta_i(t_{i0})$  ( $i = 1, 2, \dots, m$ ) associated with different defects are mutually independent and have identical prior distributions (*iid*). Note that the prior distributions of the model parameters involved in the HGP-based model are the same as those involved in the NHGP-based model except that  $\kappa$  is deterministic and set equal to unity.



### 2.5.3 Likelihood Functions of the ILI Data

Define  $\mathbf{y}_i = (y_{i1}, y_{i2}, \dots, y_{ij}, \dots, y_{in})'$  and  $\mathbf{x}_i = (x_{i1}, x_{i2}, \dots, x_{ij}, \dots, x_{in})'$ . Given  $\mathbf{x}_i$ , it follows from Eqs. (2.3) and (2.4) as well as the above-mentioned assumptions that  $\mathbf{y}_i$  is characterized by a multivariate normal distribution with a mean vector of  $\mathbf{a} + \mathbf{b}\mathbf{x}_i$  and a variance matrix of  $\Sigma_{E_i}$ , where  $\mathbf{a} = (a_1, a_2, \dots, a_j, \dots, a_n)'$  and  $\mathbf{b}$  is an  $n$ -by- $n$  diagonal matrix with diagonal elements equal to  $b_j$  ( $j = 1, 2, \dots, n$ ). The likelihood of the inspection data  $\mathbf{y}_i$  conditional on the latent parameters  $\Delta x_{ij}$  can then be written as

$$L(\mathbf{y}_i | \Delta \mathbf{x}_i) = (2\pi)^{-\frac{n}{2}} |\Sigma_{E_i}|^{-\frac{1}{2}} \exp\left(-\frac{1}{2} (\mathbf{y}_i - (\mathbf{a} + \mathbf{b}\mathbf{x}_i))' (\Sigma_{E_i})^{-1} (\mathbf{y}_i - (\mathbf{a} + \mathbf{b}\mathbf{x}_i))\right) \quad (2.8)$$

with  $\Delta \mathbf{x}_i = (\Delta x_{i1}, \Delta x_{i2}, \dots, \Delta x_{ij}, \dots, \Delta x_{in})$ , and  $x_{ij} = \sum_{k=1}^j \Delta x_{ik}$ .

### 2.5.4 Likelihood Functions of Model Parameters

It follows from Eq. (2.5) and the property of the Gamma distribution (i.e.  $\Delta x_{ij}$  and  $\Delta x_{ik}$  ( $j \neq k$ ) are mutually independent for a given defect  $i$  conditional on  $\alpha$ ,  $\kappa$ ,  $\beta_i$  and  $t_{i0}$ ) that the joint probability density function of  $\Delta \mathbf{x}_i$  is

$$\begin{aligned} f_{\Delta \mathbf{x}_i}(\Delta \mathbf{x}_i | \Delta A_{ij}, \beta_i) &= \prod_{j=1}^n f_{\Delta x_{ij}}(\Delta x_{ij} | \Delta A_{ij}, \beta_i) \\ &= \prod_{j=1}^n \beta_i^{\Delta A_{ij}} \Delta x_{ij}^{\Delta A_{ij}-1} e^{-\Delta x_{ij} \beta_i} / \Gamma(\Delta A_{ij}) \end{aligned} \quad (2.9)$$

where  $\Delta \mathbf{x}_i = (\Delta x_{i1}, \Delta x_{i2}, \dots, \Delta x_{in})'$ .

Further denote  $\Delta \mathbf{x} = (\Delta \mathbf{x}_1, \Delta \mathbf{x}_2, \dots, \Delta \mathbf{x}_m)$ ,  $\boldsymbol{\beta} = (\beta_1, \beta_2, \dots, \beta_m)$  and  $\mathbf{t}_0 = (t_{10}, t_{20}, \dots, t_{m0})$ . Assume that  $\Delta x_{ij}$  and  $\Delta x_{lj}$  ( $i \neq l$ ) are mutually independent for given inspection  $j$  conditional on  $\alpha$ ,  $\kappa$ ,  $\beta_i$  and  $t_{i0}$ ; that is, the growths of different defects are spatially independent. Given that  $\beta_i$  and  $t_{i0}$  are defect-specific and only depends on the growth of the  $i^{\text{th}}$  defect (i.e.  $\Delta \mathbf{x}_i$ ) and that  $\alpha$  and  $\kappa$  are common for the growth of all defects (i.e.  $\Delta \mathbf{x}$ ), the likelihood function of  $\Delta \mathbf{x}_i$  conditional on  $\alpha$ ,  $\kappa$ ,  $\beta_i$  and  $t_{i0}$  ( $i = 1, 2, \dots, m$ ), as well as the

likelihood functions of  $\Delta \mathbf{x}$  conditional on  $\alpha$ ,  $\kappa$ ,  $\boldsymbol{\beta}$  and  $\mathbf{t}_0$  are therefore obtained from Eqs. (2.10a) and (10b), respectively.

$$\begin{aligned} L(\Delta \mathbf{x}_i | \alpha, \kappa, \boldsymbol{\beta}_i, \mathbf{t}_{i0}) &= \prod_{j=1}^n f_{\Delta x_{ij}}(\Delta x_{ij} | \Delta A_{ij}, \beta_i) \\ &= \prod_{j=1}^n \beta_i^{\Delta A_{ij}} \Delta x_{ij}^{\Delta A_{ij}-1} e^{-\Delta x_{ij} \beta_i} / \Gamma(\Delta A_{ij}) \end{aligned} \quad (2.10a)$$

$$\begin{aligned} L(\Delta \mathbf{x} | \alpha, \kappa, \boldsymbol{\beta}, \mathbf{t}_0) &= \prod_{i=1}^m \prod_{j=1}^n f_{\Delta x_{ij}}(\Delta x_{ij} | \Delta A_{ij}, \beta_i) \\ &= \prod_{i=1}^m \prod_{j=1}^n \beta_i^{\Delta A_{ij}} \Delta x_{ij}^{\Delta A_{ij}-1} e^{-\Delta x_{ij} \beta_i} / \Gamma(\Delta A_{ij}) \end{aligned} \quad (2.10b)$$

### 2.5.5 Posterior Distribution

Denote the uncertain parameters in the growth model by  $\boldsymbol{\theta}$ . The joint prior distribution of  $\boldsymbol{\theta}$ ,  $\pi(\boldsymbol{\theta})$ , can be combined with the likelihood,  $L(\mathbf{D} | \boldsymbol{\theta})$ , of the observed data  $\mathbf{D}$  according to Bayes' theorem to lead to the joint posterior distribution of  $\boldsymbol{\theta}$ ,  $p(\boldsymbol{\theta} | \mathbf{D})$  (Gelman 2004):

$$p(\boldsymbol{\theta} | \mathbf{D}) = \frac{L(\mathbf{D} | \boldsymbol{\theta}) \pi(\boldsymbol{\theta})}{\int L(\mathbf{D} | \boldsymbol{\theta}) \pi(\boldsymbol{\theta}) d\boldsymbol{\theta}} \propto L(\mathbf{D} | \boldsymbol{\theta}) \pi(\boldsymbol{\theta}) \quad (2.11)$$

where “ $\propto$ ” represents proportionality. In a hierarchical framework, i.e. the distribution parameters (denoted by  $\boldsymbol{\omega}$ ) of the prior distribution of  $\boldsymbol{\theta}$  also considered to be uncertain, the joint posterior distribution of the parameters  $\boldsymbol{\theta}$  and  $\boldsymbol{\omega}$ , denoted by  $p(\boldsymbol{\theta}, \boldsymbol{\omega} | \mathbf{D})$ , is given by

$$p(\boldsymbol{\theta}, \boldsymbol{\omega} | \mathbf{D}) = \frac{L(\mathbf{D} | \boldsymbol{\theta}) \pi(\boldsymbol{\theta} | \boldsymbol{\omega}) \pi(\boldsymbol{\omega})}{\int \dots \int L(\mathbf{D} | \boldsymbol{\theta}) \pi(\boldsymbol{\theta} | \boldsymbol{\omega}) \pi(\boldsymbol{\omega}) d\boldsymbol{\theta} d\boldsymbol{\omega}} \propto L(\mathbf{D} | \boldsymbol{\theta}) \pi(\boldsymbol{\theta} | \boldsymbol{\omega}) \pi(\boldsymbol{\omega}) \quad (2.12)$$

The derivation of the full conditional posterior distribution of the individual parameter in the growth model given by Eq. (2.1) is shown in Appendix A. The MCMC simulation techniques implemented in the software *OpenBUGS* (Lunn et al. 2009) were employed to numerically evaluate the marginal posterior distributions of the parameters.

### 2.5.6 Hierarchical Representation of the Growth Model

The aforementioned corrosion growth model can be represented by the directed acyclic graph (DAG) (Spiegelhalter 1998) as depicted in Fig. 2.3. Ellipses and rectangles in Fig. 2.3 symbolize the stochastic and known deterministic parameters (or nodes), respectively, in the analysis. Single- and double-edged arrows denote the stochastic links and deterministic functional links, respectively. Three levels of parameters are involved in Fig. 2.3. The first level includes the inspection data, i.e. the defect depths reported by inspections, which are associated with measurement errors characterized by  $\mathbf{a}$ ,  $\mathbf{b}$  and  $\Sigma_{Ei}$ . The second level includes the latent variables that consist of the actual depths at the times of inspections and increments of the actual depths between two consecutive inspections as well as the scale parameters  $\Delta A_{ij}$  ( $i = 1, 2, \dots, m; j = 1, 2, \dots, n$ ). This level captures the stochastic characteristics and temporal variability of the defect growth path. The third level includes the basic parameters of the gamma process model (i.e.  $\alpha$ ,  $\kappa$ ,  $\beta_i$  and  $t_{i0}$ ). The known quantities as shown in Fig. 2.3 include the parameters of the prior distributions of  $\alpha$ ,  $\kappa$ ,  $\beta_i$  and  $t_{i0}$  (i.e.  $p_1, q_1, p_2, q_2, p_3, q_3, p_4$  and  $q_4$ ), the background information,  $t_{ij}$  ( $j = 1, 2, \dots, n$ ), as well as the measurement errors. Note that  $p_1$  ( $q_1$ ),  $p_2$  ( $q_2$ ) and  $p_4$  ( $q_4$ ) denote the shape (rate) parameters of the gamma distributions of  $\alpha$ ,  $\kappa$  and  $\beta_i$ , respectively, and  $p_3$  and  $q_3$  denote the lower and upper bounds of the uniform distribution of  $t_{i0}$ . Furthermore, the parameter  $\kappa = 1$  in the DAG for the HGP-based model.

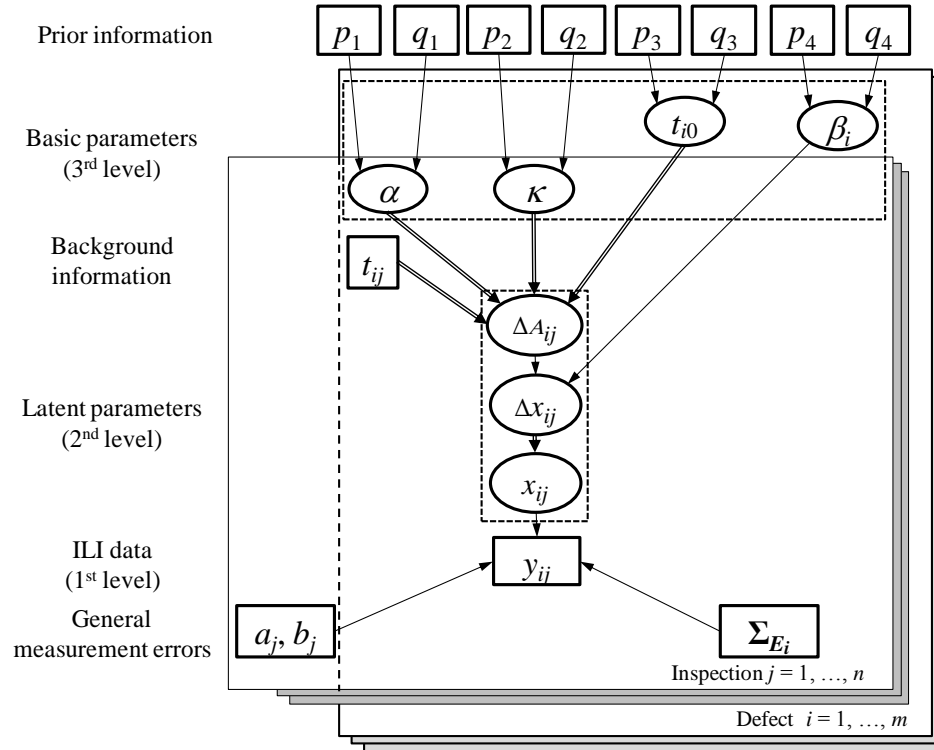


Figure 2.3 Hierarchical structure of the growth model

### 2.5.7 MCMC Simulation-based Bayesian Updating Procedures

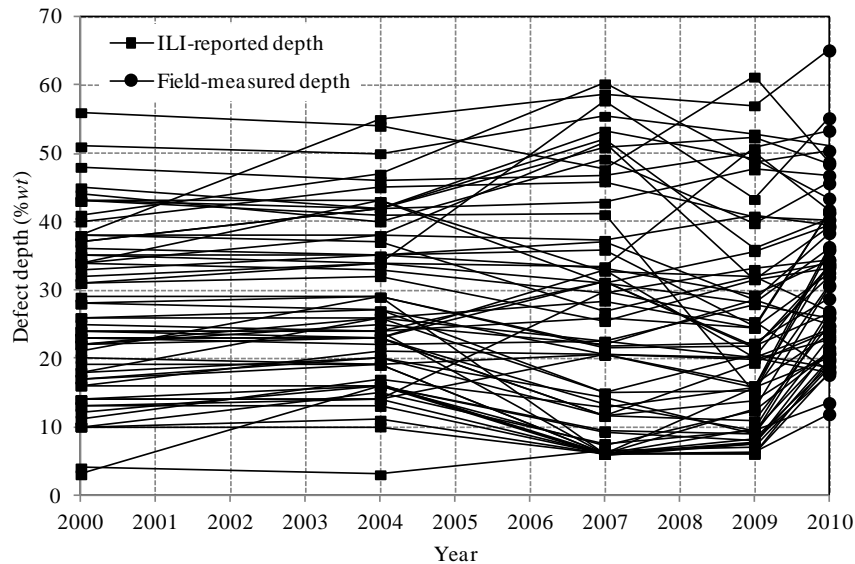
It follows from the description in Section 2.5.1 and the full conditional posterior distributions in Appendix A that a hybrid of these algorithms (e.g. the M-H algorithm and Gibbs Sampler) was employed in this study to carry out the MCMC simulation (Gelman 2004). Without loss of generality, a step-by-step procedure based on a hybrid of the M-H algorithm and Gibbs sampler to sequentially generate the random samples of the parameters in the growth model is included in Appendix B.

## 2.6 Model Validation

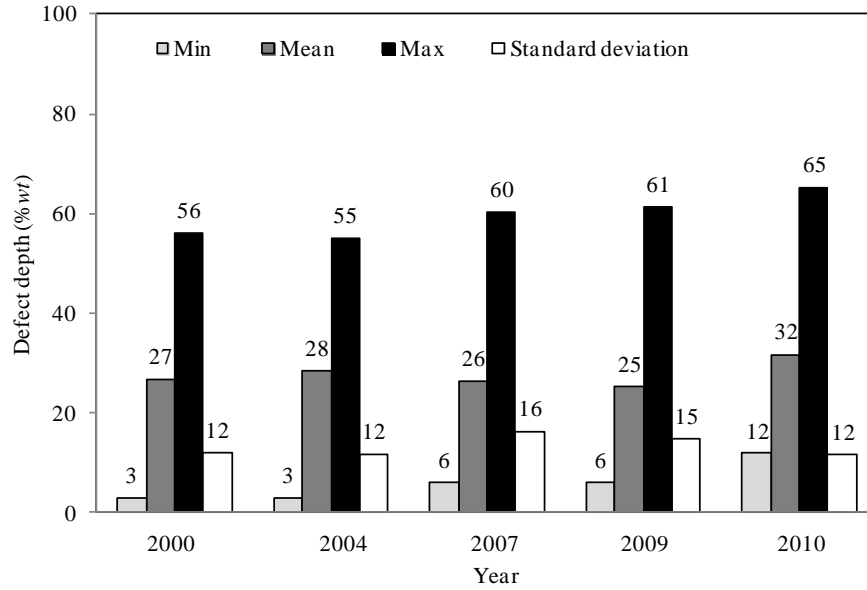
### 2.6.1 General

In this section, the growth models were developed for 62 external corrosion defects collected from a pipeline that was constructed in 1972 and is currently in service in Alberta, Canada. The 62 defects were inspected by high-resolution magnetic flux leakage

(MFL) tools in 2000, 2004, 2007 and 2009, and were excavated, field measured and recoated in 2010. The field-measured depths were assumed to be free of measurement errors (Al-Amin et al. 2012), which implies that the actual depths of the 62 defects in 2010 are known. The general information of the data sets described above is depicted in Figure 2.4, including the apparent growth paths of these defects as indicated by the ILI-reported data and field-measured depths shown in Figure 2.4(a) and the statistics (i.e. the minimum, mean and maximum values as well as the standard deviation) of the data sets shown in Figure 2.4(b). The symbol  $wt$  denotes the pipe wall thickness, and the symbol  $\%wt$  denotes the percentage of pipe wall thickness and is the unit of the defect depth reported by the MFL tools. The number at the top of each bin shown in Figure 2.4(b) denotes the value of the particular statistical property. All the 62 defects are external metal-loss corrosion defects, and therefore considered to have similar underlying corrosion mechanisms. The large scattering shown in Fig. 2.4 can be attributed to two factors: 1) the defects spread over a long section of the pipeline (approximately 82 km long) that has been in service for a long time, i.e. since 1972; therefore, the variability of the actual depths of these defects is expected to be high, and 2) the measurement uncertainties associated with the ILI tools further increase the variability of the ILI-reported depths. Furthermore, due to the measurement error associated with the ILI data, some growth paths shown in Fig. 2.4(a) decrease over time.



(a) Apparent growth paths indicated by the ILI-reported and field-measured depths



(b) Statistics of the ILI-reported and field-measured data

Figure 2.4 General information of the ILI-reported and field-measured data

The measurement errors associated with these ILI tools as well as the correlation between the random scattering errors associated with different ILI tools were quantified using a Bayesian methodology described in Al-Amin et al. (2012). The calibrated biases, the random scattering errors associated with individual ILI tools as well as the correlations between the random scattering errors of different ILI tools used in 2000, 2004, 2007 and 2009 are as follows:  $a_1 = a_2 = 2.04$  (%wt),  $a_3 = -15.28$  (%wt) and  $a_4 = -10.38$  (%wt);  $b_1 = b_2 = 0.97$ ,  $b_3 = 1.4$  and  $b_4 = 1.13$ ;  $\sigma_1 = \sigma_2 = 5.97$  (%wt),  $\sigma_3 = 9.05$  (%wt) and  $\sigma_4 = 7.62$  (%wt);  $\rho_{12} = 0.82$ ,  $\rho_{13} = \rho_{23} = 0.7$ ,  $\rho_{14} = \rho_{24} = 0.72$  and  $\rho_{34} = 0.78$  (Al-Amin et al. 2012), where the subscripts ‘1’, ‘2’, ‘3’ and ‘4’ denote the parameters associated with the ILI data obtained in 2000, 2004, 2007 and 2009, respectively. Note that the above-mentioned parameters were calibrated based on the ILI-reported depths for 128 static defects that were repaired prior to 2000 and ceased growth (Al-Amin et al. 2012). Although these static defects are different from the 62 active defects used in this study, the calibrated measurement errors are applicable because both the static and active defects are located on the same pipeline and were sized by the same ILI tools.

The three sets of ILI data obtained in 2000, 2004 and 2007 were used to carry out the Bayesian updating and evaluate the probabilistic characteristics of the parameters of the growth models for each of the 62 defects. The growth model was then validated by comparing the actual depths of the defects in 2010 with the corresponding depths predicted by the growth model. The ILI data obtained in 2009 were intentionally excluded from the analysis so that the prediction from the growth model is over a reasonably long period (i.e. 3 years). The application and validation of the NHGP- and HGP-based growth models are illustrated in the following sections.

### 2.6.2 NHGP-based Growth Model

The NHGP-based growth model was first applied to the 62 corrosion defects described in Section 2.6.1. The parameters of the hyper prior distributions, i.e. the parameters at the top level of Fig. 2.3, were specified as follows:  $p_1 = 1$ ,  $q_1 = 1$ ,  $p_2 = 1$ ,  $q_2 = 1$ ,  $p_3 = 0$ ,  $q_3 = 28$  (year),  $p_4 = 1$  and  $q_4 = 1$ . The values of  $p_1$ ,  $q_1$ ,  $p_2$ ,  $q_2$ ,  $p_4$  and  $q_4$  imply that the means and variances of  $\alpha$ ,  $\kappa$  and  $\beta_i$  are all equal to unity. It follows from Section 2.5.2 that  $q_3$  denote the time elapsed since the installation time of the pipeline (i.e. year 1972) up to the time of the first inspection (i.e. year 2000) and therefore equals 28 years. A total of 20,000 MCMC simulation sequences were generated with the first 2000 sequences considered as the burn-in period (Gelman et al. 2004) and therefore discarded. The samples in the rest of the sequences were used to evaluate the probabilistic characteristics of the parameters in the growth models.

To predict the growth of the corrosion defects, two scenarios, denoted as Scenarios I and II were considered and employ the posterior mean and median values of model parameters, respectively. A comparison between the predicted depths,  $x_p$ , in 2010 with the corresponding field-measured depths,  $x_a$ , for the 62 defects is shown in Fig. 2.5 for both scenarios. The predicted depth for a given defect shown in Fig. 2.5 is the mean depth evaluated according to the NHGP with the model parameters (i.e.  $\alpha$ ,  $\kappa$ ,  $\beta_i$  and  $t_{i0}$ ) assumed to be deterministic and set equal to the mean (median) values of the corresponding marginal posterior distributions obtained from the MCMC simulation for Scenario I (II). Figure 2.5 suggests that the predictions given by the proposed model are

reasonably good in that about 90% of the predicted depths fall within the region bounded by the two lines representing actual depth  $\pm 10\%wt$  (these two bounding lines are commonly used in the pipeline industry as a confidence interval for the accuracy of the inspection tool and are adopted in this study as a metric for the predictive accuracy of the corrosion growth model). The predicted depths show significant deviation (defined as the absolute difference between the predicted and actual depths being greater than 10 %wt) from the corresponding actual depths for only six defects, with the maximum absolute deviation being approximately 20 %wt for Scenario I and 19 %wt for Scenario II.

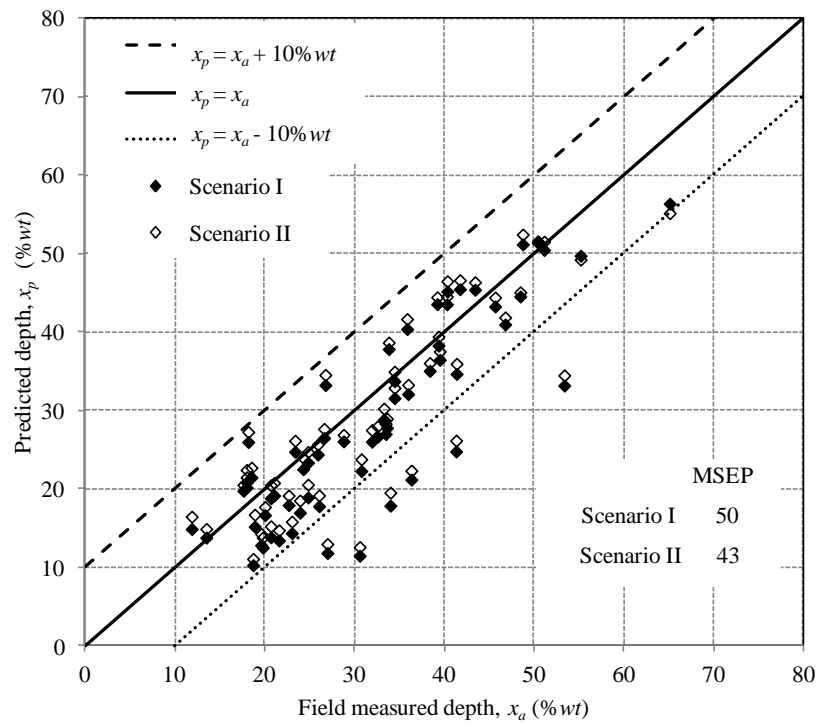


Figure 2.5 Comparison of the predicted and field-measured depths

The mean squared error of prediction (MSEP) (Harville & Jeske 1992), defined by 
$$\text{MSEP} = \frac{1}{N} \sum_{i=1}^N (x_{pi} - x_{ai})^2$$
, was employed to quantitatively evaluate the predictive accuracy of the two scenarios described above, where  $x_{pi}$  and  $x_{ai}$  denote the predicted and field-measured depths of the  $i^{\text{th}}$  defect, respectively, and  $N$  is the total number of defects employed in the model validation (i.e.  $N = 62$ ). The lower is the MSEP associated with a given model, the higher is its predictive accuracy. The MSEP values shown in Fig. 2.5



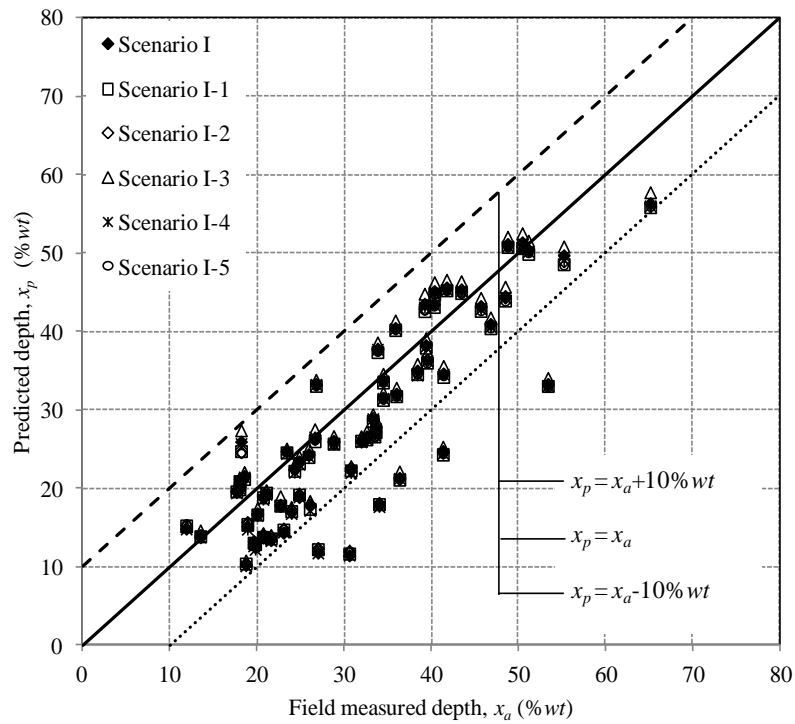
suggest that the predictive accuracy corresponding to the median values of the model parameters is somewhat higher than that corresponding to the mean values for the NHGP-based model.

Sensitivity analyses with respect to the prior distributions of  $\alpha$ ,  $\kappa$  and  $\beta_i$  were carried out and are described in the following section. A total of six sensitivity cases based on Scenarios I (II) described above were considered and are summarized in Table 2.1. Comparisons of the model-predicted and field-measured depths for the sensitivity cases are depicted in Fig. 2.6. The MSEP values corresponding to the sensitivity cases are summarized in Table 2.1. For all the sensitivity cases, the predictive accuracy corresponding to the median values of the model parameters is higher than that corresponding to the mean values. Table 2.1 and Fig. 2.6 further indicate that the impact of prior distributions of  $\alpha$  and  $\kappa$  on the predictive accuracy of the growth model is small as long as the prior distribution of  $\beta_i$  is selected as a gamma distribution with a mean of unity and a coefficient of variation (COV) of 100% (i.e.  $p_4 = q_4 = 1$ ). Further investigation indicated that the growth model is highly sensitive to the prior distribution of  $\beta_i$  regardless of the prior distributions of  $\alpha$  and  $\kappa$ ; convergence of the Markov chains of  $\alpha$  and  $\kappa$  in the MCMC simulation could not be achieved if the parameters (i.e.  $p_4$  and  $q_4$ ) of the prior distributions of  $\beta_i$  were not set to unity. Of the six scenarios shown in Table 2.1, Scenario II-3 has the highest predictive accuracy as the corresponding MSEP value is 41, which is the smallest among the MSEP values associated with the 6 scenarios considered. Given the prior distributions of  $\alpha$  and  $\beta_i$ , the prior mean, standard deviation and COV of the growth of the depth over the first year since  $t_{i0}$  are approximately equal to  $E[\alpha]/E[\beta_i]$ ,  $E[\alpha^{0.5}]/E[\beta_i]$ , and  $E[\alpha^{-0.5}]$ , respectively. The prior distributions of  $\alpha$  and  $\beta_i$  summarized in Table 2.1 implies that  $E[\alpha]/E[\beta_i]$  ranges from 1 to 10 %wt,  $E[\alpha^{0.5}]/E[\beta_i]$  ranges from 1 to 3.2 %wt, and  $E[\alpha^{-0.5}]$  ranges from 32% to 100%. Those values suggest that each set of prior distributions of  $\alpha$  and  $\beta_i$  summarized in Table 2.1 is informative. From this perspective, the predictions are influenced by both the prior distributions of  $\alpha$  and  $\beta_i$  and the information represented by the ILI data, and therefore have no marked difference as indicated by the MSEP values given in Table 2.1. Furthermore, results shown in Table 2.1 suggest that  $\kappa$  can be assigned a non-informative prior distribution

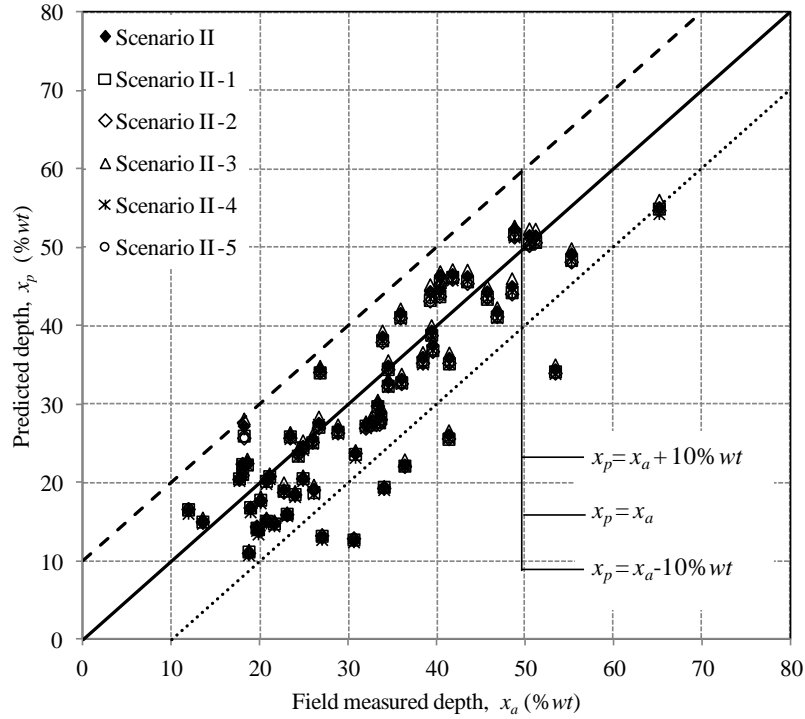
and inferred from the information implied in the ILI data, which is not unexpected because  $\kappa$  characterizes the trend of the mean growth path.

Table 2.1 Summary of sensitivity scenarios for the NHGP-based model

Scenario	$\alpha$		$\kappa$		$\beta_i$		Model parameter	MSEP	Percentage (%)
	$p_1$	$q_1$	$p_2$	$q_2$	$p_4$	$q_4$			
I (II)	1	1	1	1	1	1	Mean (median)	50 (43)	90 (90)
I (II)-1	10	1						50 (43)	
I (II)-2	0.001	0.001	48 (43)						
I (II)-3	1	1	10	1				46 (41)	
I (II)-4			0.001	0.001				51(45)	
I (II)-5	0.001	0.001	0.001	0.001	49(43)				



(a)



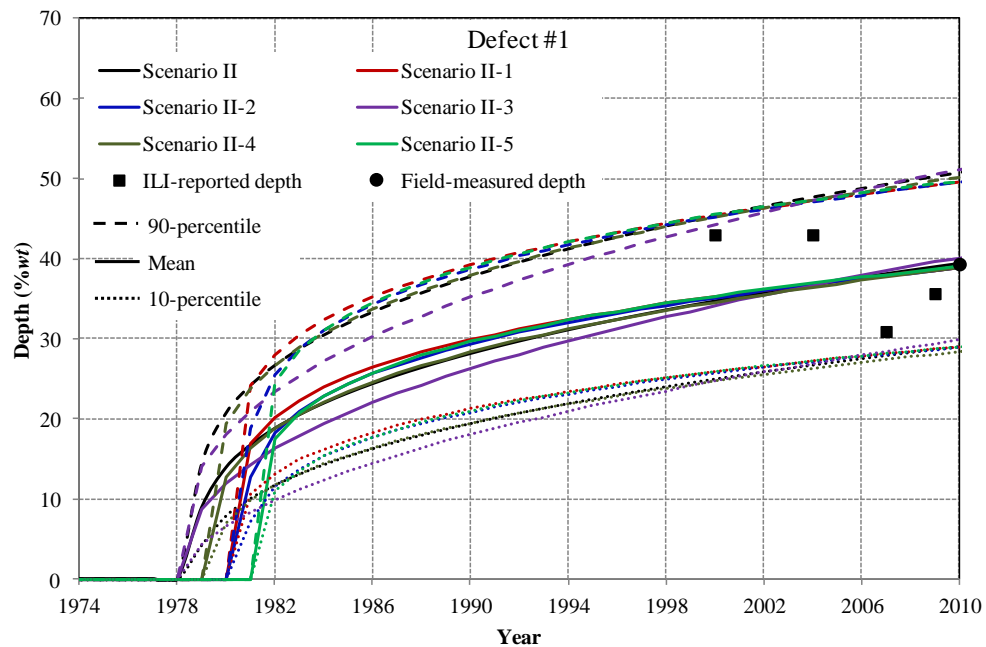
(b)

Figure 2.6 Comparison of the predicted and field-measured depths for different scenarios

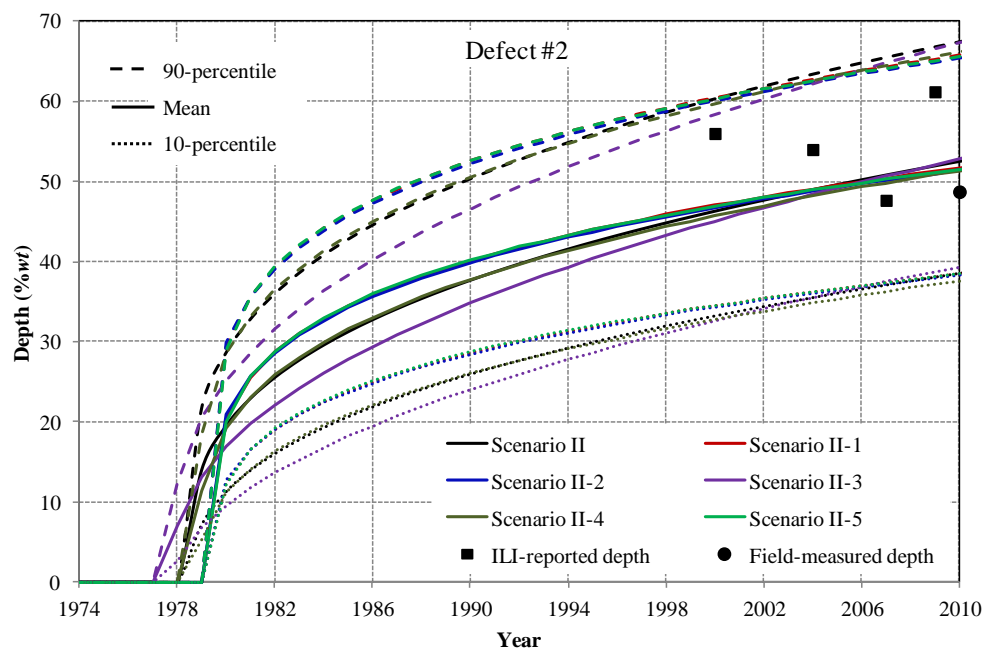
Figures 2.7(a) through 2.7(j) depict the mean, 10- and 90-percentile values, for ten selected defects, Defects #1, #2, #3, #7, #12, #13, #14, #15, #22 and #60, respectively. For a given defect, the mean,  $\mu_i(t)$ , and standard deviation,  $\sigma_i(t)$ , of the defect depth at time  $t$  were calculated using Eqs. (2.2a) and (2.2b), i.e.  $\mu_i(t) = \alpha(t-t_{i0})^\kappa/\beta_i$  and  $\sigma_i(t) = (\alpha(t-t_{i0})^\kappa/\beta_i^2)^{0.5}$ , where  $\alpha$ ,  $\kappa$ ,  $t_{i0}$  and  $\beta_i$  were treated as deterministic quantities and set equal to their corresponding mean (or median) values of the marginal posterior distributions evaluated from the MCMC simulation. The 10- and 90-percentile values of the predicted depth at time  $t$  were quantified according to the fact that the depth follows a gamma distribution with a shape parameter of  $\alpha(t-t_{i0})^\kappa$ , a rate parameter of  $\beta_i$  and a cumulative distribution function (CDF) given by  $F(X(t) \leq x(t)) = \gamma(\alpha(t-t_{i0})^\kappa, \beta_i x(t))/\Gamma(\alpha(t-t_{i0})^\kappa)$ , where  $\gamma(w, z)$  is the so-called incomplete gamma function and given as  $\gamma(w, z) = \int_0^z v^{w-1} e^{-v} dv$  (Ang and Tang 1975). For comparison, the ILI-reported depth in 2000, 2004, 2007 and 2009 are shown in the same figure as well. Figure 2.7 indicates that the predictions

obtained from the model for Defects #1, #2, #3, #13, #14, #15 and #60 are reasonably good, but the predicted depths for Defects #7, #12 and #22 are markedly lower than the actual depths for all scenarios considered, for example, about 15, 18 and 18 %wt lower than the actual depths for Scenario II-3. The poor prediction can be partially attributed to the relatively large measurement errors that are involved in the ILI data for the three defects. This is also reflected in Figs. 2.7(c), 2.7(e) and 2.7(i), which show that the defect depths reported by the three ILI tools in 2000, 2004 and 2007 are similar but much lower than the actual depth in 2010.

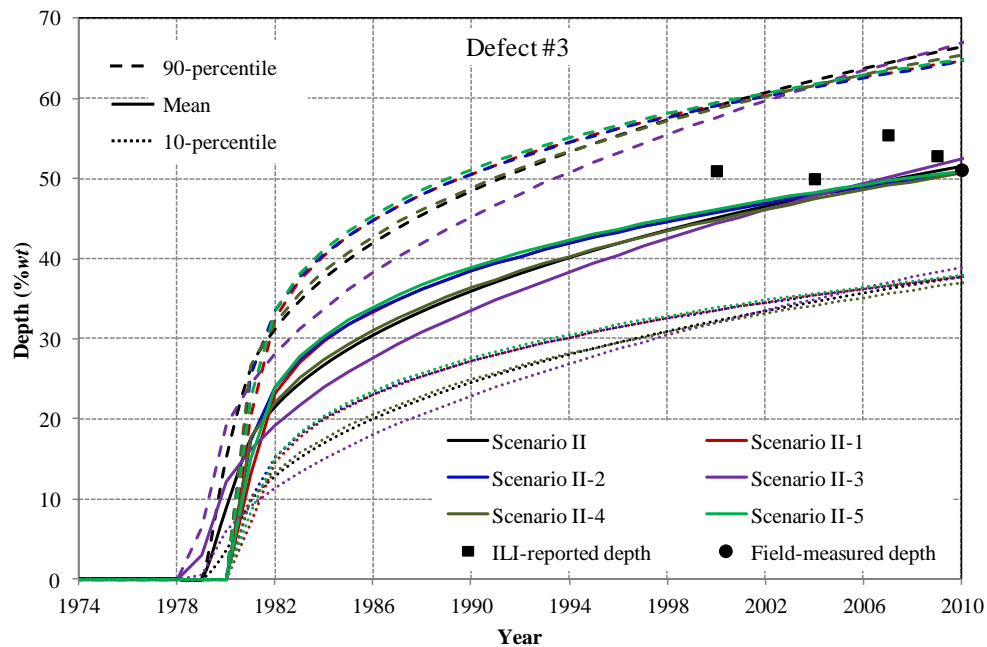
Note that the initiation time in the growth model plays an important role in characterizing the growth of defect. If the ILI data for a particular defect indicate a fast growing trend for the defect, it is likely to be identified by the Bayesian inference as a relatively new defect with a large initiation time. This observation is consistent with the experimental results reported in the literature (Provan and Rodriguez 1989; Aziz 1956) indicating that metal-loss corrosion tends to have a higher growth rate at the early stage of the corrosion process. In the present study, for example, the ILI data for Defect #60 suggest a higher growth rate than those for Defects #1 and #2; therefore, the mean of the initiation time obtained from MCMC simulation for Defect #60 is 15 years larger than that for Defect #1 and 16 years larger than that for Defect #2 for Scenario II-3.



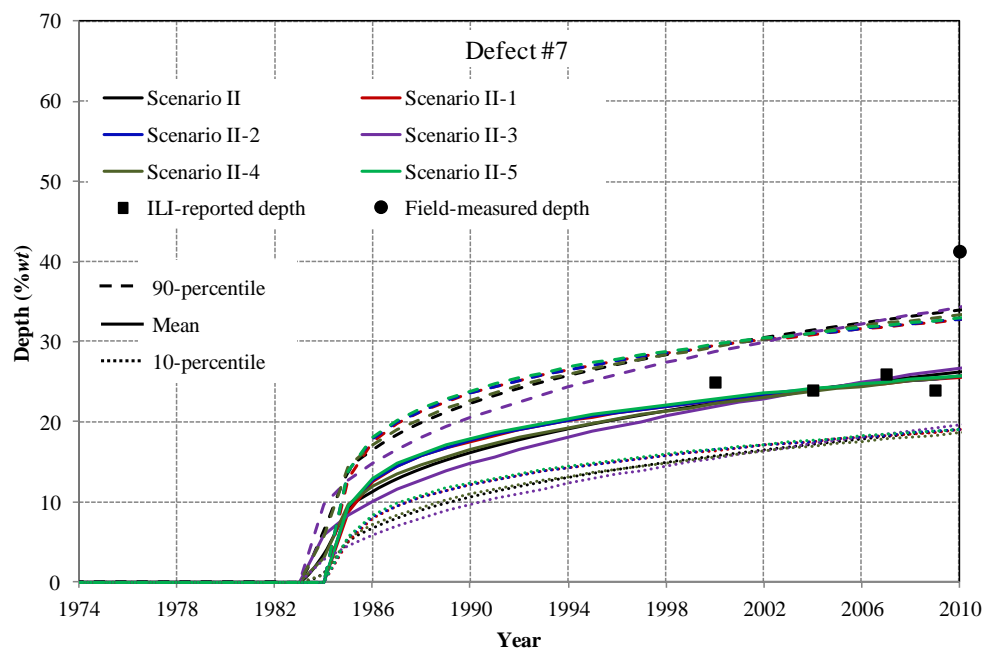
(a)



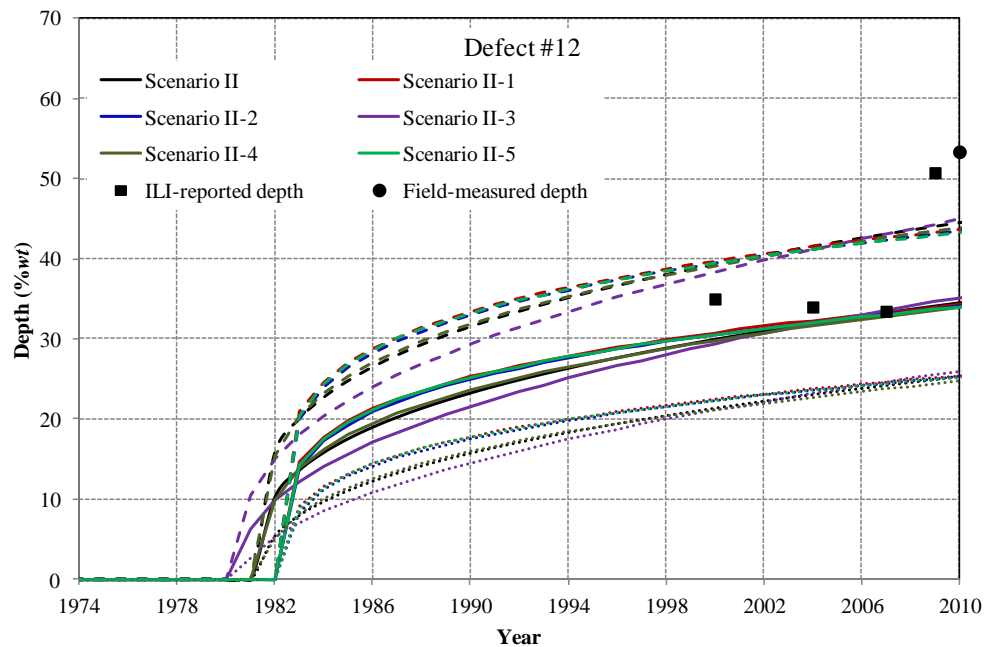
(b)



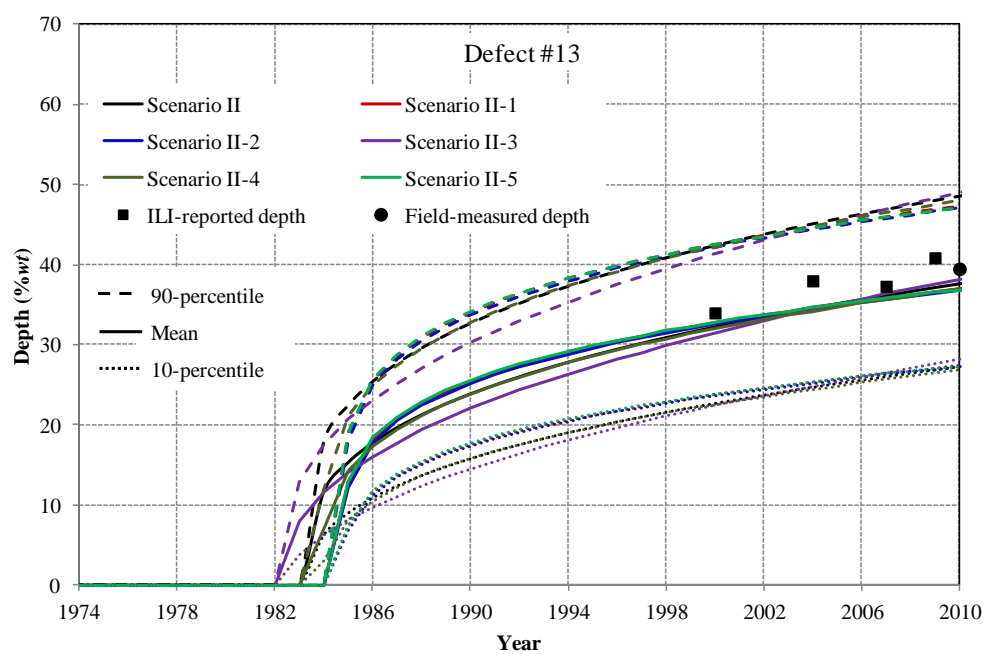
(c)



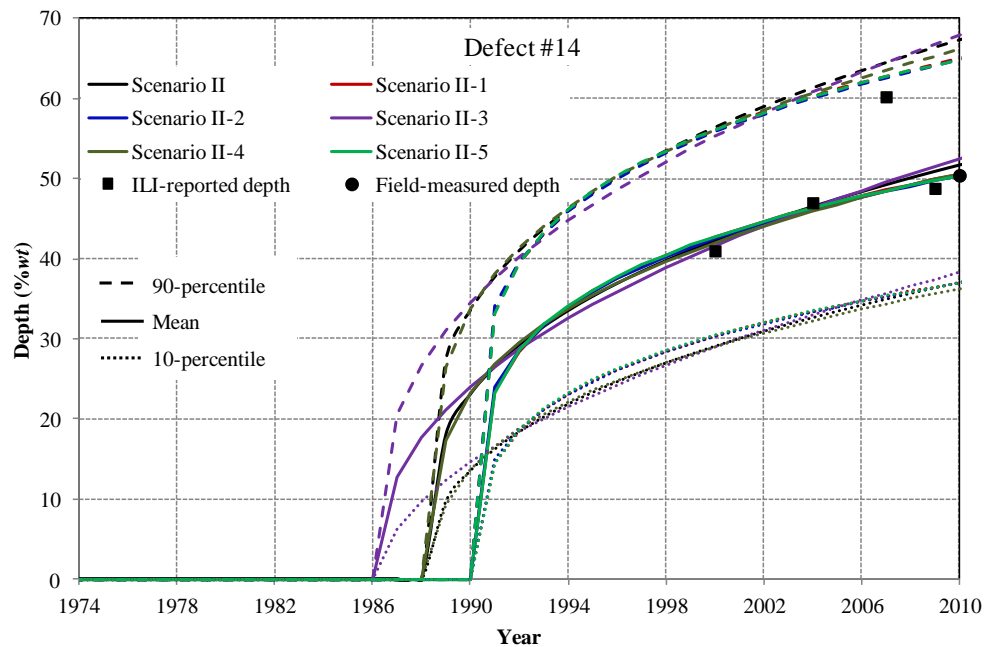
(d)



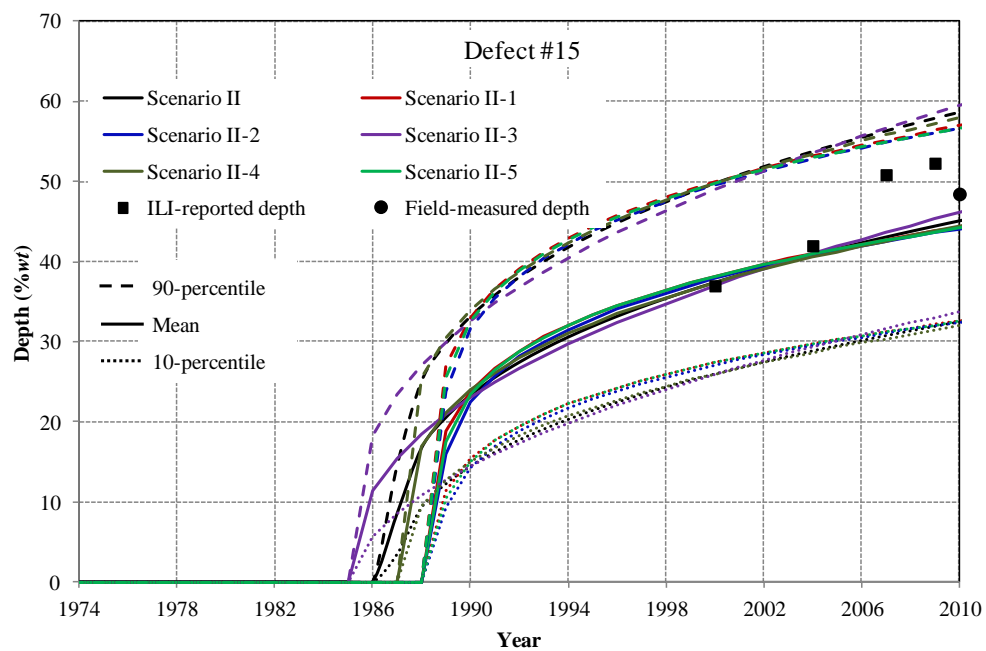
(e)



(f)

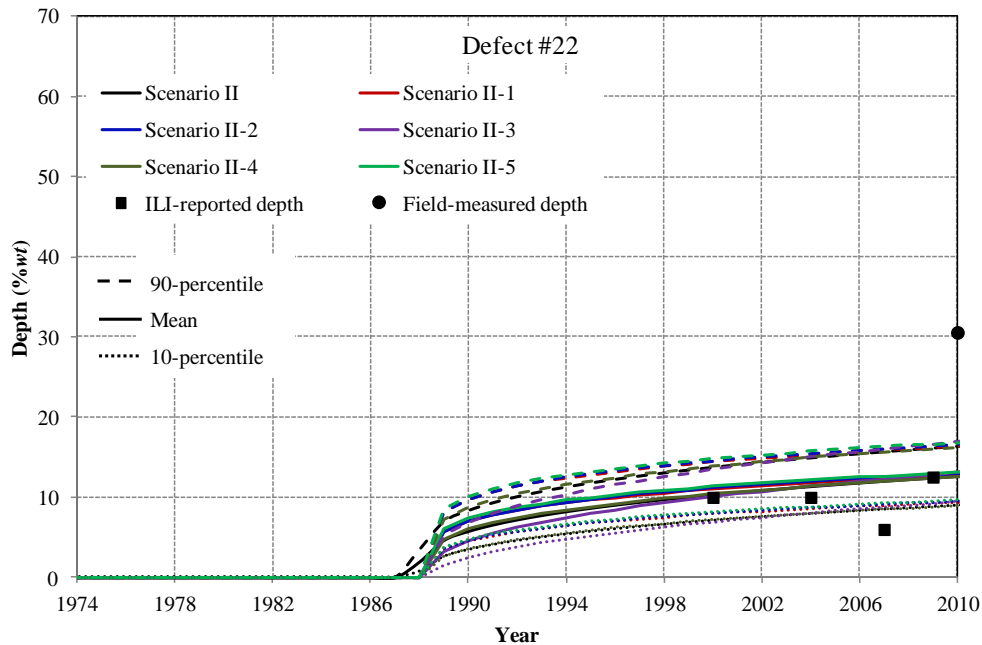


(g)

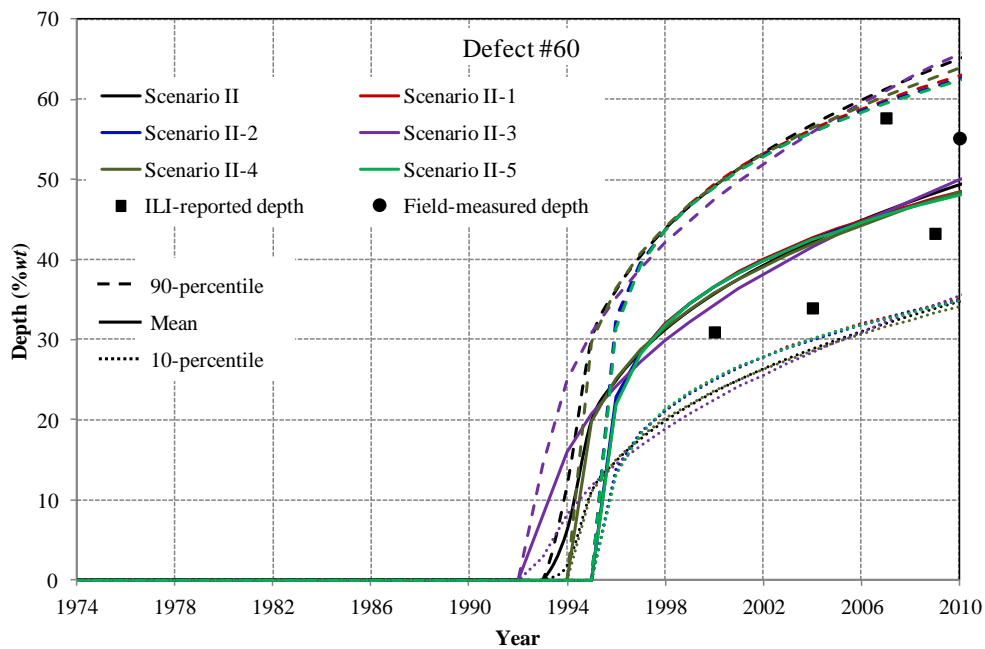


(h)





(i)



(j)

Figure 2.7 Predicted growth paths of ten defects using NHGP-based models

Furthermore, Figure 2.7 also indicates that the prior distributions of  $\alpha$ ,  $\kappa$  and  $\beta_i$  have a marked impact on the predicted growth paths, including the mean, 10- and 90- percentile values, at the early stage of forecasting period, especially in the first unit time interval since defect initiation; however, this impact becomes small and even negligible as time increases up to the time of field measurement.

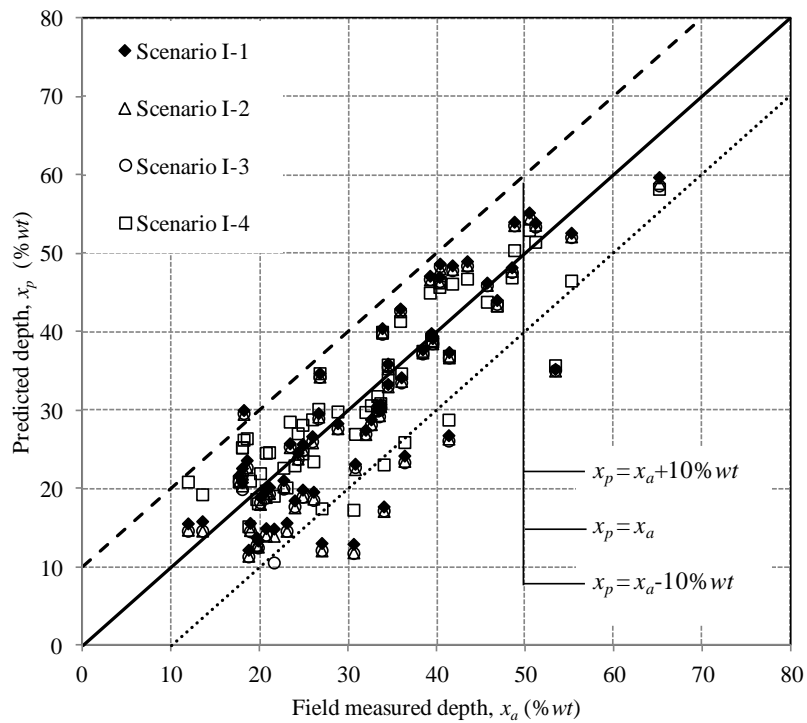
### 2.6.3 HGP-based Corrosion Growth Model

In this section, the HGP-based model (i.e.  $\kappa = 1$ ) was applied to the same set of defects considered in Section 2.6.2. For this model, four cases were considered with respect to the prior distributions of  $\alpha$ ,  $\beta_i$  and  $t_{i0}$ , which are summarized in Table 2.2. Similar to the NHGP-based model presented in Section 2.6.2, the four cases allow investigation of the impact of both the posterior values (i.e. mean or median) and prior distributions of model parameters on the predictive accuracy of the HGP-based growth models. The joint posterior distribution of the model parameters involved in the HGP-based growth model was evaluated using the same number of MCMC simulation sequences (i.e. 18,000) as described in Section 2.6.2.

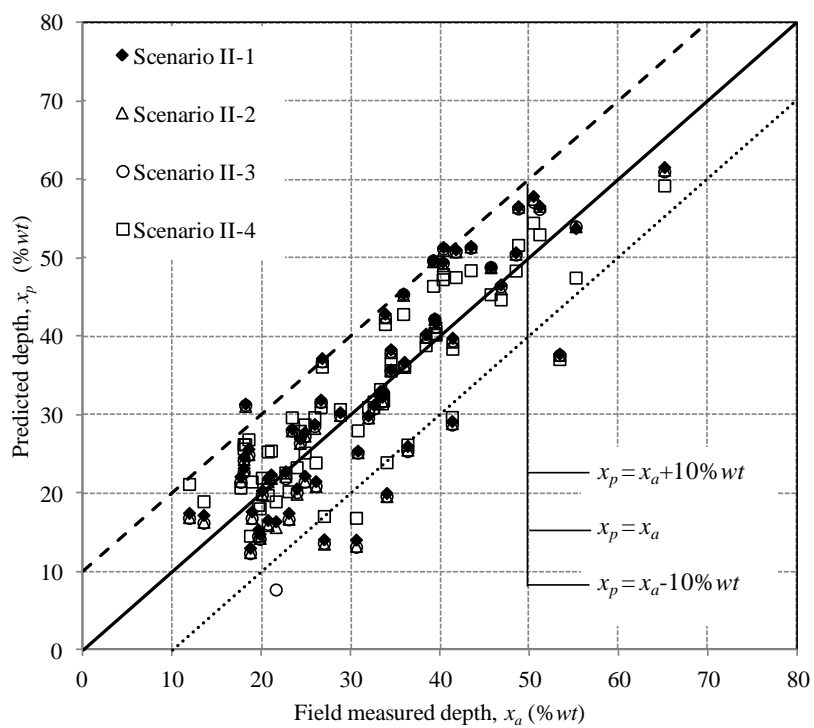
Table 2.2 Summary of sensitivity scenarios for the HGP-based model

Scenario	$\alpha$		$\beta_i$		Model parameter	MSEP ((% wt) <sup>2</sup> )	Percentage (%)
	$p_1$	$q_1$	$p_4$	$q_4$			
I (II)-1	10	1	1	1	Mean (median)	44 (45)	89 (87)
I (II)-2	1	1				47 (45)	89 (87)
I (II)-3	0.001	0.001				48 (46)	89 (85)
I (II)-4	10	1				31 (33)	94 (95)

Figure 2.8 depicts the comparison of the predicted and field-measured depths for the 62 defects corresponding to the cases summarized in Table 2.2. The predicted depths shown in Figs. 2.8(a) and 2.8(b) were obtained in the same manner as those shown in Figure 2.6(a) and 2.6(b), respectively. The observations obtained from Fig. 2.6 are equivalently applicable to Fig. 2.8.



(a)

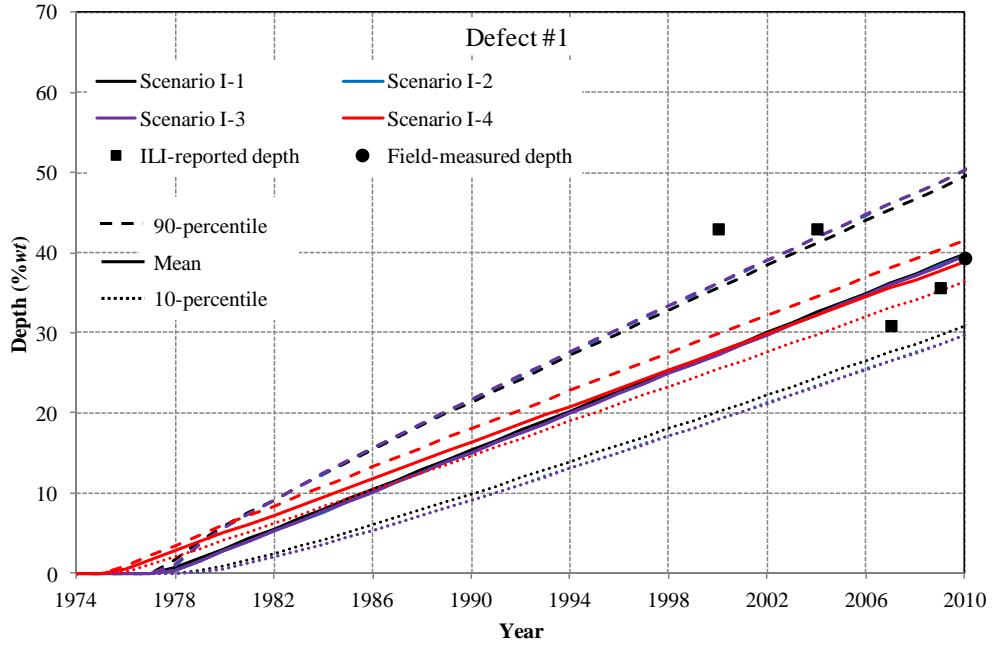


(b)

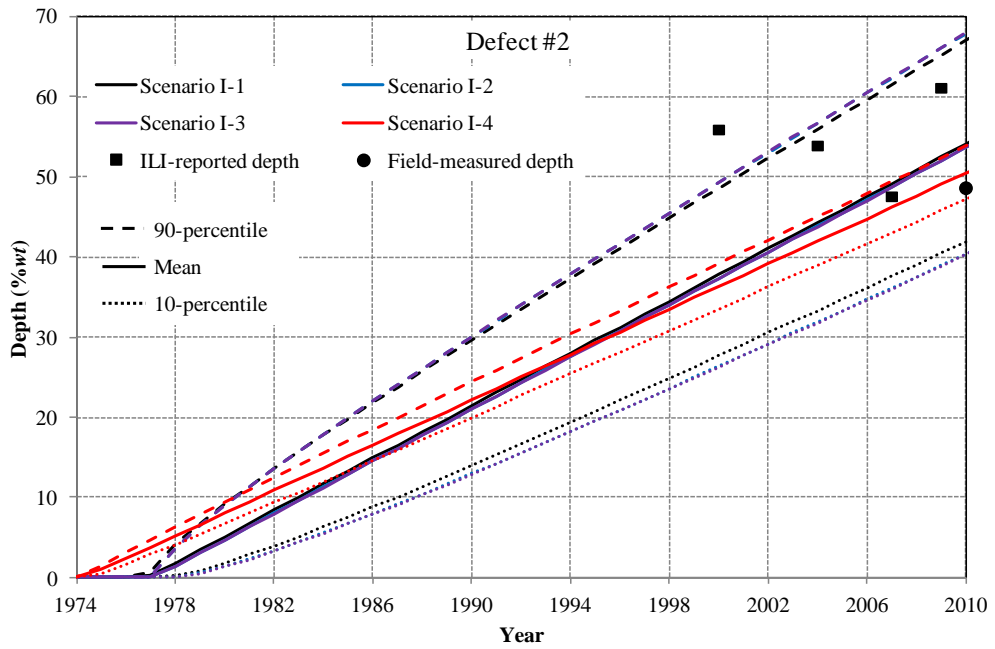
Figure 2.8 Comparison of the predicted and field-measured depths for different scenarios

The MSEP values shown in Table 2.2 suggest that the predictive accuracies of the HGP-based models corresponding to the posterior mean values of the model parameters in general are higher than those corresponding to the posterior median values, which is contrary to the predictive accuracies associated with the NHGP-based models. Furthermore, the MSEP values indicate that the mean of prediction at year 2010 is slightly sensitive to the prior distribution of  $\beta_i$ , but not sensitive to the prior distribution of  $\alpha$ . The impact of the prior distributions of  $\alpha$  and  $\beta_i$  on the predicted growth paths is shown in Figure 2.9.

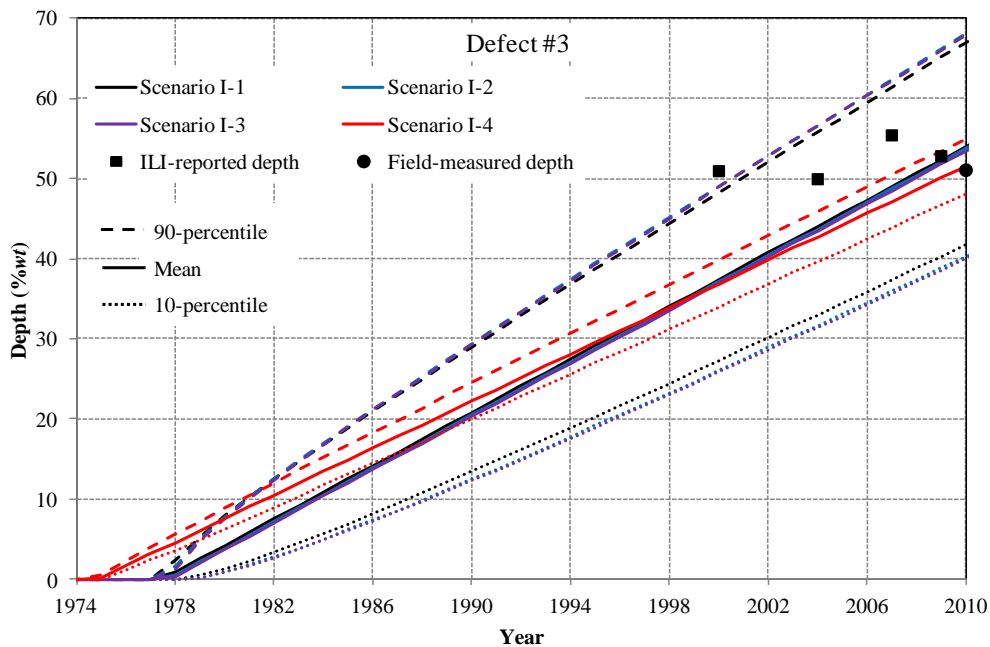
Figure 2.9 shows the mean, 10- and 90-percentile values of the predicted growth paths based on the HGP-based models for the same defects as shown in Fig. 2.7. In Fig. 2.9, the mean and standard deviation of the defect depth for a given defect  $i$  at time  $t$  equal  $\alpha(t-t_0)/\beta_i$  and  $(\alpha(t-t_0)/\beta_i^2)^{0.5}$ , respectively. Figure 2.9 indicates that the percentile values of predicted growth paths are markedly sensitive to the prior distribution of  $\beta_i$ , whereas the mean growth paths are slightly sensitive to the prior distributions of  $\beta_i$ . The predicted growth paths are insensitive to the prior distribution of  $\alpha$ . Furthermore, it can be observed that the mean growth rate differs from defect to defect, which is expected in that  $t_0$  and  $\beta$  were assumed to be defect-specific. For example, among the ten defects corresponding to Scenario I-1 shown in Fig. 2.9, Defect #60 has the highest growth rate equal to 2.2 %wt/year, followed by Defects #14, #3, #2, #15, #13, #1, #12, #7 and #22 in a descending order, which equal to 1.9, 1.7, 1.6, 1.6, 1.3, 1.2, 1.1, 0.9 and 0.6 %wt/year, respectively. The comparison of the HGP- and NHGP-based models is described in detail in the next section.



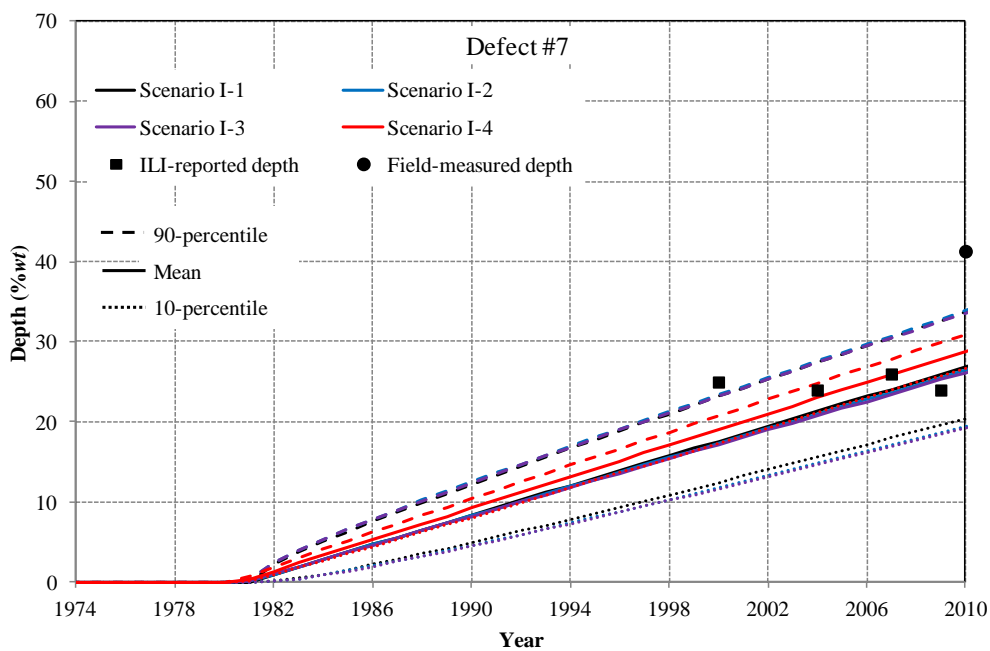
(a)



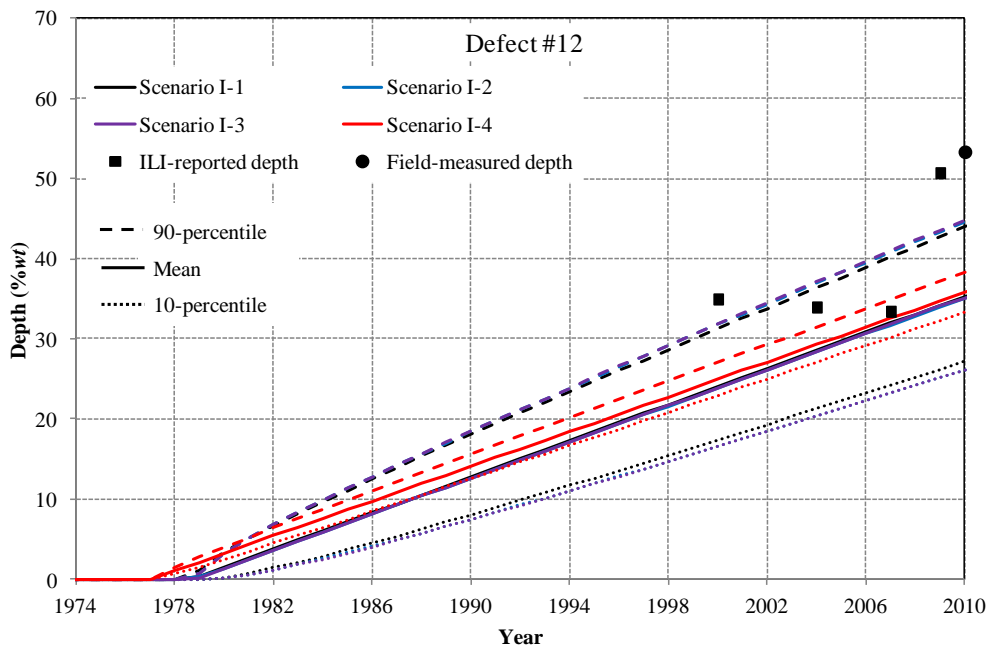
(b)



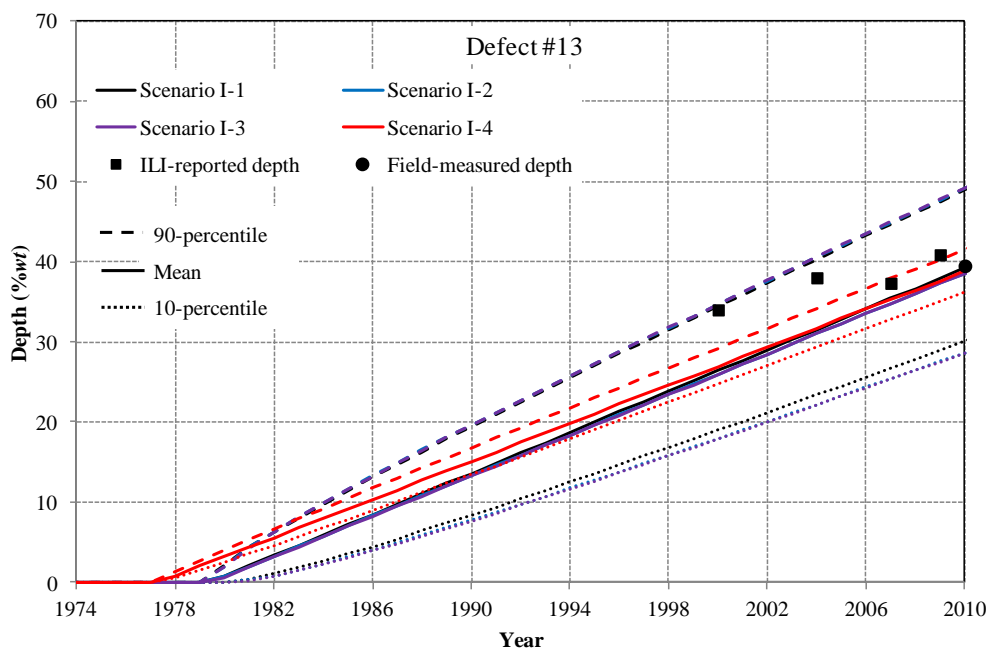
(c)



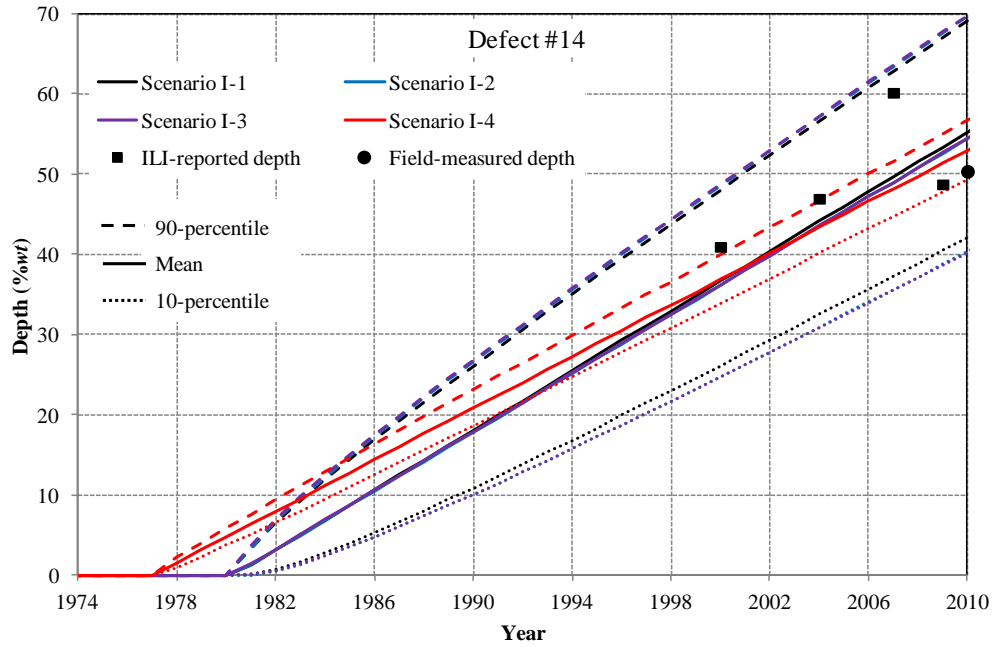
(d)



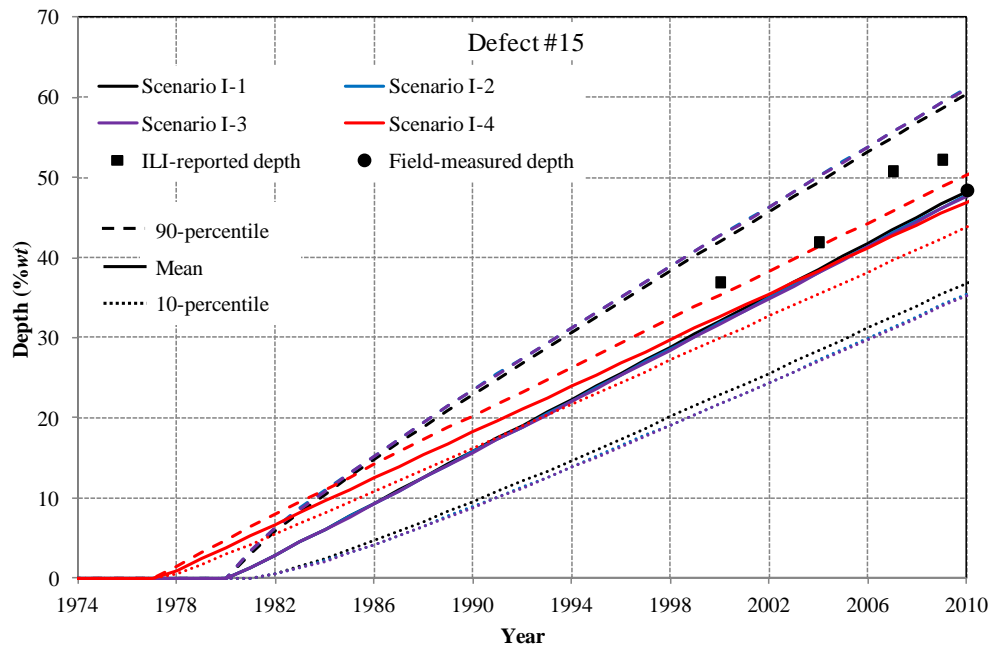
(e)



(f)

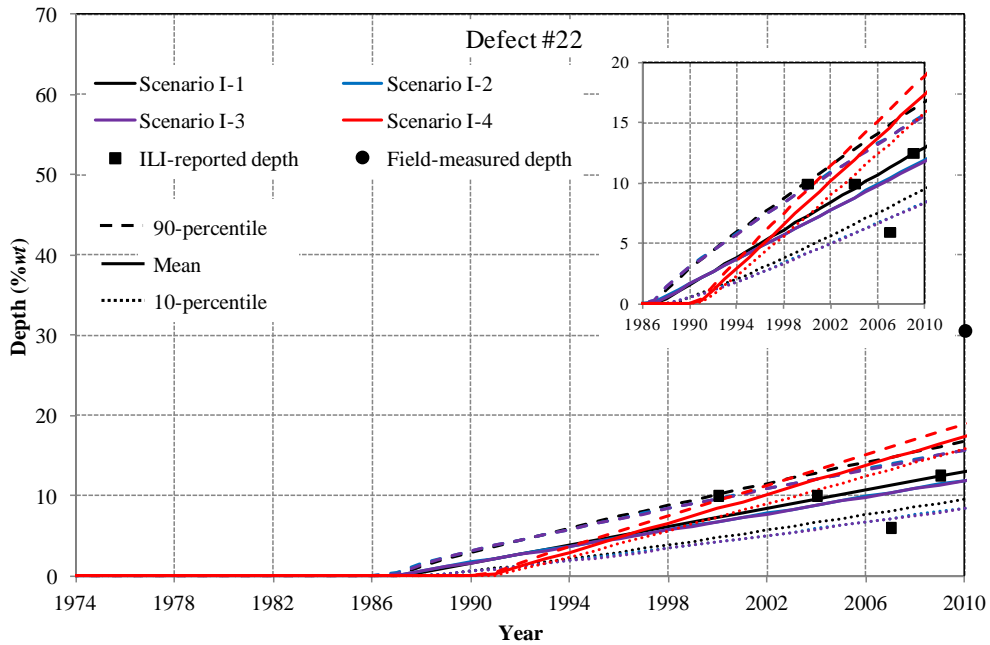


(g)

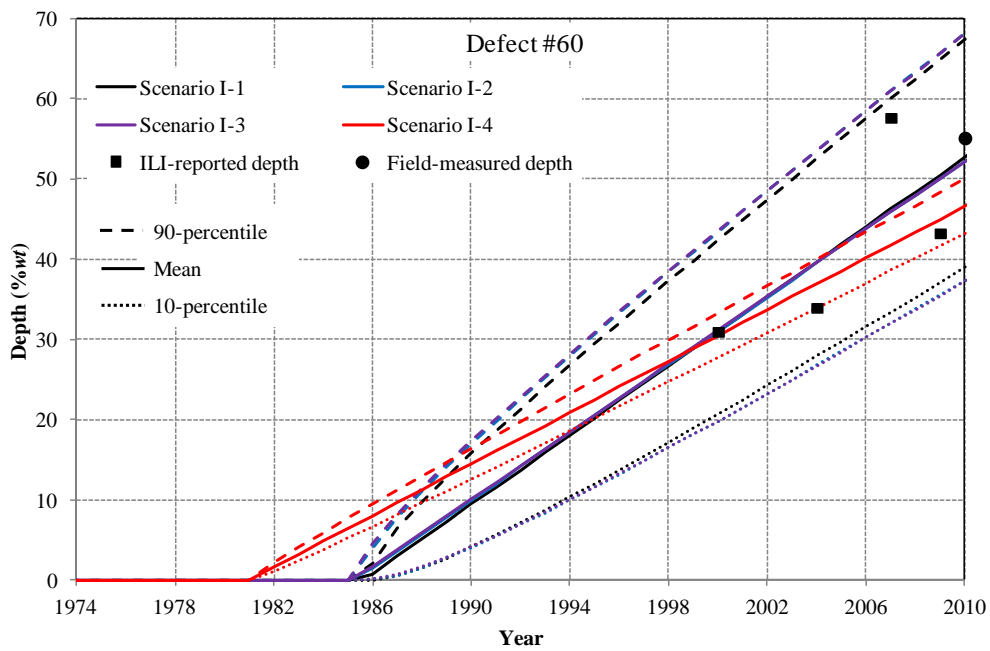


(h)





(i)



(j)

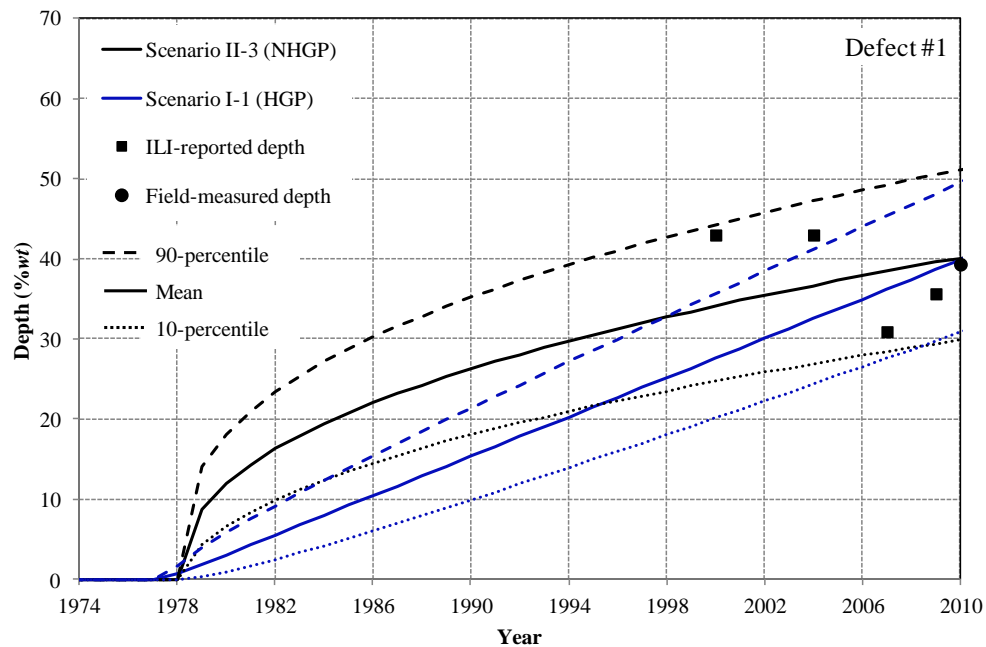
Figure 2.9 Predicted growth paths of ten defects using HGP-based model

Note that the 80% confidence interval of the prediction (i.e. the difference between the 10- and 90-percentile values) corresponding to Scenario I-4 is markedly narrower than those corresponding to Scenarios I-1 through I-3 for all defects shown in Figure 2.9. This observation is mainly because the prior distribution of  $\beta_i$  in Scenarios I-1 through I-3 has a smaller mean (i.e. unity) compared with that in Scenario I-4 (i.e. ten) and leads to a smaller posterior mean of  $\beta_i$ . It follows that smaller values of  $\beta_i$  result in larger standard deviations and 80% confidence intervals of the (gamma distributed) defect depth at a given time. On the other hand, the prior distributions of  $\alpha$  and  $\beta_i$  corresponding to the first three Scenarios in Table 2.2 suggest that  $E[\alpha]/E[\beta_i]$  and  $E[\alpha^{0.5}]/E[\beta_i]$  (i.e. the approximate prior mean and standard deviation of the growth rate, respectively) range from 1 to 10 %wt and from 1 to 10 %wt, respectively, which are similar to those corresponding to the scenarios summarized in Table 2.1. In contrast, the prior distributions of  $\alpha$  and  $\beta_i$  specified in Scenario I-4 indicate that  $E[\alpha]/E[\beta_i]$  and  $E[\alpha^{0.5}]/E[\beta_i]$  equal 1 %wt and 0.32 %wt, respectively, the latter of which is somewhat unrealistic. From this standpoint, it is remarked that the prior distribution of  $\beta_i$  specified in Scenario I-4 is too restrictive; in other words, the predicted growth is significantly influenced by the prior distribution of  $\beta_i$ . Based on the above observation, such overly-restrictive prior distribution of  $\beta_i$  (e.g. the prior distribution in Scenario I-4) is not suggested in the analysis although the mean prediction is the best, as indicated by the MSE values in Table 2.2.

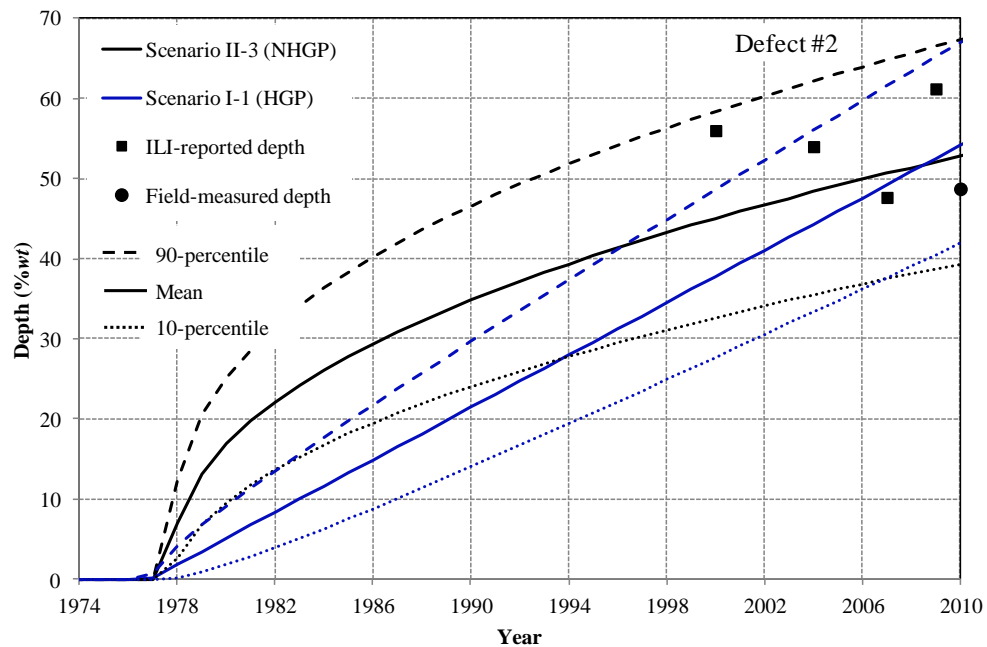
#### 2.6.4 Comparison of the NHGP- and HGP-based Corrosion Growth Models

The NHGP- and HGP-based models were compared in this section in terms of the predicted growth path and the probability density function (PDF) of the defect depth. The predicted growth paths of the ten defects show in Sections 2.6.2 and 2.6.3 based on the NHGP- and HGP-based models are shown in Figure 2.10, where Scenario II-3 (i.e.  $p_1 = 1$ ,  $q_1 = 1$ ;  $p_2 = 10$ ,  $q_2 = 1$ ;  $p_4 = 1$  and  $q_4 = 1$ ) is considered for the NHGP-based models and Scenarios I-1 (i.e.  $p_1 = 10$ ,  $q_1 = 1$ ;  $p_4 = 1$  and  $q_4 = 1$ ) are considered for the HGP-based models. Figure 2.10 suggests that for a given defect the initiation times associated with the HGP- and NHGP-based models are marginally different. The initiation times

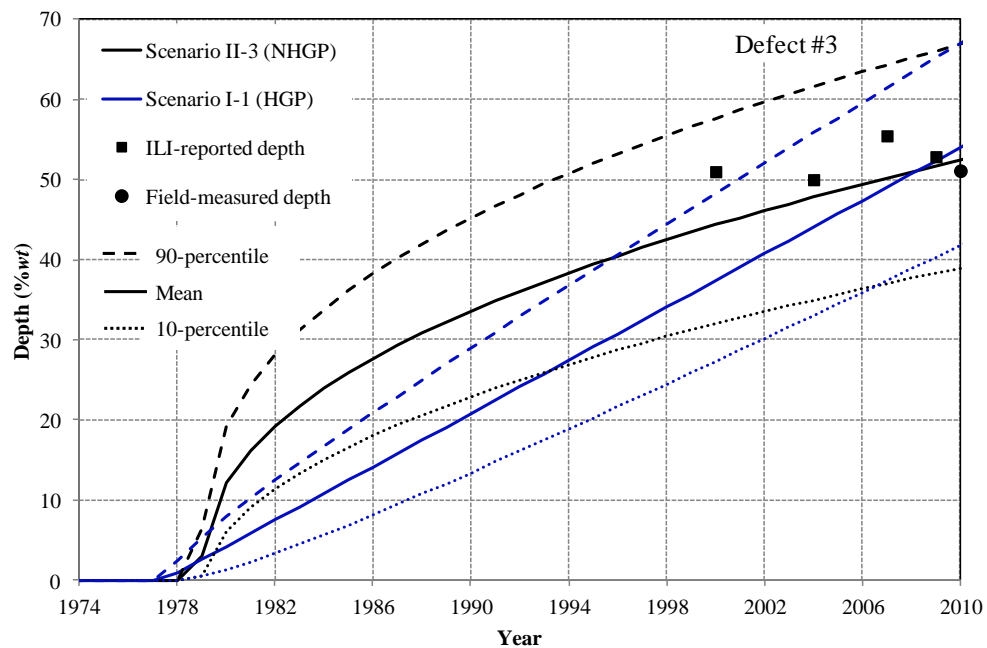
associated with the NHGP-based model, in general, are about 2-5 years larger than those associated with the HGP-based model for the ten defects plotted. The overall predicted growth paths between the times of defect initiation and excavation obtained from the HGP-based model markedly differ from those obtained from the NHGP-based model. This is expected in that the shape parameter was assumed a linear function of time in the former, and a power-law function of time in the latter.



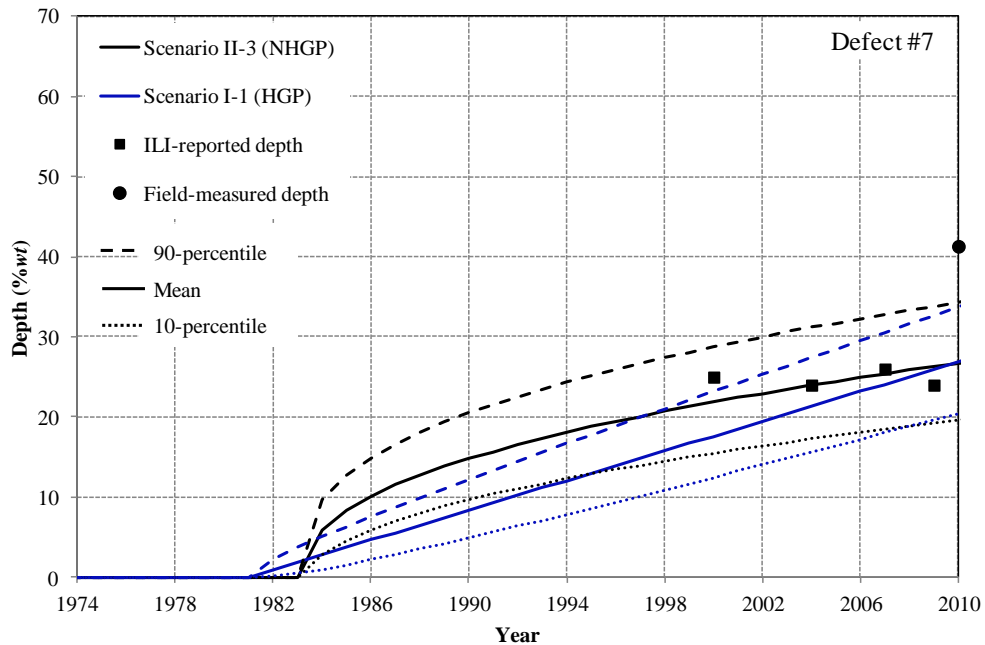
(a)



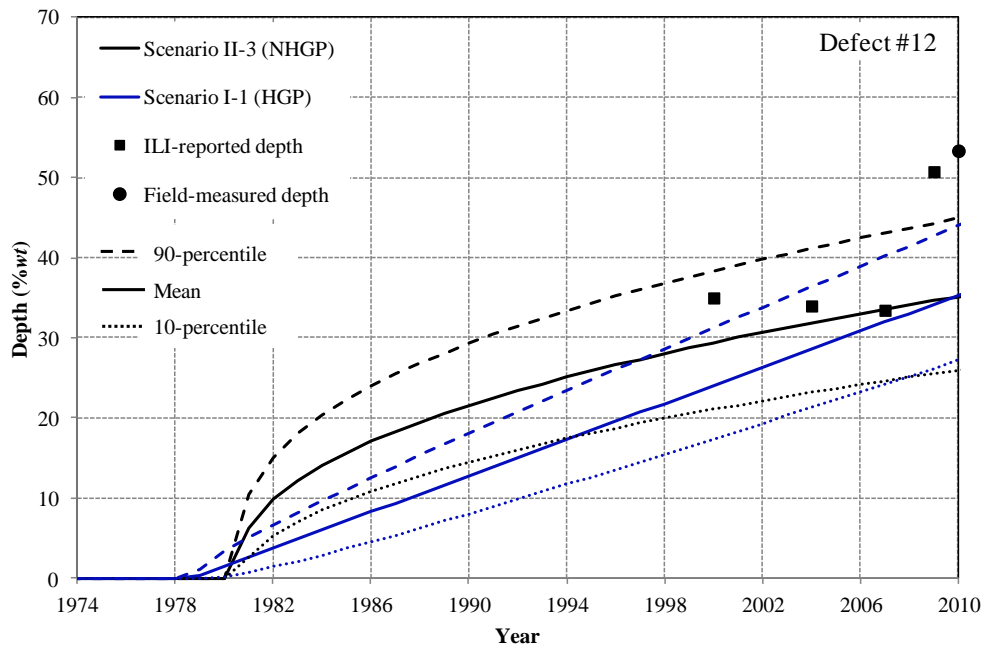
(b)



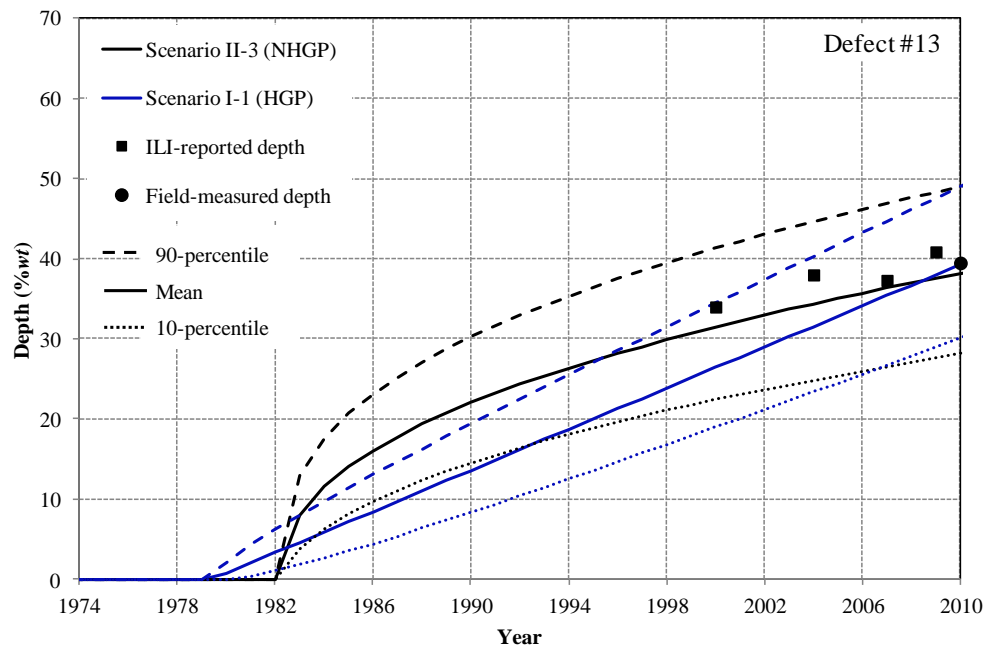
(c)



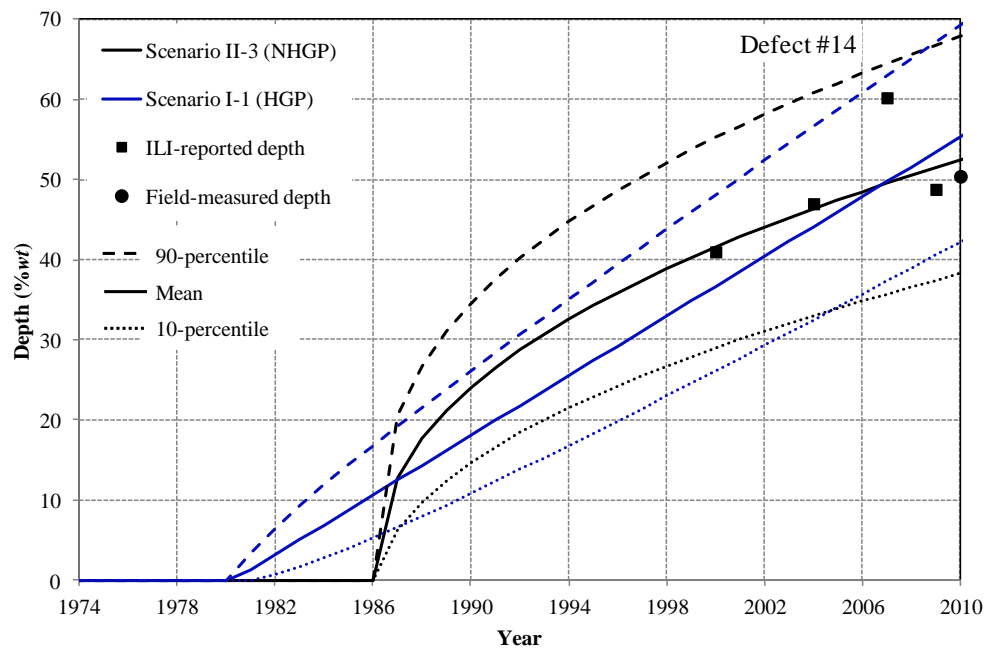
(d)



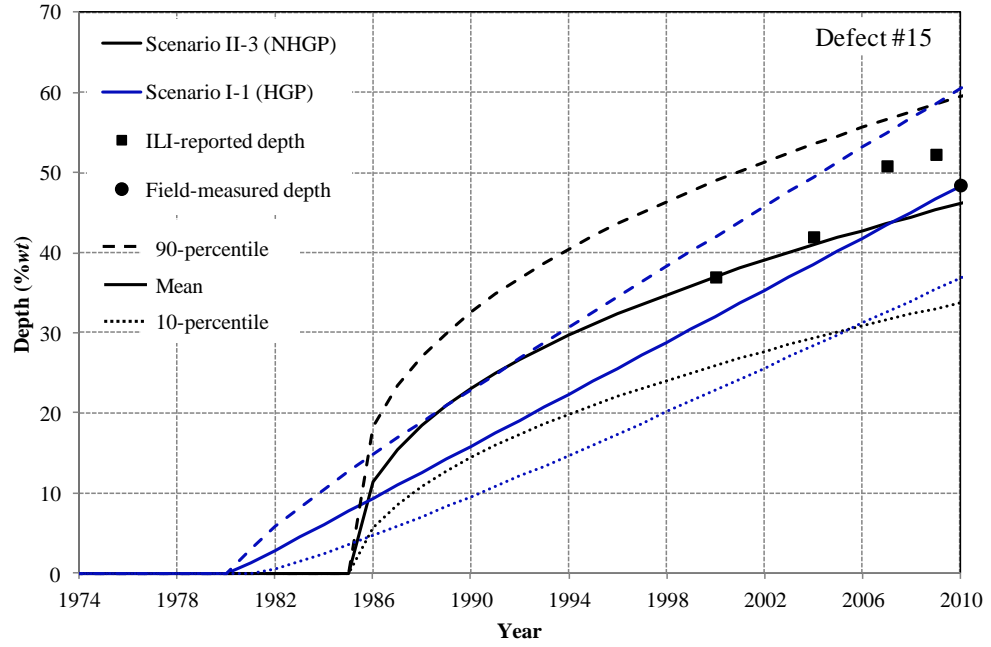
(e)



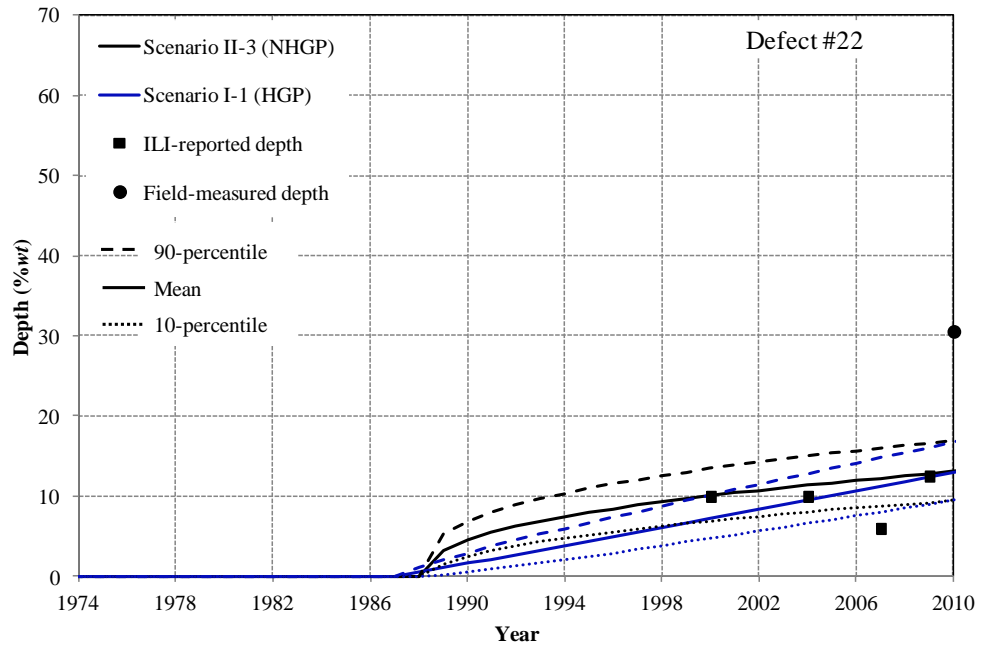
(f)



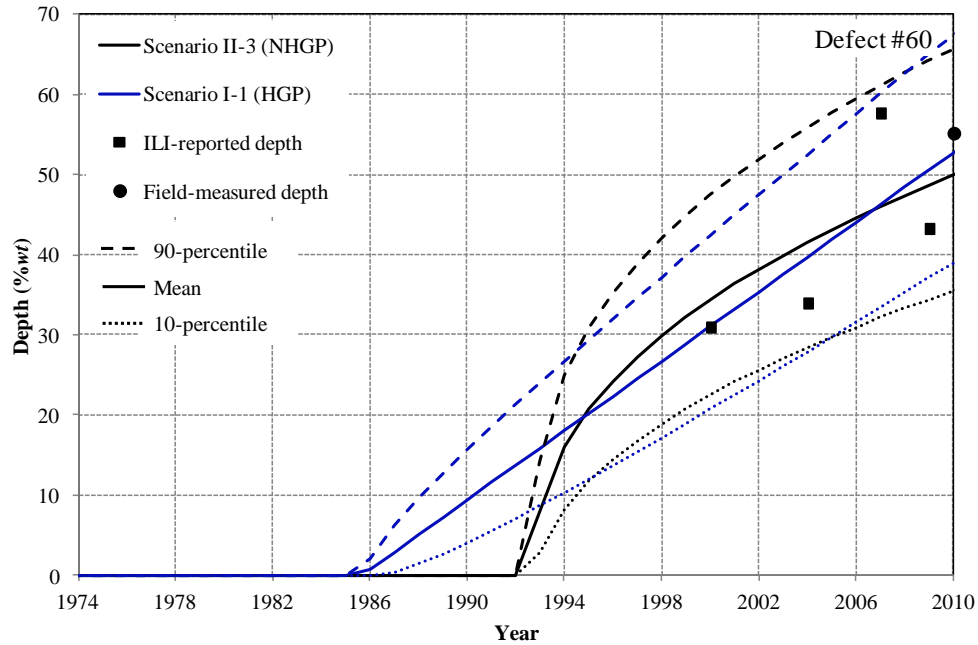
(g)



(h)



(i)



(j)

Figure 2.10 Comparison of the growth paths of a given defect corresponding to NHGP- and HGP-based models

To compare the PDF curves of defect depth obtained from the NHGP- and HGP-based growth models, the two scenarios considered in Fig. 2.10 were considered in this section. A comparison of the time-dependent PDF curves of defect depths of an arbitrarily selected defect, i.e. Defect #3, associated with the two scenarios is depicted in Fig. 2.11, where ten PDF curves corresponding to a ten-year forecasting period from 2000 to 2009 are included. Furthermore, the defect-specific PDF curves of Defect #1 through #10 at an arbitrarily selected time, i.e. year 2009, are depicted in Fig. 2.12. Figure 2.11 indicates that the mean and standard deviation of defect depth are increasing as time increases, which is expected because both of them are increasing function of time as reflected by Eqs. (2.2a) and (2.2b). The means of the predicted depths from the NHGP-based models are in general larger than those obtained from the HGP-based models over the ten-year forecasting period. As time increases, the difference between the means of predicted depth associated with the two growth models becomes small and even can be negligible at year 2009.



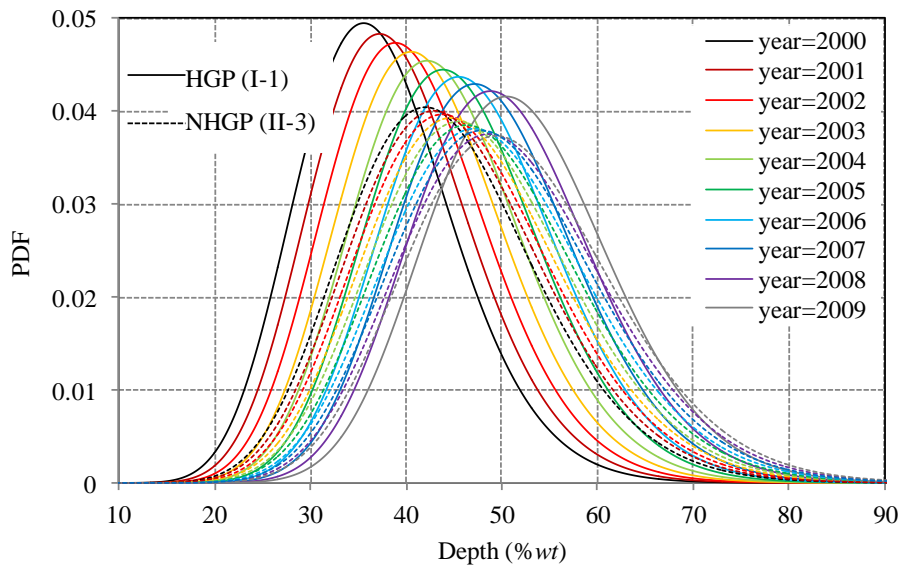


Figure 2.11 Time-dependent PDF curves of defect depth of Defect #3 at years 2000-2009

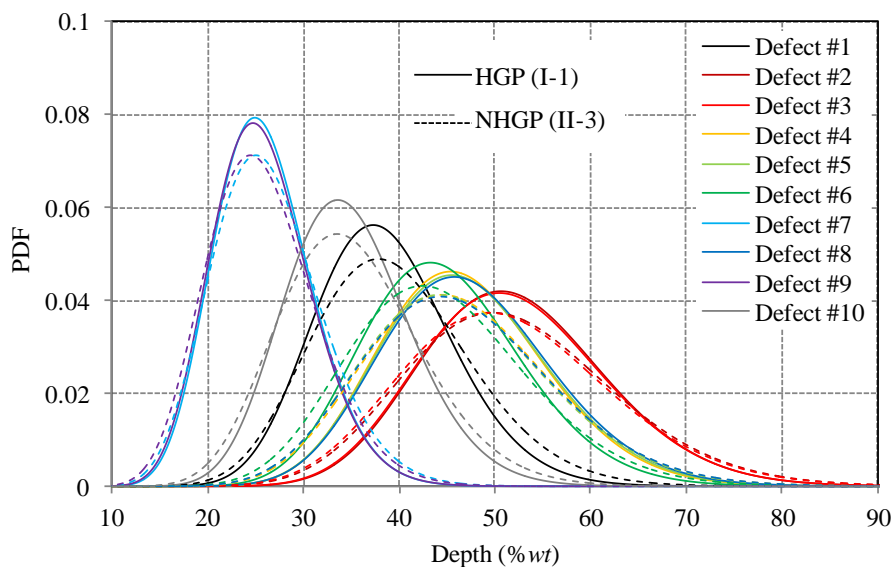


Figure 2.12 PDF curves of defect depths of Defects #1-10 at year 2009

Figure 2.12 suggests that the PDF curves of the defect depth at a given forecasting time are different from defect to defect, which is attributed to that both the initiation time and rate parameter in the growth models are defect-specific. The observations associated

with the mean and standard deviation of the predicted depth obtained from the HGP- and NHGP-based models shown in Fig. 2.12 are similar to those shown in Fig. 2.11.

## 2.7 Conclusions

This chapter describes a gamma process-based model to characterize the growth of metal-loss corrosion defects on oil and gas pipelines. Two sets of models were considered in this study, namely the non-homogeneous process- (NHGP-) and homogeneous gamma process- (HGP-) based models. The shape parameter of the gamma process is assumed to be a power-law function of time in the former, and a linear function of time in the latter, whereas the scale parameter of the gamma process was assumed to be time-independent and defect-specific for both the NHGP- and HGP-based models. Furthermore, the corrosion initiation time for individual defect is accounted for in the growth models. All the parameters involved in each of the models were assumed to be uncertain and evaluated using the hierarchical Bayesian methodology based on the inspection data obtained from multiple ILI runs. The biases, measurement errors as well as the correlations between the random scattering errors associated with the ILI tools were also taken into account in the Bayesian inference. The Markov Chain Monte Carlo (MCMC) simulation was employed to carry out the Bayesian updating and derive the posterior distributions of the parameters in the growth models.

An example involving real ILI data for a gas pipeline was used to illustrate the proposed models. The parameters of the growth models for 62 external corrosion defects that were field measured and recoated were evaluated based on the defect depths reported by multiple ILI runs prior to the field measurement. The parameters were then used to predict the depths of the defects at the time of the field measurements. The predicted defect depths were compared with the corresponding field-measured depths to validate the growth model. The analysis results suggested that the model proposed in this study in general characterizes the growth of the defect depth reasonably well: the absolute differences between the predicted depths and the field-measured depths are less than or equal to 10 %wt for about 90% of the 62 defects. The model predictions are relatively poor for some defects, for which large measurement errors are involved in the ILI data.

Sensitivity analyses indicated that the predictions given by the NHGP-based growth models are insensitive to the prior distribution of  $\alpha$  and  $\kappa$  given a particular prior distribution of  $\beta_i$  (i.e.  $p_4 = q_4 = 1$ ) and highly sensitive to the prior distribution of  $\beta_i$  regardless of the prior distributions of  $\alpha$  and  $\kappa$ . Furthermore, the prior distributions of  $\alpha$ ,  $\kappa$  and  $\beta_i$  in the NHGP-based model have a marked impact on the mean, 10- and 90-percentile values of predicted growth path at the early stage of forecasting period, and a negligibly small impact on the predictions at the time of field measurements. On the other hand, sensitivity analyses indicated that the predictions given by the HGP-based growth model are sensitive to the prior distribution of  $\beta_i$ , but insensitive to that of  $\alpha$ . The prior distributions of  $\alpha$  and  $\beta_i$  have a marginal impact on the mean predicted growth paths; however, only the prior distribution of  $\beta_i$  has a marked impact on percentile values of the predicted growth paths. Sensitivity analyses further suggested that, in general, using the mean (median) values of the marginal posterior distributions of model parameters leads to a better prediction for all scenarios considered for the HGP- (NHGP-) based models.

Comparative analyses indicated that, for a given defect, the initiation time associated with the NHGP-based model is slightly larger than that associated with the HGP-based model. Furthermore, the predicted growth paths over the period of time from defect initiation to excavation obtained from the HGP-based model are markedly different from those obtained from the NHGP-based model, which is expected because different time-dependent functions were assumed for the shape parameters involved in the two growth models. Furthermore, a comparison of the MSEP values of the best predictions corresponding to the two growth models (i.e. Scenario II-3 of the NHGP-based model and Scenario I-1 of the HGP-based model) indicated that the HGP-based model leads to better predictions than the NHGP-based model.

The proposed model provides a powerful framework to deal with various uncertainties involved in the corrosion growth modeling based on the ILI data and will facilitate the corrosion management of oil and gas pipelines.

## Reference

- Al-Amin, M., Zhou, W., Zhang, S., Kariyawasam, S. and Wang, H. (2012). Bayesian model for the calibration of ILI tools. Proceedings of IPC 2012, IPC2012-90491, ASME, Calgary, Canada.
- Ang, A. H. S. and Tang, W. H. (1975). Probability Concepts in Engineering Planning and Design, Volume I: Basic Principles. John and Wiley & sons, NY.
- Aziz, P. M. (1956). Application of the statistical theory of extreme values to the analysis of maximum pit depth data for aluminum. Corrosion, 12(10): 495-506.
- Cheng, T. and Pandey, M. D. (2012). An accurate analysis of maintenance cost of structures experiencing stochastic degradation. Structure and Infrastructure Engineering, 8(4): 329-39.
- Cheng, T. and Pandey, M. D. and van der Weide, J. A. M (2012). The probability distribution of maintenance cost of a system affected by the gamma process of degradation: Finite time solution. Reliability Engineering and System Safety, 108: 65-76.
- Chib, S. and Greenberg, E. (1995). Understanding the Metropolis-Hastings algorithm. The American Statistician, 49(4): 327-335.
- Fuller, W. A. (1987). Measurement Error Models, John Wiley & Sons, Inc., NY.
- Gelfand, A. and Smith, A. (1990). Sampling-based approaches to calculating marginal densities. Journal of the American Statistical Association, 85(410): 398-409.
- Gelman, A., Carlin, J. B., Stern, H. S. and Rubin, D. B. (2004). Bayesian Data Analysis (2nd edition). Chapman & Hall/CRC, NY.
- Harville, D. A. and Jeske, D. R. (1992). Mean squared error of estimation or prediction under a general linear model. Journal of the American Statistical Association, 87: 724-731.
- Jaech, J. L. (1985). Statistical Analysis of Measurement Errors, John Wiley & Sons, Inc., NY.

- Jasa, T. and Xiang, N. (2009). Efficient estimation of decay parameters in acoustically coupled-spaces using slice sampling, *Journal of Acoustical Society of America*, 126(3): 1269-1279.
- Jonhson, R. A. (2000). *Probability and Statistics for Engineers* (6th edition). Prentice-Hall Inc, US.
- Kariyawasam, S. and Peterson, W. (2010). Effective Improvements to Reliability Based Corrosion Management, *Proceedings of IPC 2010, IPC2010-31425*, ASME, Calgary.
- Kallen, M. J. and van Noortwijk, J. M. (2005). Optimal maintenance decisions under imperfect inspection. *Reliability Engineering and System Safety*, 90(2-3): 177-185.
- Lunn, D., Spiegelhalter, D., Thomas, A. and Best, N. (2009). The BUGS project: evolution, critique and future directions (with discussion). *Statistics in Medicine*, 28: 3049-82.
- Lynch, Scott M. (2007). *Introduction to Applied Bayesian Statistics and Estimation for Social Scientists*, Springer, NY.
- Maes, M. A., Faber, M. H. and Dann, M. R. (2009). Hierarchical modeling of pipeline defect growth subject to ILI uncertainty. *Proceedings of the ASME 2009 28th International Conference on Ocean, Offshore and Arctic Engineering*, Honolulu, Hawaii, USA, OMAE2009-79470.
- Neal, R. M. (2003). Slice sampling. *The Annals of Statistics*, 31(3): 705-767.
- Provan, J. W. and Rodriguez III, E. S. (1989). Part I: Development of Markov description of pitting corrosion. *Corrosion*, 45: 178-192.
- Spiegelhalter, D. J. (1998). Bayesian graphic modeling: A case-study in monitoring health outcomes. *Applied Statistics*, 47: 115-33.
- van Noortwijk, J. M. (2009). A survey of the application of Gamma process in maintenance. *Reliability Engineering System Safety*, 94: 2-21.
- van Noortwijk, J. M., van der Weide, J. A. M., Kallen, M. J. and Pandey, M. D. (2007). Gamma process and peaks-over-threshold distribution for time-dependent reliability. *Reliability Engineering System Safety*, 92: 1651-58.

- van Noortwijk, J. M. and van Gelder, P. H. A. J. M. (1996). Optimal maintenance decisions for berm breakwaters. *Structural Safety*, 18(4): 293-309.
- Wang, X. (2008). A Pseudo-likelihood estimation method for nonhomogeneous gamma process model with random effects. *Statistica Sinica*, 18: 1153-1163.
- Yuan, X. X., Pandey, M. D. and Bickel, G. A. (2008). A probabilistic model of wall thinning in CANDU feeders due to flow-accelerated corrosion. *Nuclear Engineering and Design*, 238(1): 16-24.
- Yuan, X. X., Mao, D. and Pandey, M. D. (2009). A Bayesian approach to modeling and predicting pitting flaws in steam generator tubes. *Reliability Engineering and System Safety*, 94: 1838-1847.
- Zhou, W., Hong, H. P. and Zhang, S. (2012). Impact of dependent stochastic defect growth on system reliability of corroding pipelines. *International Journal Pressure Vessels and Piping*, 96-97: 68-77.
- Zhang, S., Zhou, W., Al-Amin, M., Kariyawasam, S. and Wang, H. (2012). Time-dependent corrosion growth modeling using multiple ILI data. *Proceedings of IPC 2012, IPC2012-90502, ASME, Calgary, Canada.*

## **Chapter 3 Inverse Gaussian Process-based Corrosion Growth Modeling Based on Imperfect Inspection Data**

### **3.1 Introduction**

Two stochastic processes analogues to the gamma process, namely the inverse Gaussian process and Wiener process were recently reported in the literature (e.g. Wang and Xu 2010; Wang 2010) in the context of modeling the degradation process. The inverse Gaussian process (IGP) consists of independent increments that follow the inverse Gaussian distribution, whereas the Wiener process consists of independent increments that follow the Gaussian distribution. Wang and Xu (2010) employed the inverse Gaussian process to model the degradation of the laser devices based on observed data. Wang (2010) used Wiener process to characterize the degradation of the strength of bridge beams based on field-measured data. Both studies used the maximum likelihood method to estimate the model parameters and ignored the measurement error associated with the inspection data. A notable drawback of using the Wiener process to model the corrosion growth is that it cannot rigorously characterize the monotonic nature of the growth, since the Gaussian distributed increments can be either positive or negative. The IGP overcomes this drawback because it is positively defined. The mathematical tractability of the IGP (Chikkara and Folks 1989; Wang and Xu 2010) also facilitates incorporating the IGP-based corrosion growth model in a Bayesian framework to evaluate and update the model parameters based on inspection data. However, to the author's best knowledge, studies of IGP-based corrosion growth models based on data obtained from imperfect inspections are unavailable in the literature.

In this study, the objective is to develop an IGP-based growth model for the depths of corrosion defects on underground pipelines by incorporating the in-line inspection (ILI) data that are subjected to measurement uncertainties. The growth model is formulated in a hierarchical Bayesian framework. The probabilistic characteristics of the model parameters are evaluated using the Markov Chain Monte Carlo (MCMC) simulation techniques. An example involving a real in-service natural gas pipeline located in

Alberta, Canada is used to illustrate and validate the proposed growth model. Parametric analysis and comparative study are also included in the example.

The rest of this chapter is organized as follow. Section 3.2 briefly describes the inverse Gaussian distribution and inverse Gaussian process. Section 3.3 presents the formulation of the IGP-based growth models for multiple corrosion defects. The formulations to evaluate the model parameters using the hierarchical Bayesian methodology are presented in Section 3.4. An example for illustrating and validating the proposed growth model is given in Section 3.5, followed by the conclusions in Section 3.6. The derivations of posterior distributions of model parameters are given in Appendix C.

### 3.2 Inverse Gaussian Process

Consider  $X$  as an inverse Gaussian-distributed random variable with a mean of  $\mu$  ( $\mu > 0$ ) and a shape parameter  $\theta$  ( $\theta > 0$ ). The probability density function (PDF) of  $X$  is given by (Chikkara and Folks 1989)

$$f_X(x|\mu, \theta) = \sqrt{\frac{\theta}{2\pi}} x^{-\frac{3}{2}} \exp\left(-\frac{\theta(x-\mu)^2}{2\mu^2 x}\right) I_{(0,\infty)}(x) \quad (3.1)$$

where  $I_{(0,\infty)}$  is an indicator function and equal to unity for  $x > 0$  and zero for  $x \leq 0$ . The variance of  $X$  equals  $\mu^3/\theta$ . The PDFs of  $X$  corresponding to different combinations of  $\mu$  and  $\theta$  are illustrated in Fig. 3.1.

Given  $\theta$  and  $\mu$ , a realization of  $X$ ,  $x$ , can be generated through three steps (Chikkara and Folks 1989; Kroses et al. 2011): 1) generate a random number  $u$  from the standard normal distribution and set  $z = u^2$ ; 2) set  $w = \mu + \mu^2 z / (2\theta) + \mu / (2\theta) (4\mu\theta z + \mu^2 z^2)^{0.5}$ , and 3) generate a random number  $u_0$  from a Bernoulli distribution with a probability of  $\mu/(\mu+w)$ , and set  $x = w$  if  $u_0 = 1$  and  $x = \mu^2/w$  otherwise.



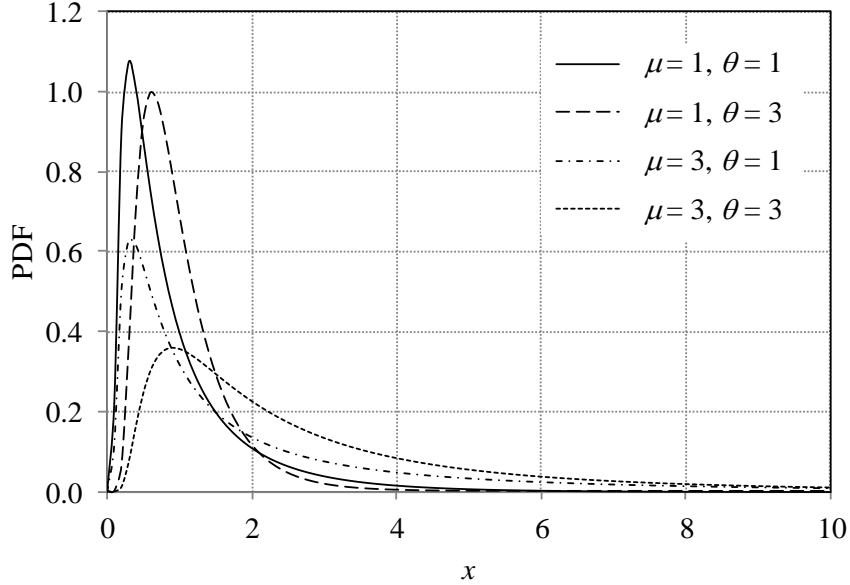


Figure 3.1 PDF function of the inverse Gaussian distribution

Let  $\{X(t); t \geq 0\}$  denote an IGP over time  $t$ . Based on Wang and Xu (2010),  $X(t)$  is parameterized by its mean or expectation function,  $\Theta(t)$ , (i.e.  $E[X(t)] = \Theta(t)$ ), and shape parameter  $\xi(\Theta(t))^2$ , where  $\xi$  is a scale parameter. It follows from Eq. (3.1) that the PDF of  $X(t)$  is given by

$$f_{X(t)}(x(t)|\theta(t), \xi(\theta(t))^2) = \sqrt{\frac{\xi}{2\pi}} \theta(t) x(t)^{-\frac{3}{2}} \exp\left(-\frac{\xi(x(t)-\theta(t))^2}{2x(t)}\right) I_{(0,\infty)}(x(t)) \quad (3.2)$$

The variance and coefficient of variation (COV) of  $X(t)$ , denoted by  $\text{Var}[X(t)]$  and  $\text{COV}[X(t)]$  respectively, are then

$$\text{Var}[X(t)] = \frac{\theta(t)}{\xi} \quad (3.2a)$$

$$\text{COV}[X(t)] = \frac{1}{\sqrt{\xi\theta(t)}} \quad (3.2b)$$

The IGP defined by Eq. (3.2) has the following properties (Wang and Xu 2010):

- (1)  $X(0) = 0$  with probability one;

(2)  $X(\tau) - X(t)$  follows an inverse Gaussian distribution with a PDF of  $f_{X(\tau)-X(t)}(x(\tau) - x(t) | \mathcal{O}(\tau) - \mathcal{O}(t), \xi(\mathcal{O}(\tau) - \mathcal{O}(t))^2)$  for all  $\tau > t \geq 0$ , and

(3)  $X(t)$  has independent increments.

Because the mean function,  $\mathcal{O}(t)$ , must be a monotonically increasing function with time  $t$ , Equation (3.2b) indicates that the COV of  $X(t)$  decreases as time increases, which is similar to that of the Gamma process (GP) (van Noortwijk 2009) described in Chapter 2. In fact, both the GP and IGP belong to the same generalized inverse Gaussian process (Johnson et al. 1994) because the inverse Gaussian and gamma distributions are two special cases of a generalized inverse Gaussian distribution (Chikkara and Folks 1989). The scale parameter (i.e.  $\xi$ ) in an IGP influences its COV but not its mean, whereas the scale parameter in a GP influences its mean but not its COV as described in Chapter 2.

### 3.3 Growth Modeling for Multiple Defects

Consider that  $m$  active corrosion defects on a given pipeline have been subjected to  $n$  inspections over a period of time. The measured depth (i.e. in the through pipe wall thickness direction) of the  $i^{\text{th}}$  defect at the  $j^{\text{th}}$  inspection,  $y_{ij}$ , ( $i = 1, 2, \dots, m; j = 1, 2, \dots, n$ ) is related to the actual depth,  $x_{ij}$ , through Eq. (2.3), i.e.  $y_{ij} = a_j + b_j x_{ij} + \varepsilon_{ij}$ , with  $a_j$  and  $b_j$  denoting the constant and non-constant biases associated with the ILI tool used in the  $j^{\text{th}}$  inspection, and  $\varepsilon_{ij}$  denoting the random scattering error associated with the ILI-reported depth of the  $i^{\text{th}}$  defect at the  $j^{\text{th}}$  inspection, and being assumed to follow a zero-mean normal distribution (Al-Amin et al. 2012).

The actual defect depth was assumed to follow an inverse Gaussian process given by Eq. (2), where  $\mathcal{O}(t)$  can be assumed to be a power-law function of time, i.e.  $\mathcal{O}(t) = \alpha(t - t_0)^\kappa$  with  $t_0$  denoting the defect initiation time, where  $\kappa > 1$ ,  $\kappa < 1$  and  $\kappa = 1$  imply that the mean growth is an accelerating, decelerating and linear trajectory over time, respectively. In this study, it is assumed that  $\kappa$  equals unity, which implies that the mean growth path is a linear function of time. Note that the IGP-based growth model with  $\kappa \neq 1$  has been reported by Qin et al. (2013).

It follows from Eq. (3.2) that the growth of the  $i^{\text{th}}$  defect between the  $(j-1)^{\text{th}}$  and  $j^{\text{th}}$  inspections,  $\Delta X_{ij}$ , is inverse Gaussian distributed and has a PDF given by  $f_{\Delta X_{ij}}(\Delta x_{ij}|\Delta \Theta_{ij}, \xi(\Delta \Theta_{ij})^2)$ . The mean value of  $\Delta X_{ij}$ ,  $\Delta \Theta_{ij}$ , is calculated by

$$\Delta \Theta_{ij} = \alpha_i(t_{ij} - t_{i,j-1}) \quad (j = 1, 2, \dots, n) \quad (3.3)$$

where  $t_{ij}$  ( $j = 1, 2, \dots, n$ ) denotes the time of the  $j^{\text{th}}$  inspection (e.g. the time elapsed since the installation of pipe up to the  $j^{\text{th}}$  inspection) for defect  $i$ ;  $t_{i0}$  denotes the initiation time of the  $i^{\text{th}}$  defect, (i.e. the time interval between the installation of pipe and the time at which the defect initiates), and  $\alpha_i$  denotes the average growth of the  $i^{\text{th}}$  defect over a unit time interval (i.e.  $\Delta t = 1$  year). The actual depth of the  $i^{\text{th}}$  defect at the time of the  $j^{\text{th}}$  inspection,  $x_{ij}$ , is then obtained by  $x_{ij} = x_{i,j-1} + \Delta x_{ij}$ , where the defect depth at  $t = t_0$  (i.e.  $x_{i0}$ ) is assumed to equal zero with a probability of one.

In the above-described model, the initiation time  $t_0$  and parameter  $\alpha$  are assumed to be defect-specific and the scale parameter  $\xi$  is assumed to be common for all defects. The formulations in the following sections are based on these assumptions. Two alternative sets of assumptions were also considered in the analysis, namely defect-specific  $t_0$  and  $\xi$  but common  $\alpha$  for all defects, as well as defect-specific  $t_0$  but common  $\xi$  and  $\alpha$  for all defects. The impact of these assumptions on the predictive capability of the growth model was investigated through parametric analyses as described in Section 3.5.

## 3.4 Bayesian Updating of the Growth Model

### 3.4.1 Likelihood Function

Denote  $\mathbf{y}_i = (y_{i1}, y_{i2}, \dots, y_{ij}, \dots, y_{in})'$ ,  $\mathbf{x}_i = (x_{i1}, x_{i2}, \dots, x_{ij}, \dots, x_{in})'$  and  $\Delta \mathbf{x}_i = (\Delta x_{i1}, \Delta x_{i2}, \dots, \Delta x_{in})'$ , with “'” representing transposition. Let  $\mathbf{E}_i = (E_{i1}, E_{i2}, \dots, E_{in})'$  denote the vector of random scattering errors associated with defect  $i$  for inspections  $j = 1, 2, \dots, n$ . Consider defect  $i$ , it follows from Eqs. (2.3) and (2.4) as well as the assumptions described in Section 2.3 of Chapter 2 (i.e. the random scattering errors were assumed to be spatially independent but temporally correlated) that the likelihood of the inspection data,  $\mathbf{y}_i$ , conditional on the growth,  $\Delta \mathbf{x}_i$ , is the same as Eq. (2.8) in Chapter 2, i.e.  $L(\mathbf{y}_i|\Delta \mathbf{x}_i)$

$= (2\pi)^{-n/2} |\boldsymbol{\Sigma}_{E_i}|^{-1/2} \exp(-0.5(\mathbf{y}_i - (\mathbf{a} + \mathbf{b}\mathbf{x}_i))' (\boldsymbol{\Sigma}_{E_i})^{-1} (\mathbf{y}_i - (\mathbf{a} + \mathbf{b}\mathbf{x}_i)))$  with  $x_{ij} = \sum_{k=1}^j \Delta x_{ik}$ , except that  $\Delta x_{ij}$  is inverse Gaussian-distributed as opposed to being gamma-distributed, where  $\mathbf{a} = (a_1, a_2, \dots, a_j, \dots, a_n)'$ ,  $\mathbf{b}$  is an  $n$ -by- $n$  diagonal matrix with diagonal elements equal to  $b_j$  ( $j = 1, 2, \dots, n$ ) and  $\boldsymbol{\Sigma}_{E_i}$  denotes the variance matrix of  $\mathbf{E}_i$  and is an  $n$ -by- $n$  matrix with the element equal to  $\rho_{jk} \sigma_j \sigma_k$  ( $j = 1, 2, \dots, n; k = 1, 2, \dots, n$ ).  $\rho_{jk}$  denotes the correlation coefficient between the random scattering errors associated with the  $j^{\text{th}}$  and  $k^{\text{th}}$  inspections, and  $\sigma_j$  and  $\sigma_k$  denote the standard deviations of the random scattering errors associated with the tools used at the  $j^{\text{th}}$  and  $k^{\text{th}}$  inspections, respectively. A Bayesian methodology has been developed (Al-Amin et al. 2012) to evaluate  $a_j$ ,  $b_j$ ,  $\sigma_j$  and  $\rho_{jk}$  ( $j = 1, 2, \dots, n; k = 1, 2, \dots, n$ ) based on the ILI-reported depths for a set of static defects (i.e. defects that have been repaired prior to the ILI and ceased growing). In this study,  $a_j$ ,  $b_j$ ,  $\sigma_j$  and  $\rho_{jk}$  were assumed to be known and deterministic quantities.

It follows from the properties of the IGP described in Section 3.2 that the joint probability density function of  $\Delta \mathbf{x}_i$  is

$$\begin{aligned}
 f_{\Delta \mathbf{x}_i}(\Delta \mathbf{x}_i | \Delta \theta_{ij}, \xi (\Delta \theta_{ij})^2) &= f_{\Delta \mathbf{x}_i}(\Delta \mathbf{x}_i | \alpha_i, t_{i0}, \xi) = \prod_{j=1}^n f_{\Delta x_{ij}}(\Delta x_{ij} | \alpha_i, t_{i0}, \xi) \\
 &= \prod_{j=1}^n \sqrt{\frac{\xi}{2\pi}} \Delta \theta_{ij} \Delta x_{ij}^{-\frac{3}{2}} \exp\left(-\frac{\xi (\Delta x_{ij} - \Delta \theta_{ij})^2}{2\Delta x_{ij}}\right) \quad (3.4)
 \end{aligned}$$

Further denote  $\Delta \mathbf{x} = (\Delta \mathbf{x}_1, \Delta \mathbf{x}_2, \dots, \Delta \mathbf{x}_m)$ ,  $\boldsymbol{\alpha} = (\alpha_1, \alpha_2, \dots, \alpha_m)$  and  $\mathbf{t}_0 = (t_{10}, t_{20}, \dots, t_{m0})$ . Assume that the growths of different defects are spatially independent; in other words,  $\Delta x_{ij}$  and  $\Delta x_{lj}$  ( $i \neq l$ ) are mutually independent for given inspection  $j$  conditional on  $\alpha_i$ ,  $\xi$  and  $t_{i0}$ . Given that  $\alpha_i$  and  $t_{i0}$  are defect-specific and only depends on the growth of the  $i^{\text{th}}$  defect (i.e.  $\Delta \mathbf{x}_i$ ) and  $\xi$  is common for the growth of all defects (i.e.  $\Delta \mathbf{x}$ ), the likelihood function of  $\Delta \mathbf{x}_i$  conditional on  $\alpha_i$ ,  $t_{i0}$  and  $\xi$  ( $i = 1, 2, \dots, m$ ), as well as the likelihood function of  $\Delta \mathbf{x}$  conditional on  $\xi$ ,  $\boldsymbol{\alpha}$  and  $\mathbf{t}_0$  are therefore obtained from Eqs. (3.5a) and (3.5b), respectively.

$$\begin{aligned}
L(\Delta \mathbf{x}_i | \alpha_i, t_{0i}, \xi) &= \prod_{j=1}^n f_{\Delta x_{ij}}(\Delta x_{ij} | \alpha_i, t_{i0}, \xi) \\
&= \prod_{j=1}^n \sqrt{\frac{\xi}{2\pi}} \Delta \theta_{ij} \Delta x_{ij}^{-\frac{3}{2}} \exp\left(-\frac{\xi(\Delta x_{ij} - \Delta \theta_{ij})^2}{2\Delta x_{ij}}\right)
\end{aligned} \tag{3.5a}$$

$$\begin{aligned}
L(\Delta \mathbf{x} | \boldsymbol{\alpha}, \mathbf{t}_0, \xi) &= \prod_{i=1}^m L(\Delta \mathbf{x}_i | \alpha_i, t_{i0}, \xi) = \prod_{i=1}^m \prod_{j=1}^n f_{\Delta x_{ij}}(\Delta x_{ij} | \alpha_i, t_{i0}, \xi) \\
&= \prod_{i=1}^m \prod_{j=1}^n \sqrt{\frac{\xi}{2\pi}} \Delta \theta_{ij} \Delta x_{ij}^{-\frac{3}{2}} \exp\left(-\frac{\xi(\Delta x_{ij} - \Delta \theta_{ij})^2}{2\Delta x_{ij}}\right)
\end{aligned} \tag{3.5b}$$

### 3.4.2 Prior and Posterior Distributions

For  $m$  active corrosion defects, a total of  $2m + 1$  basic parameters are included in the growth model described in Section 3.3, namely  $m$  defect-specific parameters  $\alpha_i$  and initiation times  $t_{i0}$  ( $i = 1, 2, \dots, m$ ) and one common scale parameter (i.e.  $\xi$ ). In this study, the gamma distribution was selected as the prior distributions of  $\alpha_i$  and  $\xi$  ( $i = 1, 2, \dots, m$ ) considering that the gamma distribution ensures  $\alpha_i$  and  $\xi$  to be positive quantities and can be conveniently made as a non-informative distribution. Furthermore, the assignment of the gamma distribution as the prior distribution of  $\xi$  improves the computational efficiency in the MCMC simulation because it leads to a conjugate posterior distribution (Gelman et al. 2004) of  $\xi$  conditional on  $\alpha_i$  and  $t_{i0}$ . The prior distribution of  $t_{i0}$  was chosen to be a uniform distribution with a lower bound of zero and an upper bound equal to the time interval between the installation of the pipeline and the first detection of defect  $i$ .  $\alpha_i$  ( $t_{i0}$ ) associated with different defects were further assumed to be mutually independent and have identical prior distributions (*iid*). Given above, the prior distributions of  $\alpha_i$ ,  $t_{i0}$  and  $\xi$  are parameterized as follows:

$$\alpha_i \sim f_G(\alpha_i | p_1, q_1) \text{ (iid for } i = 1, 2, \dots, m) \tag{3.6a}$$

$$t_{i0} \sim f_U(t_{i0} | p_2, q_2) \text{ (iid for } i = 1, 2, \dots, m) \tag{3.6b}$$

$$\xi \sim f_G(\xi | p_3, q_3) \quad (3.6c)$$

where  $f_G(\cdot)$  and  $f_U(\cdot)$  denote the PDFs of the gamma and uniform distributions;  $p_1$  ( $q_1$ ) and  $p_3$  ( $q_3$ ) denote the shape (rate) parameter of the gamma distributions of  $\alpha_i$  and  $\xi$ , respectively, and  $p_2$  and  $q_2$  denote the lower and upper bounds of the uniform distribution of  $t_{i0}$ .

It follows from the Bayesian theorem (see Section 2.5.5 of Chapter 2) that the posterior distributions of model parameters can be derived and are given in Appendix C. The MCMC simulation techniques implemented in the software *OpenBUGS* (Lunn et al. 2009) were employed in this study to numerically evaluate the marginal posterior distributions of the parameters. Without loss of generality, the procedures based on a hybrid of the Metropolis-Hasting (M-H) algorithm and Gibbs sampler (Gelman et al. 2004) to sequentially generate the random samples of the parameters in the growth model are depicted in a flowchart as shown in Fig. 3.2, where  $s$  denotes the counter for the simulation trial;  $N_s$  denotes the total number of sequence of samples generated in the MCMC simulation, and  $p(\bullet)$  denotes the conditional posterior distribution of a given model parameter (see Appendix C). The inverse Gaussian distribution was defined in *OpenBUGS* (Lunn et al. 2009) through the generic distribution option.

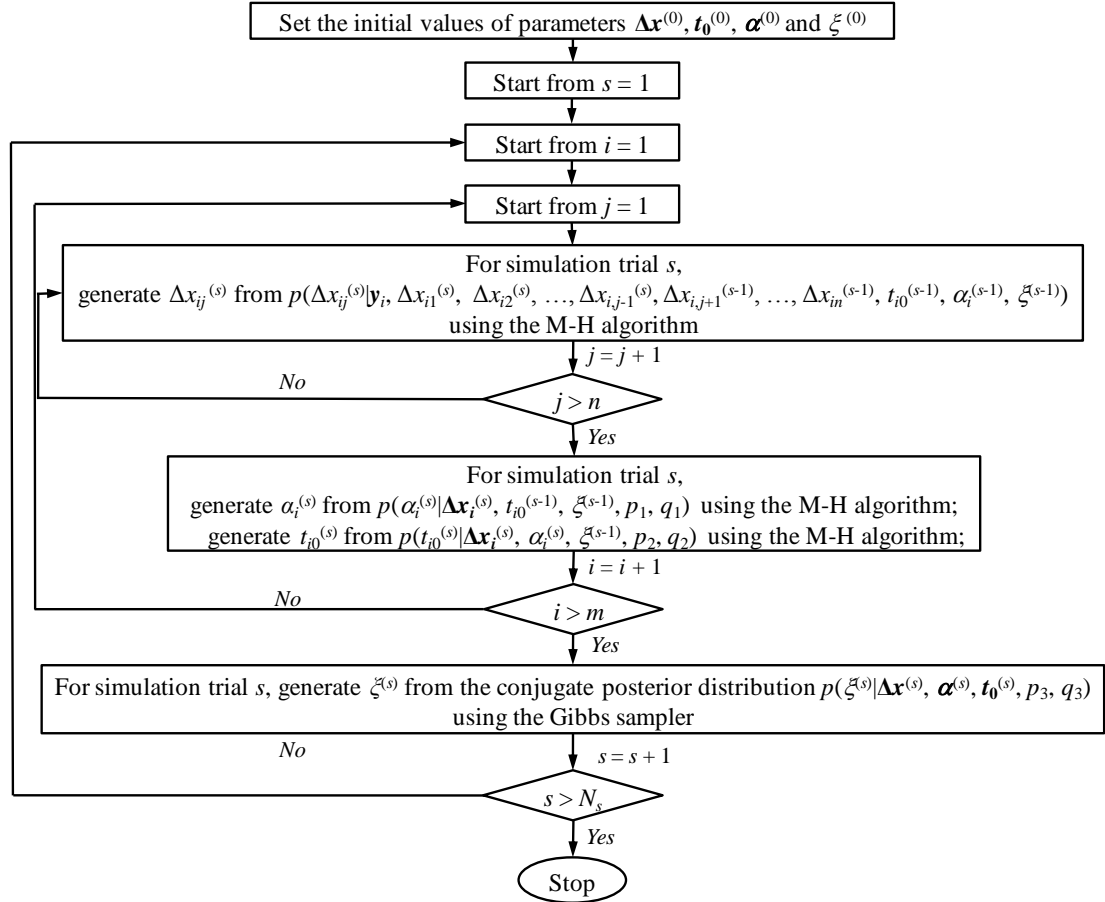


Figure 3.2 Flowchart of the MCMC simulation-based Bayesian updating procedures

### 3.4.3 Hierarchical Representation of the Growth Model

A visualization of the aforementioned corrosion growth model is given by the directed acyclic graph (DAG) (Spiegelhalter 1998) as depicted in Fig. 3.3, where ellipses and rectangles symbolize the stochastic and deterministic parameters, respectively; single-edged arrows denote the stochastic links, whereas double-edged arrows denote the deterministic functional links. Three levels of parameters are involved in Fig. 3.3. The first level includes the ILI data that are associated with measurement errors characterized by  $\mathbf{a}$ ,  $\mathbf{b}$  and  $\Sigma_{E_i}$ . The second level includes the latent variables that consist of the actual depths at the times of inspections and increments of the actual depths between two consecutive inspections as well as the mean ( $\Delta\theta_{ij}$ ) of  $\Delta x_{ij}$  ( $i = 1, 2, \dots, m; j = 1, 2, \dots, n$ ). This level captures the stochastic characteristics and temporal variability of the defect growth path. The third level includes the basic parameters of the inverse Gaussian

process model (i.e.  $\alpha_i$ ,  $t_{i0}$  and  $\xi$ ). The known quantities including the parameters of the distributions of the basic parameters (i.e.  $p_1$ ,  $q_1$ ,  $p_2$ ,  $q_2$ ,  $p_3$  and  $q_3$ ), the background information,  $t_{ij}$  ( $j = 1, 2, \dots, n$ ), as well as the measurement errors are also shown in Fig. 3.3.

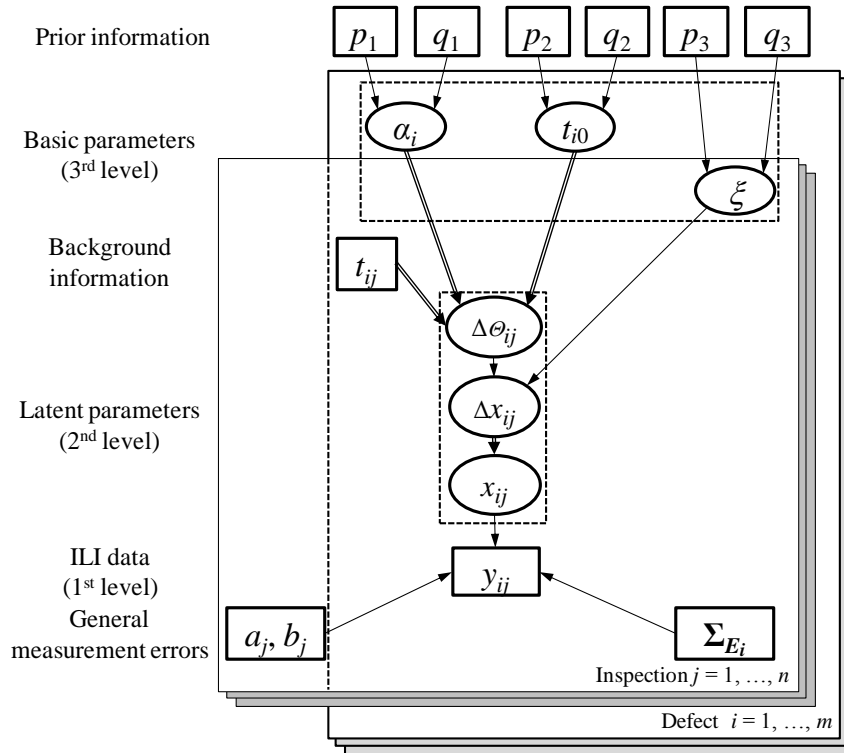


Figure 3.3 DAG of the growth model

## 3.5 Example

### 3.5.1 Illustration and Validation of Growth Model

In this section, the growth models were applied to the 62 external corrosion defects described in Section 2.6.1 of Chapter 2. The same sets of ILI data (i.e. the ILI-reported depth in 2000, 2004 and 2007) were used to carry out the Bayesian updating. The parameters of the hyper prior distributions, i.e. the parameters at the top level of Fig. 3.3, were specified as follows:  $p_1 = 1$ ,  $q_1 = 1$ ,  $p_2 = 0$  (year),  $q_2 = 28$  (year),  $p_3 = 1$ ,  $q_3 = 1$ . A total of 20,000 MCMC simulation sequences were generated with the first 2000 sequences considered as the burn-in period (Gelman et al. 2004) and therefore discarded.



The samples in the rest of the sequences were used to evaluate the probabilistic characteristics of the parameters in the growth models. A comparison between the predicted depths,  $x_p$ , in 2010 with the corresponding field-measured depths,  $x_a$ , for the 62 defects is shown in Fig. 3.4.

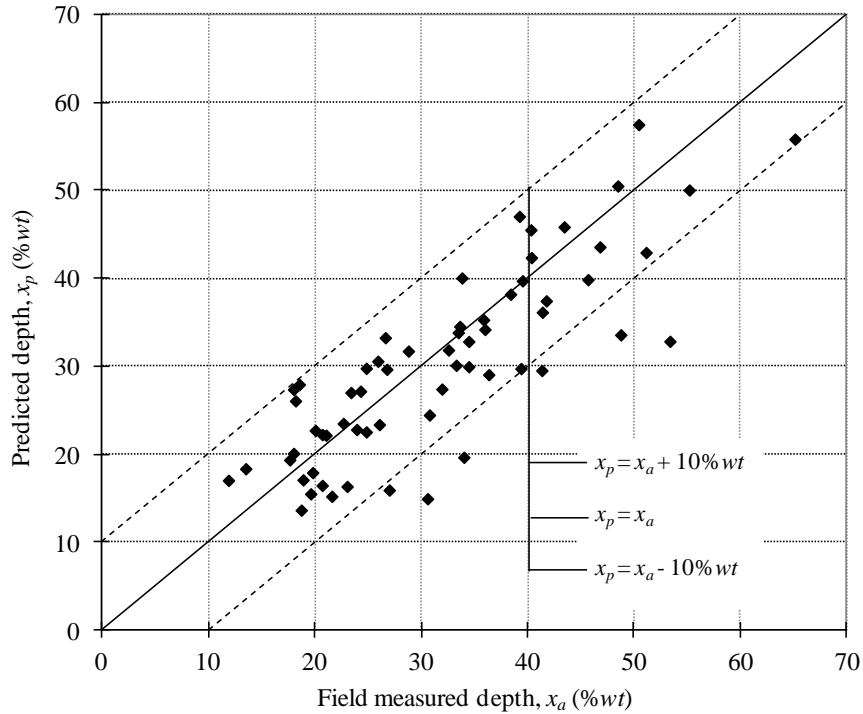
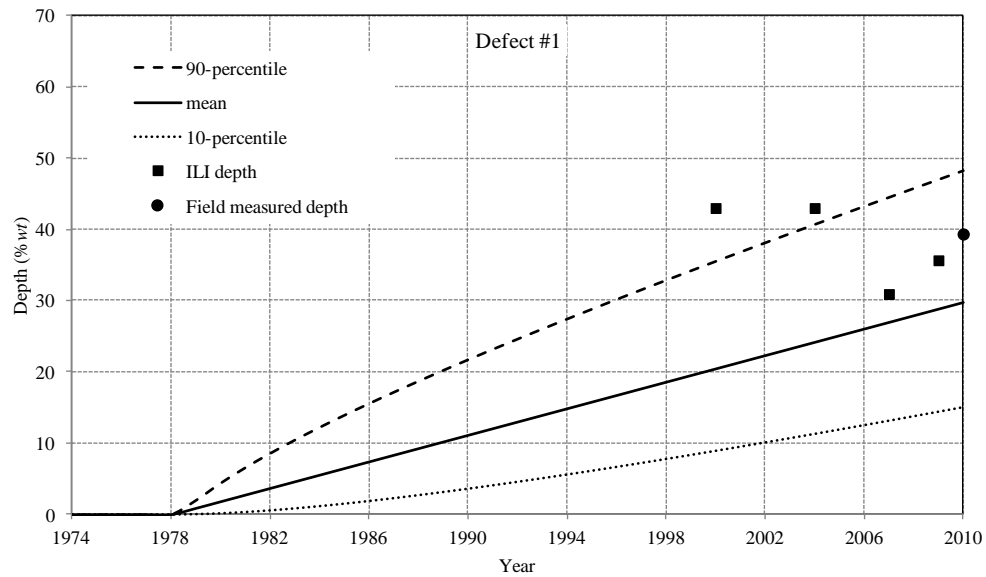


Figure 3.4 Comparison of the predicted depths in 2010 with the corresponding field-measured depths

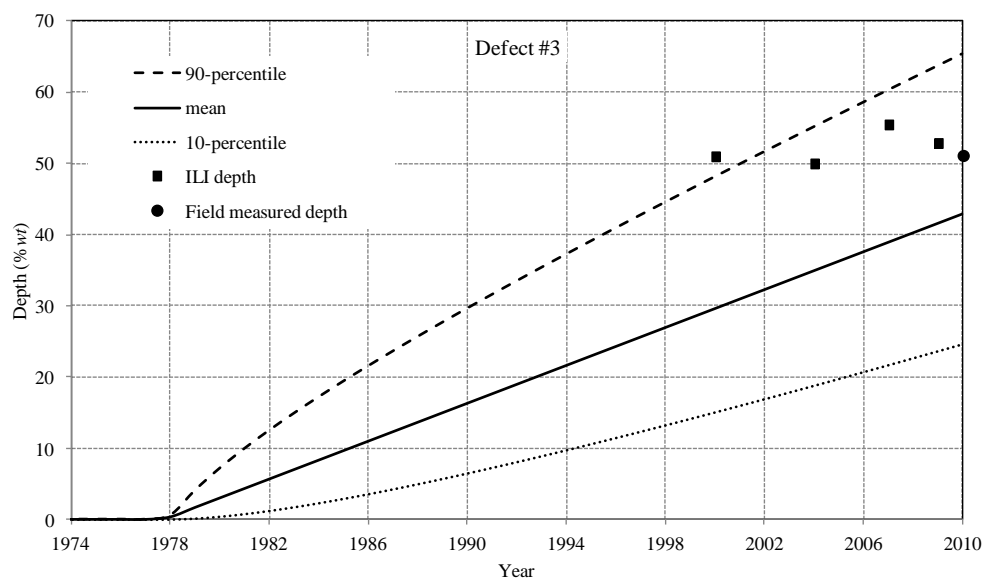
The predicted depth for a given defect shown in Fig. 3.4 is the mean depth predicted from the IGP-based model with the model parameters (i.e.  $\alpha_i$ ,  $t_{i0}$  and  $\xi$ ) assumed to be deterministic and set equal to the median values of the corresponding marginal posterior distributions obtained from the MCMC simulation. Figure 3.4 suggests that the proposed model can provide reasonably good predictions for majority of the defects considered, as the predicted depths for 90% of the 62 defects fall within the region bounded by the two lines representing actual depth  $\pm 10\%$  wt. Note that the two bounding lines are commonly used in the pipeline industry as a confidence interval for the accuracy of the inspection tool and are adopted in this study as a metric for the predictive accuracy of the corrosion growth model. The predicted depths show significant deviation (defined as the absolute

difference between the predicted and actual depths being greater than 10 %wt) from the corresponding actual depths for only six defects, with the maximum absolute deviation being approximately 15 %wt.

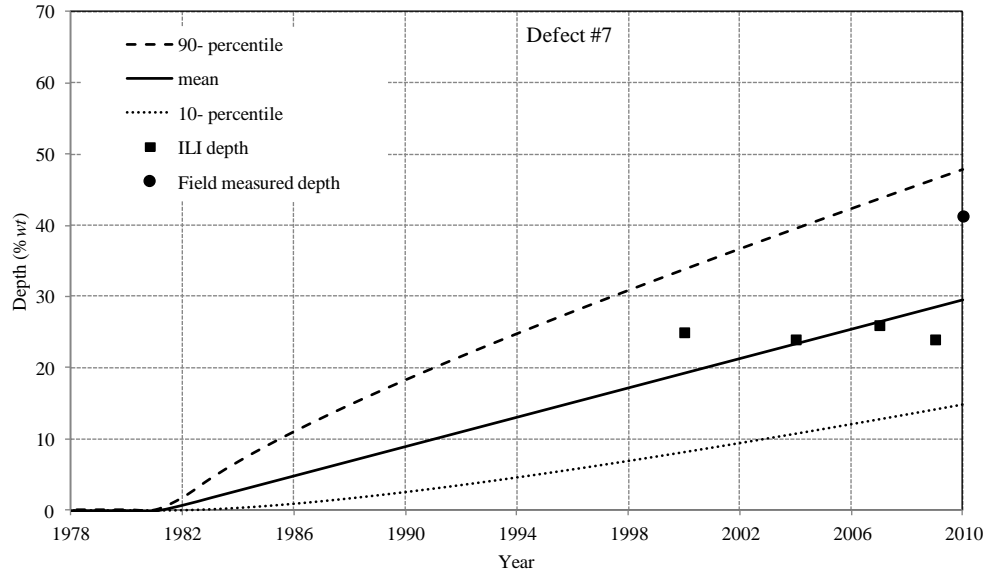
The mean, 10- and 90-percentile values of the growth paths for ten arbitrarily selected defects, i.e. Defects #1, #3, #7, #13, #15, #18, #19, #22, #50 and #60, are plotted in Figs. 3.5(a) through 3.5(j), respectively. For a given defect, the 10- and 90-percentile values were evaluated assuming the defect depth at a given time follows an inverse Gaussian distribution with a cumulative distribution function (CDF) of  $P(X(t) \leq x(t)) = 1 - \Phi((\xi/x(t))^{0.5}(\Theta(t) - x(t))) + \exp(2\xi\Theta(t))\Phi(-(\xi/x(t))^{0.5}(\Theta(t) + x(t)))$  (Chikkara and Folks 1989; Kroses et al. 2011; Wang and Xu 2010), where  $\Phi(\bullet)$  denotes the CDF of the standard normal distribution. The mean of the predicted growth path of the  $i^{\text{th}}$  defect (i.e.  $\Theta_i(t)$ ) was obtained from  $\Theta_i(t) = \alpha_i(t - t_{i0})$  with  $\alpha_i$  and  $t_{i0}$  equal to their median values evaluated from the MCMC simulations and  $t$  varying from zero to 38 years (i.e. from years 1972 to 2010) with an increment of one year, where  $\Theta_i(t) = 0$  if  $t \leq t_{i0}$ . For comparison, the corresponding ILI-reported depths in 2000, 2004, 2007 and 2009 as well as the field-measured depth in 2010 are also plotted in the same figure. The results indicate that the predicted average growth rate differs from defect to defect; this is expected because the parameter  $\alpha$ , which represents the average growth rate, is assumed to be defect-specific. For example, the average growth rate of Defects #19 is the highest among the ten defects plotted and equals to 1.9 %wt/yr, followed by Defects #60, #15, #3, #13, #18, #7, #1, #22 and #50 with average growth rates equal to 1.8, 1.7, 1.4, 1.3, 1.2, 1.0, 0.9, 0.7 and 0.6 %wt/yr, respectively.



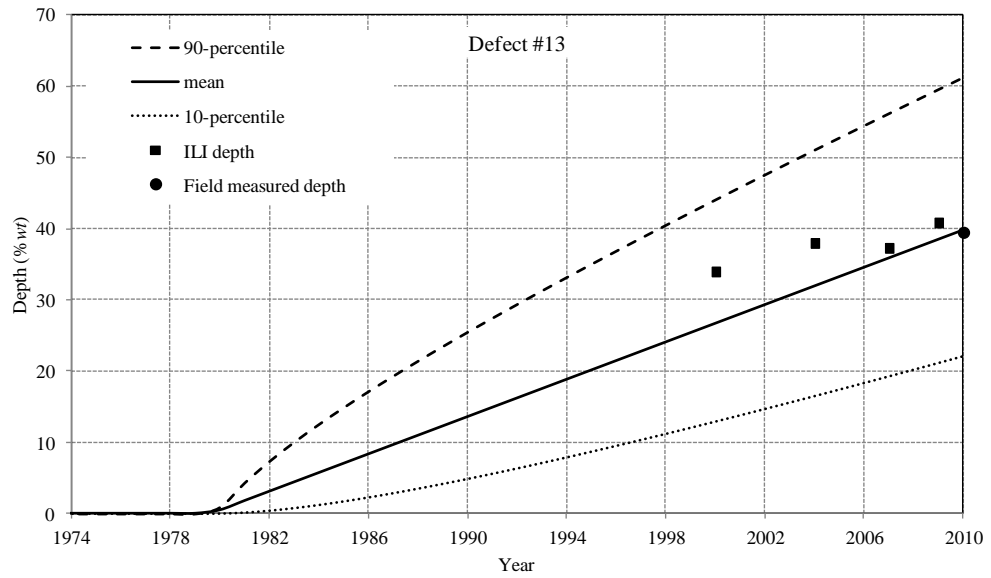
(a)



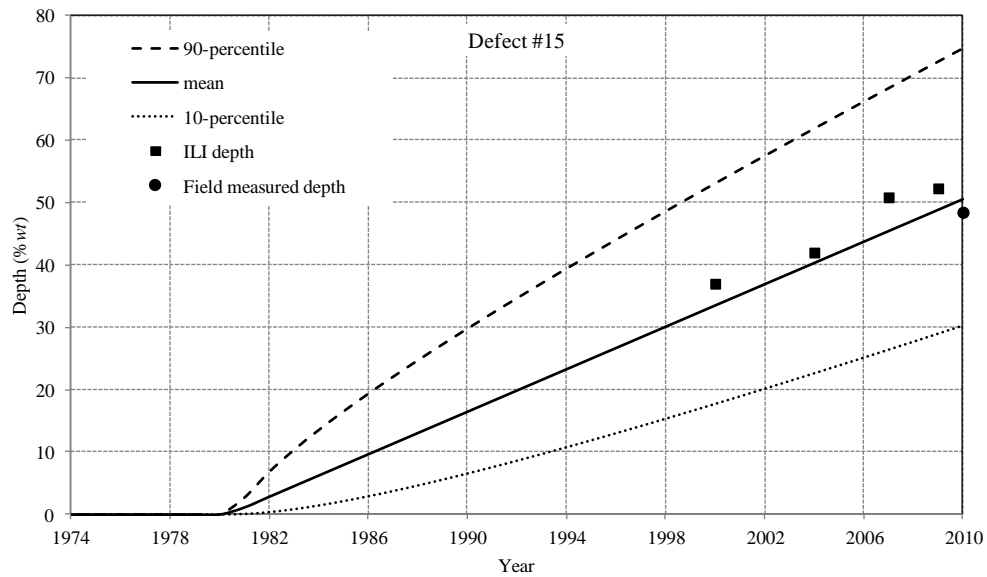
(b)



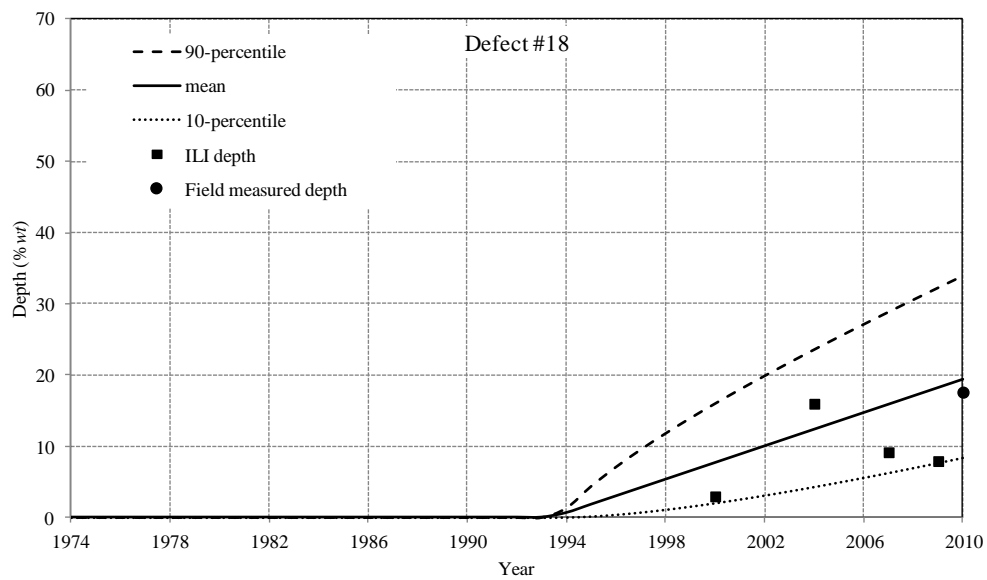
(c)



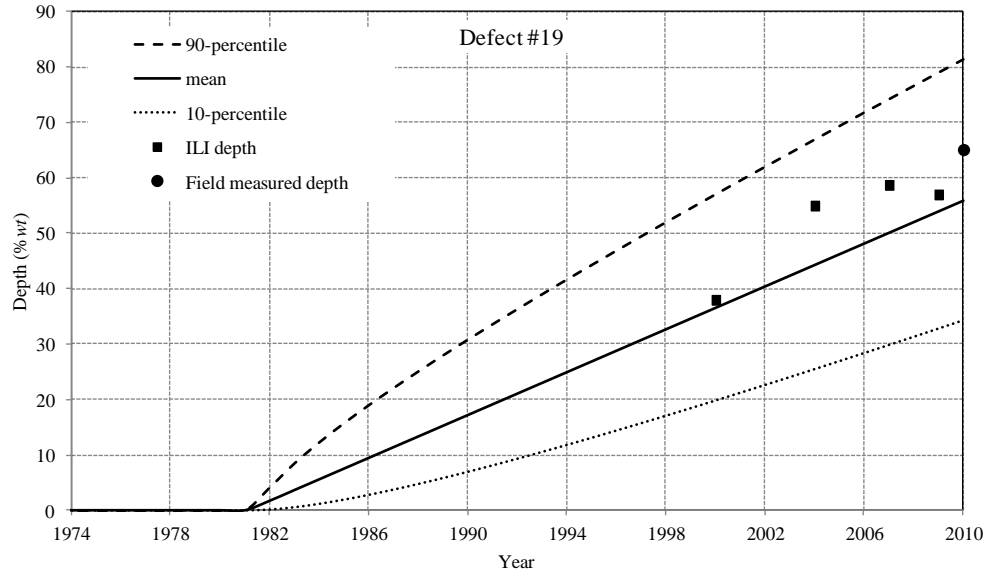
(d)



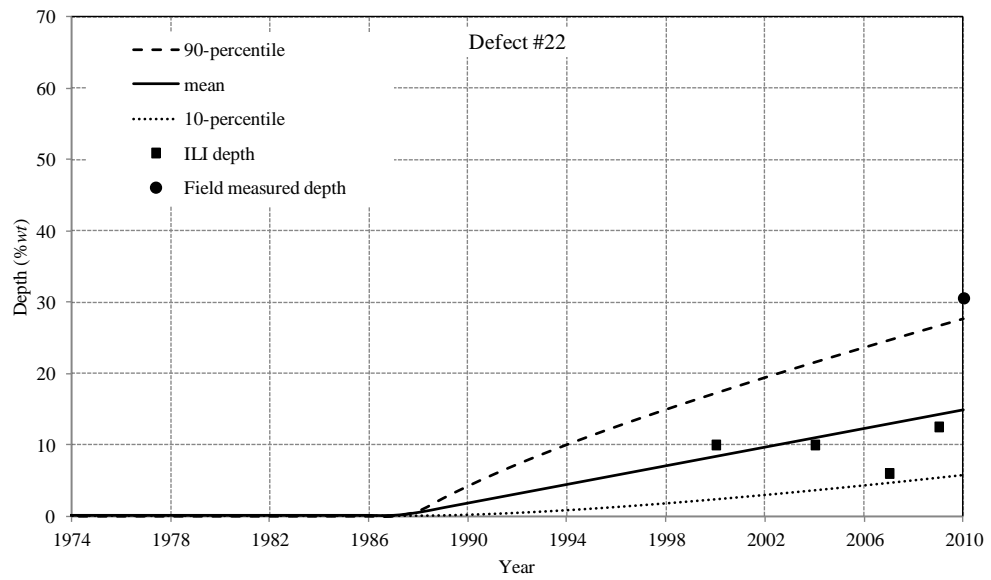
(e)



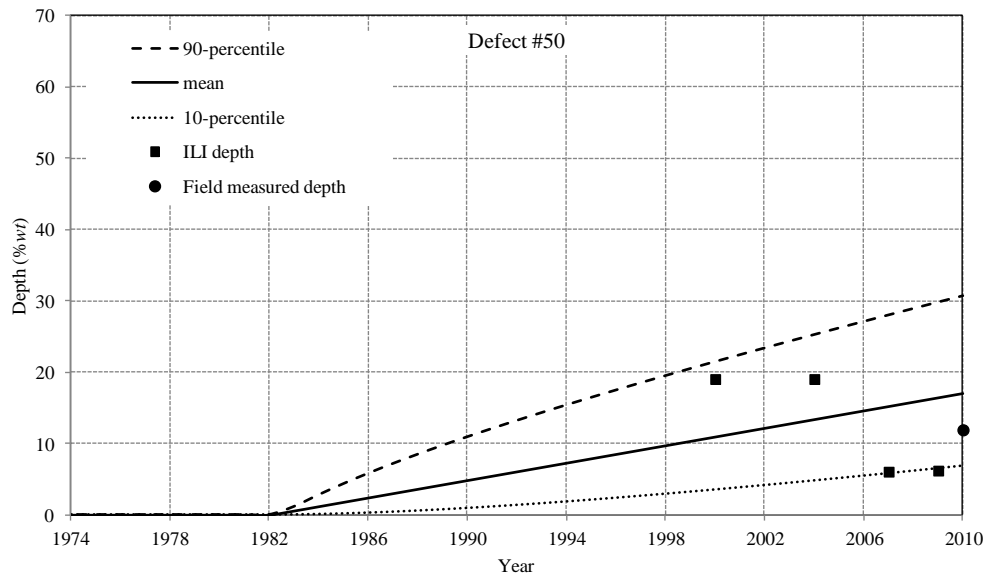
(f)



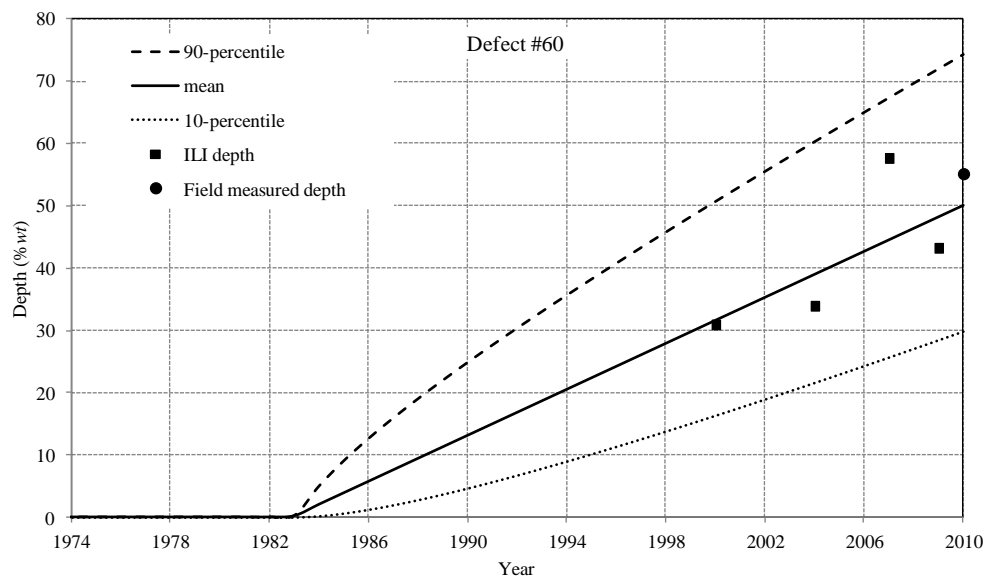
(g)



(h)



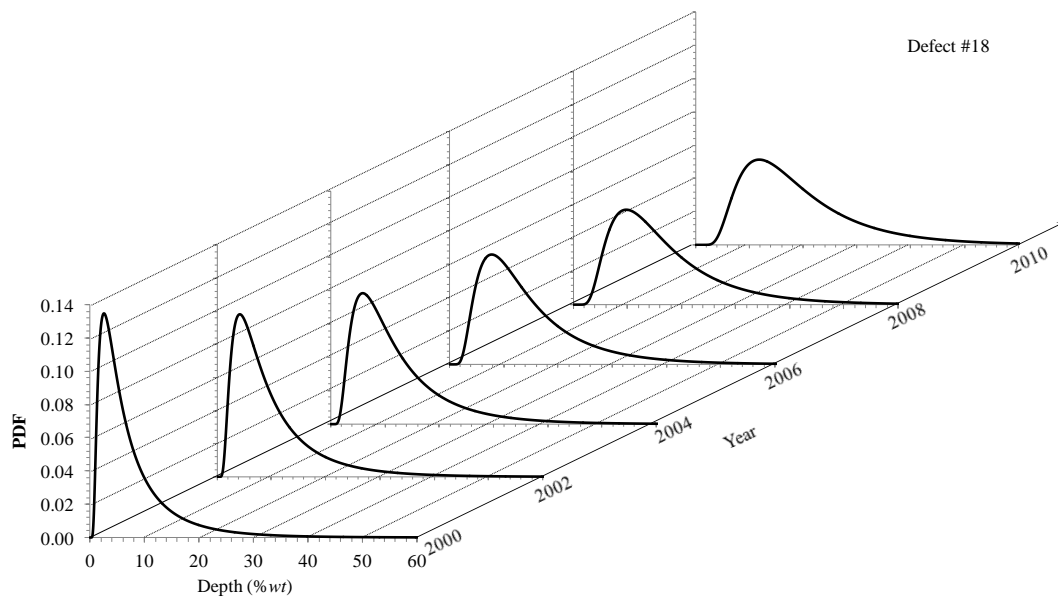
(i)



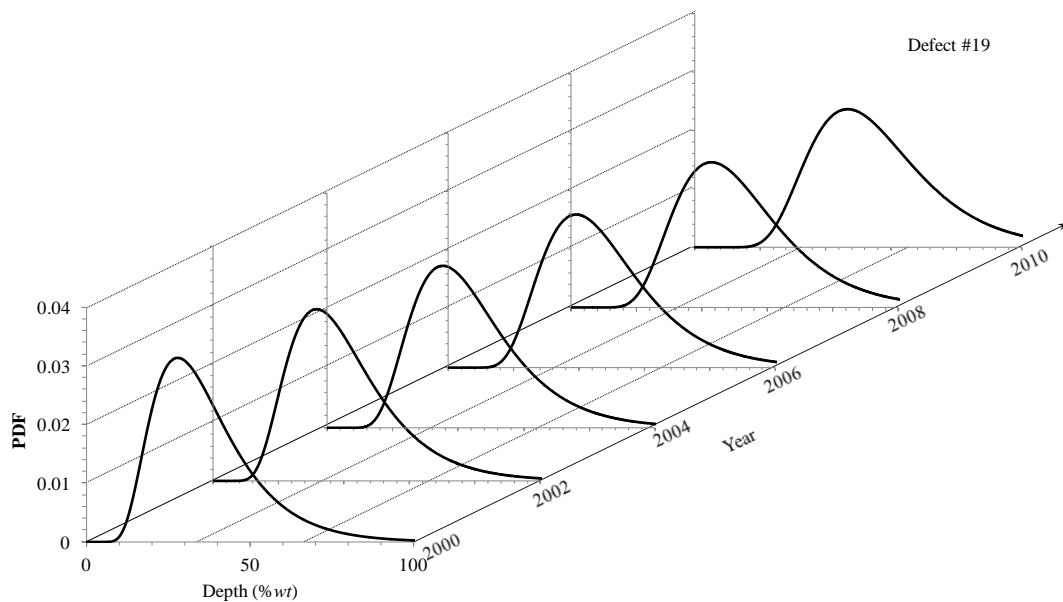
(j)

Figure 3.5 Predicted growth path of a given defect

To illustrate the time-variant nature of the growth model, the PDF curves of defect depths corresponding to years 2000, 2002, 2004, 2006, 2008 and 2010 are depicted in Fig. 3.6(a) for Defect #18 and in Fig. 3.6(b) for Defect #19, respectively. Figure 3.6 indicates that the mean and variance of the predicted depth increase as time increases, which is expected.



(a)



(b)

Figure 3.6 Time-dependent PDF of the defect depth

### 3.5.2 Parametric Analysis

To investigate the impact of the assumptions with respect to the model parameters on the predictive capability of the growth model, three additional scenarios, denoted by



Scenarios II, III and IV, were considered. The parameters  $\alpha$  and  $\xi$  were assumed to be either defect-specific or common in these scenarios. For brevity, the baseline case used to evaluate the results shown in Figs. 3.4 through 3.6 is referred to as Scenario I, where  $\alpha$  is defect-specific and  $\xi$  is common for all defects ( $t_0$  was assumed to be defect-specific for all four scenarios). Table 3.1 summarizes the characteristics of  $\alpha$  and  $\xi$  in the four scenarios. The prior distributions of  $\alpha$  and  $\xi$  used in Scenarios II, III and IV are the same as those specified in Scenario I. The analysis procedure used to evaluate the model parameters in Scenario I were repeated to evaluate the model parameters in Scenarios II through IV. The comparisons of predictions corresponding to the four scenarios are described in the following.

Table 3.1 Comparison of four scenarios for the growth model

Scenario	$\alpha$	$\xi$	$t_0$	Percentage of predictions within actual depth $\pm 10 \% wt$	MSEP $((\% wt)^2)$
I	defect-specific	common	defect-specific	90	43
II	defect-specific	defect-specific		90	45
III	common	common		76	68
IV	common	defect-specific		82	60

The predicted defect depths in 2010 corresponding to Scenarios I through IV are compared with the field-measured depths in Fig. 3.7. The percentages of the predicted depths falling within the actual depths  $\pm 10 \% wt$  for the four scenarios are summarized in Table 3.1. The figure suggests that the predicted depths corresponding to Scenarios III and IV show markedly more deviations from the actual depths compared with those corresponding to Scenario I, whereas the predictions corresponding to Scenario II are slightly different from those corresponding to Scenario I. The mean squared error of prediction (MSEP) (Bunke and Droge 1984; Harville and Jeske 1992) as described in Chapter 2 was employed to quantitatively evaluate the predictive accuracy of each model considered. The higher is the predictive accuracy of a give model, the lower is its corresponding MSEP. The MSEPs associated with Scenarios I, II, III and IV are

summarized in Table 3.1. These results suggest that the growth model corresponding to Scenario I has the highest predictive accuracy followed by II, IV and III in a descending order. Furthermore, the growth models employing defect-specific  $\alpha$  (i.e. Scenarios I and II) on average have a higher predictive accuracy than those employing common  $\alpha$  (i.e. Scenarios III and IV), whereas whether  $\xi$  is defect specific or common for all defects has a small impact on the predictive accuracy of the growth model.

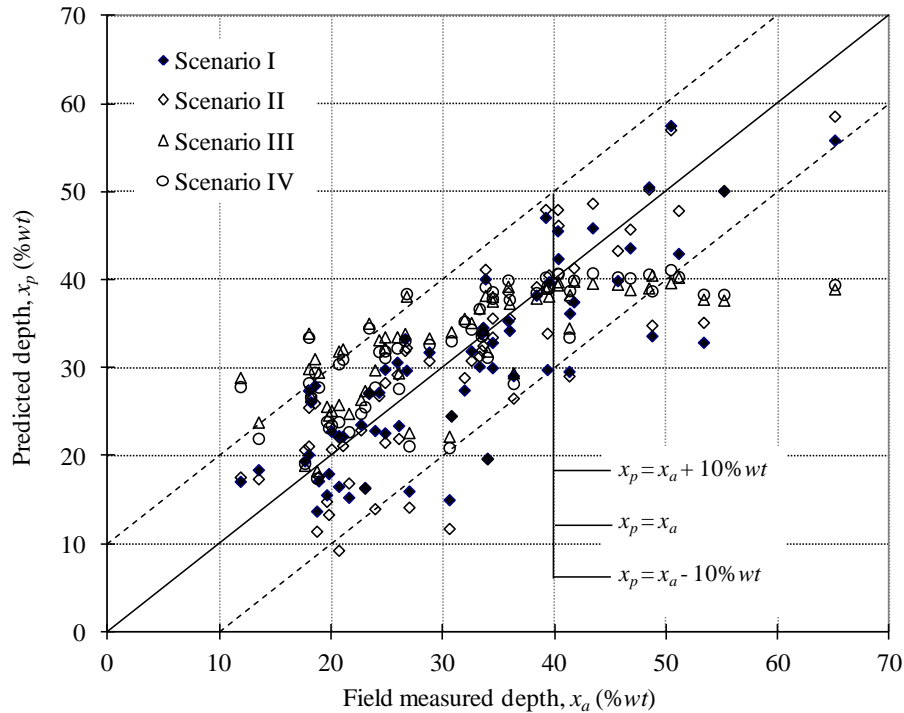
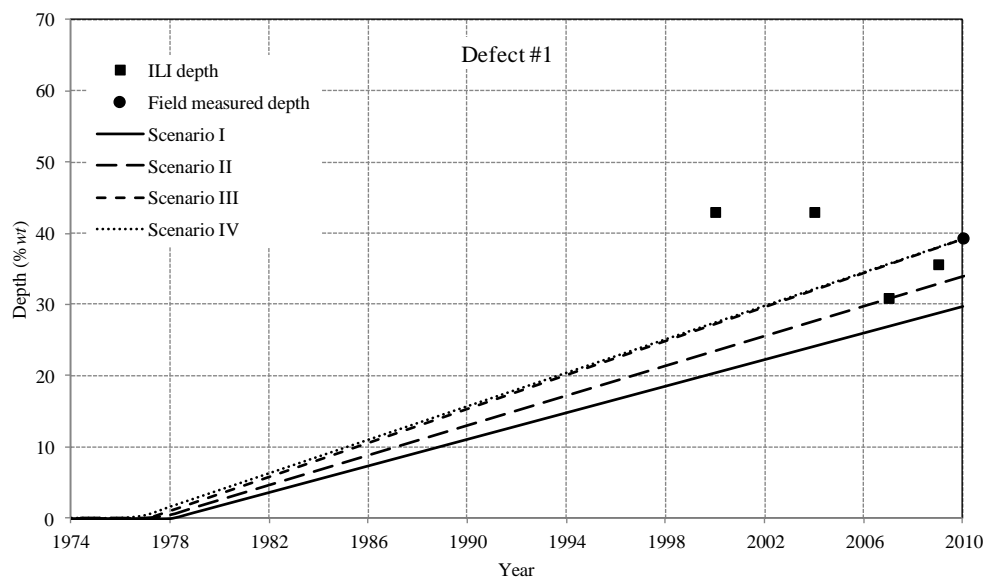


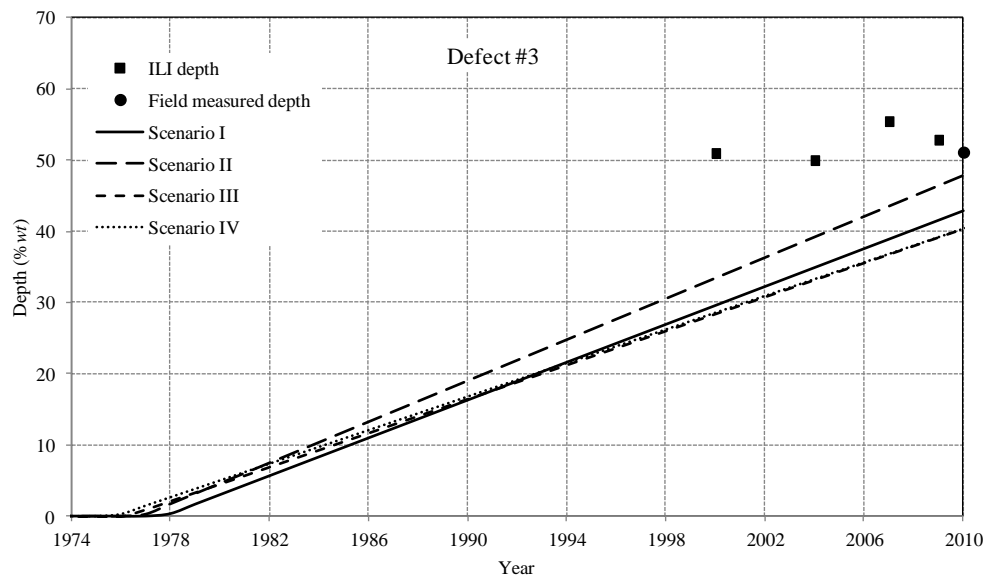
Figure 3.7 Comparison of the mean predicted depth with the field-measured depths corresponding to Scenarios I, II, III and IV

The mean predicted growth paths corresponding to the four scenarios for the same ten defects plotted in Fig. 3.5 are plotted in Figs. 3.8(a) through 3.8(j), respectively. Also shown in the figures are the depths reported by the ILI tools as well as the actual depth obtained from the field measurement. Consistent with the aforementioned observation, Figure 3.8 reveals that predictions corresponding to Scenarios I and II are more accurate than those corresponding to Scenarios III and IV for six (i.e. Defects #3, #13, #15, #19, #50 and #60) of the ten defects shown in the figure. However, the predicted depths for Defects #1, #7 and #22 based on the assumption of defect-specific  $\alpha$  deviate significantly

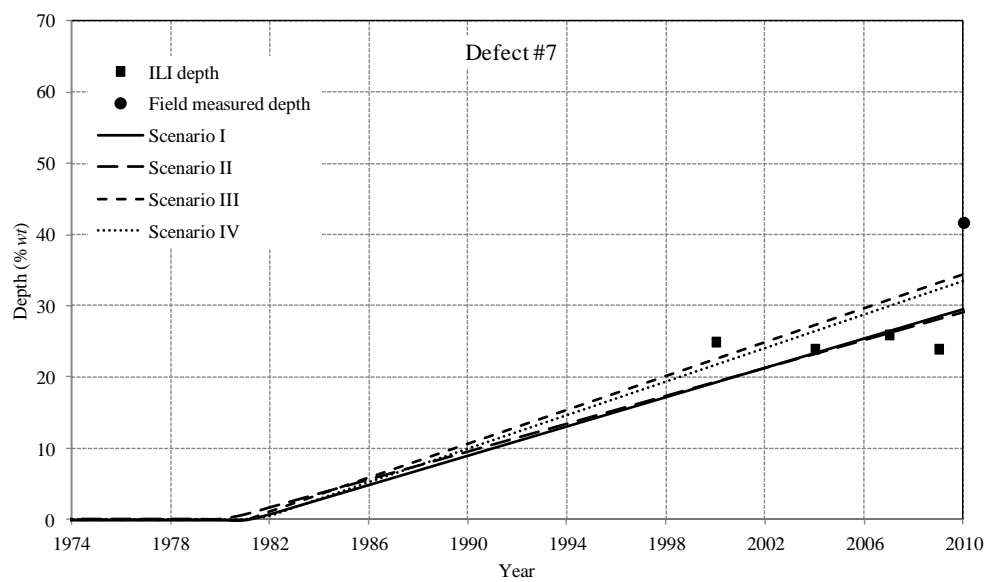
from the actual depths (about 10%, 12% and 15 %wt, respectively). This can be attributed to the slow growth rate as indicated by the ILI data in 2000, 2004 and 2007, which are likely associated with large measurement errors such that the ILI data cannot reflect the actual growth of this particular defect. The deviation of the predicted depth from the field-measured depth however becomes smaller (less than 10 %wt) for Defects #1, #7 and #22 if the parameter  $\alpha$  is assumed to be common for all defects. This implies that the assumption of common  $\alpha$  allows the growth model to borrow information from the other defects and improves to certain extent the accuracy of the prediction for this particular defect.



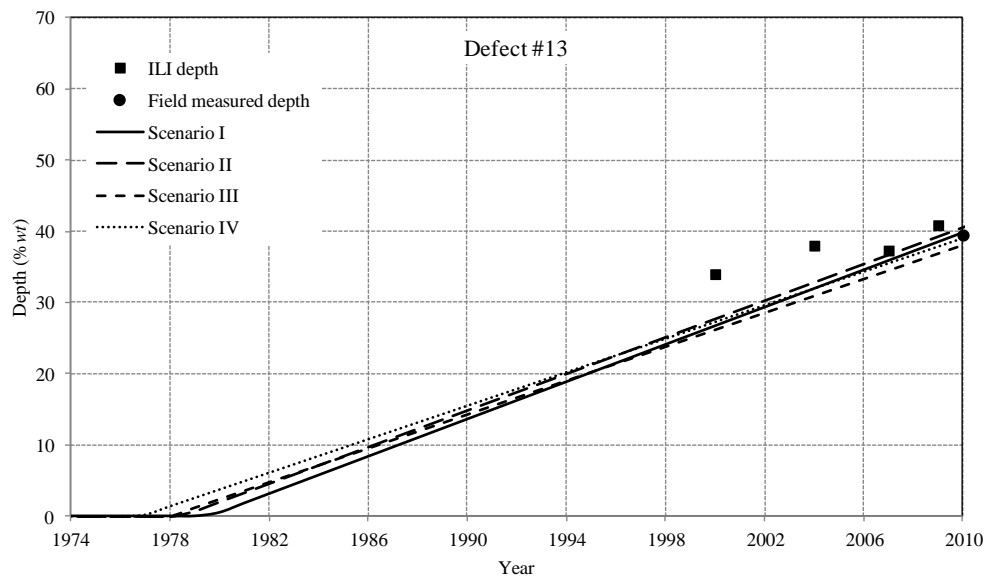
(a)



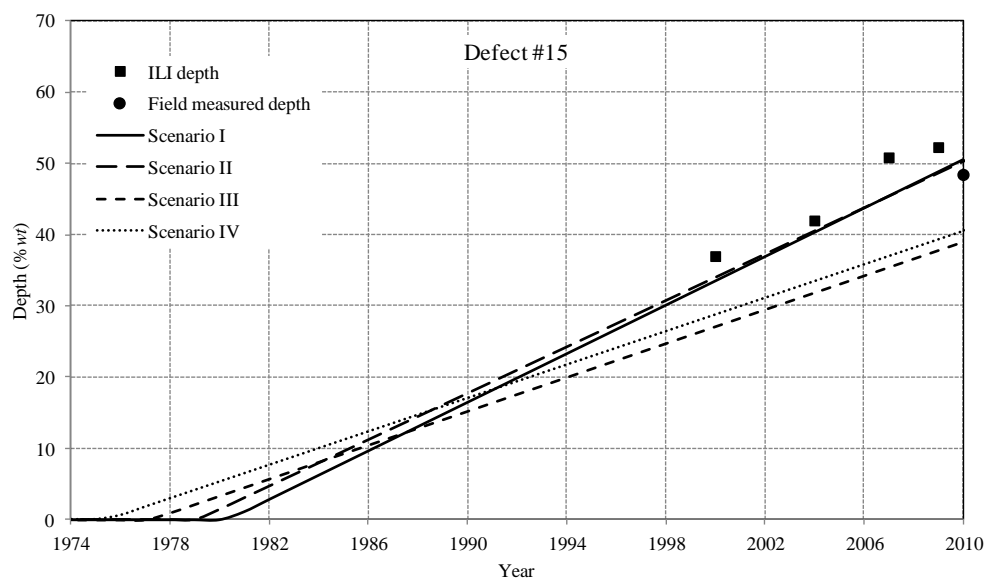
(b)



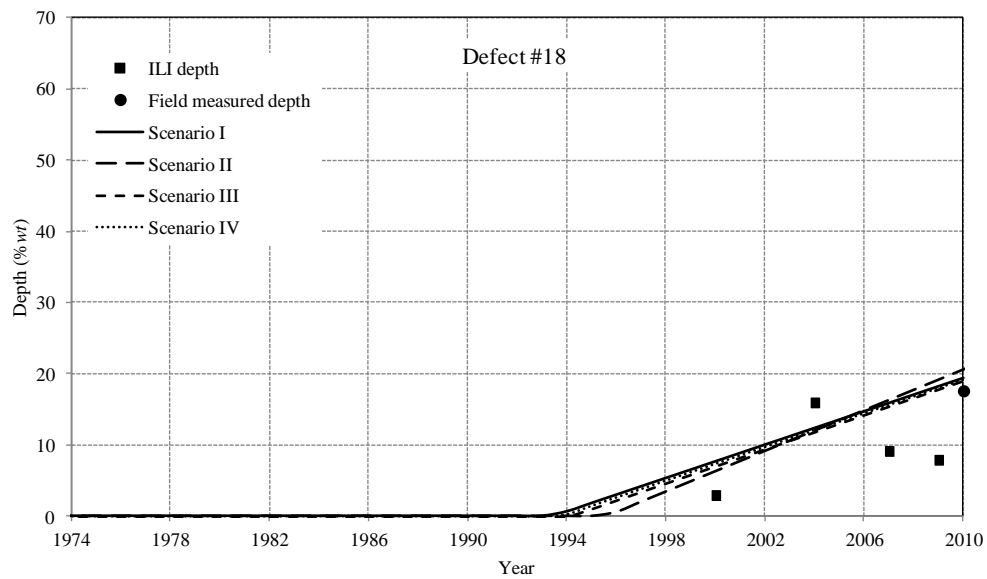
(c)



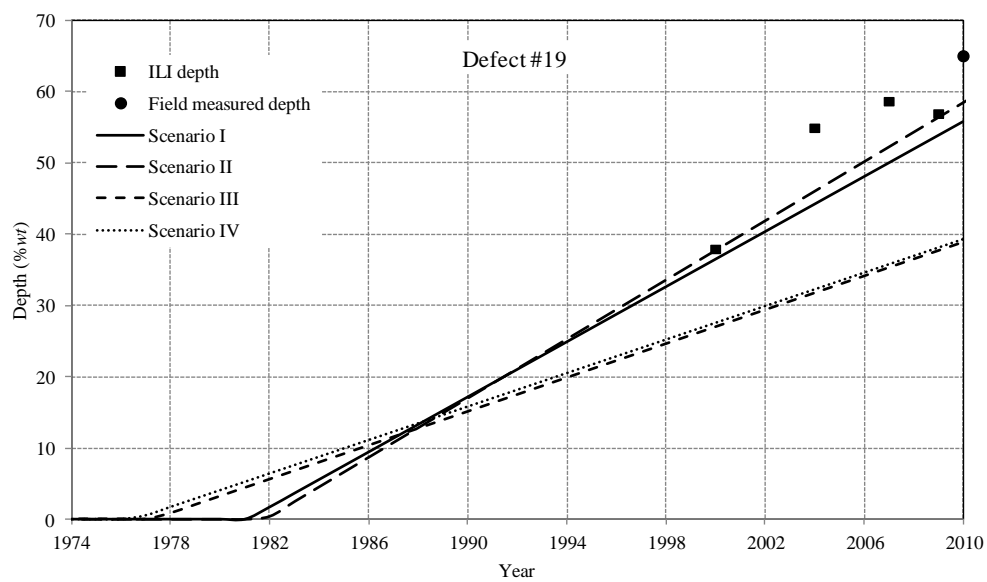
(d)



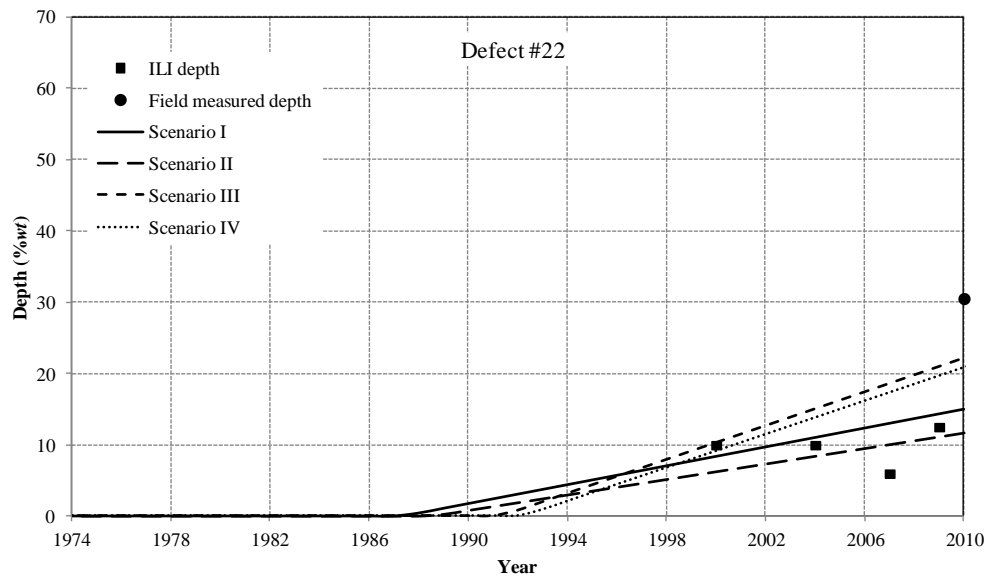
(e)



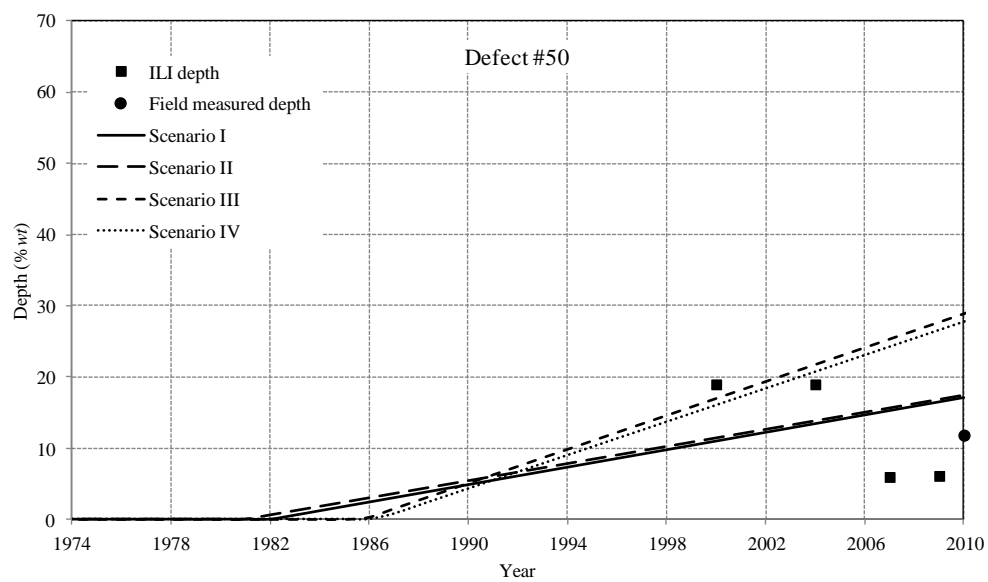
(f)



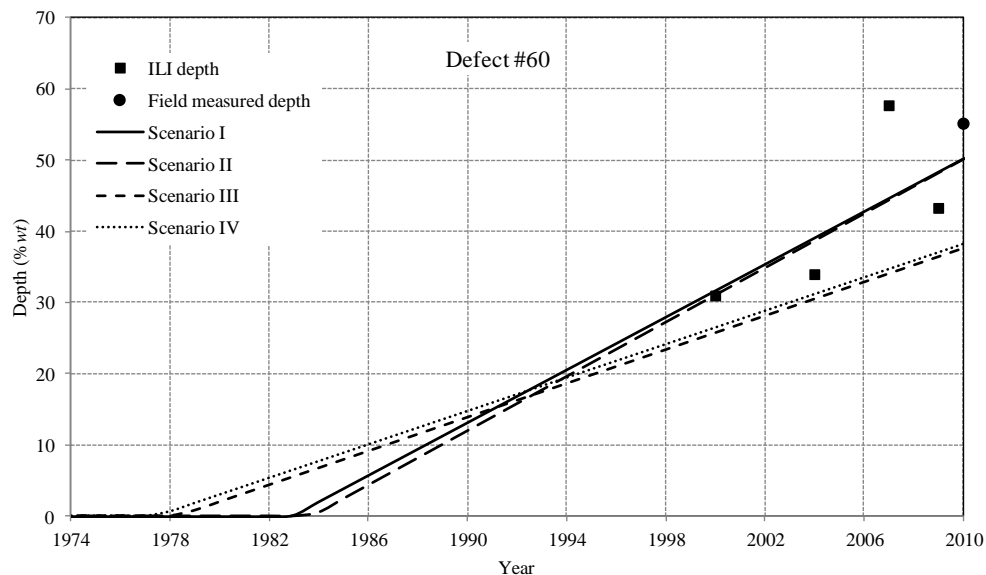
(g)



(h)



(i)



(j)

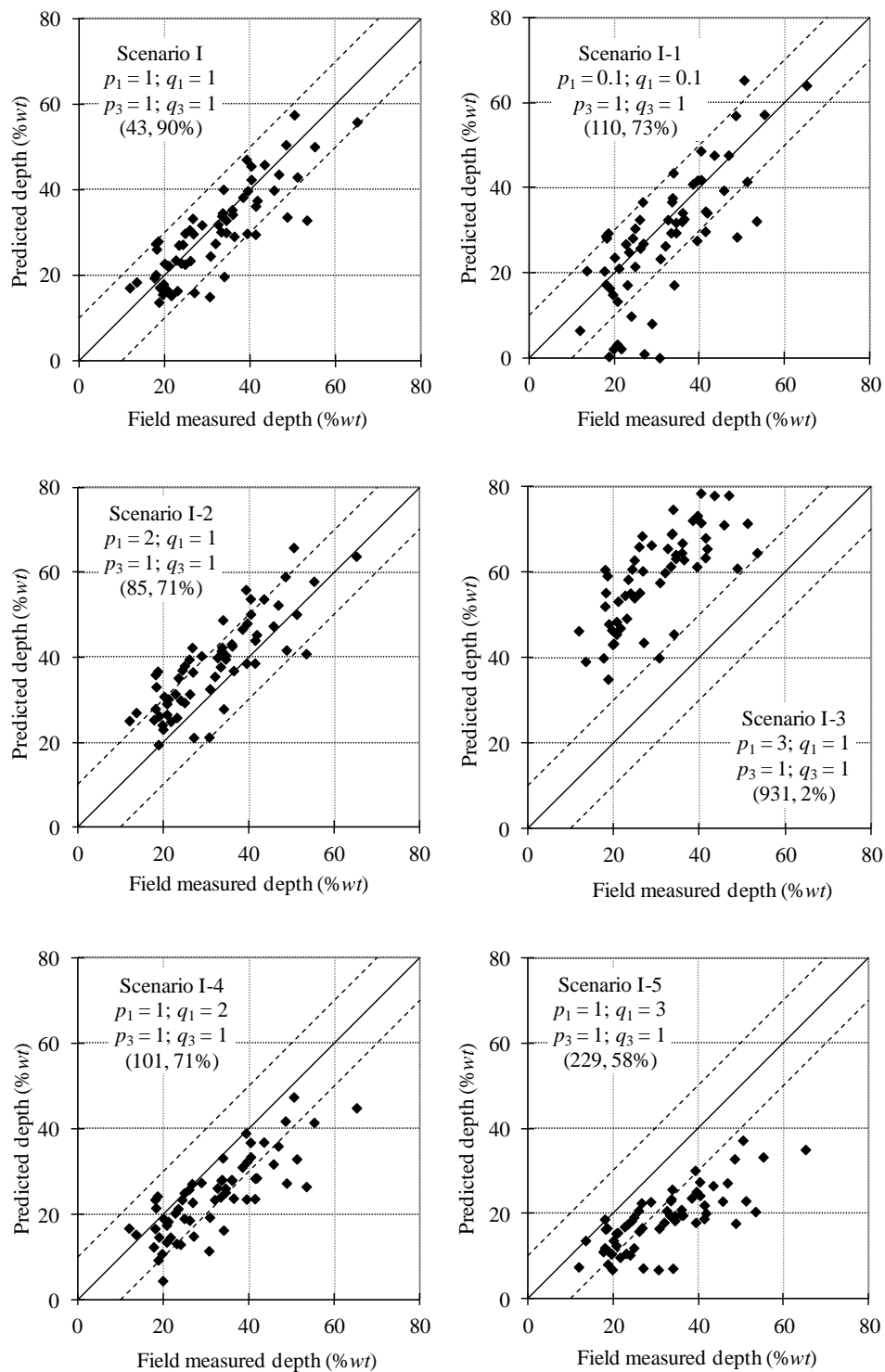
Figure 3.8 Comparison of the mean predicted growth paths corresponding to Scenarios I, II, III and IV

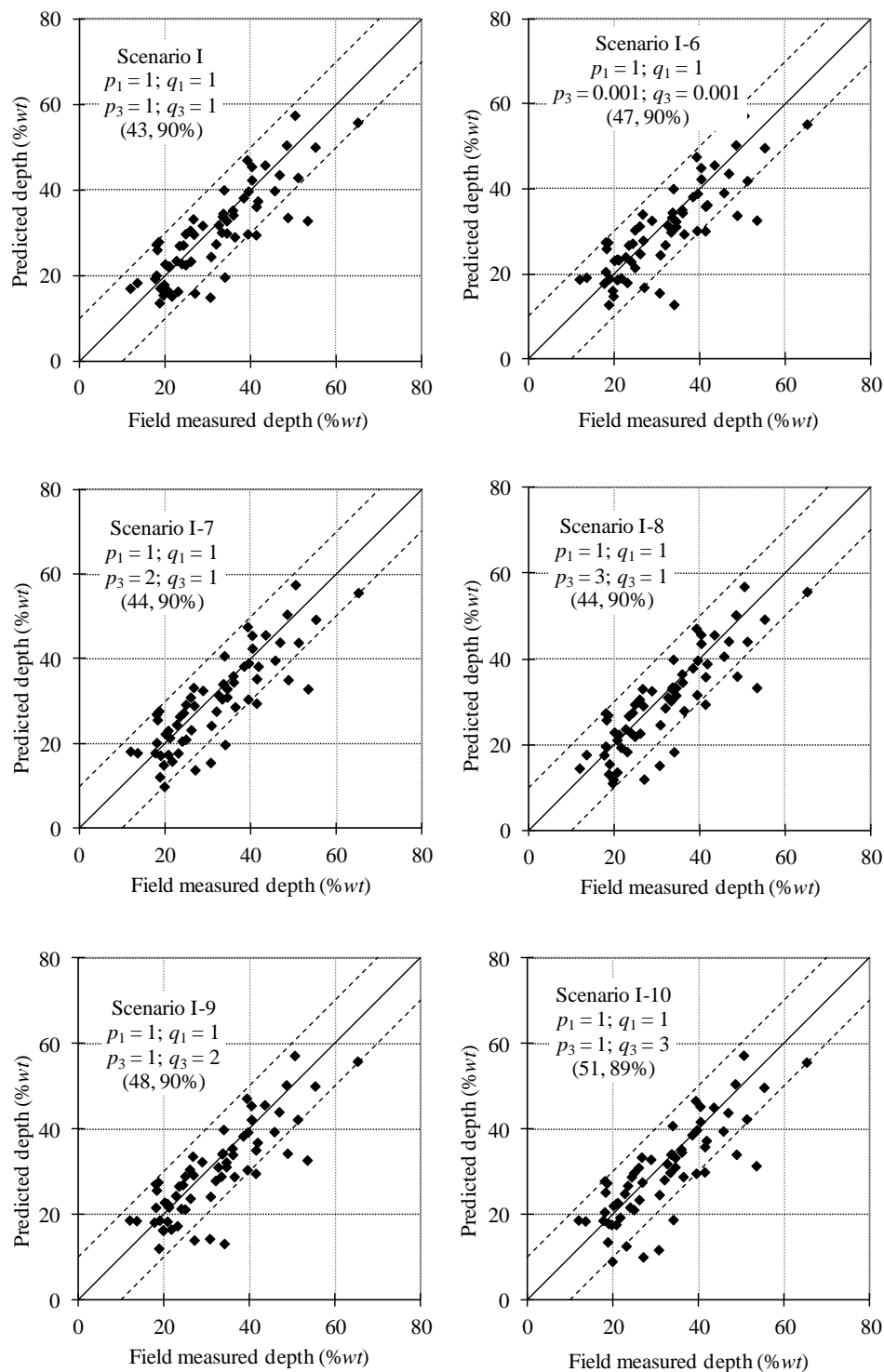
To investigate the impact of the prior distributions of the model parameters on the predictive quality of the growth model, ten scenarios with respect to the prior distributions of  $\alpha$  and  $\xi$  were considered, denoted by Scenarios I-1 through I-10, respectively. The notation was used to emphasize that the ten scenarios are the same as Scenario I except that different values were specified for the distribution parameters (i.e.  $p_1$ ,  $q_1$ ,  $p_3$  and  $q_3$ ) of the prior distributions of  $\alpha$  and  $\xi$ . Figure 3.9 depicts the comparison of the predictions corresponding to Scenarios I and I-1 through I-10. The values of  $p_1$ ,  $q_1$ ,  $p_3$  and  $q_3$  associated with each individual scenario are shown in the figure as well with the two numbers in brackets denoting the MSEP value and percentage of predictions within actual depth  $\pm 10$  %wt (i.e. the two dashed bounding lines in Fig. 3.9) associated with this particular scenario, respectively.

The results shown in Fig. 3.9 indicate that the prediction obtained from Scenario I is the best because its MSEP value is the lowest; it was also observed that the prior distributions specified in Scenario I leads to a good convergence of the MCMC simulation. Figures 3.9(a) and 3.9(b) suggest that the prediction is highly sensitive to the



prior distribution of  $\alpha$  but insensitive to that of  $\xi$ . This observation is expected because the mean predicted depth (i.e.  $\Theta(t) = \alpha(t - t_0)$ ) is only dependent on  $\alpha$  and  $t_0$ . Figure 3.9(a) indicates that a high mean value (i.e.  $p_1/q_1$ ) of the prior distribution of  $\alpha$  tends to overestimate the corrosion growth (e.g. Scenarios I-2 and I-3), whereas a low mean value of the prior distribution of  $\alpha$  tends to underestimate the corrosion growth (e.g. Scenarios I-4 and I-5). This makes sense as the parameter  $\alpha$  represents the mean of growth rate. On the other hand, a large variance (i.e.  $p_1/q_1^2$ ) of the prior distribution of  $\alpha$  also leads to a poor prediction as reflected by a comparison of the predictions corresponding to Scenarios I and I-1 shown in Fig. 3.9(a). For example,  $p_1 = 0.1$  and  $q_1 = 0.1$  in Scenario I-1 and  $p_1 = 3$  and  $q_1 = 1$  in Scenario I-3 imply that the mean and coefficient of variation (COV) of  $\alpha_i$  (i.e. the average growth rate of the  $i^{\text{th}}$  defect) equal 1 %wt/yr and 316% for Scenario I-1, and 3 %wt/yr and 58% for Scenario I-3, respectively. This prior knowledge about the growth rate in both scenarios might be too distant from the realistic scenario to lead to a good convergence of the MCMC simulation as well as good estimate of the posterior distributions. The prior distribution of  $\alpha$  in Scenario I (i.e.  $p_1 = q_1 = 1$ ) implies that the mean and COV of the growth rate equal 1 %wt/yr and 100%, respectively, which are considered reasonably representative of the reality. From this perspective, the prior distribution of  $\alpha$  specified in Scenario I can be regarded, to certain extent, as an informative distribution. Figure 3.9(b) indicates that the impact of the prior distribution of  $\xi$  on the prediction is in general negligible. A non-informative distribution is therefore suggested as the prior distribution of  $\xi$  for the Bayesian inference. The comparison highlights the importance of properly selecting the prior distributions for the Bayesian updating.

(a) Impact of the prior distribution of  $\alpha$  on the predictive quality of the growth model



(b) Impact of the prior distribution of  $\xi$  on the predictive quality of the growth model

Figure 3.9 Impact of the prior distributions of  $\alpha$  and  $\xi$  on the predictive quality of the growth model

### 3.5.3 Comparisons with the GP-based and Conventional Growth Models

In this section, the IGP-based growth model (Scenario I only) was compared with the homogeneous gamma process- (HGP-) based and conventional growth models. The HGP-based model II-1 described in Chapter 2 was used in this comparative study, i.e. the median values of the posterior distributions of the parameters in the HGP-based model were used to predict the defect depth in 2010.

The conventional growth model employed in this study is a deterministic linear growth model with a growth rate that is constant in time and defect-specific, which has been widely adopted by the pipeline operators. The growth rate of a given defect is usually evaluated from the depths reported by two recent ILIs (Nessim et al. 2008; Huysse and van Roodselaar 2010) and is then assumed to remain constant in the future. In this study, the ILI-reported depths in 2004 and 2007 were used to evaluate the defect-specific growth rate. It follows from Eq. (2.3) and the calibrated biases presented in Section 2.6.1 that the growth rate for defect  $i$ , denoted by  $r_i$ , can be estimated by  $r_i = ((y_{i3} - a_3)/b_3 - (y_{i2} - a_2)/b_2)/(t_3 - t_2)$ . Note that the measurement error in the ILI data may cause  $r_i$  to be negative. In this case,  $r_i$  was set to zero because the actual defect depth cannot decrease; the corresponding predicted depth in 2010,  $x_{pi}$ , is then obtained from  $x_{pi} = (y_{i3} - a_3)/b_3 + r_i\Delta t$ , where  $\Delta t$  denotes the interval between the time of the last inspection (i.e. year 2007) up to the time of prediction (i.e. year 2010) and therefore equals three years. The comparison of the predictions for the 62 defects given by the three growth models is depicted in Fig. 3.10. The MSEP value and percentage of predictions within actual depth  $\pm 10\%$  associated with each of the three growth models are also shown in the same figure. The results indicate that the difference between the predictions corresponding to the IGP- and HGP-based models is negligible, whereas the conventional growth model leads to markedly poorer predictions compared with the two Bayesian growth models.

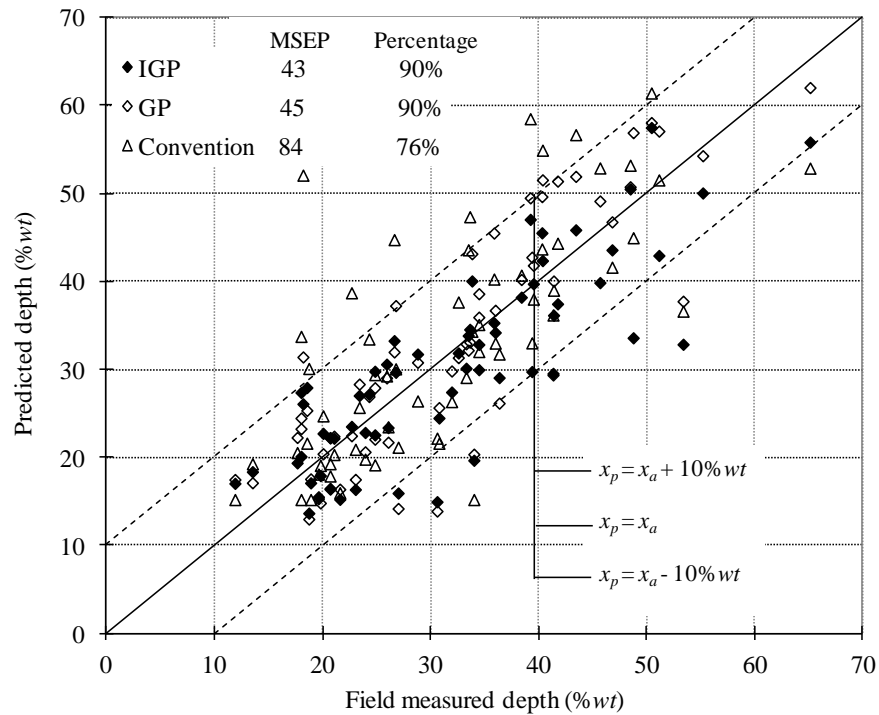


Figure 3.10 Comparison of the predictions of the IGP-, GP-based and conventional models

### 3.6 Conclusions

An inverse Gaussian process-based model was proposed to characterize the growth of depths of metal-loss corrosion defects on underground energy pipelines. The model includes a parameter  $\alpha$  that defines the average growth rate over time, the corrosion initiation time  $t_0$ , and a scale parameter  $\xi$ . All the parameters were assumed to be uncertain and evaluated using the hierarchical Bayesian methodology based on the inspection data obtained from multiple ILI runs. The biases, random scattering errors as well as the correlations between the random scattering errors associated with the ILI tools were accounted for in the Bayesian inference. Markov Chain Monte Carlo simulation techniques were employed to carry out the Bayesian updating and numerically evaluate the posterior distributions of the parameters in the growth model.

The application of the proposed model was illustrated using an example involving real ILI data collected from a natural gas pipeline that is described in Chapter 2. The growth

models were developed for 62 external corrosion defects that have been subjected to multiple ILI runs and were excavated, field measured in ditch and mitigated. The ILI data obtained from the inspections prior to the field measurement were used to carry out the Bayesian updating and evaluate the model parameters in the growth models corresponding to the 62 corrosion defects considered. The median values of the updated model parameters were then used to predict the depths of the defects at the time of the field measurements. The predictive quality of the growth model was validated by comparing the predicted defect depths with the corresponding field-measured depths.

While the corrosion initiation time  $t_0$  was assumed to be defect-specific, four scenarios in which the model parameters  $\alpha$  and  $\xi$  were assumed to be either defect-specific or common for all defects were considered to investigate the impact of these assumptions on the predictive accuracy of the growth model. Scenario I (i.e. the baseline case) assumes that  $\alpha$  is defect-specific and  $\xi$  is common for all defects; Scenario II assumes that  $\alpha$  and  $\xi$  are both defect-specific; Scenario III assumes that  $\alpha$  and  $\xi$  are both common for all defects, and Scenario IV assumes that  $\alpha$  is common for all defects and  $\xi$  is defect-specific.

The analysis results suggest that the model corresponding to the baseline case predicts the growth of the defect depth reasonably well: the absolute deviations of the predicted depths from the field-measured depths are less than or equal to 10 %wt for 90% of the 62 defects. The assumption of defect-specific  $\alpha$  generally leads to a better prediction than the assumption of common  $\alpha$  for all defects regardless of whether  $\xi$  is assumed to be defect-specific or common for all defects. Of the four scenarios considered, the MSEF corresponding to Scenario I is the lowest, which indicates the highest predictive accuracy; the MSEF corresponding to Scenario II is only marginally higher than that of Scenario I. On the other hand, the MSEFs corresponding to Scenarios III and IV (both assuming  $\alpha$  common for all defects) are markedly higher than those of Scenarios I and II. Sensitivity analysis suggests that the prior distribution of  $\alpha$  has a significant impact on the predictive accuracy of the growth model whereas the impact of the prior distribution of  $\xi$  on the predictive accuracy is negligible. The proposed model provides a viable

alternative to predict the corrosion growth on energy pipelines based on imperfect inspection data and will facilitate the corrosion management of pipelines.

## Reference

- Al-Amin, M., Zhou, W., Zhang, S., Kariyawasam, S. and Wang, H. (2012). Bayesian model for the calibration of ILI tools. Proceedings of IPC 2012, IPC2012-90491, ASME, Calgary, Canada.
- Bunke, O. and Droge, B. (1984). Estimators of the mean squared error of prediction in linear regression. *Technometrics*, 26: 145-155.
- Chikkara, R. S. and Folks, J. L. (1989). *The Inverse Gaussian Distribution: Theory, Methodology and Application*. Marcell Dekker, New York.
- Gelman, A., Carlin, J. B., Stern, H. S. and Rubin, D. B. (2004) *Bayesian Data Analysis*, (2nd edition). Chapman & Hall/CRC, NY.
- Harville, D. A. and Jeske, D. R. (1992). Mean squared error of estimation or prediction under a general linear model. *Journal of the American Statistical Association*, 87: 724-731.
- Huyse, L. and van Roodselaar, A. (2010). Effects of inline inspection sizing uncertainties on the accuracy of the largest features and corrosion rate statistics. Proceedings of 8th International Pipeline Conference, ASME, Calgary, Alberta, Canada, 403-413.
- Johnson, N. L., Kotz, S. and Balakrishnan, N. (1994). *Continuous Univariate Distributions*. Vol. 1, Wiley Series in Probability and Mathematical Statistics: Applied Probability and Statistics, (2nd edition), John Wiley & Sons, NY.
- Kroes, D. P., Taimre, T. and Botev, Z. I. (2011). *Handbook of Monte Carlo Methods*. John Wiley & Sons, Inc., NJ.
- Lunn, D., Spiegelhalter, D., Thomas, A. and Best, N. (2009). The BUGS project: evolution, critique and future directions (with discussion). *Statistics in Medicine*, 28: 3049-82.

- Nessim, M., Dawson, J., Mora, R. and Hassanein, S. (2008). Obtaining corrosion growth rates from repeat in-line inspection runs and dealing with the measurement uncertainties, Proceedings of 7th International Pipeline Conference, ASME, Calgary, Alberta, Canada, 593-600.
- Qin, H., Zhang, S. and Zhou, W. (2013). Inverse Gaussian process-based corrosion growth modeling and its application in the reliability analysis for energy pipelines. *Frontiers of Structural and Civil Engineering*, 7(3): 276-287.
- Seshadri, V. (1999). *The Inverse Gaussian Distribution: Statistical Theory and Application*. Springer, NY.
- Spiegelhalter, D. J. (1998). Bayesian graphic modeling: A case-study in monitoring health outcomes. *Applied Probability and Statistics*, 47: 115-33.
- van Noortwijk, J. M. (2009). A survey of the application of gamma process in maintenance. *Reliability Engineering and System Safety*, 94: 2-21.
- Wang, X. and Xu, D. (2010). An inverse Gaussian process model for degradation data. *Technometrics*, 52(2): 188-197.
- Wang, X. (2010). Wiener processes with random effects for degradation data. *Journal of Multivariate Analysis*, 101: 340-351.



## **Chapter 4 Geometric Brownian Motion-based Corrosion Growth Modeling Based on Imperfect Inspection Data**

### **4.1 Introduction**

The use of the Markov chain, gamma process and inverse Gaussian process to model the metal-loss corrosion growth on pipelines has been reported in the literature (e.g. Hong 1999; Valor et al. 2007; Timashev et al. 2008; Caleyó et al. 2009; Zhou et al. 2012; Zhang et al. 2013). In particular, the Bayesian methodology has been employed to evaluate the parameters of the gamma and inverse Gaussian processes-based corrosion growth models using in-line inspection (ILI) data that are associated with measurement errors, which has been described in Chapters 2 and 3, respectively.

The gamma and inverse Gaussian processes-based models respectively assume that the corrosion process consists of a series of independent gamma- and inverse Gaussian-distributed increments, which are also independent of the state of corrosion (e.g. the overall defect depth and length at a given time) (Zhang et al. 2012; Zhang and Zhou 2013; Zhang et al. 2013). Both models are therefore referred to as the state-independent model (Guida and Pulcini 2013). The Markov chain- (MC-) based models reported by Hong (1999) and Caleyó et al. (2009) assume the corrosion process as a transition of a series of discrete damage states, governed by the so-called transition probability function. These models imply that the corrosion increment depends on the current corrosion state (referred to as the state-dependent model). The main limitations of the MC-based models include (1) the accuracy of the model is sensitive to the total number of discrete damage states (Hong 1999, Guida and Pulcini 2011), and (2) it is not straightforward to evaluate the transition probability function when the inspection data are imperfect.

Recently, an inverse gamma process-based model, as an alternative to the MC-based model, was reported by Guida and Pulcini (2013) to characterize the state-dependent deterioration process. The inverse gamma process-based model does not require discretization of the damage state or evaluation of the transition probability function (Guida and Pulcini 2013); however, this model is somewhat complex because a

complicated expression of the state-dependent conditional probability density function (PDF) of the increments is involved.

The Brownian motion (or Wiener process) and geometric Brownian motion have been widely reported for modeling degradation (e.g. Whitemore and Schenkelberg 1997; Park and Padgett 2005; Gebraeel and Pan 2008; Wang 2010; Ye et al. 2012). The geometric Brownian motion differs from the Brownian motion in that the former characterizes the logarithm of the degradation as a Brownian motion. However, a notable drawback of using both the Brownian motion and geometric Brownian motion to model the corrosion growth is that they cannot rigorously characterize the monotonic nature of growth, since the Gaussian-distributed increments of a Brownian motion can be either positive or negative.

To evaluate the reliability of bridge beams with degrading capacities, Elsayed and Liao (2004) employed the geometric Brownian motion to characterize the degradation rate; that is, the logarithm of the degradation rate of the bridge beam capacity was characterized by a Brownian motion. This model ensures the degradation process to be monotonic, which is an improvement over the previously proposed Brownian motion-based degradation models. Furthermore, the current growth rate depends on the previous growth rate, which implicitly makes the growth rate dependent on the current state of the degradation; therefore, the model is state-dependent. The maximum likelihood method was used to estimate the model parameters using the degradation data subjected to measurement error. Note that the measurement error considered in the study is somewhat simplistic, represented by a Gaussian-distributed additive random term with a mean of zero and a standard deviation that is invariant among different inspections. The potential bias in the inspection data as well as the correlation between the measurement errors associated with different inspections were not considered.

It is observed that the state-dependent growth models for corrosion on underground steel pipelines reported in the literature are all based on Markov chains and therefore have notable drawbacks as discussed above. Motivated by this observation, the geometric Brownian motion is explored in this study for characterizing the growth rate of

depths of corrosion defects on underground pipelines. Compared with the work of Elsayed and Liao (2004), the present work is novel in the following four aspects. First, the corrosion initiation time is incorporated in the growth model. Second, the model is applicable to individual defects, i.e. defect-specific. This is more advantageous than, for example, a segment-specific growth model in that the defect-specific model takes into account the heterogeneity of the corrosion data along the pipeline and facilitates the identification of the critical defects. Third, a realistic characterization of the measurement error associated with the inspection data is incorporated in the model, which includes the bias, random scattering error and correlation between the random scattering errors associated with different inspections. Finally, the model is formulated in a hierarchical Bayesian framework, and the Markov Chain Monte Carlo (MCMC) simulation techniques are used to evaluate the probabilistic characteristics of the model parameters by incorporating inspection data obtained from multiple ILI runs.

The chapter is organized as follows. Section 4.2 gives a brief description of the standard Brownian motion, the usual form of the Brownian motion-based degradation model as well as the geometric Brownian motion-based degradation rate model. Sections 4.3 and 4.4 present the Bayesian updating of the corrosion growth model and the methodology to predict the defect growth, respectively. An example involving ILI data collected from a real in-service natural gas pipeline to illustrate and validate the proposed growth model is given in Section 4.5, followed by conclusions in Section 4.6.

## **4.2 Brownian Motion-based Degradation Model**

### **4.2.1 Standard Brownian Motion**

A standard Brownian motion (or Wiener process) is a continuous-time stochastic process  $W = \{W(t); t \geq 0\}$  with the following properties (Beichelt and Fatti 2002).

- (1)  $W$  has a continuous path with  $W(0) = 0$  and  $W(t) \in (-\infty, +\infty)$ ;

(2)  $W$  has stationary and independent increments. In other words, for any  $t_1 < t_2 \leq t_3 < t_4$ ,  $W(t_2) - W(t_1)$  and  $W(t_4) - W(t_3)$  are independent normally distributed with zero mean and variances equal to  $t_2 - t_1$  and  $t_4 - t_3$ , respectively, and

(3)  $W$  is a Gaussian process: for all  $t > 0$ ,  $W(t)$  is normally distributed with a mean of zero and a variance of  $t$ .

#### 4.2.2 Usual Form of Brownian Motion-based Degradation Model

Consider a degradation process  $\{X(t) > 0; t > 0\}$ . The well-adopted form of the Brownian motion-based model to characterize  $X(t)$  is (e.g. Whitmore and Schenkelberg 1997; Wang 2010):

$$X(t) = A(t) + \sigma W(t) \quad (4.1)$$

where  $A(t)$  is the drift term, a positive and non-decreasing deterministic function of time, e.g.  $A(t) = \lambda t$ , with  $\lambda$  ( $\lambda > 0$ ) denoting the deterministic drift parameter;  $\sigma$  denotes the diffusion parameter, and  $W(t)$  is the standard Brownian motion defined in Section 4.2.1. Equation (4.1) indicates that  $X(t)$  is a Brownian motion with independent increments  $\Delta X(t) = X(t + \Delta t) - X(t)$ , where  $\Delta X(t)$  is normally distributed and has a mean of  $\Delta A(t) = A(t + \Delta t) - A(t)$  and a variance of  $\sigma^2 \Delta t$ . Furthermore, Equation (4.1) implies that the mean of the degradation trajectory (i.e.  $A(t)$ ) is positive and monotonic increasing over time; however, a particular realization of the degradation trajectory given by Eq. (4.1) is not necessarily both positive and monotonically increasing, as shown in Figure 4.1, which illustrates five realizations of the Brownian motion characterized by Eq. (4.1) with  $\lambda$  and  $\sigma^2$  equal to 0.5 and 4, respectively, as well as the mean of the Brownian motion (i.e.  $A(t)$ ). Therefore, this model cannot properly characterize the positive and monotonically increasing nature of corrosion growth.

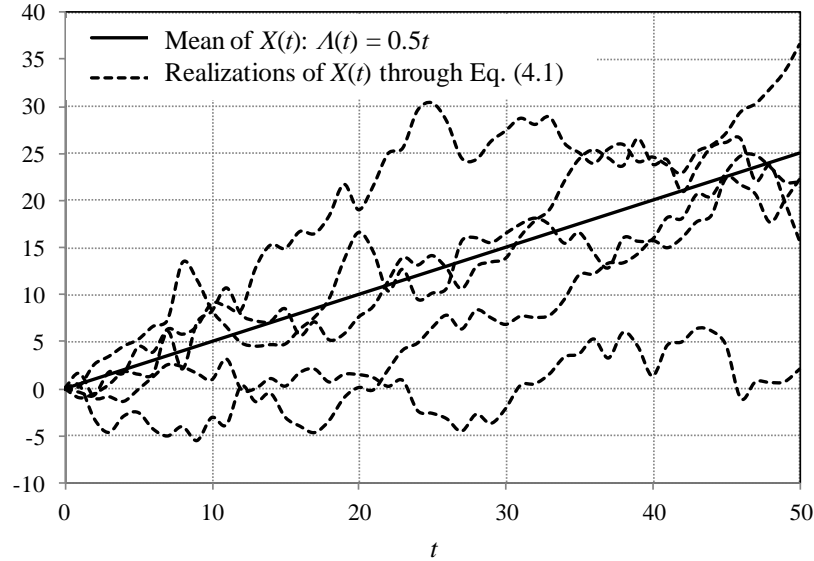


Figure 4.1 Illustration of realizations of the Brownian motion

Considering that the desirable model to characterize the degradation process must be positive, Park and Padgett (2005) proposed the geometric Brownian motion to model the degradation process. In this model, the logarithm of  $X(t)$  is defined as a Brownian motion, that is

$$\ln(X(t)) = \Lambda(t) + \sigma W(t) \quad (4.2)$$

where  $\ln(X(t))$  has the same properties as those of  $X(t)$  indicated by Eq. (4.1). It can be inferred that the model given by Eq. (4.2) still does not guarantee  $X(t)$  to be monotonically increasing although it ensures  $X(t)$  to be positively defined. To overcome the underlying drawbacks of the degradation models given by Eqs. (4.1) and (4.2), the geometric Brownian motion-based growth rate model developed by Elsayed and Liao (2004) is used in this study and described in the following sections.

#### 4.2.3 Geometric Brownian Motion-based Growth Rate Model

The geometric Brownian motion-based growth rate (GBMGR) model is different from Eqs. (4.1) and (4.2) in that the GBMGR model characterizes the growth rate of the defect depth as a geometric Brownian motion.

Elsayed and Liao (2004) proposed that the instantaneous degradation rate at time  $t$ ,  $r(t)$ , be given by

$$r(t) = r_0 \exp(\beta t + \sigma W(t)) \quad (4.3a)$$

i.e.

$$\ln(r(t)) = \ln(r_0) + \beta t + \sigma W(t) \quad (4.3b)$$

where  $r_0$  denotes the initial degradation rate, and  $\beta$  and  $\sigma$  denote the drift and diffusion parameters, respectively. Implicit in Eq. (4.3b) is that  $\ln(r(t_2)) - \ln(r(t_1)) = \beta \Delta t + \sigma W(\Delta t)$  with  $\Delta t = t_2 - t_1$  and  $t_2 > t_1$ . It follows that the logarithm of the instantaneous degradation rate at the present time  $t_2$ ,  $\ln(r(t_2))$ , can be related to that at the previous time  $t_1$ ,  $\ln(r(t_1))$ , through the Brownian motion given by Eq. (4.1); that is,  $\ln(r(t_2)) = \ln(r(t_1)) + \beta \Delta t + \sigma W(\Delta t)$ . This implies that  $r(t_2)$  is dependent on the current state of the degradation; therefore, the GBMGR model is a state-dependent model.

If the ILI data are available from multiple inspections, characterization of the growth of the corrosion defect can be established from the perspective of modeling the instantaneous growth rate at times of the inspections based on the GBMGR model described above. The GBMGR model adopted in this study to characterize the growth of corrosion defects on pipelines is described as follows.

Suppose that  $m$  active corrosion defects on a given pipeline have been inspected  $n$  times. Let  $x_{ij}$  denote the actual depth (i.e. in the through pipe wall thickness direction) of defect  $i$  at the time of the  $j^{\text{th}}$  inspection,  $t_{ij}$ . In practice, the time interval between two consecutive inspections is not necessarily constant (see Figure 4.2). Two key assumptions are involved in this model. First, the instantaneous growth rate at time  $t_{i,j-1}$ , denoted by  $r_{i,j-1}$ , is greater than zero and remains constant between the time interval  $\Delta t_{i,j-1} = t_{ij} - t_{i,j-1}$  ( $j = 1, 2, 3, \dots, n$ ) with  $t_{i0}$  denoting the initiation time of defect  $i$ ; that is,  $r_{i,j-1}$  equals the average growth rate within  $\Delta t_{i,j-1}$  and  $r_{i,j-1} = (x_{ij} - x_{i,j-1})/\Delta t_{i,j-1}$ . This assumption implies that the actual growth path is approximated by a piecewise linear path defined based on the inspection intervals; the constant growth rate within a given inspection

interval is considered a reasonable practical choice, as long as the inspection interval is not too long (say,  $\leq 5$  years). Second, the differences of the logarithms of  $r_{ij}$  and  $r_{i,j-1}$ , denoted by  $\eta_{ij}$  ( $j = 1, 2, 3, \dots, n-1$ ), are independent and normally-distributed with a mean of  $\beta\Delta t_{i,j-1}$  and a variance of  $\sigma^2\Delta t_{i,j-1}$  ( $\beta$  and  $\sigma^2$  are constant but uncertain parameters), i.e.  $\eta_{ij} \sim N(\beta\Delta t_{i,j-1}, \sigma^2\Delta t_{i,j-1})$ , with  $N(\bullet)$  denoting the normal distribution function. The notations are schematically illustrated in Figure 4.2. For simplicity,  $r_{i0}$  and  $\eta_{ij}$  shown in Figure 4.2 are referred to as the initial average growth rate and the random noise of the average growth rate, respectively.

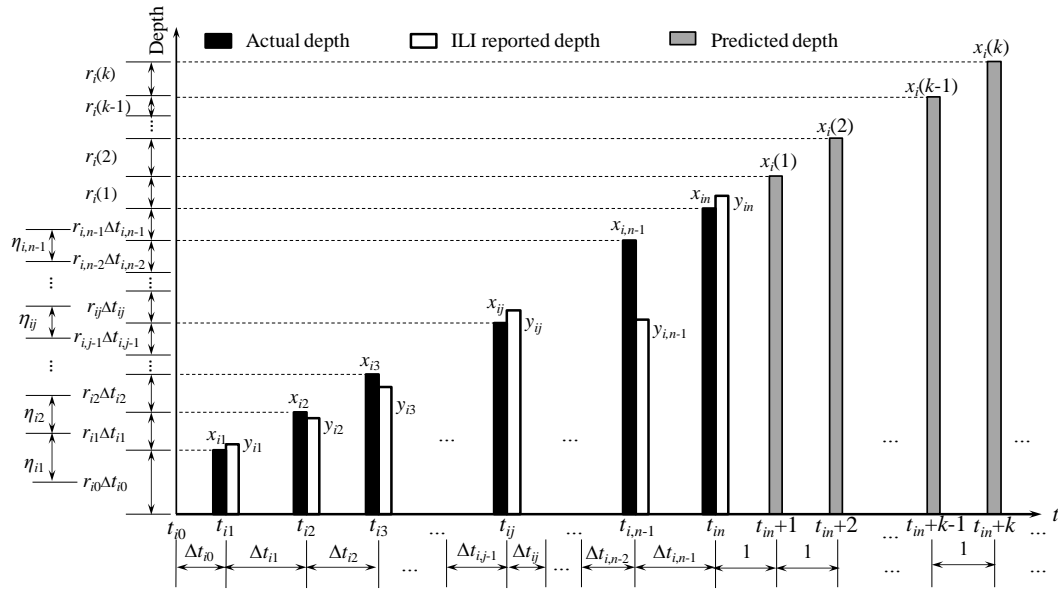


Figure 4.2 Illustration of notations

It follows from the above-mentioned assumptions and Eq. (4.3) that  $\ln(r_{ij})$ , as indicated by Eq. (4.4), can be characterized by a Brownian motion:

$$\ln(r_{ij}) = \ln(r_{i,j-1}) + \beta\Delta t_{i,j-1} + \sigma W(\Delta t_{i,j-1}) \quad (j = 1, 2, 3, \dots, n-1) \quad (4.4)$$

where the drift parameter  $\beta$  defines the deterministic trend in the difference between the logarithms of average growth rates corresponding to two consecutive inspection intervals (i.e.  $\ln(r_{ij})$  and  $\ln(r_{i,j-1})$ ); the standard Brownian motion  $W(t)$  characterizes the random noise in the change from  $\ln(r_{i,j-1})$  to  $\ln(r_{ij})$ , and the diffusion parameter  $\sigma$  is a scaling factor that quantifies the uncertainty in the random noise, i.e.  $\sigma^2\Delta t_{i,j-1}$  being the variance

of the random noise. Note that as per the definition of  $W(t)$  the variance of the random noise increases linearly with the length of the time interval between the current and previous inspections, which appears reasonable given that the growth rate is averaged over the time interval.

Given a realization of  $\ln(r_{i,j-1})$ ,  $\beta$  and  $\sigma$ , Equation (4.4) indicates that  $\ln(r_{ij})$  follows a normal distribution with a mean of  $\ln(r_{i,j-1}) + \beta\Delta t_{i,j-1}$  and a variance of  $\sigma^2\Delta t_{i,j-1}$ , i.e.  $\ln(r_{ij}) \sim N(\ln(r_{i,j-1}) + \beta\Delta t_{i,j-1}, \sigma^2\Delta t_{i,j-1})$ . This normal distribution essentially defines the transition probability from  $\ln(r_{i,j-1})$  to  $\ln(r_{ij})$ . It follows that  $r_{ij}$  is lognormally distributed with the mean and variance, denoted by  $E[r_{ij}]$  and  $V[r_{ij}]$  respectively, expressed as

$$E[r_{ij}] = r_{i,j-1} \exp\left(\left(\beta + \frac{1}{2}\sigma^2\right)\Delta t_{i,j-1}\right) \quad (4.5a)$$

$$V[r_{ij}] = (r_{i,j-1})^2 \exp\left((2\beta + \sigma^2)\Delta t_{i,j-1}\right) [\exp(\sigma^2\Delta t_{i,j-1}) - 1] \quad (4.5b)$$

The depth at the time of the  $j^{\text{th}}$  inspection,  $x_{ij}$ , can be calculated through

$$x_{ij} = x_{i,j-1} + r_{i,j-1}\Delta t_{i,j-1} \quad (4.6)$$

where the defect depth at  $t = t_{i0}$  (i.e.  $x_{i0}$ ) is assumed to equal zero with a probability of one.

It must be emphasized that Eq. (4.4) should be interpreted as  $r_{ij}$  following a lognormal distribution, given  $\beta$  and  $\sigma$ , and a realization of  $r_{i,j-1}$ . Equation (4.5a) indicates that different combinations of the values of  $\beta$  and  $\sigma$  can lead to  $E[r_{ij}]$  equal to, greater than or less than  $r_{i,j-1}$ , which implies that the GBMGR model, as pointed out by Elsayed and Liao (2004), is able to characterize a linear, an accelerating, and a decelerating mean growth path; however, a specific assumption about the mean growth path is not required. From this standpoint, this model is more flexible than the gamma process- and inverse Gaussian process-based models reported in the literature (Pandey et al. 2009; Zhang and Zhou 2013; Zhang et al. 2013) in that the latter models typically assume the mean growth path to be a linear or power-law function of time. The GBMGR model is also more advantageous than the Markov chain models developed by Hong (1999) and Caleyó et al.



(2009) in that it does not require discretizing the damage state or evaluating the transition probability. The GBMGR model proposed in this study is considered suitable for pipelines for which multiple (say,  $\geq 3$ ) sets of ILI data are available and the inspection interval is not too long (say,  $\leq 5$  years). Such pipelines are not uncommon in practice.

### 4.3 Bayesian Updating of the Growth Model

#### 4.3.1 Likelihood Function

Denote  $\mathbf{y}_i = (y_{i1}, y_{i2}, \dots, y_{ij}, \dots, y_{in})'$  and  $\boldsymbol{\eta}_i = (\eta_{i0}, \eta_{i1}, \dots, \eta_{i,n-1})'$ , with “'” representing transposition. For defect  $i$ , it follows from the relationship between the measured and actual depths defined by Eq. (2.8) in Chapter 2 that the likelihood function of the inspection data,  $\mathbf{y}_i$ , conditional on  $r_{i0}$ ,  $\boldsymbol{\eta}_i$  and  $t_{i0}$  can be expressed as:

$$L(\mathbf{y}_i | r_{i0}, \boldsymbol{\eta}_i, t_{i0}) = (2\pi)^{-\frac{n}{2}} |\boldsymbol{\Sigma}_{E_i}|^{-\frac{1}{2}} \exp\left(-\frac{1}{2}(\mathbf{y}_i - (\mathbf{a} + \mathbf{b}\mathbf{x}_i))' (\boldsymbol{\Sigma}_{E_i})^{-1} (\mathbf{y}_i - (\mathbf{a} + \mathbf{b}\mathbf{x}_i))\right) \quad (4.7)$$

where  $\mathbf{a} = (a_1, a_2, \dots, a_n)'$ ;  $\mathbf{b}$  is an  $n$ -by- $n$  diagonal matrix with the  $j^{\text{th}}$  element equal to  $b_j$ , with  $a_j$  and  $b_j$  denoting the constant and non-constant biases associated with the ILI tool used in the  $j^{\text{th}}$  inspection;  $\mathbf{x}_i = (x_{i1}, x_{i2}, \dots, x_{ij}, \dots, x_{in})'$  with the  $j^{\text{th}}$  element  $x_{ij} = r_{i0} \sum_{k=1}^j \exp(\sum_{l=1}^k \eta_{i,l-1}) \Delta t_{i,k-1}$  and  $\eta_{i0} = 0$ , and  $\mathbf{E}_i = (E_{i1}, E_{i2}, \dots, E_{in})'$  denote the vector of random scattering errors associated with defect  $i$  for inspections  $j = 1, 2, \dots, n$  and is characterized by a multivariate normal distribution with a zero mean and a variance matrix,  $\boldsymbol{\Sigma}_{E_i}$ , with the elements  $(\boldsymbol{\Sigma}_{E_i})_{kl}$  equal to  $\rho_{kl} \sigma_k \sigma_l$  ( $k, l = 1, 2, \dots, n$ ), where  $\sigma_k$  and  $\sigma_l$  denote the standard deviation of the random scattering error associated with the tool used at the  $k^{\text{th}}$  and  $l^{\text{th}}$  inspections, and  $\rho_{kl}$  denotes the correlation coefficient between the random scattering errors associated with the  $k^{\text{th}}$  and  $l^{\text{th}}$  inspections (Al-Amin et al. 2012).

Further denote  $\boldsymbol{\eta} = (\boldsymbol{\eta}_1, \boldsymbol{\eta}_2, \dots, \boldsymbol{\eta}_m)$  and  $\mathbf{t}_0 = (t_{10}, t_{20}, \dots, t_{m0})$  and assume  $\eta_{ij}$  and  $\eta_{lj}$  ( $i \neq l$ ) are independent of each other for given inspection  $j$  conditional on  $\beta$ ,  $\sigma^2$ ,  $t_{i0}$  and  $t_{l0}$ ; that is, the exchangeability condition (Bernardo and Smith 2007) is applicable to  $\eta_{ij}$  ( $i = 1,$

2, ..., m) for a given inspection  $j$ . Given that both  $\beta$  and  $\sigma^2$  were assumed to be common for all the defects over all the time intervals, the likelihood function of  $\boldsymbol{\eta}$  conditional on  $\beta$ ,  $\sigma^2$  and  $\mathbf{t}_0$  is given by

$$\begin{aligned}
 L(\boldsymbol{\eta}|\boldsymbol{\beta}, \sigma^2, \mathbf{t}_0) &= \prod_{i=1}^m \prod_{j=1}^{n-1} L(\eta_{ij}|\beta, \sigma^2, t_{i0}) \\
 &= \sigma^{-m(n-1)} (2\pi)^{-m(n-1)/2} \left( \prod_{i=1}^m \prod_{j=1}^{n-1} \Delta t_{i,j-1} \right)^{-1/2} \exp \left( -\frac{1}{2\sigma^2} \sum_{i=1}^m \sum_{j=1}^{n-1} \frac{(\eta_{ij} - \beta \Delta t_{i,j-1})^2}{\Delta t_{i,j-1}} \right)
 \end{aligned}
 \tag{4.8}$$

where  $L(\eta_{ij}|\beta, \sigma^2, t_{i0})$  denotes the likelihood function of  $\eta_{ij}$  conditional on  $\beta$ ,  $\sigma^2$  and  $t_{i0}$ , i.e.  $N(\beta \Delta t_{i,j-1}, \sigma^2 \Delta t_{i,j-1})$ . It is noted that the potential spatial correlation between individual defects (given distribution parameters) was not considered in the above formulation due to a lack of suitable data (i.e. a set of closely spaced corrosion defects with known depths) to quantify the correlation.

### 4.3.2 Prior and Posterior Distributions

The aforementioned growth model includes a total of  $m(n + 1)$  basic parameters, namely  $m$  initial average growth rates ( $r_{i0}$ ) and initiation times  $t_{i0}$  ( $i = 1, 2, \dots, m$ ) and  $m(n - 1)$  random noises of the average growth rate  $\eta_{ij}$  ( $i = 1, 2, \dots, m; j = 1, 2, \dots, n - 1$ ), as well as another two hyper parameters (i.e.  $\beta$  and  $\sigma^2$ ). The average growth rates over the other time intervals  $r_{ij}$  ( $i = 1, 2, \dots, m; j = 1, 2, \dots, n - 1$ ) and the depths at the time of inspections  $x_{ij}$  ( $i = 1, 2, \dots, m; j = 1, 2, \dots, n$ ) are latent parameters that facilitate the establishment of the likelihood of the inspection data conditional on the basic parameters. In this study, the gamma distribution was selected as the prior distributions of  $r_{i0}$  ( $i = 1, 2, \dots, m$ ) and  $\sigma^2$  considering that the gamma distribution ensures  $r_{i0}$  and  $\sigma^2$  to be positive quantities and can be conveniently made as a non-informative distribution (Gelman et al. 2004). The PDF of a gamma distributed random variable  $Z$  is parameterized by  $f_Z(z) = B^A z^{A-1} \exp(-Bz) / \Gamma(A)$  for  $z > 0$ ,  $A > 0$  and  $B > 0$ , with  $A$  denoting the shape parameter and  $B$  denoting the rate parameter (i.e. the inverse of the scale

parameter). The normal distribution was assigned as the prior distribution of  $\beta$  because  $\beta$  can be either positive or negative as described in Section 4.2.3. The prior distribution of  $t_{i0}$  was chosen to be a uniform distribution with a lower bound of zero and an upper bound equal to the time interval between the installation of the pipeline and the first detection of defect  $i$ . The  $r_{i0}(t_{i0})$  associated with different defects were further assumed to be mutually independent with the identical prior distribution (*iid*). The hierarchical structure of the growth model represented by the directed acyclic graph (or DAG) (Spiegelhalter 1998) is shown in Figure 4.3, where the parameters defined at the top level (i.e.  $p_1, q_1, p_2, q_2, p_3, q_3, p_4$  and  $q_4$ ) indicate the distribution parameters of the prior distributions of the basic and hyper parameters. More specifically,  $p_1$  and  $q_1$  denote the lower and upper bounds of the uniform prior distribution of  $t_{i0}$ ;  $p_2$  and  $q_2$  denote the mean and precision (or the inverse of variance) of the normal prior distribution of  $\beta$ , and  $p_3$  ( $q_3$ ) and  $p_4$  ( $q_4$ ) denote the shape (rate) parameters of the gamma prior distributions of  $\sigma^2$  and  $r_{i0}$ , respectively.

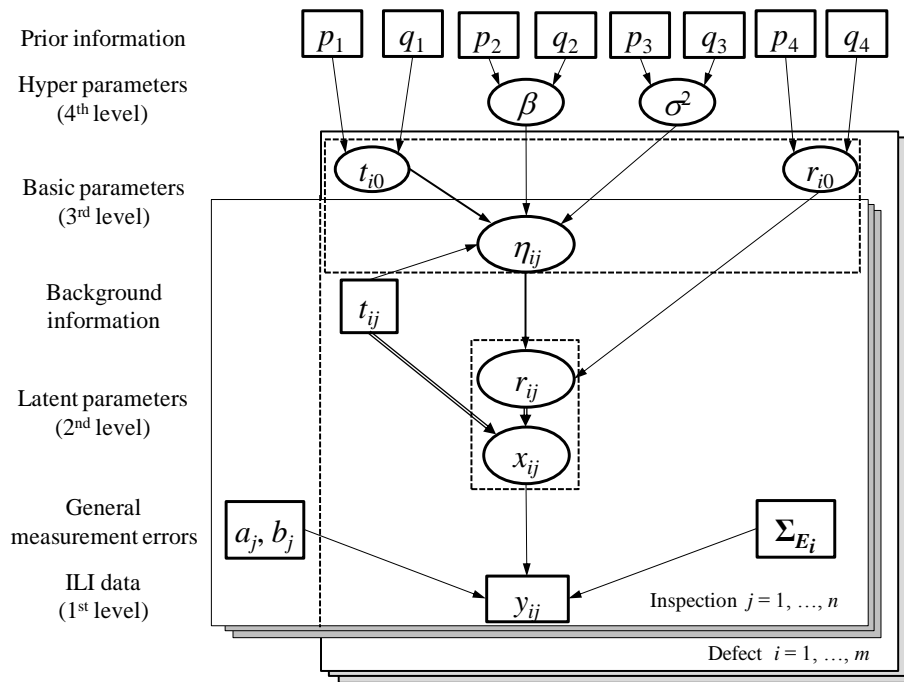


Figure 4.3 DAG representation of the growth model

Given the likelihood functions presented in Section 4.3.1 and the prior distributions described in Section 4.3.2, the full conditional posterior distributions of model parameters

were derived based on the Bayesian theorem given by Eq. (2.12) in Chapter 2 and are given in Appendix C. It is very difficult, if not impossible, to obtain the posterior marginal distributions of model parameters analytically, as implied by the full conditional posterior distributions of model parameters given in Appendix C. Therefore, the MCMC simulation techniques implemented in the software *OpenBUGS* (Lunn et al. 2009) were employed to numerically evaluate the marginal distributions of the parameters. A flowchart for illustrating the aforementioned methodology is shown in Figure 4.4, where the prediction is described in Section 4.4.

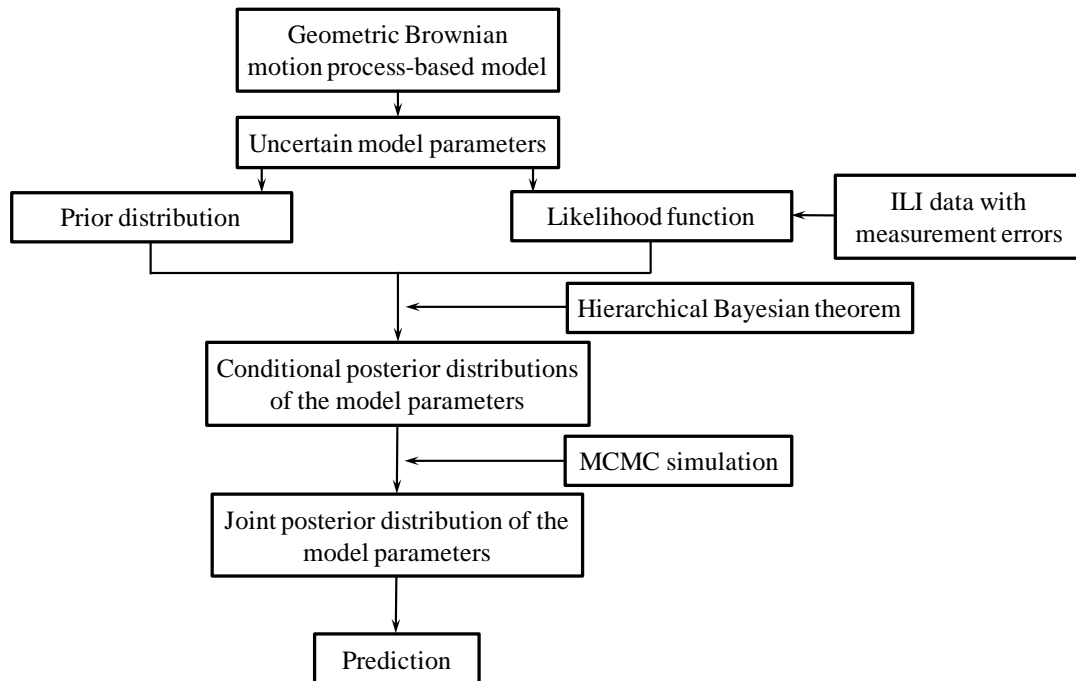


Figure 4.4 Illustration of the Bayesian updating of the growth model

## 4.4 Prediction

This section presents the approaches to predict the growth of defect depth based on the parameters (i.e.  $x_{in}$ ,  $r_{i,n-1}$ ,  $\beta$  and  $\sigma^2$ ) evaluated from the MCMC simulation. Without loss of generality, the time step for prediction is assumed to be a unit length, e.g. one year. Let  $r_i(k)$  and  $x_i(k)$  denote the average growth rate and depth corresponding to the  $k^{\text{th}}$ -step ( $k = 1, 2, \dots$ ) prediction (see Figure 4.2) since the most recent inspection considered in the Bayesian updating, respectively, i.e. the average growth rate within the time interval from  $t_n + k - 1$  to  $t_n + k$ , and depth at time  $t_n + k$ . Three approaches, namely the predictive

analysis-based approach, mean value-based approach and extrapolation-based approach, were considered for the prediction of  $x_i(k)$  and are described in the following sections. Note that the first approach incorporates the uncertainties associated with all the updated model parameters in the prediction of  $x_i(k)$  and therefore is the so-called predictive analysis (Kruschke 2010), whereas the latter two approaches involve simplifying assumptions that make them more amenable to practical application than the predictive analysis-based approach.

#### 4.4.1 Predictive Analysis-based Approach

Based on Eq. (4.4), the logarithm of the predicted growth rate corresponding to the  $k^{\text{th}}$  step (i.e.  $\ln(r_i(k))$ ) follows a Gaussian distribution given by

$$\ln(r_i(k)) \sim \begin{cases} N(\ln(r_{i,n-1}) + \beta\Delta t_{i,n-1}, \sigma^2\Delta t_{i,n-1}) & (k = 1) \\ N(\ln(r_i(k-1)) + \beta, \sigma^2) & (k \geq 2) \end{cases} \quad (4.9)$$

The predicted defect depth corresponding to the  $k^{\text{th}}$  step is then given by

$$x_i(k) = x_{in} + \sum_{l=1}^k r_i(l) \quad (4.10)$$

Note that  $x_{in}$ ,  $r_{i,n-1}$ ,  $\beta$  and  $\sigma^2$  in Eqs. (4.9) and (4.10) are uncertain. To evaluate the probabilistic characteristics of  $r_i(k)$  and  $x_i(k)$ , a sequence of sets of samples of  $r_{i,n-1}$ ,  $\beta$  and  $\sigma^2$  generated from the MCMC simulation was used first to compute the means and variances of  $r_i(k)$ , which can then be used to generate samples of  $r_i(k)$ . The samples of  $r_i(k)$  were subsequently used to obtain samples of  $x_i(k)$  from Eq. (4.10). In this study,  $N_0$  samples of  $r_i(k)$  and  $N_0$  samples of  $x_i(k)$  were used to evaluate their corresponding probabilistic characteristics, where  $N_0$  is the total number of sample sequences obtained from the MCMC simulation excluding those within the burn-in period. Note that the number of samples of  $r_i(k)$  and  $x_i(k)$  (i.e.  $N_0$ ) is set the same as the number of sample sets generated in the MCMC simulations for the sole purpose of facilitating the implementation of the program in *OpenBUGS*. Both the median and mean values of  $x_i(k)$  can be used to predict the actual depth at the  $k^{\text{th}}$  step.

#### 4.4.2 Mean Value-based Approach

Let  $E[r_i(k)]$  and  $V[r_i(k)]$  denote the mean and variance of  $r_i(k)$  ( $k = 1, 2, \dots$ ), respectively. It follows from Eq. (4.9) that  $E[r_i(k)]$  and  $V[r_i(k)]$  can be obtained as follows:

$$E[r_i(k)] = \begin{cases} r_{i,n-1} \exp\left(\left(\beta + \frac{1}{2}\sigma^2\right)\Delta t_{i,n-1}\right) & (k = 1) \\ r_i(k-1) \exp\left(\beta + \frac{1}{2}\sigma^2\right) & (k \geq 2) \end{cases} \quad (4.11a)$$

$$V[r_i(k)] = \begin{cases} (r_{i,n-1})^2 \exp\left((2\beta + \sigma^2)\Delta t_{i,n-1}\right) [\exp(\sigma^2\Delta t_{i,n-1}) - 1] & (k = 1) \\ (r_i(k-1))^2 \exp(2\beta + \sigma^2) [\exp(\sigma^2) - 1] & (k \geq 2) \end{cases} \quad (4.11b)$$

Further assume  $x_{in}$  and  $r_i(l)$  ( $l = 1, 2, \dots, k$ ) to be mutually independent. Then the mean and variance of  $x_i(k)$ , denoted by  $E[x_i(k)]$  and  $V[x_i(k)]$  respectively, can be evaluated by:

$$E[x_i(k)] = E[x_{in}] + \sum_{l=1}^k E[r_i(l)] \quad (4.12a)$$

$$V[x_i(k)] = V[x_{in}] + \sum_{l=1}^k V[r_i(l)] \quad (4.12b)$$

The use of Eq. (4.12) to predict the defect depth was also considered in this study. To this end, the median or mean values of  $r_{i,n-1}$ ,  $\beta$  and  $\sigma^2$  obtained from the MCMC simulation can be substituted into Eqs. (4.11a) and (4.11b) to evaluate  $E[r_i(k)]$  and  $V[r_i(k)]$ .

#### 4.4.3 Extrapolation-based Approach

If the temporal variability of the growth path over the forecasting period is ignored, the predicted depths can also be approximately obtained by extrapolating the current growth rate (i.e.  $r_{i,n-1}$ ) into the future, i.e.  $x_i(k) = x_{in} + k \cdot r_{i,n-1}$ , where  $x_{in}$  and  $r_{i,n-1}$  can be set to the corresponding median or mean values evaluated from the MCMC simulation. A comparison of the predictive quality corresponding to the above-mentioned approaches is given in Section 4.5.

## 4.5 Example

### 4.5.1 Model Validation

In this section, the growth models were developed for the 62 external corrosion defects described in Section 2.6.1 of Chapter 2. The same sets of ILI data (i.e. the ILI-reported depth in 2000, 2004 and 2007) were used to carry out the Bayesian updating. The parameters of the prior distributions, i.e. the parameters at the top level of Figure 4.3, were specified as follows:  $p_1 = 0$  (year),  $q_1 = 28$  (year),  $p_2 = 0$  (year<sup>-1</sup>),  $q_2 = 10000$  (year<sup>2</sup>),  $p_3 = 10$ ,  $q_3 = 10$  (year),  $p_4 = 1$  and  $q_4 = 1$  (year/%wt). It follows from Section 4.3.3 that  $q_1$  denotes the time elapsed since the installation time of the pipeline (i.e. 1972) up to the time of the first inspection (i.e. 2000) and therefore equals 28 years. The values of  $p_2$  and  $q_2$  imply that the normal prior distribution of  $\beta$  has a mean of zero and a standard deviation of 0.01 (year<sup>-1</sup>), which is an informative prior distribution considering that the deterministic change between the average growth rates corresponding to two consecutive inspection intervals is likely to be small because the inspection intervals are not long ( $\leq 4$  years). The values of  $p_3$  and  $q_3$  ( $p_4$  and  $q_4$ ) imply that the mean and variance of the prior distribution of  $\sigma^2$  ( $r_{i0}$ ) equal 1 (year<sup>-1</sup>) and 0.1 (year<sup>-2</sup>) (1 (%wt/year) and 1 (%wt/year)<sup>2</sup>), respectively. A total of 20,000 MCMC simulation sequences were generated with the first 2000 sequences considered as the burn-in period (Gelman et al. 2004) and therefore discarded. The samples in the rest of the sequences were used to evaluate the probabilistic characteristics of the parameters in the growth models. Six scenarios were considered and summarized in Table 4.1 in terms of predicting the defect depths in 2010. It should be emphasized that the predicted defect depths in 2010 in Scenarios I and II are respectively the median and mean values of the 18,000 samples (i.e. equal to the total number of MCMC sequences excluding the number of sequences in the burn-in period) of the defect depth in 2010 per the predictive analysis-based approach, as described in Section 4.4.1. On the other hand, the predictions corresponding to Scenarios III through VI are based on the median or mean values of the model parameters per mean value- and extrapolation-based approaches as described in Sections 4.4.2 and 4.4.3, respectively. A comparison between the predicted depths,  $x_p$ , in 2010 based on Scenario I and the corresponding field-measured depths,  $x_a$ , for the 62 defects is shown in Figure 4.5.

Table 4.1 Summary of the six scenarios for model prediction

Scenario	Approach of prediction	Values of prediction and parameters employed in prediction
I (Baseline)	Predictive analysis-based*	Median
II		Mean
III	Mean value-based <sup>+</sup>	Median
IV		Mean
V	Extrapolation-based <sup>+</sup>	Median
VI		Mean

\*: Predictions are the median or mean values of the predicted depths.

+: The median or mean values of the model parameters are used to evaluate the predicted depths.

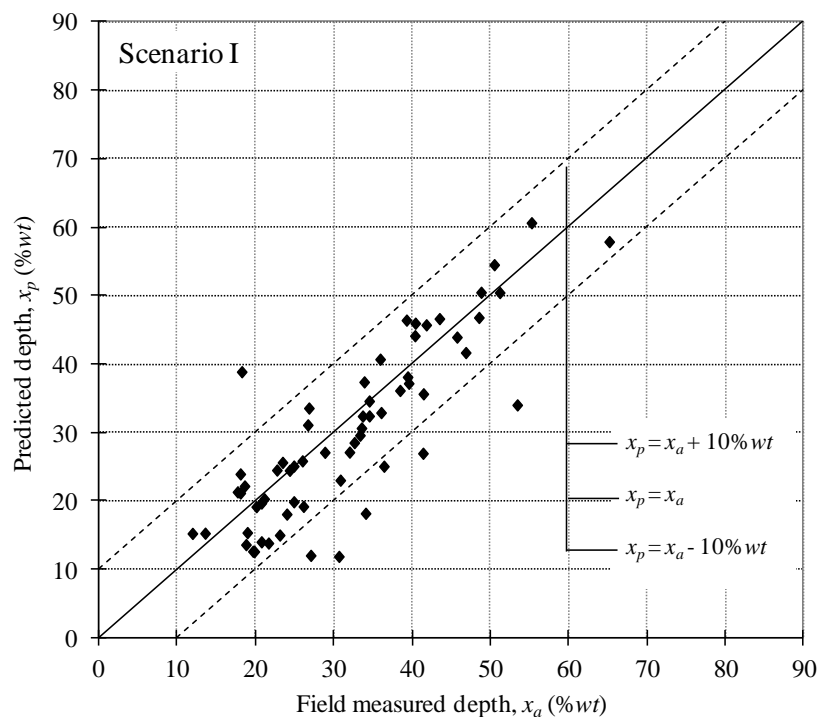


Figure 4.5 Comparison of the predicted and field-measured depths in 2010 for Scenario I

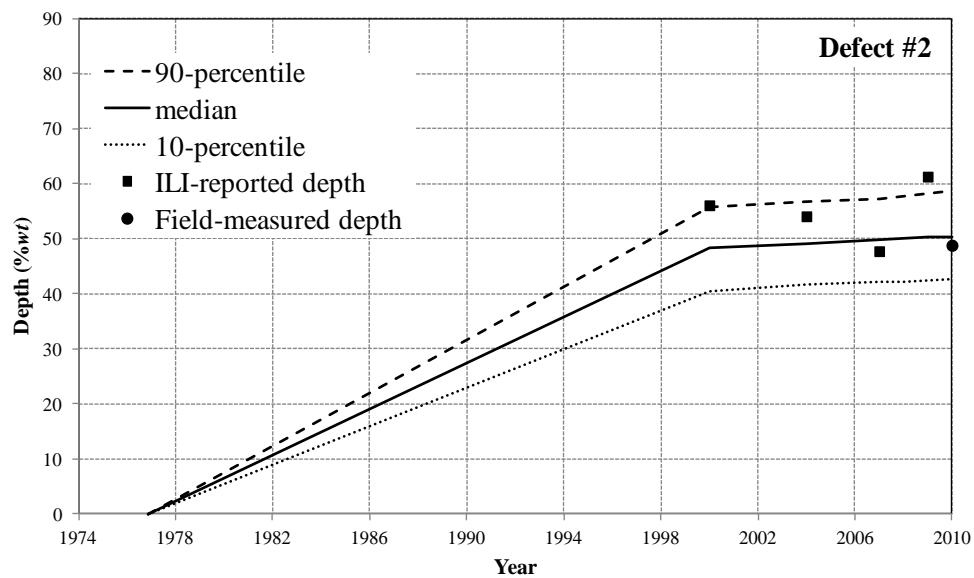
Figure 4.5 suggests that the proposed model can predict the corrosion growth reasonably well for a majority of the defects considered, as the predicted depths for 89%



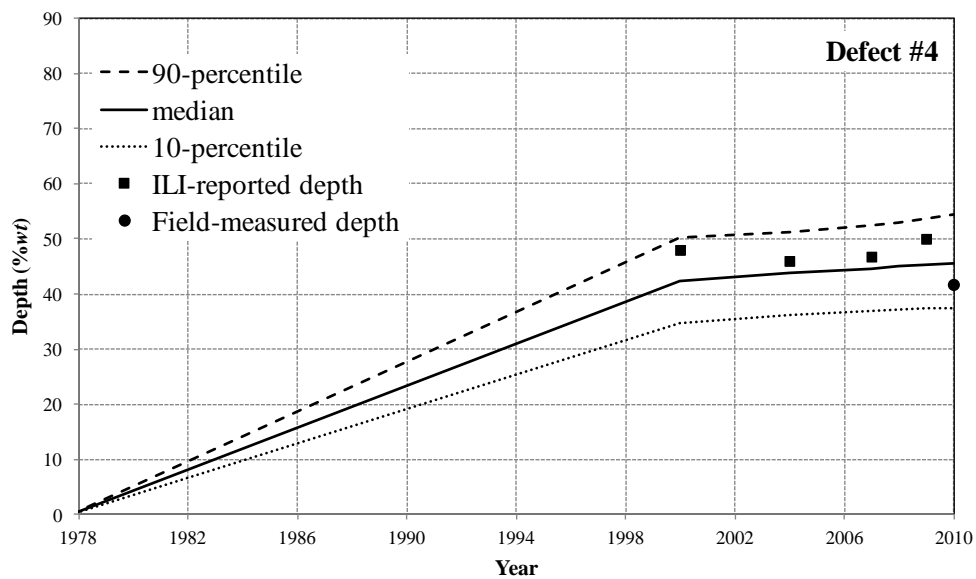
of the 62 defects fall within the region bounded by the two dashed lines, with the top and bottom lines representing  $x_p = x_a \pm 10\%wt$ , respectively. Note that the two bounding lines are commonly used in the pipeline industry as a confidence interval for the accuracy of the inspection tool and were adopted in this study as a metric for the predictive accuracy of the corrosion growth model. To illustrate the deviation of the predicted depths from the actual depths, one solid line representing  $x_p = x_a$  is also plotted along with the two bounding lines in the same figure. The predicted depths show significant deviation (defined as the absolute difference between the predicted and actual depths being greater than  $10\%wt$ ) from the corresponding actual depths for seven defects, with the maximum absolute deviation being approximately  $21\%wt$  (Defect #49).

The median, 10- and 90-percentile values of the growth paths for ten arbitrarily selected defects, i.e. Defects #2, #4, #5, #7, #15, #18, #19, #49, #60 and #61, are plotted in Figures 4.6(a) through 4.6(j), respectively. The median, 10- and 90-percentile values were evaluated using the samples of  $x_i(k)$  generated based on each sequence of model parameters obtained from MCMC simulations. For comparison, the corresponding ILI-reported depths in 2000, 2004, 2007 and 2009 as well as the field-measured depth in 2010 are also plotted in the same figure. Figure 4.6 shows that the predicted growth paths are, as expected, piecewise linear. The results indicate that the predicted growth path differs from defect to defect; this is expected because the parameter  $t_{i0}$  and  $r_{i0}$  are assumed to be defect-specific. The use of Eqs. (4.9) and (4.10) to predict the growth of the defect depth implies that the predicted depth is largely influenced by the predicted average growth rate over the time interval between the last two inspections, i.e.  $r_{i,n-1}$ . The investigation further indicates that the statistics of  $r_{i,n-1}$  are markedly impacted by the last two sets of ILI data used in the Bayesian updating. Therefore, if the inspection data in the last two inspections are subjected to large measurement errors, the predicted average growth rate is expected to deviate markedly from the actual average growth rate and therefore leads to a poor prediction for the defect depth. For example, the ILI-reported depth in 2007 for Defect #49 shown in Figure 4.6(h) involves relatively large measurement errors, as inferred from a comparison with the ILI data reported in 2000,

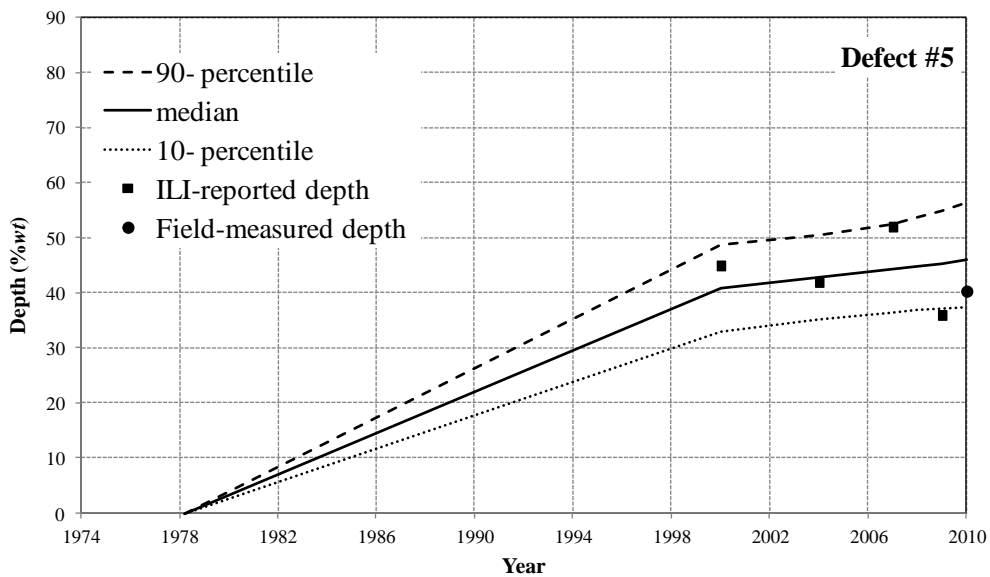
2004 and 2009, and field-measured data. This is considered the main reason for a poor prediction for Defect #49.



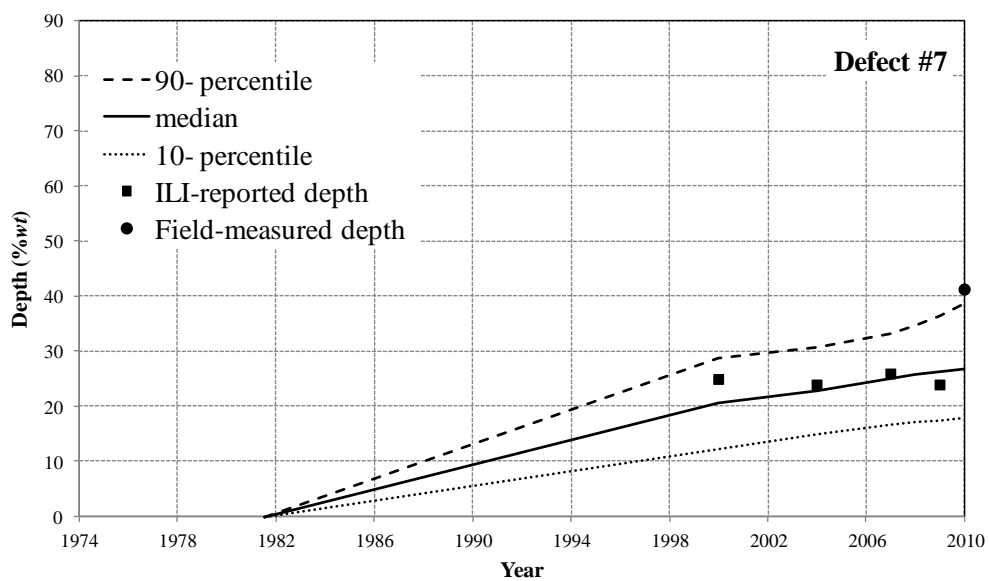
(a)



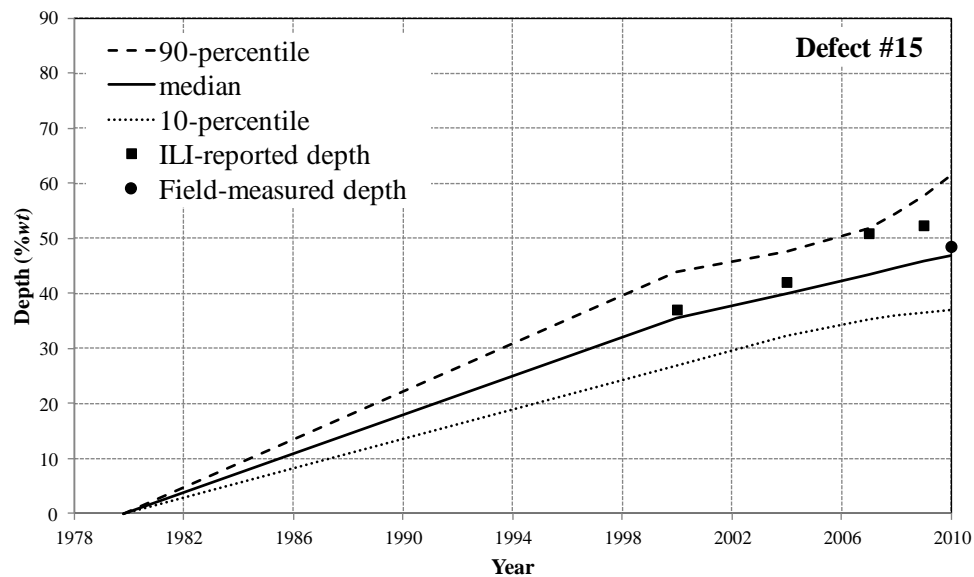
(b)



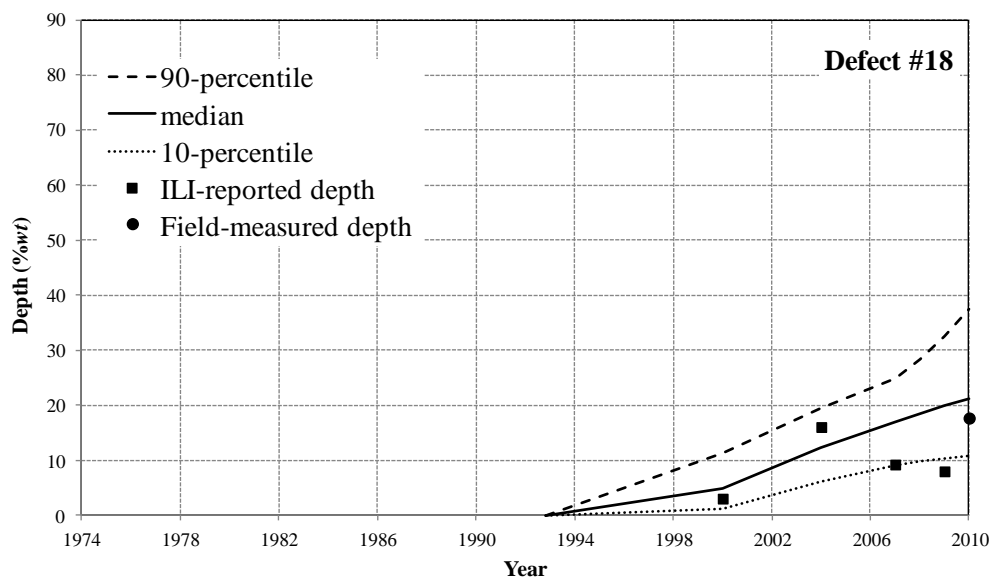
(c)



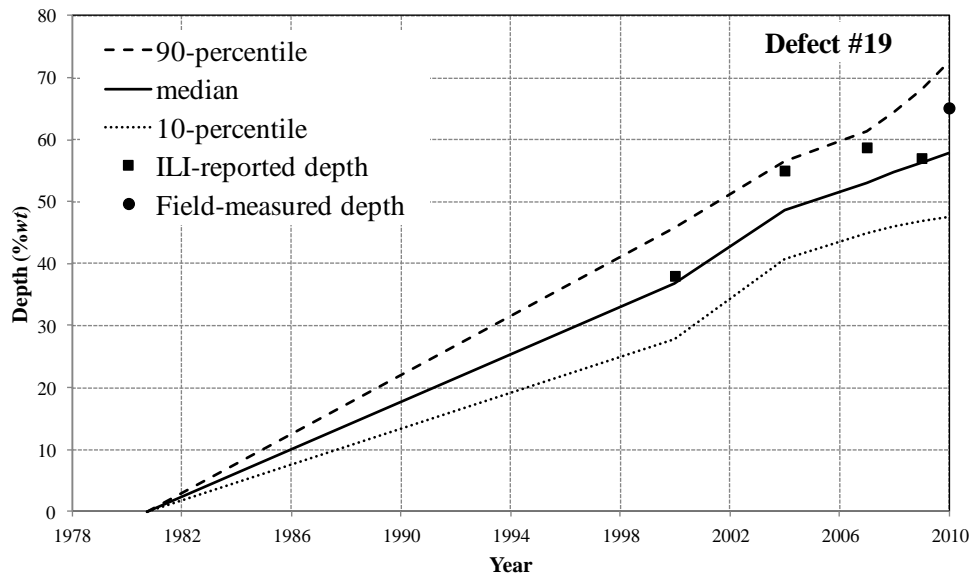
(d)



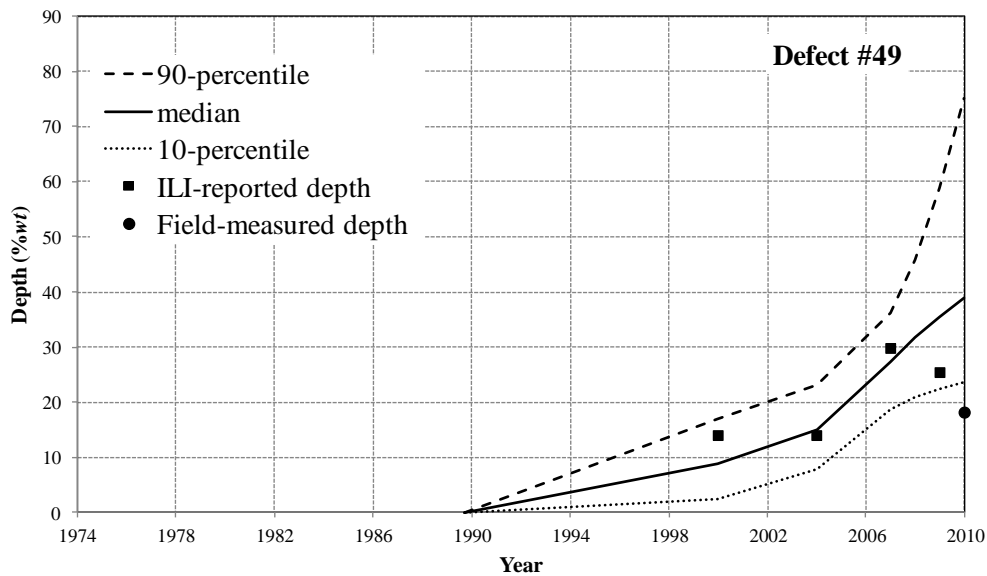
(e)



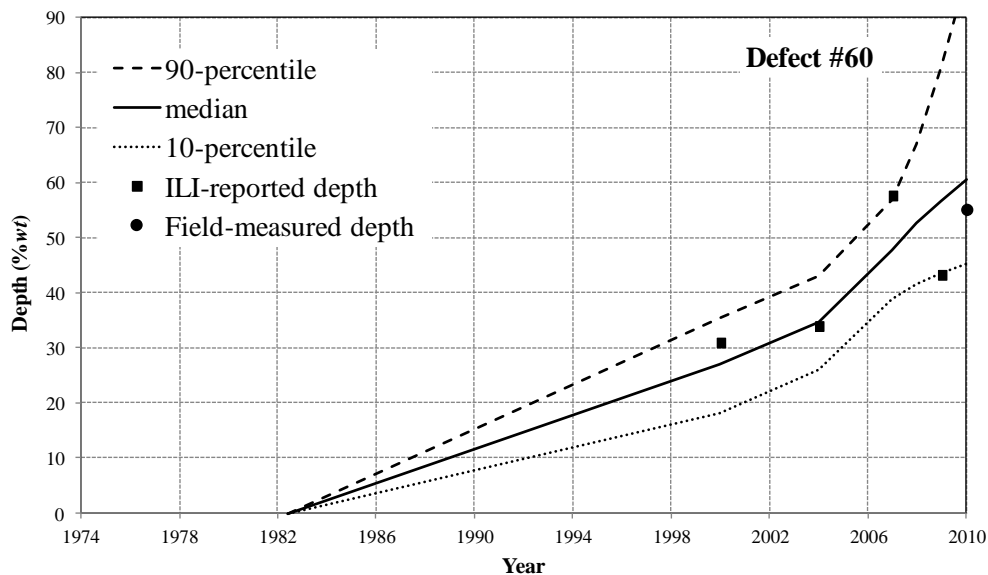
(f)



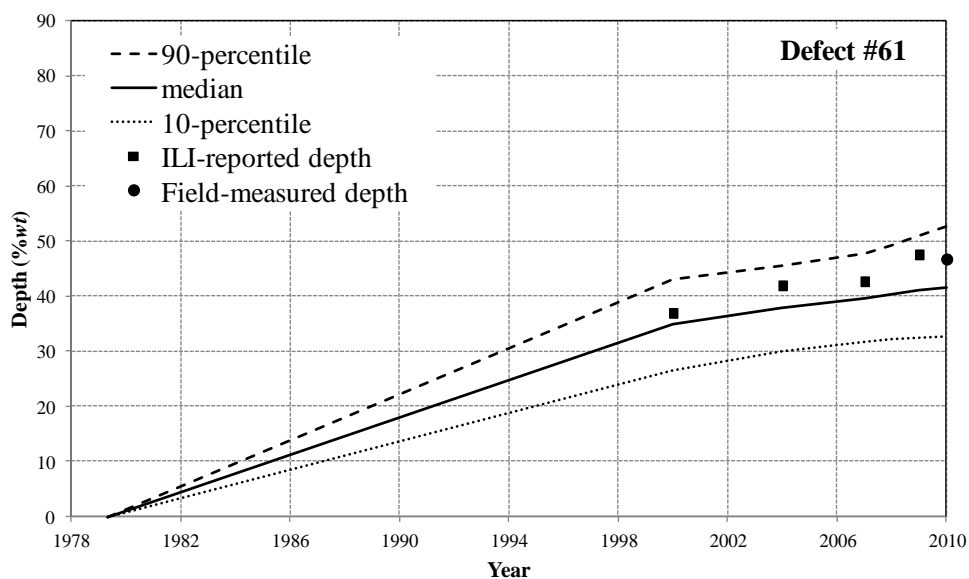
(g)



(h)



(i)

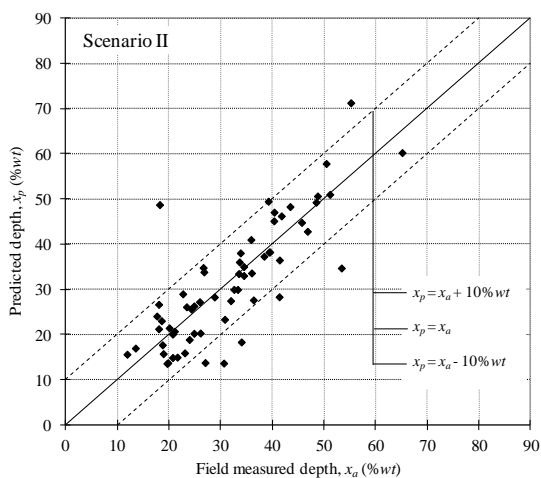


(j)

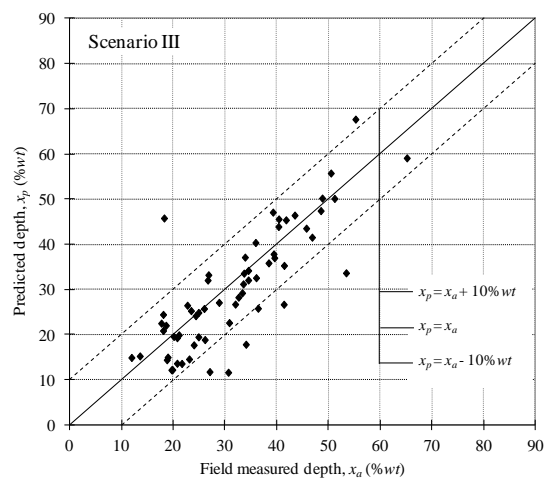
Figure 4.6 Predicted growth paths for Defects #2, #4, #5, #7, #15, #18, #19, #49, #60 and #61

To investigate the differences of the predictions corresponding to the six scenarios described in Table 4.1, the comparison of the predicted depths in 2010 with the field-measured depths corresponding to Scenarios II through VI are plotted in Figures 4.7(a)

through 4.7(e), respectively. The overall comparison of the predictions associated with the six scenarios considered is depicted in Figure 4.7(f). The corresponding MSEP (i.e. mean squared error of prediction) (Bunke and Droge 1984; Harville and Jeske 1992) values as stated in Chapter 2 as well as the percentage of total number of defects falling within the bounded region associated with each of the six scenarios are also shown in Figure 4.7(f). Figure 4.7(f) indicates that MSEP values associated with Scenarios II through V are slightly larger than those associated with Scenarios I and VI. It also indicates that the predictive accuracy of Scenario VI, i.e. the approximate method based on the mean values of  $x_{i,n}$  and  $r_{i,n-1}$ , is statistically the same as that of Scenario I given that the predictions corresponding to both scenarios have the same MSEP values. This suggests that the approximate method corresponding to Scenario VI is adequate to predict the growth of corrosion defect, although it ignores the temporal variability of the growth over the forecasting period.



(a)



(b)

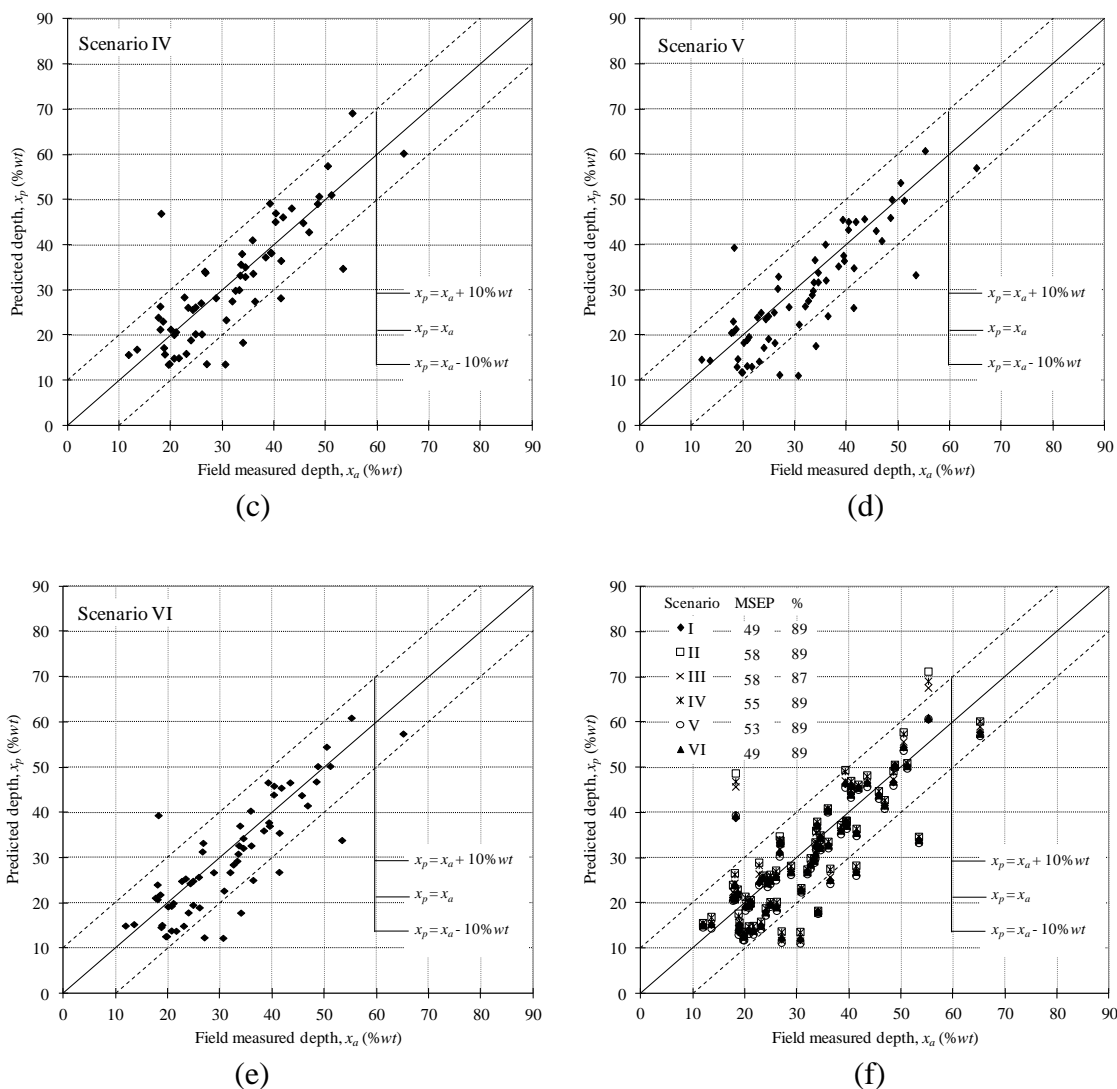
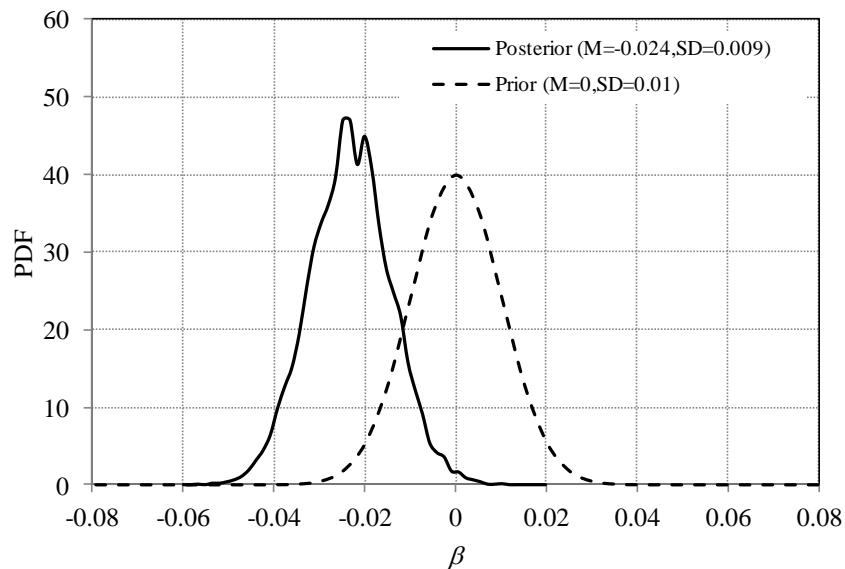


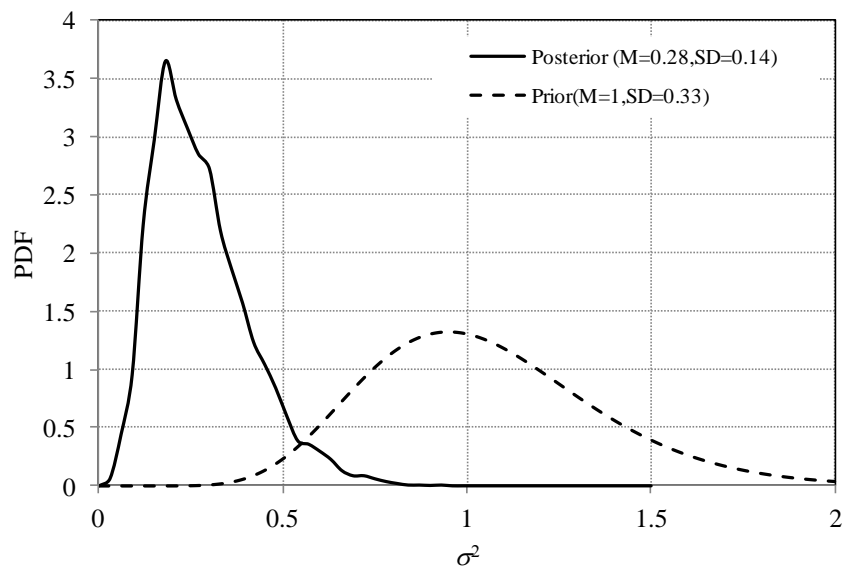
Figure 4.7 Comparison of the predictions corresponding to Scenarios I through VI

The posterior distributions of  $\beta$  and  $\sigma^2$  evaluated using the MCMC samples are plotted in Figure 4.8(a) and 4.8(b), respectively, where the symbols M and SD denote the mean and standard deviation, respectively. For comparison, the prior distributions of  $\beta$  and  $\sigma^2$  specified in the Bayesian updating are plotted in the same figure as well. The marked difference between the probability density functions of the prior and posterior distributions shown in Figure 4.8 illustrates the contribution of the information implied in the ILI data that the Bayesian approach used to update the prior knowledge of model parameters.





(a)



(b)

Figure 4.8 The prior and posterior distributions  $\beta$  of  $\sigma^2$ 

#### 4.5.2 Comparison with Other Growth Models

In this section, the proposed GBM-based growth model is compared with the homogeneous gamma process- (HGP-) and inverse Gaussian process- (IGP-) based

models stated in Chapters 2 and 3, respectively, as well as the conventional linear growth model stated in Section 3.5.3 of Chapter 3. Scenario II-1 of the HGP-based model and Scenario I of the IGP-based model (i.e. the posterior median values of the model parameters were used to predict the depth for both models) were considered in the comparison. The predictions corresponding to the GBM-based model were obtained from the approximate approach (i.e. the results corresponding to Model 1-3 shown in Figure 4.5). The comparison of the predictions for the 62 defects given by the four growth models is shown in Figure 4.9. The MSEP value and percentage of predictions within the two bounding lines associated with each of the four models are also shown in the same figure. The results indicate that the predictions corresponding to the proposed model is similar to the HGP- and IGP-based models, whereas the conventional linear growth model leads to significantly poorer predictions compared with the three Bayesian growth models.

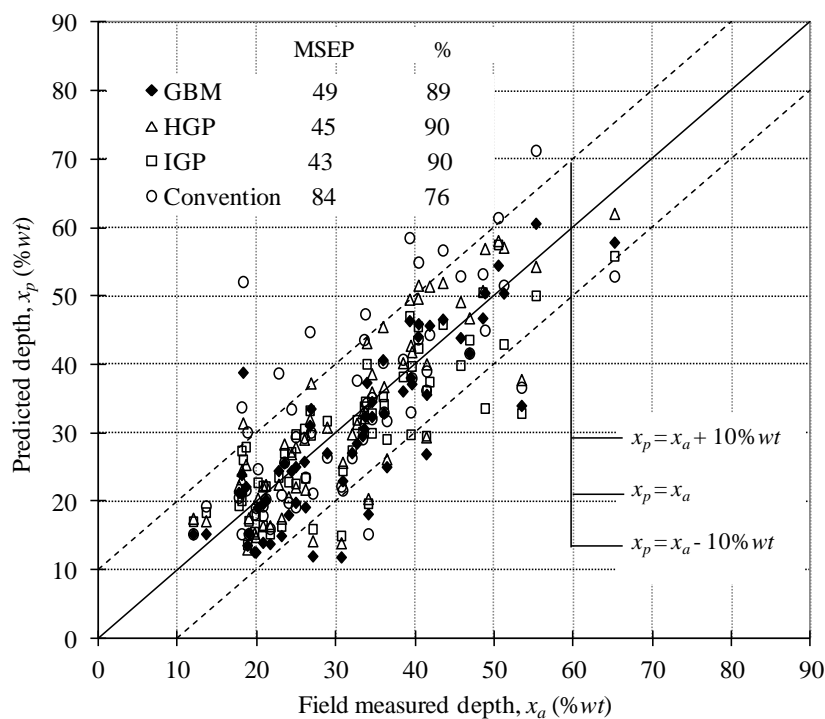


Figure 4.9 Comparison with the HGP- and IGP-based and conventional growth models

## 4.6 Conclusions

The geometric Brownian motion-based growth rate (GBMGR) model is formulated in a hierarchical Bayesian framework to characterize the growth of depths of individual metal-loss corrosion defects on underground steel pipelines based on imperfect ILI data. The model approximates the actual growth path of a corrosion defect with a piecewise linear path, and characterizes the average growth rate between two consecutive inspections as a geometric Brownian motion. The model is a state-dependent growth model in that the growth rate is implicitly dependent on the current state of corrosion, and is more advantageous than the Markov chain-based state-dependent models because it does not require discretizing the damage state or evaluating the transition probability. Compared with the gamma process- and inverse Gaussian process-based growth models reported in the literature, which consist of independent increments and are state-independent, the proposed model does not involve specific assumptions about the mean growth path (e.g. linear or power-law function of time) and therefore is more flexible. The model is suitable for pipelines whereby multiple sets of ILI data (say,  $\geq 3$ ) are available and the inspection interval is not too long (say,  $\leq 5$  years).

The Markov Chain Monte Carlo simulation techniques were employed to carry out the Bayesian updating and numerically evaluate the posterior marginal distributions of the parameters in the growth model based on the ILI data. A general form of the measurement error in the ILI data was considered, which includes the biases, random scattering error as well as correlations between the random scattering errors associated with different ILI tools. An example involving real ILI data collected from a natural gas pipeline that is currently in service in Alberta, Canada was used to illustrate and validate the proposed model. The growth models were developed for 62 external corrosion defects that have been subjected to multiple ILI runs and were excavated, field measured in ditch and recoated. The ILI data obtained from the inspections prior to the field measurement were used to carry out the Bayesian updating and evaluate the model parameters in the growth models corresponding to the 62 corrosion defects considered. The predictive quality of the growth model was demonstrated by comparing the predicted defect depths with the corresponding field-measured depths.

The analysis results indicate that the predicted defect depths obtained from the predictive analysis (i.e. the uncertainties in all of the updated model parameters included) agree reasonably well with the corresponding field-measured depths: the absolute deviations between the two depths are less than or equal to 10% *wt* for 89% of the 62 defects. The approximate approach for prediction, which extrapolates the current growth rate based on the posterior mean values of the model parameters, can also give a reasonably good prediction. The prediction is sensitive to the predicted average growth rate over the time interval between the last two inspections, the statistics of which are significantly influenced by the last two sets of ILI data included in the Bayesian updating. Results of a comparative study suggest that the predictive capability of the proposed model is similar to that of the homogeneous gamma process- and inverse Gaussian process-based Bayesian growth model, but is markedly better than that of the conventional linear growth model commonly used in the pipeline industry.

The proposed model offers a viable alternative to predicting the corrosion growth on oil and natural gas pipelines based on imperfect inspection data and will facilitate the corrosion management of underground pipelines.

## References

- Al-Amin, M., Zhou, W., Zhang, S., Kariyawasam, S. and Wang, H. (2012). Bayesian model for the calibration of ILI tools. Proceedings of International Pipeline Conference (IPC), IPC2012-90491, ASME, Calgary.
- Beichelt, F. E. and Fatti, L. P. (2002). Stochastic processes and their applications. Taylor and Francies, NY.
- Bernardo, J. and Smith, A. F. M. (2007). Bayesian theory. John Wiley & Sons Inc, NY, USA.
- Bunke, O. and Droge, B. (1984). Estimators of the mean squared error of prediction in linear regression. Technometrics, 26: 145-155.
- Caleyo, F., Velázquez, J.C., Valor, A. and Hallen, J. M. (2009). Markov chain modelling of pitting corrosion in underground pipelines. Corrosion Science, 51(9): 2197-2207.

- Elsayed, E. A. and Liao, H. T. (2004). A geometric Brownian motion model for field degradation data. *International Journal of Material and Product Technology*, 20(1-3): 51-72.
- Fuller, W. A. (1987). *Measurement error models*. John Wiley & Sons, Inc., New York, NY, USA.
- Gebraeel, N. and Pan, J. (2008). Prognostic degradation models for computing and updating residual life distributions in a time-varying environment. *IEEE Transactions on Reliability*, 57(4): 539-550.
- Gelman, A., Carlin, J. B., Stern, H. S. and Rubin, D. B. (2004). *Bayesian data analysis* (2nd edition). Chapman & Hall/CRC, NY.
- Guida, M. and Pulcin, G. (2011). A continuous-state Markov model for age- and state-dependent degradation process. *Structural Safety*, 33(6): 354-366
- Guida, M. and Pulcin, G. (2013). The inverse Gamma process: A family of continuous stochastic models for describing state-dependent deterioration phenomena. *Reliability Engineering and System Safety*, 120: 72-79.
- Harville, D. A. and Jeske, D. R. (1992). Mean squared error of estimation or prediction under a general linear model. *Journal of the American Statistical Association*, 87: 724-731.
- Hong, H. P. (1999). Inspection and maintenance planning of pipeline under external corrosion considering generation of new defects. *Structural Safety*, 21(3): 203-222.
- Huyse, L. and van Roodselaar A. (2010). Effects of inline inspection sizing uncertainties on the accuracy of the largest features and corrosion rate statistics, *Proceedings of 8<sup>th</sup> International Pipeline Conference*, ASME, Calgary, Alberta, Canada, 403-413.
- Jaech, J. L. (1985). *Statistical analysis of measurement errors*. John Wiley & Sons, Inc., New York, NY, USA.
- Kruschke, J. K. (2010). *Doing Bayesian Data Analysis: A Tutorial with R and BUGS* (1<sup>st</sup> edition). Academic Press, Waltham, Massachusetts, USA.

- Lunn, D., Spiegelhalter, D., Thomas, A. and Best, N. (2009). The BUGS project: evolution, critique and future directions (with discussion). *Statistics in Medicine*, 28: 3049-82.
- Nessim, M., Dawson, J., Mora, R. and Hassanein, S. (2008). Obtaining corrosion growth rates from repeat in-line inspection runs and dealing with the measurement uncertainties. *Proceedings of 7<sup>th</sup> International Pipeline Conference*, ASME, Calgary, Alberta, Canada, 593-600.
- Pandey, M. D., Yuan, X. X. and van Noortwijk, J. M. (2009). The influence of temporal uncertainty of deterioration on life-cycle management of structures. *Structure and Infrastructure Engineering*, 5(2): 145-156.
- Park, C. and Padgett, W. J. (2005). Accelerated degradation models for failure based on geometric Brownian motion and gamma processes. *Lifetime Data Analysis*, 11, 511-527.
- Spiegelhalter, D.J. (1998). Bayesian graphic modeling: A case-study in monitoring health outcomes. *Applied Statistics*, 47: 115-33.
- Timashev, S. A., Malyukova, M. G., Poluian, L. V. and Bushinskaya, A. V. (2008). Markov description of corrosion defects growth and its application to reliability based inspection and maintenance of pipelines. *Proceedings of International Pipeline Conference (IPC)*, IPC2008-64546, ASME, Calgary.
- Valor, A., Caleyó, F., Alfonso, L., Rivas, D. and Hallen, J. M. (2007). Stochastic modeling of pitting corrosion: a new model for initiation and growth of multiple corrosion pits. *Corrosion Science*, 49: 559-579.
- Wang, X. (2010). Wiener processes with random effects for degradation data. *Journal of Multivariate Analysis*, 101: 340-351.
- Whitemore, G. A. and Schenkelberg, F. (1997). Modeling accelerated degradation data using Wiener diffusing with a time scale transformation. *Lifetime Data Analysis*, 3(1): 27-45.
- Ye, Z. S., Shen, Y. and Xie, M. (2012). Degradation-based burn-in with preventive maintenance. *European Journal of Operational Research*, 221: 360-367.

- Zhang, S. and Zhou, W. (2013). System reliability of corroding pipelines considering stochastic process-based models for defect growth and internal pressure. *International Journal of Pressure Vessels and Piping*, 111-112(11): 120-130.
- Zhang, S., Zhou, W., Al-Amin, M., Kariyawasam, S. and Wang, H. (2012). Time-dependent corrosion growth modeling using multiple ILI data. *Proceedings of International Pipeline Conference (IPC), IPC2012-90502, ASME, Calgary.*
- Zhang, S., Zhou, W. and Qin, H. (2013). Inverse Gaussian process-based corrosion growth model for energy pipelines considering sizing error in inspection data. *Corrosion Science*, 73(10): 309-320.
- Zhou, W., Hong, H. and Zhang, S. (2012). Impact of dependent stochastic defect growth on system reliability of corroding pipelines. *International Journal of Pressure Vessels and Piping*, 96-97: 68-77.

## **Chapter 5 System Reliability of Corroding Pipelines Considering Stochastic Process-based Models for Defect Growth and Internal Pressure**

### **5.1 Introduction**

Metal-loss corrosion threatens the structural integrity and safe operation of oil and gas pipelines worldwide (Cosham et al. 2007; Nessim et al. 2009). The reliability-based corrosion management program is being increasingly used in the pipeline industry because it provides a reasonable framework to account for the various uncertainties (e.g. measurement error, and randomness associated with the corrosion growth and material properties) that impact the development of suitable maintenance strategies. The reliability-based pipeline corrosion management typically includes three tasks, namely periodic high-resolution inline inspections (ILIs) to detect and size corrosion defects on a given pipeline, failure probability evaluation of the pipeline based on the inspection results and mitigation of defects.

The majority of reliability analyses of corroding pipelines reported in the literature (e.g. Ahammed 1998; Pandey 1998; Caleyó et al. 2002; Amirat et al. 2006; Teixeira et al. 2008; Zhou 2010; Zhou et al 2012 ) employed random variable-based growth models for the depth (i.e. in the through pipe wall thickness direction) and length (i.e. in the longitudinal direction of the pipe) of the corrosion defect. Furthermore, the internal pressure of the pipeline is typically assumed to be either a (time-independent) random variable or a deterministic quantity while in reality the internal pressure varies with time and should be characterized as a stochastic process. A simple stochastic process, the Ferry-Borges process, was employed in (Zhou 2010) to model the internal pressure for evaluating the system reliability of corroding pipelines. However, the Ferry-Borges process, which characterizes the internal pressures over individual years as independent random variables, is somewhat simplistic; therefore, more realistic and sophisticated models for the internal pressure are desirable for the reliability analysis. Note that sophisticated stochastic process-based load models have been employed in the reliability



analysis of building structures (Madsen 2006; Melchers 1999; El-Reedy 2009), e.g. the Poisson Square Wave Process (PSWP) for modelling the sustained live loads.

This chapter presents a methodology to evaluate the system reliability of onshore natural gas pipelines containing multiple active metal-loss corrosion defects subjected to internal pressure. The methodology employs the growth models described in Chapters 2 through 4 to characterize the growth of depths of corrosion defects and PSWP to model the internal pressure of the pipeline. The simple Monte Carlo simulation is used to evaluate the system reliability of the pipeline in terms of three distinctive failure modes, namely small leak, large leak and rupture (Zhou 2010). The methodology can be incorporated in a reliability-based pipeline integrity management program to assist engineers in selecting suitable strategies for corrosion maintenance.

The remainder of the chapter is organized as follows. Section 5.2 briefly summarizes the growth models and describes the approach of generating the growth path in a simulation trial based on a given growth model; Section 5.3 presents the internal pressure model; the limit state functions associated with different failure modes and methodology for evaluating the time-dependent system reliability of corroding pipelines containing multiple active corrosion defects are presented in Section 5.4; an example to illustrate above-described methodologies and investigate the impact of the growth models on the time-dependent failure probabilities is shown in Section 5.5, followed by the conclusions in Section 5.6.

## **5.2 Time-dependent Corrosion Growth Models**

Four growth models, namely the non-homogeneous gamma process- (NHGP-), homogeneous gamma process- (HGP-), inverse Gaussian process- (IGP-) and geometric Brownian motion- (GBM-) based growth models, as described in Chapters 2 through 4, were considered in this chapter to carry out the time-dependent reliability analysis of corroding pipelines containing multiple active corrosion defects. Without loss of generality, suppose  $m$  corrosion defects, each of which has  $n$  sets of ILI data obtained from different ILI runs, were used to carry out the Bayesian updating. It follows from Chapters 2 through 4 that  $t$  denotes the time elapsed since the installation of pipeline;  $t_{i0}$  ( $i$

$= 1, 2, \dots, m$ ) denotes the initiation time of the  $i^{\text{th}}$  defect (e.g. time elapsed since the installation of pipeline up to the time at which the defect start to growth), and  $t_{ij}$  denotes the time of the  $j^{\text{th}}$  inspection for the  $i^{\text{th}}$  defects. Let  $T$  (years) denote the forecasting period of time-dependent reliability analysis starting from the most recent inspection that was carried out  $t_{in}$  years after the installation of the pipeline, and  $d_i(t_{in} + \tau)$  ( $\tau = 1, 2, \dots, T$ ) denote the actual depth of the  $i^{\text{th}}$  defect at the forecasting year  $\tau$  since the last inspection considered in the Bayesian updating. The model-specific procedure to generate the depth of the  $i^{\text{th}}$  defect at year  $t_{in} + \tau$  (i.e. forecasting year  $\tau$ ),  $d_i(t_{in} + \tau)$ , is described as follows.

### 5.2.1 Gamma Process-based Model

It follow from Equation (2.1) in Chapter 2 that the growth of the depth of the  $i^{\text{th}}$  defect within the  $t^{\text{th}}$  year ( $t = 1, 2, \dots, t_{in} + \tau$ ), denoted by  $\Delta d_{it}(1)$ , follows a gamma distribution with a probability density function (PDF) given by

$$f_G(\Delta d_{it}(1) | \Delta A_{it}, \beta_i) = \beta_i^{\Delta A_{it}} \Delta d_{it}(1)^{\Delta A_{it}-1} e^{-\Delta d_{it}(1)\beta_i} / \Gamma(\Delta A_{it}) I_{(0, \infty)}(t) \quad (5.1)$$

where  $\Delta A_{it}$  and  $\beta_i$  denote the shape and rate parameters associated with the growth of defect  $i$  within the  $t^{\text{th}}$  year, respectively;  $\Gamma(\cdot)$  is the gamma function, and  $I_{(0, \infty)}(t)$  is the indication function and equals unity if both  $\Delta d_{it}(1) > 0$  and  $t > t_{i0}$ , and zero otherwise. It follows from Eq. (2.6) that  $\Delta A_{it} = \alpha$ , ( $t \geq t_{i0} + 1$ ), for the homogeneous gamma process (HGP) and  $\Delta A_{it} = \alpha(t-t_{i0})^\kappa - \alpha(t-1-t_{i0})^\kappa$ , ( $t \geq t_{i0} + 1$ ), for the non-homogeneous gamma process (NHGP). Given a simulation trial,  $d_i(t_{in} + \tau)$  can be generated as follows:

(1) generate  $\Delta d_{it}(1)$  ( $t = 1, 2, \dots, t_{in} + \tau$ ) from the gamma distribution given by Eq. (5.1) with  $\alpha$ ,  $\beta_i$ ,  $\kappa$  and  $t_{i0}$  equal to their corresponding posterior mean or median values evaluated from the MCMC simulation;

(2) calculate  $d_i(t_{in} + \tau) = \sum_{t=1}^{t_{in}+\tau} \Delta d_{it}(1)$ , ( $\tau = 1, 2, \dots, T$ ).

### 5.2.2 Inverse Gaussian Process-based Model

The inverse Gaussian process-based growth model, as described in Chapter 3, implies that  $\Delta d_{it}(1)$  follows an inverse Gaussian distribution characterized by a PDF given by

$$f_{IG}(\Delta d_{it}(1)|\alpha_i, \xi(\alpha_i)^2) = \sqrt{\frac{\xi}{2\pi}} \alpha_i (\Delta d_{it}(1))^{-\frac{3}{2}} \exp\left(-\frac{\xi(\Delta d_{it}(1)-\alpha_i)^2}{2\Delta d_{it}(1)}\right) I_{(0,\infty)}(t) \quad (5.2)$$

where  $\alpha_i$ ,  $\xi$  and  $\xi(\alpha_i)^2$  denote the mean, scale and shape parameters associated with  $\Delta d_{it}(1)$ , respectively, and  $I_{(0,\infty)}(t)$  denotes the indication function and is the same as that in Eq. (5.1). Based on the same procedure as described in Section 5.2.1,  $d_i(t_{in} + \tau)$  can be generated from Eq. (5.2) with  $\alpha_i$ ,  $\xi$  and  $t_{i0}$  equal to their corresponding posterior mean or median values evaluated from the MCMC simulation.

### 5.2.3 Geometric Brownian Motion-based Model

Given a realization of  $x_{in}$ ,  $r_{i,n-1}$ ,  $\beta$  and  $\sigma^2$  generated from the MCMC simulation, it follows from Eqs. (4.9) and (4.10) in Chapter 4 that the samples of  $d_i(t_{in} + \tau)$  ( $\tau = 1, 2, \dots, T$ ) can be obtained through Eq. (5.3) given by

$$d_i(t_{in} + \tau) = x_{in} + \sum_{l=1}^{\tau} r_i(t_{in} + l) \quad (5.3a)$$

$$\ln(r_i(t_{in} + \tau)) \sim \begin{cases} N(\ln(r_{i,n-1}) + \beta \Delta t_{i,n-1}, \sigma^2 \Delta t_{i,n-1}) & (\tau = 1) \\ N(\ln(r_i(t_n + \tau - 1)) + \beta, \sigma^2) & (\tau \geq 2) \end{cases} \quad (5.3b)$$

where  $r_i(t_{in} + \tau)$  denotes the average growth of defect depth within the  $\tau^{\text{th}}$  year of forecasting of defect  $i$ .

## 5.3 Time-dependent Internal Pressure Model

The internal pressure at a given location,  $P(t)$ , was modeled by the Poisson Square Wave Process (PSWP) (Madsen 2006; Straub and Faber 2007) in this study. A PSWP consists of a series of pulses, each of which has uncertain magnitude and duration (see Fig. 5.1). The number of pulses,  $Z$ , within a given period of time  $\Delta T$  follows a Poisson

distribution with a probability mass function of  $P(Z = z|\lambda) = (\lambda\Delta T)^z \exp(-\lambda\Delta T)/z!$ , where  $\lambda$  denotes the mean occurrence rate per unit time (or Poisson rate). This implies that the durations of individual pulses are independent exponentially distributed random variables with a mean duration equal to  $1/\lambda$  (Ang and Tang 1975; Cinlar 1975). The magnitudes of different pulses,  $P$ , are independent and identically distributed random variables characterized by a PDF of  $f_P(p)$ . In this study, It is assumed in accordance with CSA (CSA 2007) that the magnitude of the internal pressure at a given time follows a Gumbel distribution with distribution parameters  $\alpha_p$  and  $\mu_p$ , i.e.  $f_P(p|\alpha_p, \mu_p) = \alpha_p \exp(-\alpha_p(p - \mu_p)) \exp(-\exp(-\alpha_p(p - \mu_p)))$ . Given the generation rate  $\lambda$  and the Gumbel-distributed magnitude of the internal pressure, the procedure for generating a realization of the Poisson square wave process over a time interval  $\Delta T$  is given as follows.

- 1) set  $T_0 = 0$  and  $i = 1$ ;
- 2) generate a random number  $u$  between zero and one; set  $\Delta t_i = -1/\lambda \cdot \ln u$  and  $T_0 = T_0 + \Delta t_i$ ;
- 3) generate a random sample of the internal pressure  $p_i$  from the Gumbel distribution and assign  $p_i$  to the interval  $\Delta t_i$ , and
- 4) if  $T_0 \geq \Delta T$ , stop; otherwise, set  $i = i + 1$  and go to step 2).

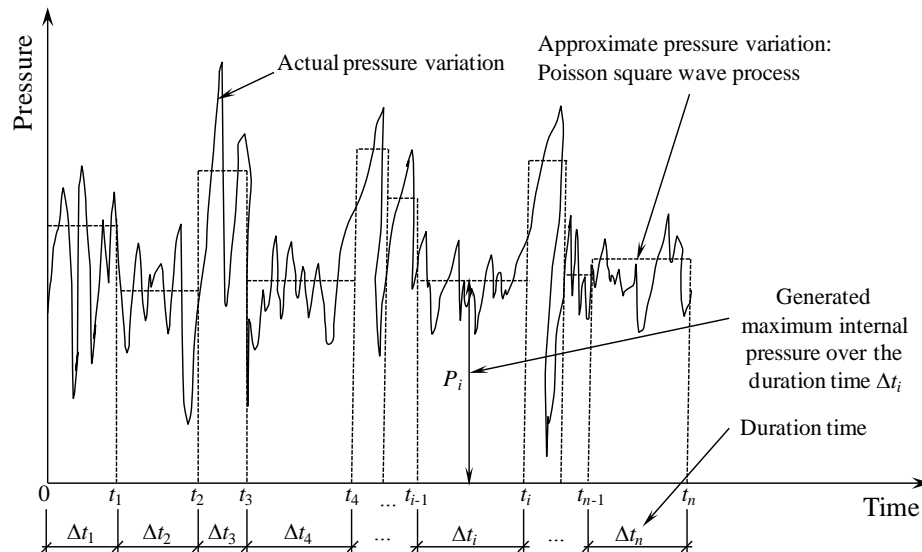


Figure 5.1 Poisson square wave process model

Figure 5.2 shows three simulated time-dependent internal pressure curves over 15 years corresponding to  $\lambda = 0.5$ ,  $\lambda = 1.0$  and  $\lambda = 2.0$  ( $\text{year}^{-1}$ ) following the above-described procedure, where the mean and coefficient of variation (COV) of the Gumbel-distributed magnitude of the internal pressure were assumed to be 5.9 MPa and 2%, respectively.

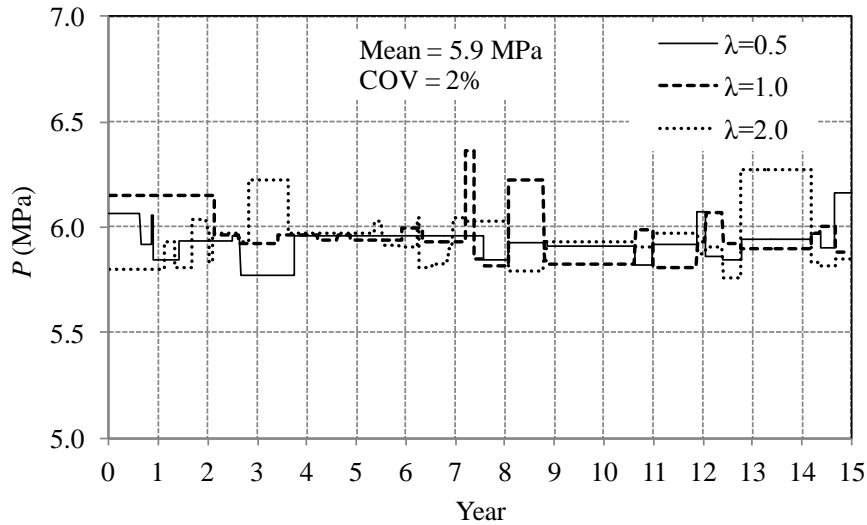


Figure 5.2 Simulated time-dependent internal pressure based on PSWP model

## 5.4 Time-dependent Reliability Evaluation of Pipeline Segment with Multiple Defects

### 5.4.1 Limit state Functions for a Single Corrosion Defect

A corroding natural gas pipeline can fail by three different failure modes, i.e. small leak, large leak and rupture, at a given corrosion defect under the internal pressure (Zhou 2010). The limit state function for defect penetrates the pipe wall, is defined as

$$g_1 = 0.8wt - d \quad (5.4)$$

where  $wt$  denotes the pipe wall thickness. The use of  $0.8wt$  as opposed to  $wt$  in Eq. (5.4) is consistent with the typical industry practice (Kariyawasam 2012) and literature (Caleyo et al. 2002), as the remaining ligament of the pipe wall is prone to developing cracks that can lead to a leak once the defect depth reaches  $0.8wt$ .

The limit state function for plastic collapse due to internal pressure at the defect is given by

$$g_2 = r_b - p \quad (5.5)$$

where  $r_b$  represents the burst pressure of a pipe containing a part-through wall corrosion defect, and can be evaluated using various mechanical models such as the ASME B31G, B31G Modified, CSA and PCORRC models.

The limit state function for unstable defect extension in the axial direction given burst is defined as

$$g_3 = r_{rp} - p \quad (5.6)$$

where  $r_{rp}$  is the rupture pressure, i.e. the pressure resistance of a pipe containing a through-wall flaw that results from the burst of the pipe at the corrosion defect. The through-wall flaw resulting from burst will undergo unstable extension in the longitudinal direction of the pipe and lead to a rupture if  $g_3 \leq 0$  (Nessim et al. 2009); otherwise, it will lead to a large leak. Note that details of  $r_p$  and  $r_{rp}$  are described in Section 5.5.1.

Utilizing  $g_1$ ,  $g_2$  and  $g_3$ , one can define a small leak as  $(g_1 \leq 0) \cap (g_2 > 0)$ , a burst as  $(g_1 > 0) \cap (g_2 \leq 0)$ , a large leak as  $(g_1 > 0) \cap (g_2 \leq 0) \cap (g_3 > 0)$ , and a rupture as  $(g_1 > 0) \cap (g_2 \leq 0) \cap (g_3 \leq 0)$ , where  $\cap$  represents a joint event. It follows that the probability of burst equals the sum of the probabilities of large leak and rupture. It should be emphasized that the limit state functions,  $g_1$ ,  $g_2$  and  $g_3$ , are all time-dependent because a) the defect grows over time and causes deterioration of the pipe resistance, and b) the internal pressure also vary with time.

#### 5.4.2 Methodology for System Reliability Analysis

The reliability analysis procedure was developed for pipe segments that have been subjected to at least one ILI. The analysis treats a pipe segment containing multiple active corrosion defects as a series system because failure at any corrosion defect within the segment implies failure of the system. It follows from Eq. (5.4) that the probability of

small leak of the pipe segment depends on the probability distribution of the maximum depth of the multiple defects in the segment. Extensive studies have been reported in the literature (e.g. Chaves and Melchers 2011; Melchers 2005) to derive the distribution of the maximum depth of multiple corrosion defects. However, it is inadequate to only derive the distribution of the maximum depth in this study because the failure probabilities corresponding to the other failure modes, i.e. large leak and rupture, depend on the defect length as well as the defect depth. Furthermore, the maximum length and maximum depth are not necessarily associated with the same defect. Given this, the simple Monte-Carlo simulation technique, which can be easily implemented to differentiate the three failure modes, was adopted to carry out the reliability analysis.

The growth of the depth of individual defect was characterized by the growth models as described in Section 5.2, whereas the defect length, consistent with the typical practice, was assumed to be static over the forecasting period, with the nominal value of the length obtained from the most recent inspection. For simplicity, the spatial variability of the material properties and internal pressure is ignored. The probabilities of small leak, large leak and rupture of the pipe segment after  $s$  years ( $s = 1, 2, \dots, T$ ) have elapsed since the last inspection,  $P_{sl}(s)$ ,  $P_{ll}(s)$  and  $P_{rp}(s)$  respectively, are evaluated according to the simulation method. A step-by-step procedure to check if the system has failed and to identify the corresponding failure mode within the forecasting period in a simulation trial is described in the following.

1) Generate samples for the pipe wall thickness ( $wt$ ), diameter ( $D$ ), ultimate tensile strength ( $\sigma_u$ ), and defect length ( $L_i$ ) ( $i = 1, 2, \dots, n_d$ ), where  $n_d$  denotes the total number of defects on the pipe segment considered and  $L_i$  denotes the length of the  $i^{th}$  defect.

2) Set the counters for small leak, large leak and rupture,  $SL(\tau)$ ,  $LL(\tau)$  and  $RP(\tau)$  ( $\tau = 1, 2, \dots, T$ ) respectively, to zero. Start from  $\tau = 1$  and carry out the following:

2.1) determine the internal pressure corresponding to forecasting year  $\tau$ ,  $p_\tau$ , based on a realization of the Poisson square wave process over the forecasting period generated according to the procedure described in Section 5.3;

2.2) generate the depth of the  $i^{\text{th}}$  defect at year  $t_{in} + \tau$  (i.e. forecasting year  $\tau$ ),  $d_i(t_{in} + \tau)$  based on the procedure described in Section 5.2.

2.3) calculate  $g_1 = 0.8wt - \max_i\{d_i(t_{in} + \tau)\}$ ;

2.4) calculate  $g_2 = \min_i\{r_{bi}(t_{in} + \tau)\} - p_\tau$ , where  $r_{bi}(t_{in} + \tau)$  denotes the burst pressure of pipe at the  $i^{\text{th}}$  defect at year  $t_{in} + \tau$ , and is obtained by substituting  $wt$ ,  $D$ ,  $\sigma_u$ ,  $L_i$  and  $d_i(t_{in} + \tau)$  into the burst pressure model considered; if  $d_i(t_{in} + \tau) > 0.8wt$ , set  $d_i(t_{in} + \tau) = 0.8wt$ ;

2.5) if  $g_1 > 0$  and  $g_2 > 0$ , set  $\tau = \tau + 1$ ;

2.6) if  $\tau \leq T$  go to Step 2.2), and

2.7) if  $g_1 \leq 0$  and  $g_2 > 0$ , set  $SL(\tau) = SL(\tau) + 1$ ; calculate  $g_3 = r_{rpm} - p_\tau$ , where  $r_{rpm}$  is the rupture pressure at the defect that has the lowest burst pressure at year  $t_{in} + \tau$ , if  $g_2 \leq 0$  and  $g_3 > 0$  set  $LL(\tau) = LL(\tau) + 1$ ; if  $g_2 \leq 0$  and  $g_3 \leq 0$  set  $RP(\tau) = RP(\tau) + 1$  (it is conservatively assumed that either a large leak or a rupture will occur if  $g_2 \leq 0$  regardless of whether  $g_1 \leq 0$  or  $g_1 > 0$ ).

By repeating the above calculation steps for  $N$  simulation trials,  $P_{sl}(s)$ ,  $P_{ll}(s)$  and  $P_{rp}(s)$  can be estimated as follows:

$$P_{sl}(s) \approx \frac{1}{N} \sum_{\tau=1}^s SL(\tau) \quad (5.7a)$$

$$P_{ll}(s) \approx \frac{1}{N} \sum_{\tau=1}^s LL(\tau) \quad (5.7b)$$

$$P_{rp}(s) \approx \frac{1}{N} \sum_{\tau=1}^s RP(\tau) \quad (5.7c)$$



## 5.5 Example

### 5.5.1 General

In this section, an example is used to illustrate the above-described methodology for the system reliability analysis. The example involves an underground natural gas pipeline that is the same as that described in Chapter 2. Two pipe segments, namely Segments 1 and 2, were selected from this pipeline to carry out the reliability analysis. Segment 1, consisting of a single pipe joint with a length of about 13.2 m, was used to illustrate the application of the proposed methodology, whereas Segment 2, consisting of many pipe joints and having a length of about 560 m, was used to investigate the impact of the growth model on the time-dependent failure probabilities. Both pipe segments have a nominal outsider diameter of 508 mm (20 inches), an operating pressure of 5.66 MPa, and a nominal wall thickness of 5.56 mm, and were made from API 5L X52 steel with a specified minimum yield strength (SMYS) of 359 MPa and a specified minimum tensile strength (SMTS) of 456 MPa.

Twenty-five active corrosion defects on Segment 1 were detected and sized by high-resolution magnetic flux leakage (MFL) tools in 2000, 2004, 2007, 2009 and 2011. It follows from Section 2.3 in Chapter 2 that the ILI data are subjected to measurement errors characterized by  $a_j$ ,  $b_j$ ,  $\sigma_j$  and  $\rho_{jk}$ , with  $a_j$  ( $b_j$ ) and  $\sigma_j$  ( $j = 1, 2, \dots, 5$  in this study) denoting the constant (non-constant) bias and the standard deviation of the random scattering error associated with the ILI tool used in the  $j$ th inspection respectively, and  $\rho_{jk}$  ( $j = 1, 2, \dots, 5; k = 1, 2, \dots, 5$ ) denoting the correlation coefficient between the random scattering errors associated with the ILI tools used in the  $j$ th and  $k$ th inspections. The above-described measurement errors associated with these ILI tools were quantified by comparing the ILI-reported and field-measured depths of 128 static defects (i.e. defects that have been recoated and ceased growing) (Al-Amin et al. 2012) as described in Section 2.6.1 of Chapter 2 and are as follows:  $a_1 = a_2 = 2.04$  (%wt),  $a_3 = -15.28$  (%wt),  $a_4 = -10.38$  (%wt) and  $a_5 = 4.84$  (%wt);  $b_1 = b_2 = 0.97$ ,  $b_3 = 1.4$ ,  $b_4 = 1.13$  and  $b_5 = 0.84$ ;  $\sigma_1 = \sigma_2 = 5.97$  (%wt),  $\sigma_3 = 9.05$  (%wt),  $\sigma_4 = 7.62$  (%wt) and  $\sigma_5 = 5.94$  (%wt);  $\rho_{12} = 0.82$ ,  $\rho_{13} = \rho_{23} = 0.7$ ,  $\rho_{14} = \rho_{24} = 0.72$ ,  $\rho_{15} = \rho_{25} = 0.82$ ,  $\rho_{34} = 0.78$ ,  $\rho_{35} = 0.71$  and  $\rho_{45} = 0.74$  (Al-

Amin et al. 2012), where the subscripts ‘1’, ‘2’, ‘3’, ‘4’ and ‘5’ denote the parameters associated with the ILI data obtained in 2000, 2004, 2007, 2009 and 2011, respectively. Segment 2 contains 10 defects selected from the 62 defects described in Chapter 2. The rationale for selecting the 10 defects is described in Section 5.5.3.

The PCORRC model (Leis and Stephens 1997) was adopted in this study to calculate the burst pressure of the pipe at a given corrosion defect, i.e.  $r_b$  in Eq. (5.5). The burst pressure is calculated as follows:

$$r_b = \xi_b \frac{2\sigma_u wt}{D} \left[ 1 - \frac{d}{wt} \left( 1 - \exp \left( \frac{-0.157L}{\sqrt{\frac{D(wt-d)}{2}}} \right) \right) \right] \quad (5.8)$$

where  $\sigma_u$  is the ultimate tensile strength of the pipe steel;  $D$  is the pipe diameter;  $L$  is the defect length, and  $\xi_b$  is a multiplicative model error term. Equation (5.8) is applicable for  $d/wt \leq 0.8$  and  $L \leq 2D$  (Fu et al. 2001; Kiefner et al. 1973).

The model developed by Kiefner et al. (Kiefner et al. 1973) for pressurized pipes containing through-wall defect was used to calculate the rupture pressure,  $r_{rp}$ , as follows:

$$r_{rp} = \frac{2\sigma_f wt}{MD} \quad (5.9a)$$

$$M = \begin{cases} \sqrt{1 + 0.6275 \frac{L^2}{Dwt} - 0.003375 \left( \frac{L^2}{Dwt} \right)^2} & L \leq \sqrt{50Dwt} \\ 3.3 + 0.032 \frac{L^2}{Dwt} & L > \sqrt{50Dwt} \end{cases} \quad (5.9b)$$

where  $M$  is the Folias factor, and  $\sigma_f$  is the flow stress and defined as  $0.9\sigma_u$  (Kiefner et al. 1973). The model error associated with Eq. (5.9a) was ignored due to a lack of relevant information in the literature.

### 5.5.2 Time-dependent Reliability Analysis Using the HGP-based Growth Model

In this section, the time-dependent system reliability of Segment 1 was evaluated considering the 25 active corrosion defects identified by ILI. The growth models for the

depths of the defects were first developed using the ILI-reported depths in 2000, 2004, 2007, 2009 and 2011. The apparent growth paths of the defects as indicated by the ILI data are shown in Fig. 5.3. Similar to Fig. 2.4(a), the decrease in the ILI-reported depths over time for some defects shown in Fig. 5.3 is attributed to the measurement error. The ILI-reported lengths in 2011 for the 25 defects, which were indicated as the numbers at top of the bins in Fig. 5.4, were adopted as the nominal defect lengths in the reliability analysis. The measurement errors (i.e. the COV value) associated with the ILI-reported lengths were assumed based on the common tool specifications that indicate a confidence interval of the actual length  $\pm 10$  mm with a probability of 80% for the measured length. The homogeneous gamma process- (HGP-) based model was adopted in this section with the parameters of the prior distributions of the model parameters identical with those specified for Scenario I-1 of the HGP-based model described in Chapter 2, i.e.  $p_1 = 10$ ,  $q_1 = 1$  (year),  $p_3 = 0$  (year),  $q_4 = 28$  (year),  $p_4 = 1$ ,  $q_2 = 1$  (%wt).

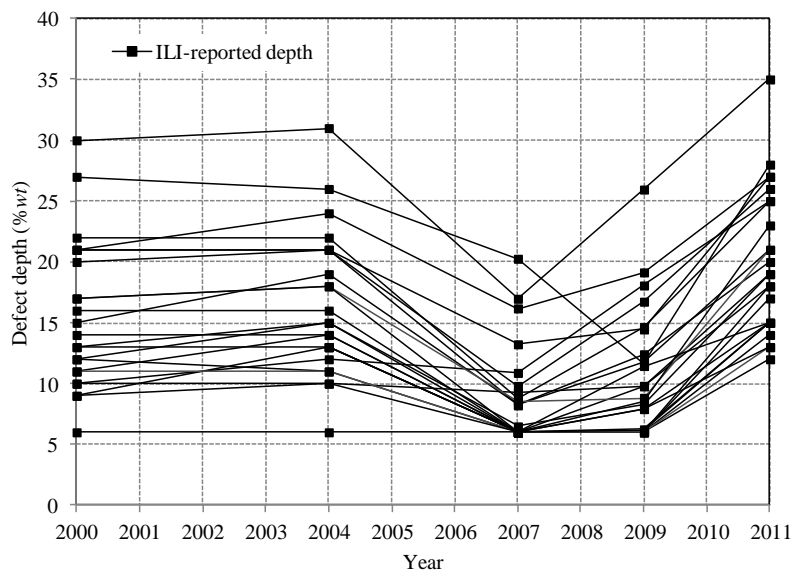


Figure 5.3 Apparent growth paths indicated by the ILI-reported depths

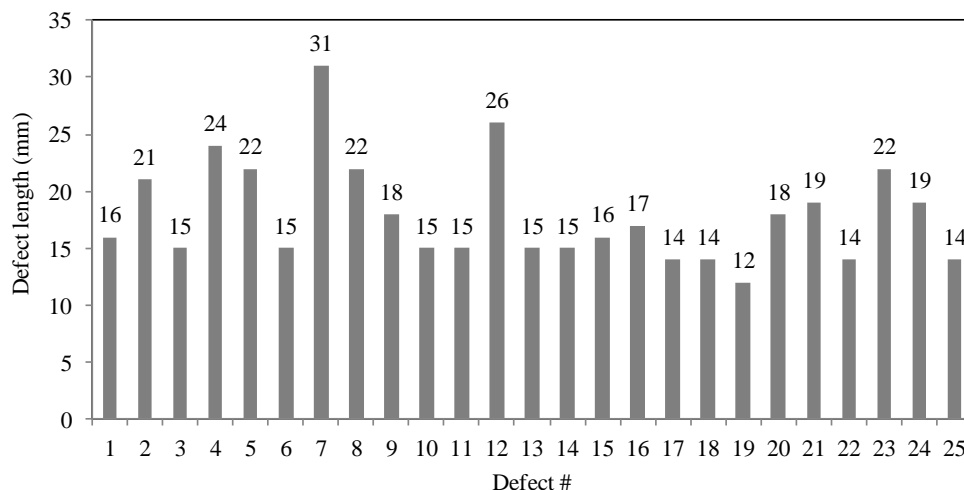


Figure 5.4 Defect lengths of 25 defects reported by the ILI in 2011

A total of 110,000 MCMC simulation sequences were generated in *OpenBUGS*; the first 10,000 sequences were considered the burn-in period and therefore discarded. A thinning interval (Gelman et al. 2004) of 10 was applied to the remaining sequences to generate 10,000 sets of MCMC samples of the growth parameters (i.e.  $\alpha$ ,  $\beta_i$  and  $t_{i0}$ ) for the defect depth, which were used to make inference of the probabilistic characteristics (e.g. mean, standard deviation and probabilistic distribution) of the growth parameters. The thinning interval reduces the autocorrelation between the samples from different MCMC sequences and therefore allows these samples to be considered approximately independent and equivalent to the samples generated from the simple Monte Carlo simulation.

The failure probabilities of the pipe joint were evaluated through  $10^6$  Monte Carlo simulation trials. To investigate the impact of the uncertainties in the growth parameters as well as the correlations between those parameters on the failure probability, three different scenarios were considered in the reliability analysis. The first scenario (denoted by Scenario I) considers the uncertainties in the growth parameters as well as their correlations by directly employing the MCMC samples of the growth parameters in the reliability analysis. To this end, a total of 2,000 sets of samples were randomly selected from the 10,000 sets of MCMC samples first. Each selected set of MCMC samples of the growth parameters were further used to generate 500 random samples of the growth path

for a given defect in the reliability analysis, which leads to a total of  $10^6$  simulation trials for the reliability analysis. The second scenario (denoted by Scenario II) considers the uncertainties in the growth parameters but ignores their correlations. In this scenario, a total of  $10^6$  simulation trials were generated in the same manner as that described in Scenario I except that the 2000 sets of samples of the growth parameters (i.e.  $\alpha$ ,  $\beta_i$  and  $t_{i0}$ ) were instead generated from their corresponding marginal distributions, therefore ignoring correlations between the growth parameters. The marginal distribution of each growth parameter was developed using the distribution fitting technique based on the 10,000 MCMC samples. The third scenario (denoted by scenario III) assumes that the growth parameters are deterministic and equal to their corresponding mean values evaluated from the MCMC simulation (i.e. the growth path was generated using the procedures described in Section 5.2.1); therefore, the uncertainties in the growth parameters and their correlations are ignored in this scenario.

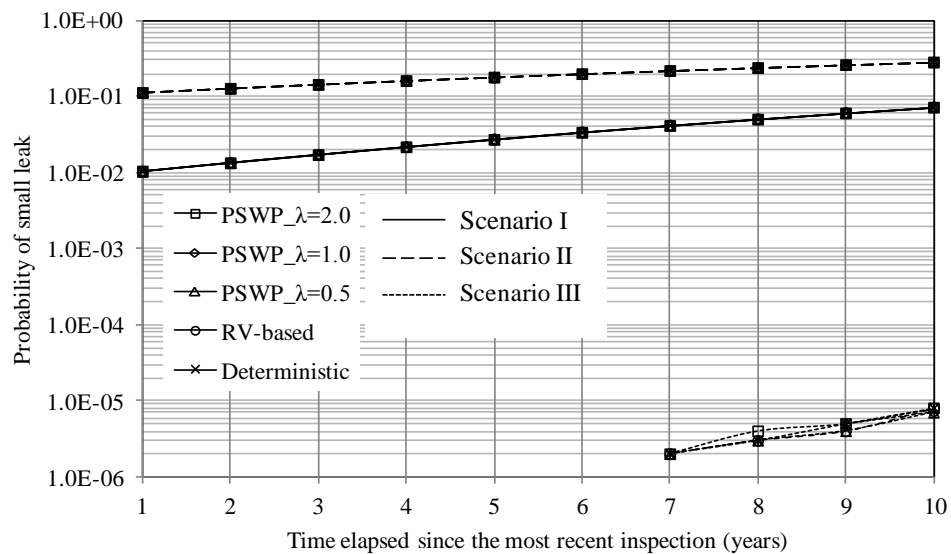
The probabilistic characteristics of the random variables involved in calculating  $r_b$  and  $r_{rp}$  are summarized in Table 5.1. All the random variables in Table 5.1 were assumed to be mutually independent. The model errors associated with individual defects were assumed to be fully correlated.

Due to a lack of the time history for the internal pressure, the generation rate (i.e.  $\lambda$ ) of the Poisson square wave process could not be quantified. Parametric analyses were therefore carried out by assuming three different values of  $\lambda$ , namely 0.5, 1.0 and 2.0 ( $\text{year}^{-1}$ ). The probability distribution of the magnitude of the internal pressure is summarized in Table 5.1. For comparison, the reliability analysis was also carried out assuming the internal pressure to be a random variable or a deterministic quantity. For the former case, the probability distribution of the internal pressure was assumed to be the same as that summarized in Table 5.1. For the latter case, the internal pressure was set equal to the mean value of the distribution of the internal pressure in Table 5.1.

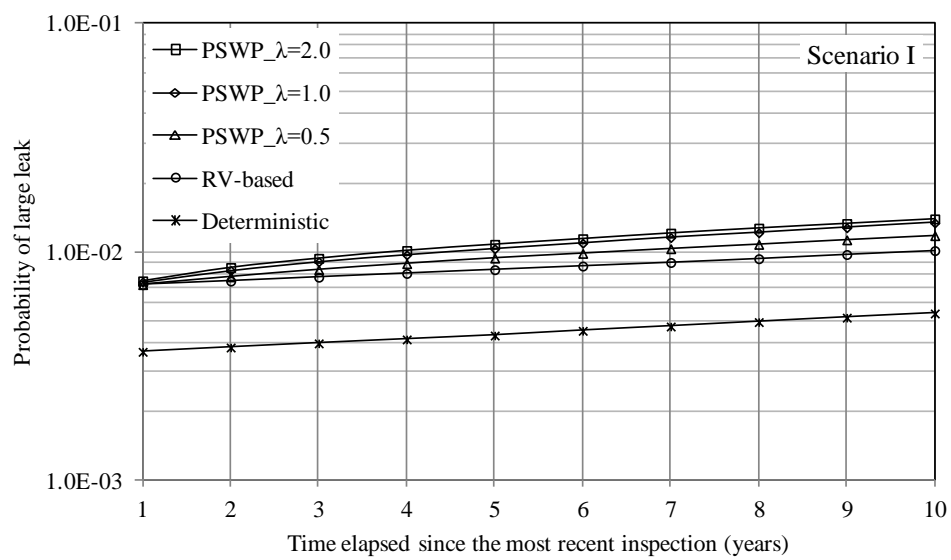
Table 5.1 Probabilistic characteristic of the random variables

Random variable	Nominal value	Unit	Mean/Nominal	COV (%)	Distribution type	Source
$L_1-L_{25}$	Given by Fig. 5.4	mm	1.0	7.8/mean	Normal	Leis and Stephens 1997
$D$	508		1.0	0.06	Normal	CSA 2007
$wt$	5.56		1.0	0.25/mean	Normal	Jiao et al. 1995
$\sigma_u$	455	MPa	1.08	3	Normal	Jiao et al. 1995
$P$	5.66		1.05	2	Gumbel	Zhou 2010; CSA 2007
$\xi_b$	1.0	N/A	1.079	26.4	Gumbel	Zhou and Huang 2012

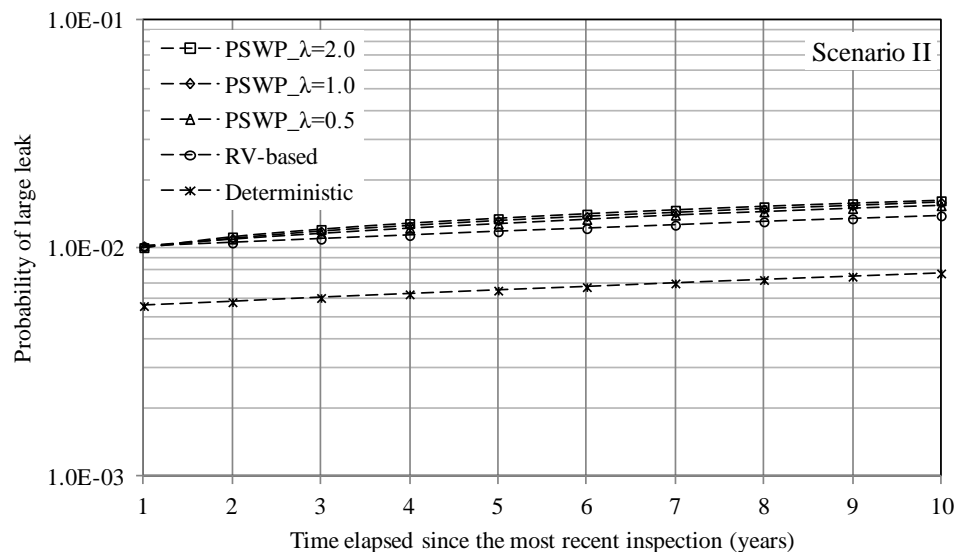
The probabilities of small leak and large leak corresponding to the three assumptions for the internal pressure (i.e. PSWP, random variable and deterministic value) and three scenarios for the growth model (i.e. Scenarios I, II and III), over a 10-year forecasting period, are shown in Fig. 5.5. The probability of rupture of this segment is too small to be evaluated based on the  $10^6$  simulation trials. For brevity, the random variable-based internal pressure model is denoted by “RV-based” in the figure. Figure 5.5(a) suggests that the pressure model has a negligible impact on the probability of small leak for a given scenario for the defect growth model; this is expected because the internal pressure only impacts burst. Figure 5.5(a) further indicates that the scenario for the growth model has a marked impact on the probability of small leak. For example, the probabilities of small leak corresponding to Scenario II (i.e. considering the uncertainties in the parameters of the growth model but ignoring their correlations) are four to ten times as high as those corresponding to Scenario I (i.e. considering the uncertainties in the model parameters and their correlations); this is mostly due to the fact that the posterior distributions of  $\alpha$  and  $\beta_i$  of the growth model are positively correlated whereas the posterior distributions of  $\beta_i$  and  $t_{i0}$  of the growth model are negatively correlated. The probabilities of small leak corresponding to Scenario I are approximately four orders of magnitude higher than those corresponding to Scenario III (i.e. assuming parameters of the growth model to be deterministic) from forecasting years 7 through 10.



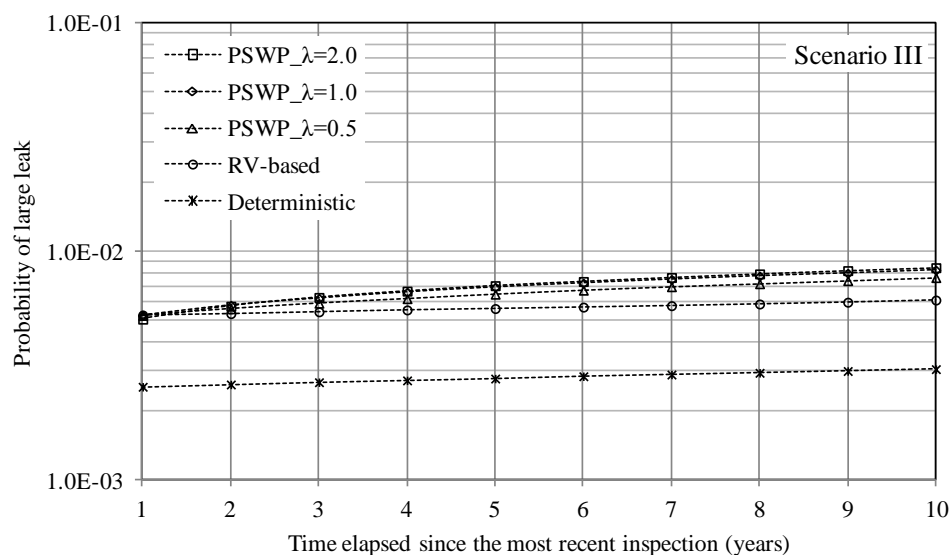
(a)



(b)



(c)



(d)

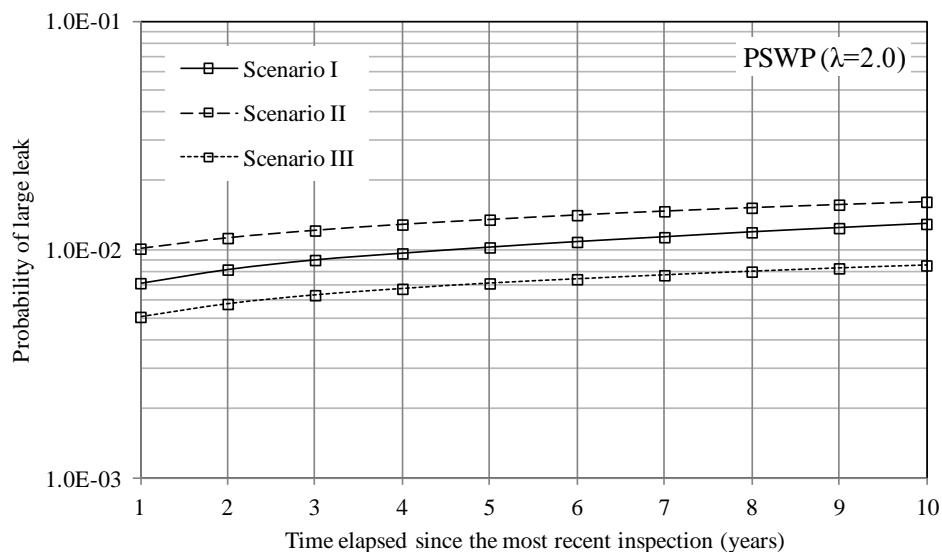
Figure 5.5 Comparison of probabilities of small leak (large leak) associated with different internal pressure models

Figures 5.5(b) through 5.5(d) indicate that, for a given scenario for the growth model, the probabilities of large leak evaluated based on the PSWP model increase marginally as  $\lambda$  increases from 0.5 to 2.0, and are slightly higher than those corresponding to the random variable-based internal pressure. The probabilities of large leak corresponding to

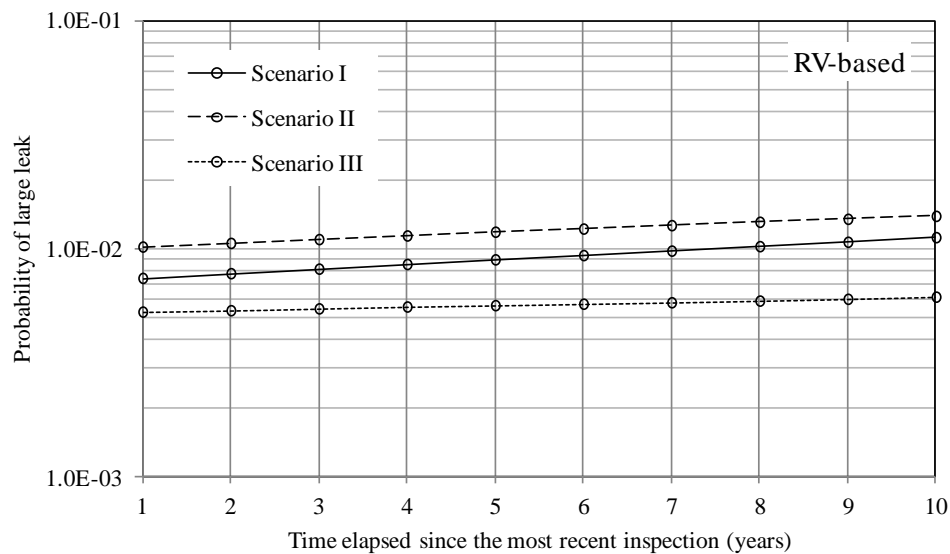


the assumption of uncertain internal pressure (characterized by either PSWP or a random variable) are about twice as high as those corresponding to the deterministic internal pressure; this indicates the importance of accounting for the uncertainty in the internal pressure in the reliability analysis, even if the uncertainty in the pressure is relatively low (the COV of the pressure magnitude being 2% in this example).

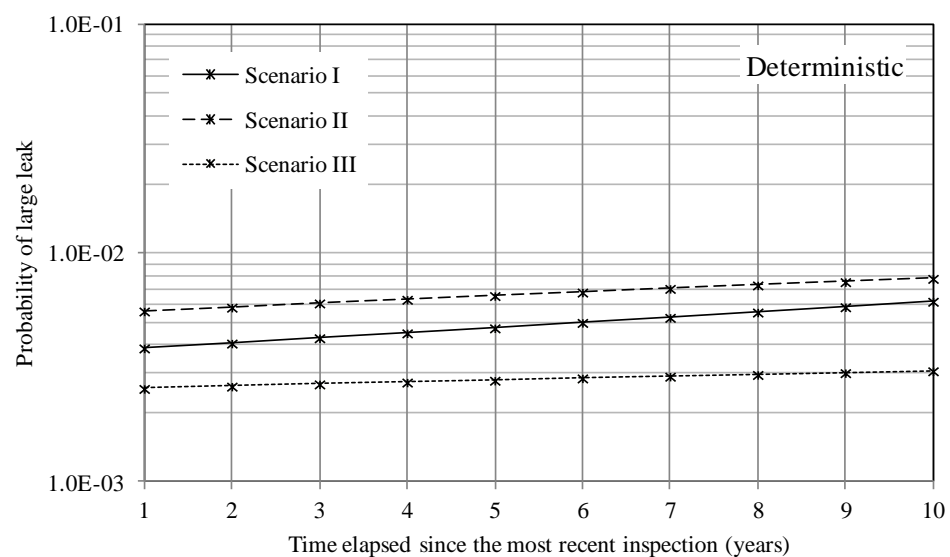
The probabilities of large leak evaluated based on Scenarios I, II and III are compared in Figs. 5.6; the internal pressure corresponding to Figs. 5.6(a), 5.6(b) and 5.6(c) is modeled by a PSWP with  $\lambda$  equal to 2.0, a random variable and a deterministic quantity, respectively. Figure 5.6 indicates that the uncertainties in the growth parameters and correlations among these parameters have a marked impact on the probability of large leak. For example, the probabilities of large leak corresponding to Scenario II (Scenario I) are about twice as high as those corresponding Scenario I (Scenario III) for a given pressure model. On the other hand, the impact of the uncertainties in the parameters of the growth model on the probability of large leak is significantly less than that on the probability of small leak. This is mainly attributed to that the probability of small leak is governed by the uncertainties in only two random variables (i.e.  $wt$  and  $d$ ) as shown in the limit state function  $g_1$ , and is therefore highly sensitive to the uncertainty in  $d$ .



(a)



(b)



(c)

Figure 5.6 Comparison of probabilities of large leak associated with three scenarios for growth model

### 5.5.3 Impact of Growth Models on the Time-dependent Reliability

The time-dependent system reliability of Segment 2 with respect to corrosion was evaluated by considering four different corrosion growth models to investigate the impact

of the growth models on the computed reliability. The 10 defects located in this segment were selected from the 62 defects for which the NHGP-, HGP-, IGP- and GBM-based growth models have been developed from the Bayesian analysis based on three sets of ILI data (i.e. ILI data in 2000, 2004 and 2007) and described in Chapters 2 through 4. Details of the growth models are summarized in Table 5.2. Although the 10 defects have been mitigated in 2010, it is assumed the defects are still active after 2010 by ignoring the mitigation. The failure probabilities of Segment 2 over a ten-year forecasting period since the most recent inspection included in the Bayesian updating (i.e. from years 2008 to 2017) were then evaluated using the simulation-based approach for each of the growth models considered. The growth path of a given defect in a given simulation trial was generated based on the procedure described in Section 5.2, with the model parameters equal to the posterior mean/median values evaluated from the Bayesian updating.

Table 5.2 Summary of the growth models

Model	Values of model parameters	ILI Data sets used in Bayesian updating	Defect population used in the Bayesian updating	Model details	MSEP ( $(\%wt)^2$ )
NHGP	median	2000, 2004 and 2007	62	See Scenario II in Chapter 2	43
HGP	mean			See Scenario I-1 in Chapter 2	44
IGP	median			See Scenario 1 in Chapter 3	43
GBM	Median			See Scenario I in Chapter 4	49

The selection of the 10 defects for the reliability analysis is based on the consideration that the absolute values of deviations between the predicted and field-measured depths for the 10 defects in 2010 are reasonably small (e.g.  $< 5 \%wt$ ) for the four growth models considered, as reflected by Fig. 5.7. This indicates that the four growth models lead to similar predicted depths for the 10 defects, which allows the comparison of the failure probabilities corresponding to different growth models to be founded on a common basis.

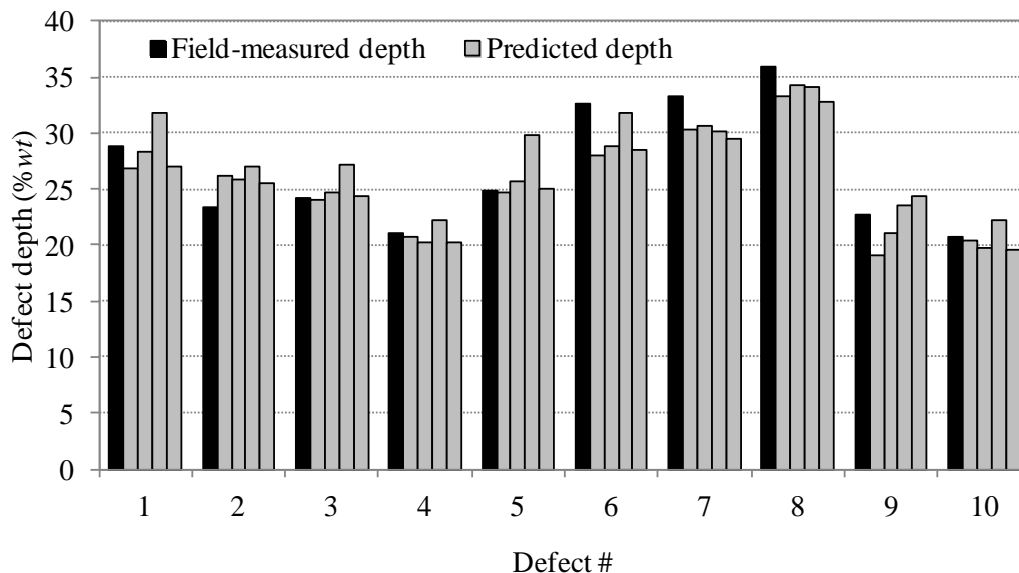
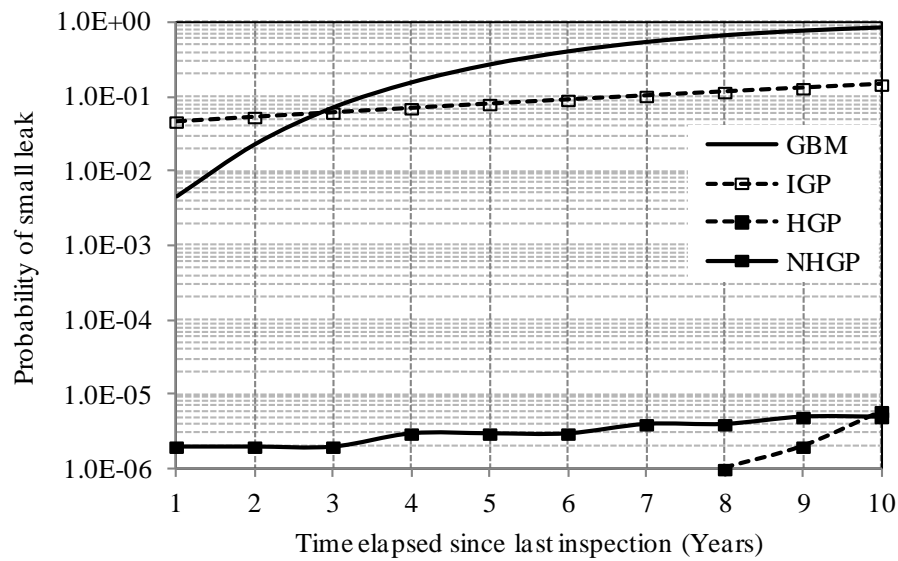


Figure 5.7 Comparison of the predicted and actual depths in 2010 for the 10 defects on Segment 2

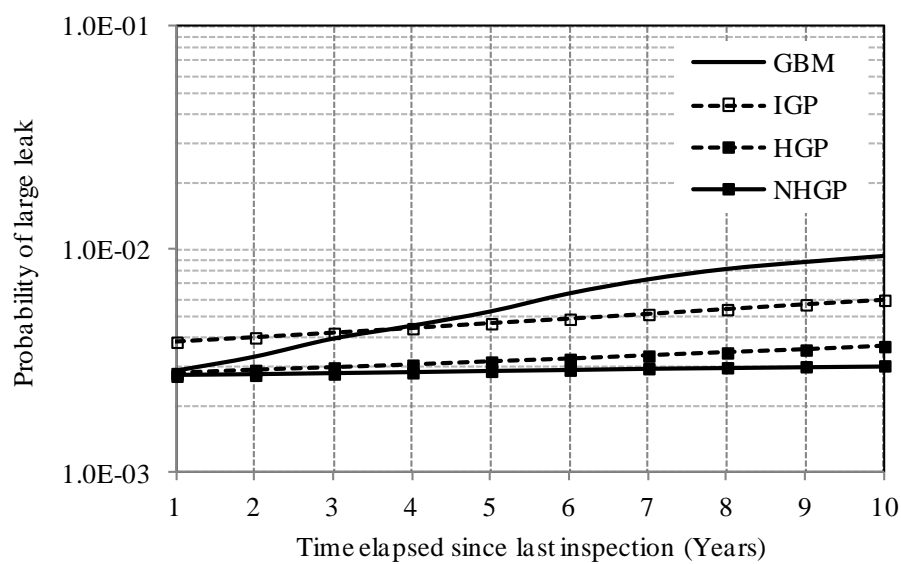
(the four grey-shaded bins for a given defect represent, from left to right, NHGP-, HGP-, IGP and GBMP-based growth models, respectively)

The probabilistic characteristics of  $D$ ,  $wt$ ,  $\sigma_u$ ,  $P$  and  $\xi_b$  are the same as those defined in Table 5.1. Furthermore, the internal pressure was assumed to be a random variable with a probability distribution the same as that summarized in Table 5.1. Due to a lack of the ILI-reported lengths of the 10 defects in the ILI of 2007, the lengths of the 10 defects, denoted by  $L_i$  ( $i = 1, 2, \dots, 10$ ), were assumed to be independent and follow an identical lognormal distribution with a mean of 30 mm and a coefficient of variation (COV) of 50% based on the information summarized in Annex O of CSA Z662 (CSA 2007).

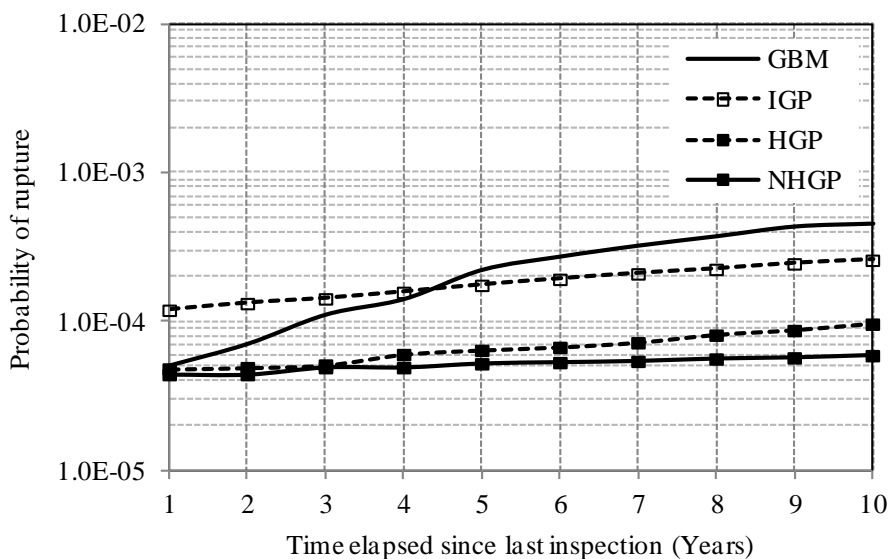
The probabilities of small leak, large leak and rupture, over a ten-year forecasting period, corresponding to the four growth models are depicted in Figs. 5.8(a) through 5.8(c), respectively. The failure probabilities were evaluated based on  $10^6$  simulation trials.



(a)



(b)



(c)

Figure 5.8 Time-dependent failure probabilities based on different growth models

Results shown in Figure 5.8(a) indicate that the probabilities evaluated using the IGP- and GBM-based models are significantly higher than those evaluated using the GP-based (i.e. HGP- and NHGP-based) models over the entire forecasting period, for example, the probabilities of small leak corresponding to the IGP-based model are about four orders of magnitude higher than those corresponding to the NHGP-based model over the entire forecasting period. On the other hand, the probabilities of small leak corresponding to the IGP-based model are higher than those corresponding to the GBM-based model if the forecasting period  $\tau$  is less than 3 years. The latter are higher than the former for  $\tau \geq 3$  years. Of the four growth models considered, the GBM-based model leads to a rapidly increasing probability of small leak over the ten-year forecasting period. For example, the probability of small leak at the end of the forecasting period is more than two orders of magnitude higher than that at the beginning of the forecasting period. It can be observed that the probabilities of small leak corresponding to the NHGP-based model differ significantly from those corresponding to the HGP-based model especially for  $\tau \leq 8$  years. Figure 5.8(a) implies that the probability of small leak is very sensitive to the growth model employed to characterize the defect depth. This is expected because only

two random variables (i.e.  $d$  and  $wt$ ) are included in the limit state function given by Eq. (5.4).

Results shown in Figs. 5.8(b) and 5.8(c) illustrate that the IGP- (GBM-) based model leads to the most conservative estimate of the failure probability for  $\tau \leq 4$  ( $\tau > 4$ ) years, which is similar as that observed from Fig. 5.8(a). Furthermore, the difference between the probabilities of large leak/rupture corresponding to the NHGP- and HGP-based models is small. The probabilities of large leak (rupture) corresponding to the IGP-based model are about two (three) times those corresponding to the GP-based models. Figure 5.8(a) and 5.8(b) suggest that the impact of the growth model on the probabilities of large leak and rupture is less pronounced than that on the probability of small leak as reflected by Fig. 5.8(a). This observation is mainly attributed to the fact that the limit state functions for large leak and rupture as given by Eqs.(5.5) and (5.6) include a total of eight random variables (as opposed to a total of two random variables involved in the limit state function for small leak). The uncertainties in parameters (e.g. the internal pressure and model error for the burst capacity model) other than the defect depth can have a large impact on the failure probabilities.

## 5.6 Conclusions

This chapter presents a methodology to evaluate the time-dependent system reliability of natural gas pipelines containing multiple active metal-loss corrosion defects. The methodology employs the homogeneous gamma process- (HGP-), non-homogeneous gamma process- (NHGP-), inverse Gaussian process- (IGP-) or geometric Brownian motion- (GBM-) based model to characterize the growth of the depth of individual corrosion defect and the Poisson square wave process (PSWP) to model the internal pressure of the pipeline. The methodology further incorporates the inspection data in the reliability analysis by using the hierarchical Bayesian method and Markov Chain Monte Carlo (MCMC) simulation to update the growth model for the defect depth. The measurement uncertainties associated with the ILI data are taken into account in the Bayesian updating. The simple Monte Carlo simulation is used to evaluate the failure

probability of the pipeline in terms of three distinctive failure modes, namely small leak, large leak and rupture.

An example involving two pipe segments (denoted as Segments 1 and 2) selected from a natural gas pipeline that is currently in service in Alberta, Canada was used to illustrate the proposed methodology and the impact of the internal pressure and corrosion growth models on the time-dependent failure probabilities of the pipe segment.

The time-dependent system reliability analysis was first carried out for Segment 1 that contains 25 active defects identified by multiple ILIs by incorporating the HGP-based corrosion growth model and PSWP-based internal pressure model. The defect length was assumed to be static, with the nominal length equal to the length reported by the most recent inspection. Three different scenarios for the growth model in terms of the uncertainties in the model parameters and their correlations were considered in the reliability analysis, namely considering the uncertainties in the model parameters and their correlations (Scenario I), considering the uncertainties in the model parameters but ignoring their correlations (Scenario II), and assuming deterministic model parameters (Scenario III). Furthermore, three assumptions for the internal pressure (i.e. Poisson square wave process (PSWP), random variable and deterministic quantity) were considered.

The analysis results suggest that the internal pressure model has a negligible impact on the probability of small leak. The probabilities of large leak corresponding to the uncertain internal pressure (characterized by either PSWP or a random variable) are approximately twice as high as those corresponding to the deterministic internal pressure. This indicates the importance of accounting for the uncertainty in the internal pressure in the reliability analysis. The analysis results also reveal that different scenarios for the growth model have a marked impact on the probabilities of small leak and large leak. For example, the probabilities of small leak corresponding to Scenario II are four to ten times as high as those corresponding to Scenario I because the posterior distributions of the shape and rate parameters in the gamma process are positively correlated, whereas the rate parameter and the initiation time in the gamma process are negatively correlated; the



probabilities of small leak corresponding to Scenario I are approximately four orders of magnitude as high as those corresponding to Scenario III. The analysis results highlight the importance of appropriately accounting for the uncertainties in the growth parameters as well as their correlations in the reliability analysis based on the proposed Bayesian growth model.

The time-dependent system reliability analysis was then carried out for Segment 2 that contains 10 active defects for which the predicted depths obtained from the four growth models agree well with the actual depths (e.g. the absolute deviations between the predicted and actual depths are less than 5 % *wt*). The internal pressure was characterized by a random variable. Analysis results suggest that the growth models have a significant impact on the probability of small leak, but a smaller impact on the probabilities of large leak and rupture. For example, over the entire forecasting period, the probabilities of small leak corresponding to the IGP-based model are about four orders of magnitude higher than those corresponding to the NHGP-based model, whereas the probabilities of large leak (rupture) corresponding to the former model are about two (three) times those corresponding to the latter model. The methodology developed in this chapter will facilitate the development of the reliability-based management of corroding pipelines.

## References

- Al-Amin, M., Zhou, W., Zhang, S., Kariyawasam, S. and Wang, H. (2012). Bayesian model for the calibration of ILI tools. Proceedings of IPC 2012, IPC2012-90491, ASME, Calgary.
- Ang, A. H. S. and Tang, W. H. (1975). Probability Concepts in Engineering Planning and Design, Volume I: Basic Principles. John and Wiley & sons, NY.
- Ahammed, M. (1998). Probabilistic estimation of remaining life of a pipeline in the presence of active corrosion defects. International Journal of Pressure Vessels and Piping, 75(4): 321-29.

- Amirat, A., Mohamed-Chateaneuf, A. and Chaoui, K. (2006). Reliability assessment of underground pipelines under the combined effect of active corrosion and residual stress. *International Journal of Pressure Vessels and Piping*, 83(2):107-17.
- Caleyo, F., Gonzalez, J. L. and Hallen, J. M. (2002). A study on the reliability assessment methodology for pipelines with active corrosion defects. *International Journal of Pressure Vessels and Piping*, 79(1): 77-86.
- Caleyo, F., Velázquez, J. C., Valor, A. and Hallen, J. M. (2009). Markov chain modelling of pitting corrosion in underground pipelines. *Corrosion Science*, 51(9): 2197-2207.
- Chaves, I. A. and Melchers, R. E. (2011). Pitting corrosion in pipeline steel weld zones. *Corrosion Science*, 53(12): 4026-4032.
- Cheng, T. and Pandey, M. D. (2012). An accurate analysis of maintenance cost of structures experiencing stochastic degradation. *Structure and Infrastructure Engineering*, 8(4): 329-39.
- Cinlar, E. (1975). *Introduction to Stochastic Processes*. Prentice-Hall Inc., Englewood, Cliffs, NJ.
- Cosham, A., Hopkins, P. and Macdonald, K. A. (2007). Best practice for the assessment of defects in pipelines—corrosion. *Engineering Failure Analysis*, 14(7): 1245-65.
- CSA (2007). *Oil and gas pipeline systems, CSA standard Z662-07*. Mississauga, Ontario, Canada: Canadian Standard Association.
- El-Reedy, M. A. (2009). *Advanced Materials and Techniques for Reinforced Concrete Structures*, CRC Press, UK.
- Fu, B., Stephens, D., Ritchie, D. and Jones, C. L. (2001). Methods for assessing corroded pipeline - review, validation and recommendations. PRCI/EPRG 13th Biennial Joint Technical Meeting, New Orleans, Louisiana, USA.
- Gelman, A., Carlin, J. B., Stern, H. S. and Rubin, D. B. (2004). *Bayesian Data Analysis* (2nd edition). Chapman & Hall/CRC, NY.

- Hong, H. P. (1999). Application of stochastic process to pitting corrosion. *Corrosion*, 55(1): 10-16.
- Hong, H. P. (1999). Inspection and maintenance planning for pipelines under external corrosion considering generation of new defects. *Structural Safety*, 21: 203-22.
- Jiao, G., Sotberg, T. and Igland, R. T. (1995). SUPERB 2M statistical data-basic uncertainty measures for reliability analysis of offshore pipelines. SUPERB project report.
- Jonhson, R. A. (2000). *Probability and statistics for engineers* (6th edition). Prentice-Hall Inc, US.
- Kariyawasam, S. (2012). Private communication.
- Kariyawasam, S. and Peterson, W. (2010). Effective improvements to reliability based corrosion management. Proceedings of 8th International Pipeline Conference 2010, ASME, IPC2010-31425, Calgary, Alberta, Canada.
- Kiefner, J. F., Maxey, W. A., Eiber, R. J. and Duffy, A. R. (1973). Failure stress levels of flaws in pressurized cylinders, progress in flaw growth and fracture toughness testing, ASTM STP 536. American Society of Testing and Materials, 461-81.
- Leis, B. N. and Stephens, D. R. (1997). An alternative approach to assess the integrity of corroded line pipe part II: alternative criterion. In: Proceedings of the 7th International Offshore and Polar Engineering Conference, Honolulu, 635-640.
- Little, J., Goldstein, M. and Jonathan, P. (2004). Spatio-temporal modelling of corrosion in an industrial furnace. *Applied Stochastic Models in Business and Industry*, 20(3): 219-238.
- Little, J., Goldstein, M., Jonathan, P. and den Heijer, K. (2004). Efficient Bayesian sampling inspection processes based on transformed spatio-temporal data. *Statistical Modelling*, 4: 299-313.
- Lunn, D., Spiegelhalter, D., Thomas, A. and Best, N. (2009). The BUGS project: evolution, critique and future directions (with discussion). *Statistics in Medicine*, 28: 3049-82.

- Madsen, H. O., Krench, S. and Linda, N. C. (2006). *Methods of Structural Safety*. Dover Publications, Inc., NY.
- Maes, M. A., Faber, M. H. and Dann, M. R. (2009). Hierarchical modeling of pipeline defect growth subject to ILI uncertainty. *Proceedings of the ASME 2009 28th International Conference on Ocean, Offshore and Arctic Engineering*, Honolulu, Hawaii, USA, OMAE2009-79470
- Melchers, R. E. (1999). *Structural Reliability Analysis and Prediction*. John Wiley and Sons, NY.
- Melchers, R. E. (2004). Pitting corrosion of mild steel in marine immersion environment - Part 2: Variability of maximum pit depth. *Corrosion (NACE)*, 60(10): 937-944.
- Nessim, M. A., Zhou, W., Zhou, J., Rothwell, B. and McLamb, M. (2009). Target reliability levels for design and assessment of onshore natural gas pipelines. *Journal of Pressure Vessel Technology ASME*, 131(6): 061701(1-12).
- Pandey, M. D. (1998). Probabilistic models for condition assessment of oil and gas pipelines. *NDT&E International*, 31(5): 349-58.
- Qin, S. and Cui, W. (2003). Effect of corrosion models on the time-dependent reliability of steel plated elements. *Marine Structure*, 16(1): 15-34.
- Spiegelhalter, D. J. (1998). Bayesian graphic modeling: A case-study in monitoring health outcomes. *Applied Statistics*, 47: 115-33.
- Straub, D. and Faber, M. H. (2007). Temporal variability in corrosion modeling and reliability updating. *Journal of Offshore Mechanics and Arctic Engineering*, 129:265-72.
- Timashev, S. A., Malyukova, M. G., Poluian, L.V. and Bushinskaya, A.V. (2008). Markov description of corrosion defects growth and its application to reliability based inspection and maintenance of pipelines. *Proceedings of IPC 2008*, IPC2008-64546, ASME, Calgary.

- Teixeira, A. P., Guedes Soares, C., Netto, T. A. and Estefen, S. F. (2008). Reliability of pipelines with corrosion defects. *International Journal of Pressure Vessels and Piping*, 85(4): 228-37.
- van Noortwijk, J. M. (2009). A survey of the application of Gamma process in maintenance. *Reliability Engineering and System Safety*, 94: 2-21.
- van Noortwijk, J. M., van der Weide, J. A. M., Kallen, M. J. and Pandey, M. D. (2007). Gamma process and peaks-over-threshold distribution for time-dependent reliability. *Reliability Engineering System Safety*, 92: 1651-58.
- Valor, A., Caleyó, F., Alfonso, L., Rivas, D. and Hallen, J. M. (2007). Stochastic modeling of pitting corrosion: A new model for initiation and growth of multiple corrosion pits. *Corrosion Science*, 49: 559-579.
- Yuan, X. X., Pandey, M. D. and Bickelb, G. A. (2008). A probabilistic model of wall thinning in CANDU feeders due to flow-accelerated corrosion. *Nuclear Engineering and Design*, 238(1): 16-24.
- Zhou, W. (2010). System reliability of corroding pipelines. *International Journal of Pressure Vessels and Piping*, 87: 587-95.
- Zhou, W. and Huang, G. X. (2012). Model error assessments of burst capacity models for corroded pipelines. *International Journal of Pressure Vessels and Piping*, 99-100: 1-8.
- Zhou, W., Hong, H. P. and Zhang, S. (2012). Impact of dependent stochastic defect growth on system reliability of corroding pipelines. *International Journal of Pressure Vessels and Piping*, 96-97: 68-77.

## **Chapter 6 Cost-based Optimal Inspection Interval for Corroding Natural Gas Pipelines Based on Stochastic Degradation Models**

### **6.1 Introduction**

Metal-loss corrosion is a major threat to the structural integrity of underground oil and gas pipelines world-wide (Cosham et al. 2007). Periodic inspection and maintenance, as a key component of the pipeline corrosion management program (Kariyawasam and Peterson 2010), is an effective means to reduce the probability of failure and maintain safe operation of the pipeline system. Determination of the optimal inspection/maintenance interval is of great importance for the pipeline operators: a too short inspection interval will result in unnecessary inspections and mitigation actions, which can be costly, whereas a too long inspection interval could lead to critical defects not mitigated in a timely manner and failures due to such defects, which can have serious safety and economic implications.

It is a challenging task to determine the optimal inspection interval in that various uncertainties are involved in the decision-making. First, the inline inspection (ILI) tools, e.g. the magnetic flux leakage (MFL) tool, are associated with certain measurement errors. Second, the deterioration or degradation of the pipe resistance due to corrosion is also uncertain and time-varying because the growth of individual corrosion defect as well as the total number of defects are uncertain and vary with time. Third, the pipe geometry, material properties and internal pressure are also uncertain in reality. Finally, the capacity model for the corroded pipeline is imperfect and therefore involves model uncertainty. The above-mentioned uncertainties need to be incorporated in the determination of the optimal inspection interval.

The selection of optimal maintenance schedules for corroding pipelines has been investigated using the reliability-based criteria (Rodriguez and Provan 1989; Morrison and Worthingham 1992; Hong 1999). Provan and Rodriguez (1989) developed a Markov process-based model for the growth of corrosion defects in the context of determining the

optimal inspection time. They considered the imperfection of inspection tools in detecting the defect, i.e. the probability of detection (PoD), but ignored the imperfection of inspection tools in sizing the defect, i.e. the measurement errors. Morrison and Worthingham (1992) employed the same corrosion growth model to determine the optimal inspection time but ignored both PoD and measurement errors associated with the inspection tools. Hong (1999) investigated the optimal inspection and maintenance schedule for corroding pipelines based on the reliability constraint. The Markov process was employed to model the growth of corrosion defects; the PoD and measurement errors associated with the inspection tool were incorporated in the failure probability evaluation, and the Poisson process was used to model the generation of new defects.

The investigations of condition-based maintenance optimization for degrading piping systems using the cost-based criterion have been reported in a few recent studies (e.g. Cheng and Pandey 2012; Gomes et al. 2013). Cheng and Pandey (2012) investigated the optimal inspection interval for a single-component degrading system using analytical methodologies, where the degradation of the system was modeled as a homogeneous gamma process and the optimal inspection interval was selected based on the minimum expected cost rule. Perfect inspection was implicitly assumed in their study. Gomes et al. (2013) used a simulation-based approach to investigate the optimal inspection interval for buried pressurized pipelines subjected to external corrosion based on the minimum expected cost rule. A single pipeline joint that contains at most one corrosion defect at a given time was considered in the analysis, which is somewhat unrealistic. A time-independent power-law model that incorporates uncertain power law parameters but a deterministic corrosion initiation time was assumed to characterize the growth of the defect depth. Although PoD of the inspection tool was incorporated in the analysis, the measurement errors of the tool were ignored. The generation of new corrosion defects was also ignored.

In this chapter, the Monte Carlo simulation is employed to investigate the optimal maintenance decision for newly-built onshore underground natural gas pipelines with respect to external metal-loss corrosion by considering the generation of corrosion defects over time and time-dependent growth of individual defects. To this end, the non-

homogeneous Poisson process is used to model the generation of new defects, and the homogeneous gamma process is used to model the growth of the defects. The minimum expected cost rule is used to select the optimal inspection interval. Both the PoD and measurement errors of the inspection tool are considered in the optimization. The investigation considers a realistic maintenance strategy and realistic costs of maintenance and failure that are consistent with the industry practice but have not been well accounted for in the literature. In particular, the excavation and repair actions are pipe joint-based as opposed to defect-based; that is, all the defects on an excavated pipe joint are mitigated by the repair actions. The failure event is defined as burst of the corroded pipeline under internal pressure, and the time-dependent probability of failure is evaluated by employing the limit state function for burst as opposed to the hazard function associated with the time-to-failure (Cox and Oakes 1984). The cost of failure includes both the direct and indirect costs, the latter of which is incorporated through the parametric analysis.

The remainder of the chapter is organized as follows. Section 6.2 presents the degradation models including the generation of new defect and the growth of the defect depth; Section 6.3 describes the uncertainties associated with ILI tools; the limit state function for burst, mitigation criteria, maintenance policy and the procedures to evaluate the expected cost rate are presented in Section 6.4; Section 6.5 presents a numerical example and parametric analysis results followed by the conclusions in Section 6.6.

## **6.2 Degradation Models**

### **6.2.1 Generation of New Defect**

Consider a reference joint of a newly-built pipeline (a typical pipe joint is approximately 12 m long). The non-homogeneous Poisson process (NHPP) was adopted to model the generation of new defects on the reference joint based on the consideration that the corrosion defects are not necessarily generated uniformly in time with a constant rate (Kuniewski et al. 2009). The total number of defects,  $N(t)$ , generated within a time interval  $[0, t]$  (e.g.  $t = 0$  denotes the time of installation of the pipeline) over the pipe joint follows a Poisson distribution with a probability mass function,  $f_P(N(t)|\Lambda(t))$ , defined as (Kulkarni 2010):



$$f_P(N(t)|\Lambda(t)) = \frac{(\Lambda(t))^{N(t)} e^{-\Lambda(t)}}{N(t)!} \quad (t > 0) \quad (6.1)$$

where  $\Lambda(t)$  denotes the expected number of defects generated over the time interval  $[0, t]$ , and  $\Lambda(t) = \int_0^t \lambda(\tau) d\tau$ .  $\lambda(\tau)$  is the assumed intensity function (or the instantaneous generation rate) corresponding to the reference pipe joint. For example, it can be assumed that  $\lambda(\tau) = \lambda_0 \tau^b$ , where  $\lambda_0$  and  $b$  are positive quantities that can be determined based on the inspection data and/or expert judgement. Note that Eq. (6.1) is simplified to a homogeneous Poisson process (HPP) if  $b$  is equal to zero, i.e. the intensity function is constant and independent of time. Three NHPP examples corresponding to  $\lambda_0 = 1, 2$  and 4 are illustrated in Fig. 6.1, where the exponent  $b$  is assumed to equal one, i.e.  $\Lambda(\tau) = \lambda_0 \tau^2/2$ . Results associated with each of the examples include the expected value, 2.5- and 97.5-percentile values as well as one realization of the NHPP.

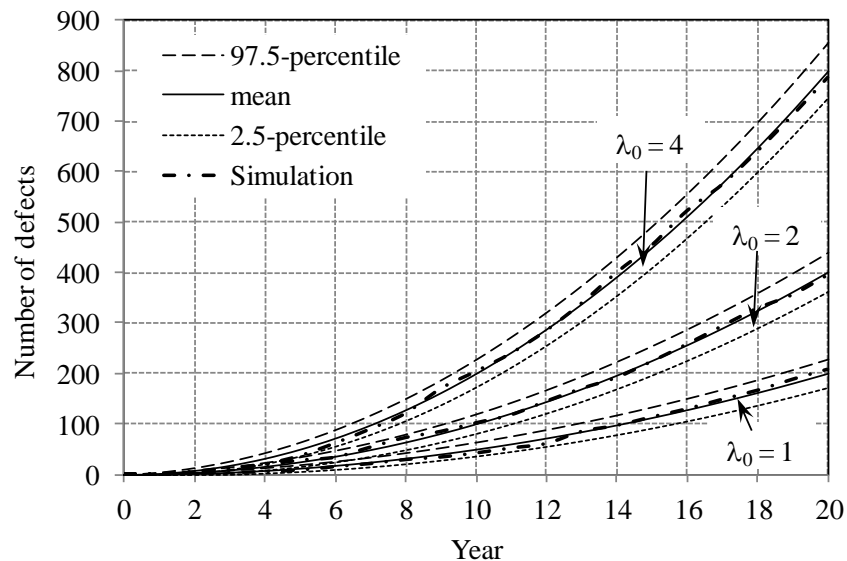


Figure 6.1 Illustration of the NHPP

Consider that  $n$  defects have been generated on the reference pipe joint up to time  $T$ . The initiation times of the  $n$  defects are denoted by  $T_1, T_2, \dots$ , and  $T_n$  ( $T_1 \leq T_2 \leq \dots \leq T_n \leq T$ ), respectively. The joint probability density function (PDF) of  $(T_1, T_2, \dots, T_n)$  conditional on  $N(T) = n$  can be expressed as (Kulkarni 2010; Beichelt and Fatti 2002):

$$f_{T_1, \dots, T_n | N(t)}(t_1, \dots, t_n | n) = \frac{n! \prod_{i=1}^n \lambda(t_i)}{[\Lambda(t)]^n} \quad (0 < t_1 < t_2 < \dots < t_n \leq T) \quad (6.2)$$

For the homogeneous Poisson process (i.e.  $b = 0$  in the intensity function), Eq. (6.2) becomes  $n!/t^n$  (Kulkarni 2010). This indicates that the joint PDF of the initiation times for HPP conditional on  $N(T) = n$  is the same as the joint PDF of the order statistics of samples of  $(U_1, U_2, \dots, U_n)$ , where  $U_1, U_2, \dots, U_n$  are  $n$  independent and identically distributed (iid) random variables that are uniformly distributed over  $[0, T]$ . This conclusion for HPP can be generalized to NHPP; that is,  $U_i$  ( $i = 1, 2, \dots, n$ ) are independent and identically distributed random variables with the distribution (Kulkarni 2010; Parzon 1962)

$$P(U_i \leq t) = \frac{\Lambda(t)}{\Lambda(T)} \quad (0 \leq t \leq T) \quad (6.3)$$

### 6.2.2 Growth of Defect

In this study, the growth of defect depth (i.e. in the through pipe wall thickness direction) was modeled by the homogeneous gamma process. The distribution of the depth of the  $i^{\text{th}}$  defect at time  $t$ ,  $d_i(t)$ , follows a gamma distribution with the PDF,  $f_G(d_i(t) | \alpha_i(t-t_{i0}), \beta_i)$ , given by

$$f_G(d_i(t) | \alpha_i(t-t_{i0}), \beta_i) = \beta_i^{\alpha_i(t-t_{i0})} d_i(t)^{\alpha_i(t-t_{i0})-1} e^{-d_i(t)\beta_i} / \Gamma(\alpha_i(t-t_{i0})) I_{(0,\infty)}(d_i(t)) \quad (6.4)$$

where  $\alpha_i(t-t_{i0})$  ( $t > t_{i0}$ ) and  $\beta_i$  denote the shape parameter and rate parameter (i.e. inverse of the scale parameter) (Ang and Tang 1975; Johnson 2000) associated with defect  $i$ , respectively, with  $t_{i0}$  denoting the initiation time of the  $i^{\text{th}}$  defect (i.e. the time elapsed since the installation of pipe up to the time at which the defect initiates), and  $I_{(0,\infty)}(d_i(t))$  denotes an indication function and equals unity if  $d_i(t) > 0$  and  $t > t_{i0}$ , and zero otherwise. Implicit in Eq. (6.4) is that the growth of the defect within one year or growth rate, denoted by  $\Delta d(1)$ , is a gamma distributed random variable, characterized by a PDF of  $f_G(\Delta d(1) | \alpha_i, \beta_i)$  with a mean of  $\alpha_i/\beta_i$  and a variance of  $\alpha_i/\beta_i^2$ . Conversely, given the mean and variance of  $\Delta d(1)$ , the values of  $\alpha_i$  and  $\beta_i$  can be obtained.

The defect length (i.e. in the pipe longitudinal direction) is expected to have a non-zero value at the initiation and equal the length of the damaged coating (Nessim and Zhou 2005); in other words, each individual defect appears on the pipe as a patch with a length and width. Consistent with the industry practice, it is assumed that the length does not grow over time and the lengths of different defects follow a predefined probability distribution.

### 6.2.3 Simulation Procedures for Generating New Defects

Let  $T$  denote the service life of the pipeline,  $\tau$  ( $\tau = 1, 2, \dots, T$ ) denote a given year within  $T$ , and  $n_T$  denote the total number of defects generated on the reference pipe joint over a period of  $T$ . Based on the defect generation and growth models described in Sections 6.2.1 and 6.2.2, respectively, the simulation procedure for generating the number of defects on the joint at year  $\tau$  is given as follows:

(1) Calculate the expected total number of defects generated over the service life,  $\Lambda(T) = \int_0^T \lambda(s)ds$ , and set the counter for the number of new defects on the joint at year  $\tau$  ( $\tau = 1, 2, \dots, T$ ),  $n(\tau)$ , to zero;

(2) Generate the total number of defects,  $n_T$ , on the joint from the Poisson distribution,  $n_T \sim f_P(N(T)|\Lambda(T))$ , and

(3) Generate the initiation times of the  $n_T$  defects from Eq. (6.3) as follows:

3.1) set  $i = 1$ ;

3.2) generate a candidate initiation time,  $\tau_0$ , between zero and  $T$ , and generate a random number,  $u$ , between zero and one;

3.3) if  $u \leq \Lambda(\tau_0)/\Lambda(T)$ , set  $t_{i0} = \tau_0$ , and  $i = i + 1$ ; otherwise, return to 3.2), and

3.4) if  $i < n_T$ , return to 3.2).

Given the values of  $t_{i0}$  ( $i = 1, 2, \dots, n_T$ ) generated in step 3.3) and the values of  $\alpha_i$  and  $\beta_i$  (determined from the mean and variance of  $\Delta d(1)$ , for example), the time-dependent

growth path of each of the  $n_T$  defects over a time interval from  $t_{i0}$  to  $t$  ( $t \geq t_{i0}$ ) can be generated from Eq. (6.4). Finally the defect lengths associated with the  $n_T$  defects can be generated from a given distribution.

## 6.3 Uncertainties Associated with the ILI Tool

### 6.3.1 Probability of Detection

The probability of detection (PoD) represents the ability of a high-resolution ILI tool to detect a true corrosion defect. It is usually a function of the defect size and parameters that characterize the inherent tool accuracy. A PoD function commonly assumed in the literature is an exponential function (Rodriguez and Provan 1989; Stephens and Nessim 2006) of the defect depth,  $d$ , defined as

$$PoD(d) = 1 - e^{-qd} \quad (6.5)$$

where  $q$  is a constant that defines the inherent tool detection capability and can be quantified from vendor-supplied tool specifications, e.g. 90% probability of detecting a defect with a depth of 10 percent of the pipe wall thickness (i.e. 10%  $w/t$ ). It follows from Eq. (6.5) that  $1/q$  represents the average depth of detectable defects.

### 6.3.2 Measurement Error

The uncertainties in sizing a detected defect are generally characterized by the biases and random scattering errors associated with the ILI tool. The depth and length of a corrosion defect measured by the ILI tool,  $d^M$  and  $L^M$  respectively, in general are related to the actual depth,  $d$ , and length,  $L$ , through the following equations (Fuller 1987; Jaech 1985):

$$d^M = c_{1d} + c_{2d}d + \varepsilon_d \quad (6.6a)$$

$$L^M = c_{1l} + c_{2l}L + \varepsilon_l \quad (6.6b)$$

where  $c_{1d}$  ( $c_{1l}$ ) and  $c_{2d}$  ( $c_{2l}$ ) denote the constant and non-constant biases (i.e. if  $c_{1d} = c_{1l} = 0$  and  $c_{2d} = c_{2l} = 1$ , the tool is unbiased) associated with the defect depth (length), respectively, and are assumed to be deterministic quantities, and  $\varepsilon_d$  and  $\varepsilon_l$  are random scattering errors associated with the measured depth and length, respectively, and are typically characterized by normal distributions with zero mean and known standard deviations quantified from tool specifications (Stephens and Nessim 2006). In this study, the random scattering errors associated with different defects for a given ILI tool were assumed to be mutually independent; that is, the spatial correlation of the random scattering errors was ignored. This is considered acceptable as long as defects are not too closely spaced. The random scattering errors associated with different ILI tools for a given defect were also assumed to be mutually independent. A recent study (Al-Amin et al. 2012) has shown that the random scattering errors associated with ILI data reported by different tools for the same defect tend to be correlated. However, such correlation was considered to have a negligible impact on the outcome of a given maintenance and therefore ignored for simplicity, based on the consideration that a pipe joint will be excavated if any given defect on the joint reaches the critical condition as explained in Section 6.4.2.

## **6.4 Optimal Condition-based Maintenance Decisions**

### **6.4.1 Limit State Function for Failure Due to Corrosion**

A corroding natural gas pipeline typically fails by either small leak or burst due to the internal pressure (CSA 2007). A small leak occurs if the corrosion defect penetrates the pipe wall prior to the plastic collapse of the remaining ligament at the defect due to the internal pressure, whereas a burst occurs if the remaining ligament undergoes plastic collapse before the defect penetrates the pipe wall. In this study, only burst was considered because the cost of a small leak is typically insignificant compared with that of a burst. Although a burst can be further classified as a large leak or a rupture based on whether or not the through-wall flaw resulting from the burst extends unstably in the longitudinal direction (CSA 2007), such a classification was not considered in this study because this study is focused on gas pipelines located in low-population-density areas (i.e.

the so-called Class 1 pipelines (CSA 2007), which are representative of the vast majority of transmission pipelines in Canada. This implies that the cost of injury and property damage due to a burst is negligible (Zhou and Nessim 2011); as a result, it is unnecessary to further classify a burst into a large leak or a rupture from the failure cost standpoint.

The limit state function,  $g$ , for burst due to a given corrosion defect is given by

$$g = r_b - p \quad (6.7)$$

where  $r_b$  is the burst pressure of the pipe at the defect;  $p$  denotes the internal pressure, and  $g \leq 0$  indicates burst at the defect. The B31G Modified model (Kiefner and Vieth 1989), which is widely used in the fitness-for-service assessment of oil and gas pipelines, was adopted to calculate  $r_b$  as follows:

$$r_b = \xi_b \frac{2wt(\sigma_y + 68.95)}{D} \left( \frac{1 - \frac{0.85d}{wt}}{1 - \frac{0.85d}{Mwt}} \right) \quad (6.8a)$$

$$M = \begin{cases} \sqrt{1 + 0.6275 \frac{L^2}{Dwt} - 0.003375 \left( \frac{L^2}{Dwt} \right)^2} & L \leq \sqrt{50Dwt} \\ 3.3 + 0.032 \frac{L^2}{Dwt} & L > \sqrt{50Dwt} \end{cases} \quad (6.8b)$$

where  $\xi_b$  denotes the model error associated with the B31G Modified model;  $wt$  and  $D$  are the wall thickness and outside diameter of the pipe, respectively, and  $\sigma_y$  is the pipe yield strength.

Note that Eq. (6.8) tends to give non-conservative predictions of  $r_b$  for defects with  $d > 0.8wt$ , and is therefore limited to defects with  $d \leq 0.8wt$  only (Kiefner and Vieth 1989). Furthermore, the probabilistic characteristics of  $\xi_b$  were developed based on the data set of defects with  $d \leq 0.8wt$ . To evaluate  $r_b$  for defects with  $0.8wt < d \leq wt$  in the optimization analysis, it is assumed in this study that the burst pressure decreases linearly from that calculated using Eq. (6.8a) at  $d = 0.8wt$  to zero at  $d = wt$ . This assumption, which is illustrated in Fig. 6.2, is considered a simple and practical extension of the B31G Modified model.

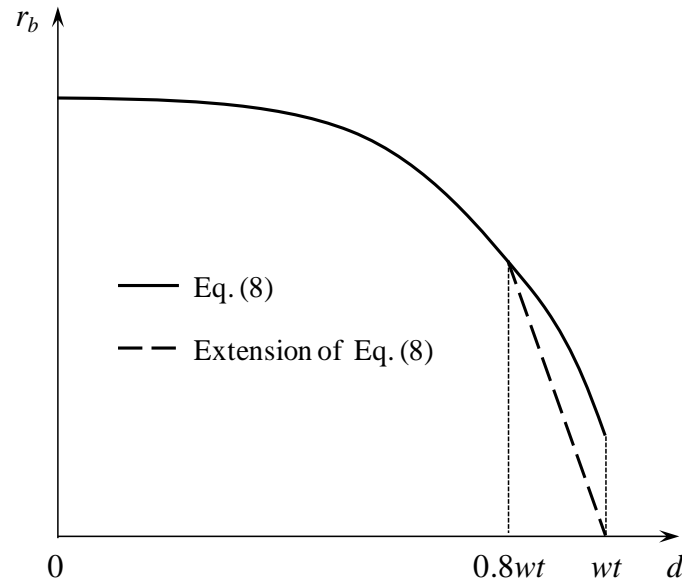


Figure 6.2 Illustration of the extension of the B31G Modified model for defects more than 80% through wall thickness

#### 6.4.2 Maintenance and Replacement Policy

It is assumed that failure (i.e. burst) at a given defect is confined to the pipe joint in which the defect is located and does not impact the adjacent joints. A burst pipe joint will be excavated and replaced immediately after failure. The maintenance actions considered in this study are consistent with typical industry practice, and involve periodic inspections using high-resolution ILI tools and subsequent excavation and repair of corroded pipe joints based on the inspection results. A pipe joint will be excavated and repaired immediately after inspection, if any defect on the joint meets one of the following two criteria:

$$d^M \geq \xi_E wt_n \quad (6.9a)$$

$$r_b^M \leq \eta_E p_n \quad (6.9b)$$

where  $wt_n$  and  $p_n$  denote the nominal pipe wall thickness and design pressure or maximum operating pressure (MOP), respectively;  $\xi_E$  ( $\xi_E < 1$ ) and  $\eta_E$  ( $\eta_E > 1$ ) are predefined safety factors associated with the two criteria, and  $r_b^M$  denotes the estimated

(as opposed to the actual) burst pressure at the defect. That is,  $r_b^M$  is evaluated from Eq. (6.8), but with  $wt$  and  $D$  replaced by  $wt_n$  and  $D_n$  ( $D_n$  is the nominal pipe outside diameter), respectively,  $d$  and  $L$  replaced by  $d^M$  and  $L^M$  respectively,  $\sigma_y$  replaced by the specified minimum yield strength (SMYS), and  $\xi_b$  set to unity.

The repair actions on an excavated pipe joint first involve completely removing the existing coating of the joint. Depending on the severity of the corrosion on the joint, recoating or recoating plus sleeving (hereafter referred to as the sleeving repair for brevity) of the joint will then be applied. The selection of recoating or sleeving can be determined based on the actual defect sizes as opposed to the ILI-reported defect sizes, because the defects on the excavated joint are always measured in the ditch and field measurements can be assumed to be error free (Al-Amin et al. 2012). A simple recoating of the joint will be carried out if every defect on the joint satisfies  $d < \xi_R wt$  (the actual wall thickness of the pipe joint is also measured during the excavation) and  $r_b' > \eta_R p_n$ , where  $r_b'$  is evaluated using Eq. (6.8), but with  $\sigma_y$  replaced by SMYS and  $\xi_b$  set to unity; the sleeving repair will be applied if  $d \geq \xi_R wt$  and/or  $r_b' \leq \eta_R p_n$  for at least one defect (referred to as the critical defect). The sleeving will cover the portion of the joint containing the critical defect(s). The parameters  $\xi_R$  and  $\eta_R$  are the safety factors associated with the two repair criteria. Note that a repaired pipe joint, regardless of the specific repair action applied, is assumed to be fully restored to the pristine condition. This is considered a reasonable assumption given that the recoating will arrest the growth of all the existing defects on the pipe joint, and the sleeved joint will have at least the same burst capacity as that of a new pipe joint, if not higher. Based on discussions with industry experts, the likelihood of a repair of being of poor quality is considered very low and therefore ignored in this study. Furthermore, it is assumed that no inspection is carried out if the inspection is scheduled upon a failure of the pipe joint or at the end of the service life of the pipeline, and no repair is applied, if required, at the end of the service life of the pipeline.

### 6.4.3 Evaluation of the Expected Cost Rate

Consider that a reference pipe joint is subjected to periodic inspections and



maintenances with a fixed time interval,  $T_I$ . Given the service life ( $T$ ), the unit costs of inspection ( $C_{IN}$ ), excavation ( $C_{EV}$ ), recoating ( $C_{RC}$ ), sleeving ( $C_{RS}$ ) and failure ( $C_F$ ) as well as the periodic inspection interval ( $T_I$ ), it follows from the assumptions in Section 6.4.2 that the total cost per unit service time or cost rate,  $C_R(T_I)$ , can be expressed as

$$C_R(T_I) = \frac{1}{T} \left( \sum_{i=1}^{n_{IN}} C_{IN} e^{-\gamma i T_I} + \sum_{i=1}^{n_{EV}} (C_{EV} + C_{Ri}) e^{-\gamma t_{EVi}} + \sum_{i=1}^{n_F} C_F e^{-\gamma t_{Fi}} \right) \quad (6.10)$$

where  $\gamma$  denotes the discount rate;  $n_{IN}$  is the total number of inspections,  $n_{EV}$  denotes the total number of excavations;  $t_{EVi}$  denotes the time of the  $i^{\text{th}}$  excavation;  $C_{Ri}$  is the cost of repair associated with the  $i^{\text{th}}$  excavation, i.e.  $C_{Ri}$  equal to either  $C_{RC}$  or  $C_{RS}$ ;  $n_F$  denotes the total number of failures, and  $t_{Fi}$  denotes the time of the  $i^{\text{th}}$  failure. Input from industry experts (Kariyawasam 2012) suggests that the cost of failure,  $C_F$ , should include not only the direct cost of replacing the failed pipe joint but also the indirect cost such as the cost of carrying out a system-wide integrity assessment demanded by the regulatory agency as a result of the failure and potential loss of business due to the failure event. The indirect failure cost can be orders of magnitude higher than the direct failure cost, but is very difficult to quantify. In this study, a parametric study was carried out to investigate the impact of the indirect cost on the optimal inspection interval as illustrated in the numerical example described in Section 6.5.

Due to uncertainties in the corrosion growth process, pipe geometric and material properties and burst capacity model,  $n_{EV}$ ,  $n_F$ ,  $t_{EVi}$  and  $t_{Fi}$  are all uncertain. Because it is very difficult to obtain analytical equations of  $C_R(T_I)$  as well as its expectation,  $E(C_R(T_I))$ , the simulation technique was adopted in this study to numerically evaluate  $E(C_R(T_I))$ .

Let  $C(T_I)$  denote the total cost corresponding to an inspection interval of  $T_I$ . Given the values of  $T$ ,  $T_I$ ,  $\gamma$ ,  $C_{IN}$ ,  $C_{EV}$ ,  $C_{RC}$ ,  $C_{RS}$ ,  $C_F$ ,  $\xi_E$ ,  $\eta_E$ ,  $\xi_R$  and  $\eta_R$ , a step-by-step procedure to evaluate  $C(T_I)$  is described as follows:

- 1) Generate the total number of defects (denoted by  $n_0$ ) on the reference joint over the period from zero to  $T$ , i.e.  $n_0 \sim f_P(N(T)|\Lambda(T))$  as well as their corresponding initiation times and growth paths following the procedures described in Section 6.2.3; generate the defect length and the model error associated with each of the  $n_0$  defects; generate the wall

thickness ( $wt$ ), yield strength ( $\sigma_y$ ), and diameter ( $D$ ), assumed to be invariant within a given joint;

2) Let  $i$  denote the inspection number, and  $n_{RC}$ ,  $n_{RS}$  and  $n_{RF}$  denote the number of defects mitigated/eliminated by recoating, sleeving and failure replacement, respectively. Set  $i = 1$ ,  $C(T_i) = 0$ ,  $n_{RC} = 0$ ,  $n_{RS} = 0$  and  $n_{RF} = 0$ ; set  $\Delta t = T_1/K$ , where  $K$  is a selected integer;

3) Set  $t_i = i \times T_1$  and  $k = 1$ ;

4) Calculate the number of remaining defects up to time  $\tau_k = (i-1) \times T_1 + k \times \Delta t$  on the joint,  $N_{\tau_k} = \sum_{0 \leq \tau \leq \tau_k} n_0(\tau)$ ;

5) Calculate the depth of the  $s^{\text{th}}$  defect at  $\tau_k$ ,  $d_s(\tau_k)$ , and identify the corresponding defect length,  $L_s$  ( $s = 1, 2, \dots, N_{j\tau_k}$ ) obtained from 2);

6) Calculate  $r_{bs,\tau_k}$  by substituting the values of  $d_s(\tau_k)$ ,  $wt$ ,  $\sigma_y$ ,  $D$ ,  $L_s$  and  $\xi$  into Eq. (6.8);

6.1) if  $g = \min_s \{r_{bs,\tau_k}\} - p > 0$ , set  $k = k + 1$ ; if  $k \leq K$  return to 4); otherwise go to 7), and

6.2) if  $g = \min_s \{r_{bs,\tau_k}\} - p \leq 0$ , calculate  $C(T_i) = C(T_i) + C_F \exp(-\gamma(i-1)T_1 + k\Delta t)$ , set  $n_{RF} = n_{RF} + n_0$ , re-generate the total number of defects on the joint (denoted by  $n_1$ ) over the period from  $\tau_k$  to  $T$ , i.e.  $n_1 \sim f_P(N(T)|\Lambda'(T))$  with  $\Lambda'(T)$  evaluated from zero to  $T - \tau_k$ , as well as their corresponding initiation times and growth paths following the procedures described in Section 6.2.3 with  $T$  replaced by  $T - \tau_k$ , and  $t_{i0} = \tau_0 + \tau_k$ ; set  $n_0 = n_1$ ; if  $\tau_k = t_i$ , set  $i = i + 1$  and return to 3), and if  $\tau_k < t_i$ , go to 7);

7) Calculate the number of remaining defects up to time  $t_i$ ,  $N_i = \sum_{0 \leq \tau \leq t_i} n_0(\tau)$ ; and calculate the corresponding growths of depth associated with each of the  $N_i$  defects;

8) Generate the measurement errors associated with the defect depth and length of the  $s^{\text{th}}$  defect ( $s = 1, 2, \dots, N_i$ ), denoted by  $\varepsilon_{ds}$  and  $\varepsilon_{ls}$ , respectively; calculate the measured depth  $d_s^M = c_{1d} + c_{2d}d_s(t_i) + \varepsilon_{ds}$ , and length  $L_s^M = c_{1l} + c_{2l}L_s + \varepsilon_{ls}$ , at time  $t_i$ , where

$d_s^M > 0$  and  $L_s^M > 0$ , and calculate  $C(T_I) = C(T_I) + C_{IN}\exp(-\gamma_i)$ . Set  $s = 1$  and carry out the following:

8.1) generate a random number  $u$  from a uniform distribution between zero and one, and calculate the PoD value associated with defect  $s$ , denoted by  $\text{PoD}_s$ , using Eq. (6.5), i.e.  $\text{PoD}_s = 1 - \exp(-qd_s)$ ;

8.2) if  $u \leq \text{PoD}_s$ , calculate  $d_s^M$  and  $r_{bs}^M$ ; if  $d_s^M \geq \xi_E w t_n$  or  $r_{bs}^M \leq \eta_E p_n$ , calculate  $C(T_I) = C(T_I) + C_{EV}\exp(-\gamma_i)$ , and re-generate the total number of defects (denoted by  $n_2$ ) over the period from  $t_i$  to  $T$ , i.e.  $n_2 \sim f_P(N(T)|\Lambda'(T))$  with  $\Lambda'(T)$  evaluated from zero to  $T - t_i$ , as well as their corresponding initiation times and growth paths following the procedures described in Section 6.2.3 with  $T$  replaced by  $T - t_i$ , and  $t_{i0} = \tau_0 + t_i$ ; set  $n_0 = n_2$ , and

8.2.1) if  $d_s \geq \xi_R w t_n$  and/or  $r_{bs}' \leq \eta_R p_n$ , calculate  $C(T_I) = C(T_I) + C_{RS}\exp(-\gamma_i)$ , set  $n_{RS} = n_{RS} + n_1$ ,  $i = i + 1$  and return to 3), and

8.2.2) if  $d_s < \xi_R w t_n$  and  $r_{bs}' > \eta_R p_n$ , calculate  $C(T_I) = C(T_I) + C_{RC}\exp(-\gamma_i)$ , set  $n_{RC} = n_{RC} + n_1$ ,  $i = i + 1$  and return to 3);

8.3) if  $u > \text{PoD}_s$ , set  $s = s + 1$ ; if  $s \leq N_i$ , return to 8.1); otherwise (i.e.  $s > N_i$ ), set  $i = i + 1$  and return to 3);

9) If  $(i-1) \times T_I + k \times \Delta t$  ( $k \leq K$ ) is less than  $T$ , repeat Steps 3) to 8).

The value of  $E(C_R(T_I))$  can be evaluated from the samples of  $C_R(T_I)$  generated from a total of  $N_s$  simulation cycles based on the above-described procedure. The above analysis can be repeated by varying the periodic inspection interval  $T_I$  from 0 to  $T$ . According to the minimum expected cost rule, the optimal inspection interval is the value of  $T_I$  that results in the minimum value of  $E(C_R(T_I))$  and is denoted by  $T_{IO}$ . Furthermore, the average annual failure probability of the pipe joint corresponding to a given inspection interval  $T_I$ , denoted by  $P_{af}(T_I)$  ( $T_I = 1, 2, \dots, T$ ), which is relevant to the selection of the optimal inspection interval subjected to the reliability constraint, can be evaluated from

the simulation results as  $P_{af}(T_I) = \sum_{i=1}^{N_s} N_{if}(T_I) / N_s / T$ , with  $N_{if}(T_I)$  denoting the total number of failures of the pipe joint over  $T$  years in the  $i^{\text{th}}$  simulation trial corresponding to inspection interval  $T_I$ .

In practice, the defect information obtained from the first ILI can be used to update the various parameters employed in the above-described analysis, e.g. PoD, the defect generation and growth models as well as the measurement errors associated with the ILI tool. The updated parameters can then be used to re-evaluate the optimal inspection interval in the subsequent years. The updating aspect of the analysis is not addressed in this study and will be dealt with in the future.

## 6.5 Example

### 6.5.1 General

An onshore underground natural gas pipeline is employed to illustrate the application of the above-described methodology in this section. The pipeline has a nominal outside diameter of 762 mm (30 inches), and a maximum operating pressure of 10.34 MPa (1500 psi), and is made from API 5L Grade X80 steel with an SMYS of 550 MPa and a specified minimum tensile strength (SMTS) of 625 MPa. The selected joint has a nominal wall thickness of 8.96 mm and a length of 12.5m. The service life of this pipeline (i.e.  $T$  in Eq. (6.10)) is assumed to be 50 years.

The pipeline at the time of installation was assumed to be defect-free. The number of defects on the pipe joint is characterized by Eq. (6.1), where  $\lambda_0$  and  $b$  were assumed to be 0.0128 and unity, respectively, i.e.  $\Lambda(t) = 0.0064t^2$ . The values of  $\lambda_0$  and  $b$  imply that the expected number of defects over a period of 50 years is 16. The growth of each defect was modeled by Eq. (6.4), and the growth rates of the depths (i.e.  $\Delta d(1)$ ) of all the defects were assumed to be independent and identically gamma-distributed with a mean of 0.2 mm/yr and a coefficient of variation (COV) of 50%. The defect length was assumed to be static and follow a lognormal distribution with a mean of 105 mm and a COV of 130% (CSA 2007). The defect lengths associated with different defects on the entire joint were assumed to be mutually independent. The model errors associated with the short and

long defects were distinguished in terms of the transition normalized defect length based on a recent study reported by Zhou and Huang (2012). Finally, the internal pressure ( $p$ ), model error ( $\xi$ ), wall thickness ( $wt$ ) and yield strength ( $\sigma_y$ ) were assumed to be invariant within the joint. The probabilistic characteristics of the parameters are summarized in Table 6.1.

Table 6.1 Probabilistic characteristic of the random variables

Random variable	Nominal value	Unit	Mean/Nominal	COV	Distribution type	Source
$L$	N/A	mm	105 <sup>(a)</sup>	130%	Lognormal	CSA 2007
$D$	762		1.0	0	Deterministic	CSA 2007
$wt$	8.96		1.0	1.5%	Normal	Jiao et al. 1995
$\sigma_y$	550	MPa	1.08	3%	Normal	Jiao et al. 1995
$P$	10.34		1.05	2%	Gumbel	CSA 2007; Zhou 2010
$\xi_b$	1.0	N/A	1.062	12.7%	Weibull <sup>(b)</sup>	Zhou and Huang 2012
			1.442	23.6%	Frechet <sup>(b)</sup>	

<sup>a</sup> The mean value of defect length is 105 mm;

<sup>b</sup> The Weibull and Frechet distributions are applicable for defects with  $L/(Dwt)^{0.5} \leq 1.5$  (i.e. short defects) and defects with  $L/(Dwt)^{0.5} > 1.5$  (i.e. long defects), respectively.

The defect depth and length reported by the ILI tool were assumed to be unbiased (i.e.  $c_{1d} = c_{1l} = 0$  and  $c_{2d} = c_{2l} = 1$  in Eqs. (6.6a) and (6.6b)), and the standard deviations of the random scattering errors of the defect depth and length were evaluated to be 7.8%  $wt$  and 7.8 mm, respectively, based on the common tool specifications that indicate a confidence interval of the actual depth  $\pm 10\%wt$  with a probability of 80% for the measured depth, and a confidence interval of the actual length  $\pm 10$  mm with a probability of 80% for the measured length. The PoD curve associated with the ILI tool was characterized by Eq. (6.5), with the PoD value equal to 90% for the defect depth of 10 %  $wt$ , i.e.  $q = 2.57 \text{ mm}^{-1}$ . Furthermore, the sizing accuracies of the ILI tools employed in different inspections were assumed to be identical. Finally, the safety factors for excavation were assumed the same as those for repair, namely  $\xi_E = \xi_R = 0.75$  and  $\eta_E = \eta_R = 1.25$ ; these values are consistent with the typical industry practice (Kariyawasam et al. 2012).

The absolute and relative unit costs of inspection, excavation, repair and failure replacement representative of the typical industry practice in Canada are summarized in Table 6.2. Note that the relative costs were employed in all the analyses in this study. As discussed in Section 6.4.3, the indirect component of the failure cost can be much higher than the direct failure cost. Due to the difficulty in quantifying the indirect cost, parametric analyses were conducted by assuming three different values of the relative failure cost, namely  $C_F = 30, 60$  and  $200$ , respectively. Additional parametric analysis scenarios were developed to investigate the impact of PoD, the safety factors in the excavation and repair criteria (i.e.  $\xi_E, \xi_R, \eta_E$  and  $\eta_R$ ), the growth rate of defect depth, the instantaneous generation rate of the generation model and defect generation model on the optimal inspection interval. These scenarios are summarized in Table 6.3, where the shaded elements indicate that the value of this parameter is the same as that in the baseline case. It should be pointed out that  $C_F = 30$  was used to investigate the impact of an overly optimistic estimate of the failure cost on the optimal inspection interval.

Table 6.2 Summary of unit costs

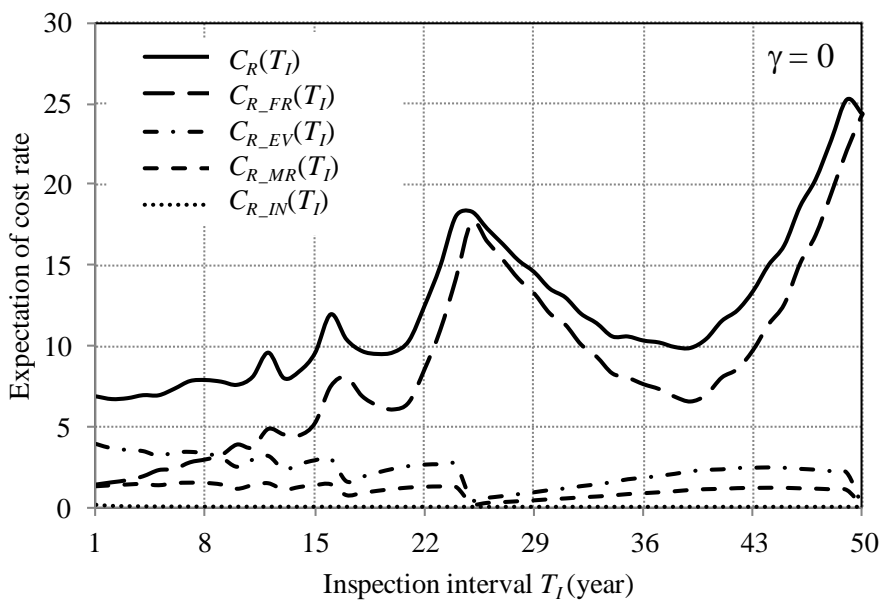
Cost item		Absolute Cost (CAD\$/joint)	Relative cost (/Joint)
Inline inspection, $C_{IN}$		70	0.0035
Corrosion defect excavation, $C_{EV}$		70,000	3.5
Recoating, $C_{RC}$		20,000	1
Sleeving, $C_{RS}$		35,000	1.75
Failure cost $C_F$	Tangible cost (i.e. excavation and replacement)	130,000	>56.5
	Intangible cost	> one million	

Table 6.3 Details of the parametric analysis

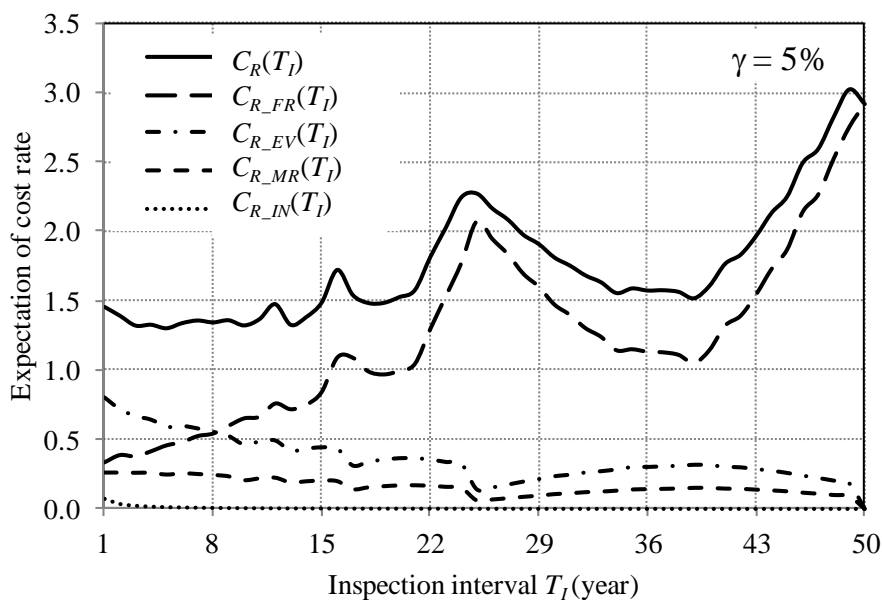
Scenario	$C_F$	$\xi_E$ and $\xi_R$	$\eta_E$ and $\eta_R$	$\overline{\Delta d(1)}$	PoD at $d = 10\% wt$	$\lambda_0$	Generation model
Baseline	60	0.75	1.25	0.2	90%	0.0128	NHPP
I	30						
	200						
II		0.5	1.5				
		0.9	1.1				
III				0.1			
				0.3			
IV					50%		
					10%		
V						0.0064	
						0.04	
VI						--	HPP

### 6.5.2 Results of Parametric Analysis

The above-described model was first applied to evaluate  $E[C_R(T_I)]$  corresponding to the baseline case specified in Table 6.3. To investigate the contribution of cost associated with each individual maintenance actions to  $E[C_R(T_I)]$ , a breakdown of  $E[C_R(T_I)]$  was obtained in terms of the expected costs of inspection, excavation, maintenance repair (including both recoating and sleeving) and failure replacement, denoted by  $E[C_{R_{IN}}(T_I)]$ ,  $E[C_{R_{EV}}(T_I)]$ ,  $E[C_{R_{MR}}(T_I)]$  and  $E[C_{R_{FR}}(T_I)]$ , respectively. The expected cost rate  $E[C_R(T_I)]$  along with the cost components as a function of the inspection interval varying from one to 50 years with an increment of one year is depicted in Fig. 6.3(a) for  $\gamma = 0$ , and Fig. 6.3(b) for  $\gamma = 5\%$ . The results shown in Fig. 6.3 indicate that  $E[C_{R_{FR}}(T_I)]$  has the highest contribution to  $E[C_R(T_I)]$  as long as  $T_I$  is, say, greater than or equal to 8 years, followed by  $E[C_{R_{EV}}(T_I)]$  and  $E[C_{R_{MR}}(T_I)]$ . The expected cost of inspection is negligible compared with those of the other maintenance actions.



(a)



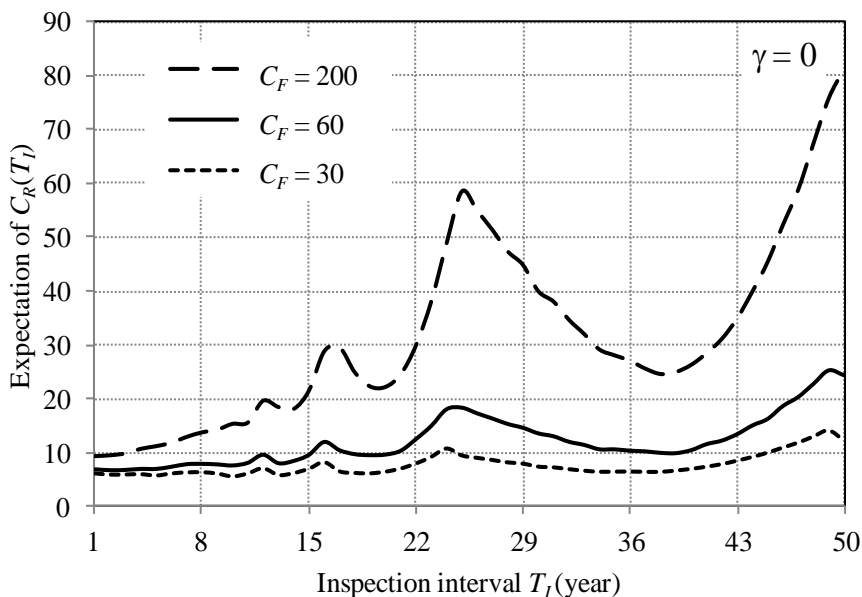
(b)

Figure 6.3 Comparison of the expected cost rates associated with different maintenance actions based on the baseline case

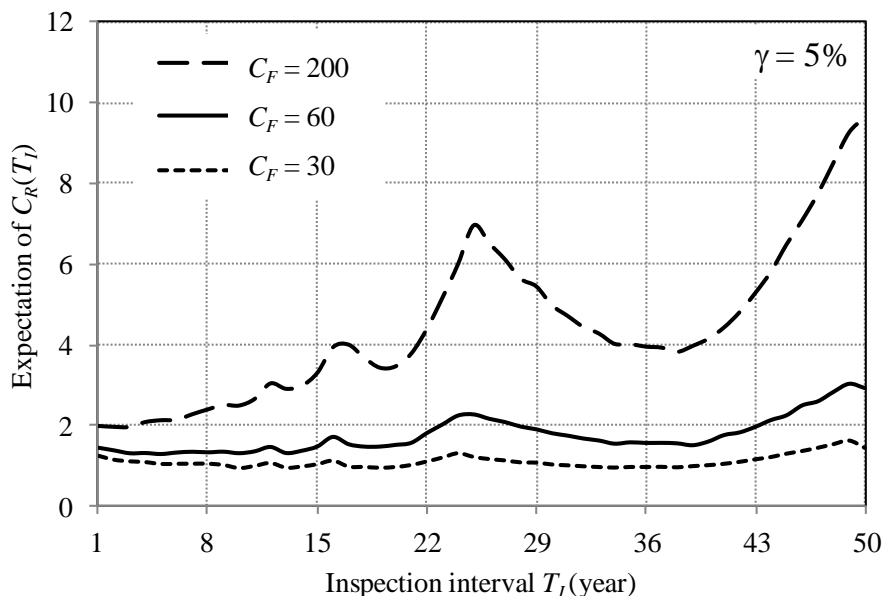
The expected cost rates corresponding to different parameters are depicted in Figs. 6.4 through 6.9, where the solid curve shown in each of the figures corresponds to the baseline case specified in Table 6.3. A notable characteristic of the curves in these



figures is the existence of multiple peaks and valleys. This is explained later in the section based on the annual failure probability curves shown in Fig. 6.10. Figure 6.4 depicts  $E[C_R(T_I)]$  versus  $T_I$  ( $T_I = 1, 2, \dots, 50$  years), where three values of  $C_F$  were considered, i.e.  $C_F = 30, 60$  and  $200$ , respectively. Figure 6.4(a), where the discount rate  $\gamma$  equals zero, indicates that  $E[C_R(T_I)]$  increases as the failure cost increases, which is expected. It also shows that the optimal inspection interval ( $T_{IO}$ ) decreases as the failure cost increases, for example,  $T_{IO}$  equals 10, 2 and 1 years for  $C_F = 30, 60$  and  $200$ , respectively. Note that  $T_{IO}$  was determined from Figure 6.4(a) based on the minimum expected cost rule as stated in Section 6.4.3, namely  $T_I$  corresponding to the minimum value of  $E[C_R(T_I)]$ . The values of  $T_{IO}$  in Figs. 6.4(b) through 6.9 were determined in the same way. If  $\gamma$  equals 5%, as shown in Fig. 6.4(b), the corresponding  $T_{IO}$  are 10, 5 and 3 years for  $C_F = 30, 60$  and  $200$ , respectively. The results shown in Fig. 6.4 suggest that an overly optimistic estimate of the failure cost (e.g.  $C_F = 30$  as opposed to 60), as expected, leads to a longer optimal inspection interval.



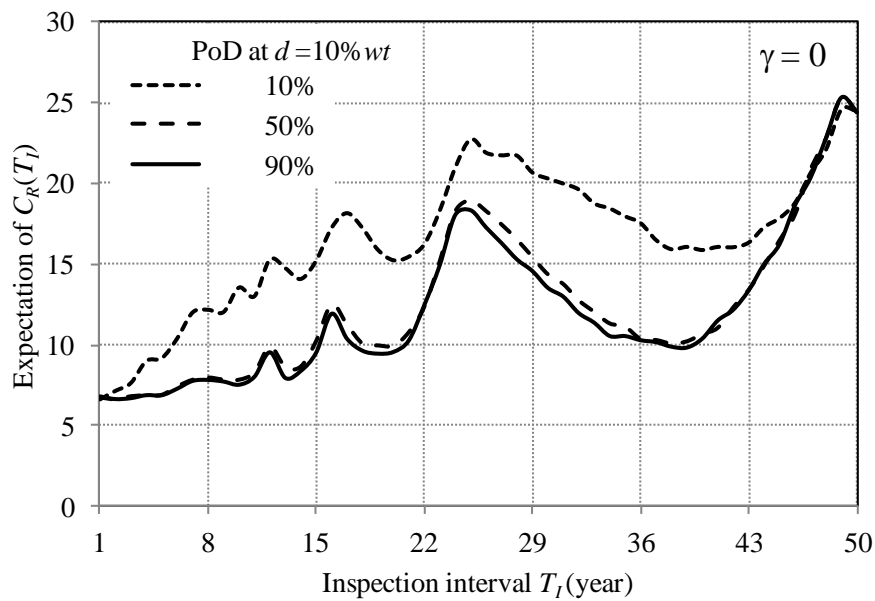
(a)



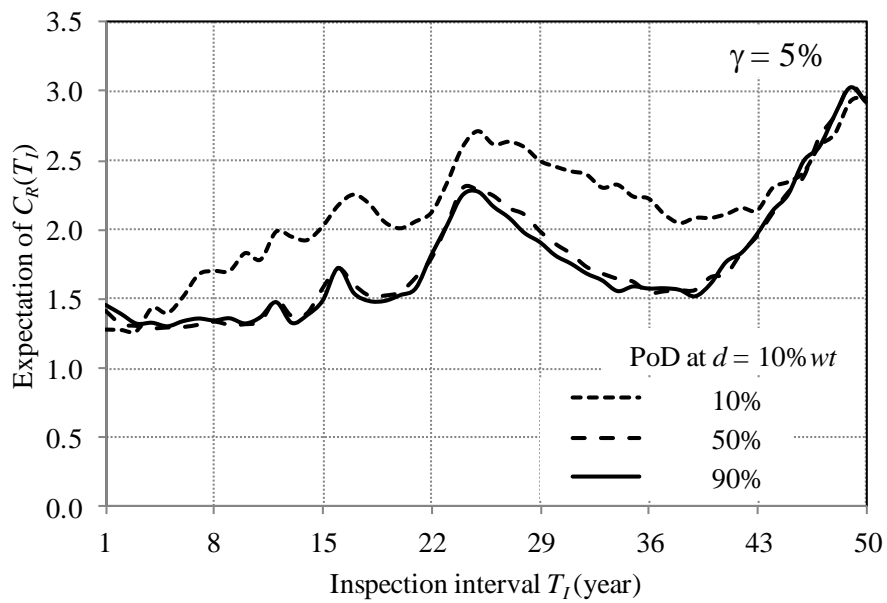
(b)

Figure 6.4 Expected cost rate vs the inspection interval  $T_I$  in term of  $C_F = 30, 60$  and  $200$ 

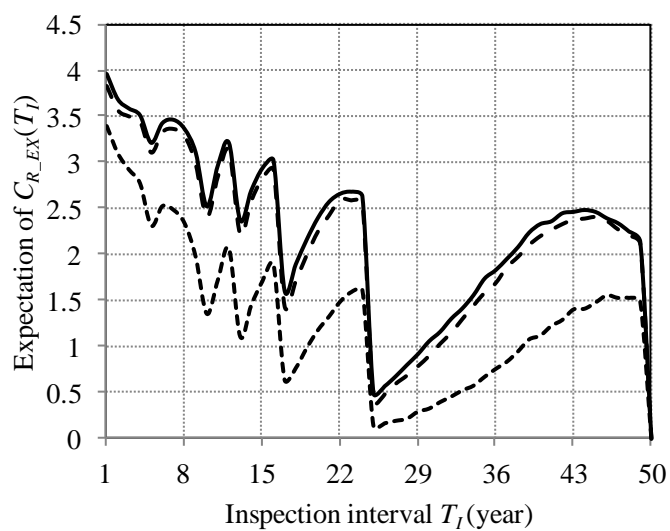
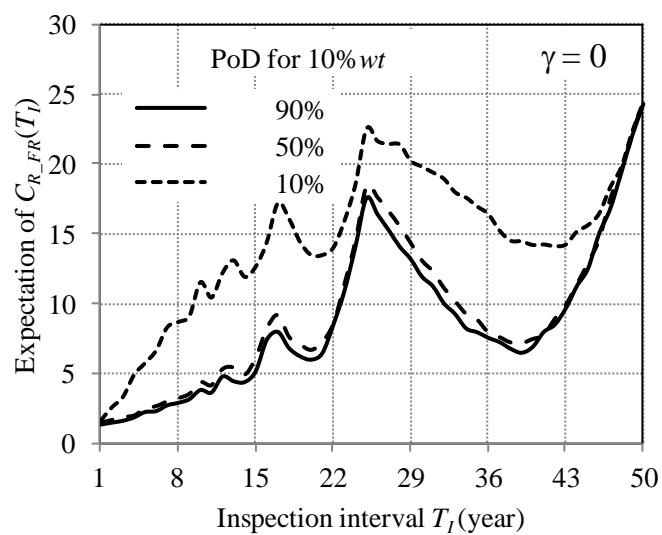
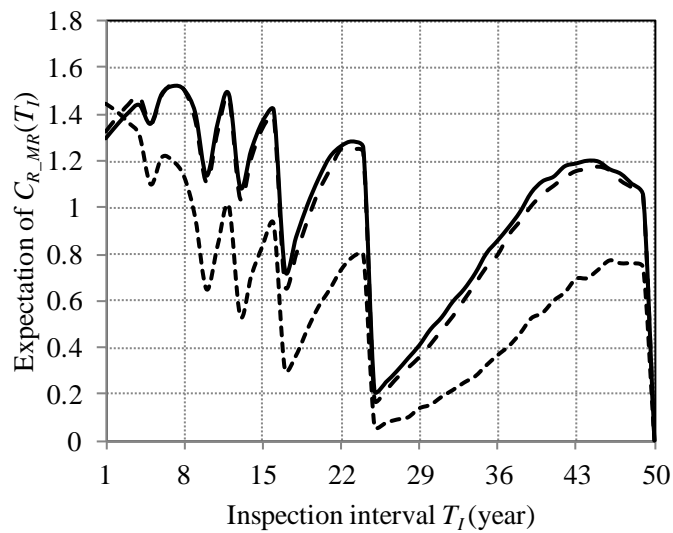
The value of  $E[C_R(T_I)]$  as a function of the inspection interval and PoD (90%, 50% or 10% for the defect depth of 10% wt) is plotted in Figure 6.5(a) for  $\gamma = 0$ , and Figure 6.5(b) for  $\gamma = 5\%$ . Figure 6.5 reveals that  $E[C_R(T_I)]$  at a given inspection interval in general increases as PoD decreases. This is mainly attributed to that a higher PoD leads to a higher likelihood to excavate and repair a given defect, and therefore lower probability of failure and expected failure cost, as indicated by Fig. 6.5(c), the latter in general having the highest contribution to  $E[C_R(T_I)]$ . The relatively small difference between the values of  $E[C_R(T_I)]$  corresponding to PoD = 90% and 50% at  $d = 10\%wt$  is attributed to the small difference between the two PoD curves as shown in Fig. 6.5(d). Furthermore, if  $T_I = 50$  years, it follows from the maintenance policy stated in Section 6.4.2 that no inspection is carried out and therefore the accuracy of ILI tool has no impact on  $E[C_R(T_I)]$ , as shown Figs. 6.5(a) and 6.5(b). Results shown in Figs. 6.5(a) and 6.5(b) suggest that the optimal inspection interval decreases as the accuracy of the ILI tool decrease, which is expected. For example,  $T_{IO} = 3, 4$  and  $5$  years for PoD = 10%, 50% and 90% at  $d = 10\%wt$ , respectively, if  $\gamma = 5\%$ .



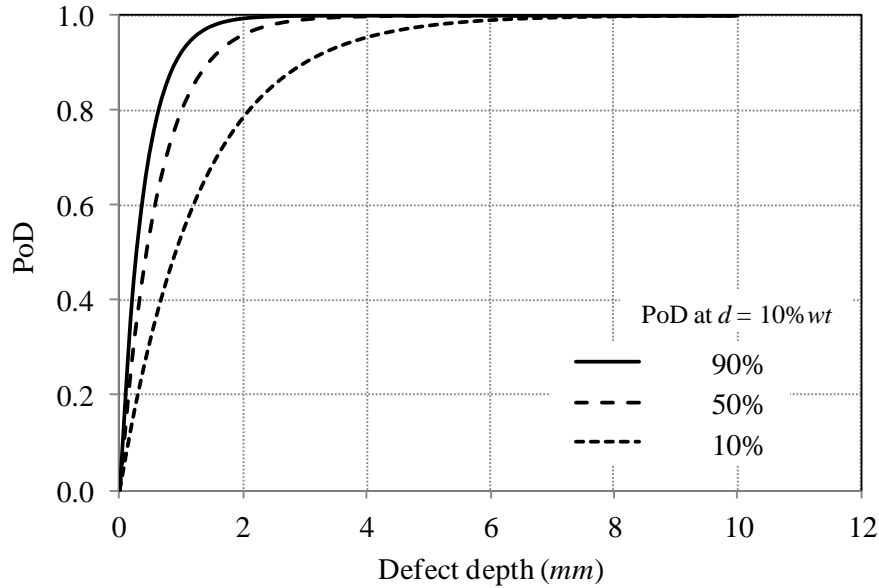
(a)



(b)



(c)

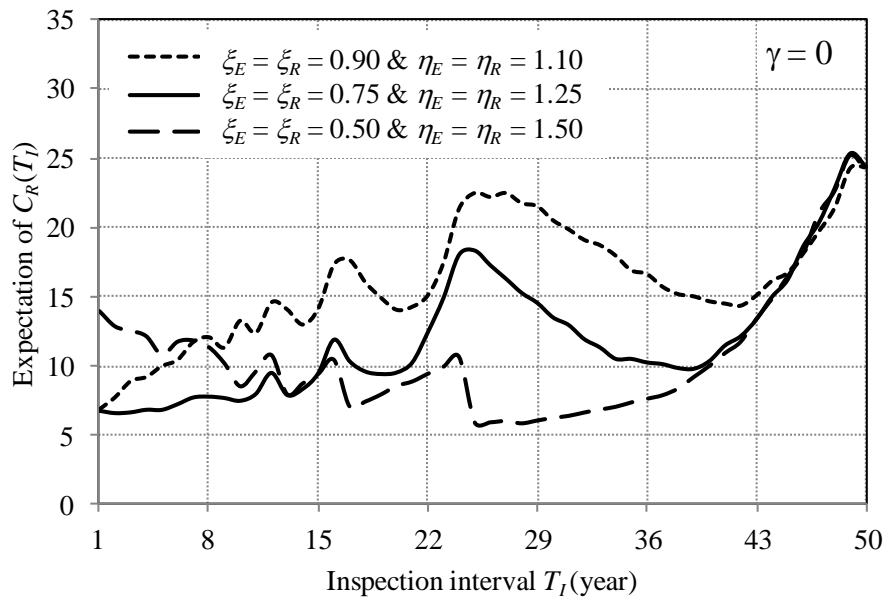


(d)

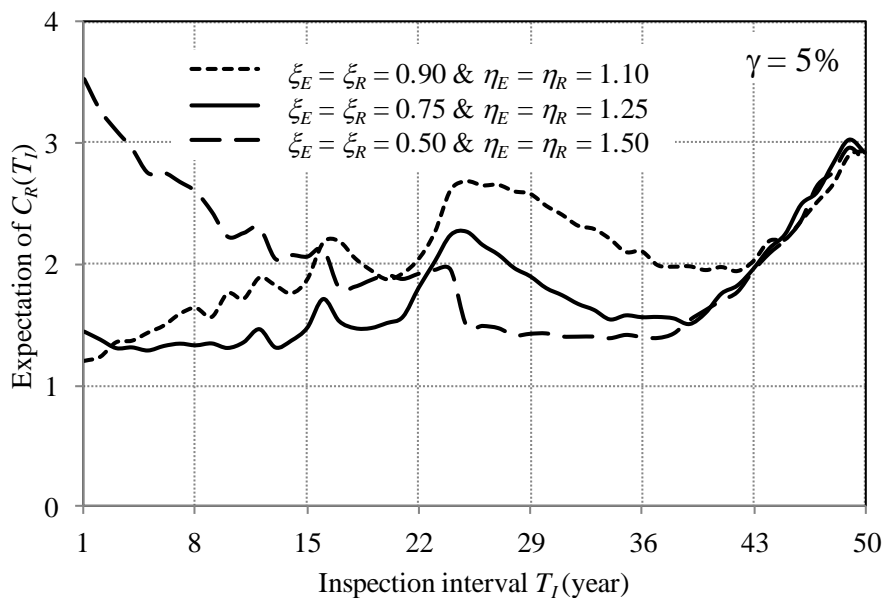
Figure 6.5 Expected cost rate vs the inspection interval  $T_I$  in term of PoD

The values of  $E[C_R(T_I)]$  corresponding to  $\xi_E = \xi_R = 0.9$  and  $\eta_E = \eta_R = 1.1$ ,  $\xi_E = \xi_R = 0.75$  and  $\eta_E = \eta_R = 1.25$  as well as  $\xi_E = \xi_R = 0.5$  and  $\eta_E = \eta_R = 1.5$ , are depicted in Fig. 6.6(a) for  $\gamma = 0$ , and in Fig. 6.6(b) for  $\gamma = 5\%$ . Figure 6.6 suggests that the values of the safety factors have a large impact on  $E[C_R(T_I)]$ . Of the three sets of safety factors considered, the most stringent set (i.e. 0.5 and 1.5) results in the highest value of  $E[C_R(T_I)]$ , if  $T_I \leq 7$  years and  $\gamma = 0$ . This observation makes sense because the more stringent safety factors are employed, the fewer failures but more excavations and repairs arise for a given inspection interval. Furthermore, investigation of the cost breakdown (see Fig. 6.6(c)) indicates that, if  $T_I \leq 7$  years, the total expected maintenance cost, denoted by  $E[C_{R_M}(T_I)]$ , (i.e. the total expected cost excludes the expected failure cost) accounts for over 95% of  $E[C_R(T_I)]$  for  $\xi_E = \xi_R = 0.5$  and  $\eta_E = \eta_R = 1.5$ , and is about 2 times (4 times) as high as that corresponding to  $\xi_E = \xi_R = 0.75$  and  $\eta_E = \eta_R = 1.25$  ( $\xi_E = \xi_R = 0.9$  and  $\eta_E = \eta_R = 1.1$ ). In such case,  $E[C_{R_{FR}}(T_I)]$  is less than  $E[C_{R_M}(T_I)]$  even though the less stringent set of safety factors lead to the higher  $P_{af}$  and  $E[C_{R_{FR}}(T_I)]$  (see Fig. 6.6(c)). If  $T_I > 7$  years, the least stringent set of safety factors (i.e. 0.9 and 1.1) lead to the highest value of  $E[C_R(T_I)]$  in that most of the critical defects are likely to be missed by the mitigation actions, which will lead to high failure probabilities and expected

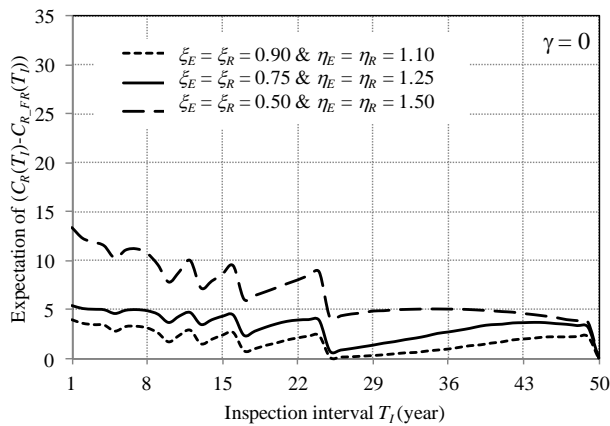
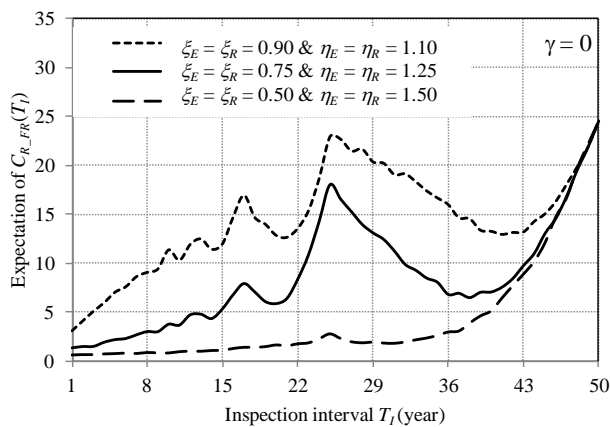
failure cost. Compared with the baseline case (i.e. 0.75 and 1.25), the more stringent safety factors (i.e. 0.5 and 1.5) increases  $T_{IO}$ , whereas the less stringent safety factors (i.e. 0.9 and 1.1) decreases  $T_{IO}$ . For example,  $T_{IO}$  equals 28 years for  $\xi_E = \xi_R = 0.5$  and  $\eta_E = \eta_R = 1.5$ , and 1 year for  $\xi_E = \xi_R = 0.9$  and  $\eta_E = \eta_R = 1.1$  if  $\gamma = 0$ ; whereas  $T_{IO}$  becomes 34 years for the former and remains to be 1 year for the latter if  $\gamma = 5\%$ . Furthermore, it is worth remarking that the safety factors 0.75 and 1.25, which are widely adopted in the pipeline industry, lead to the lowest expected cost for a range of inspection intervals that are commonly used in the industry (say, between 2 to 15). This suggests that the current industry practice in terms of the safety factors for excavation and repair is quite cost-effective.



(a)



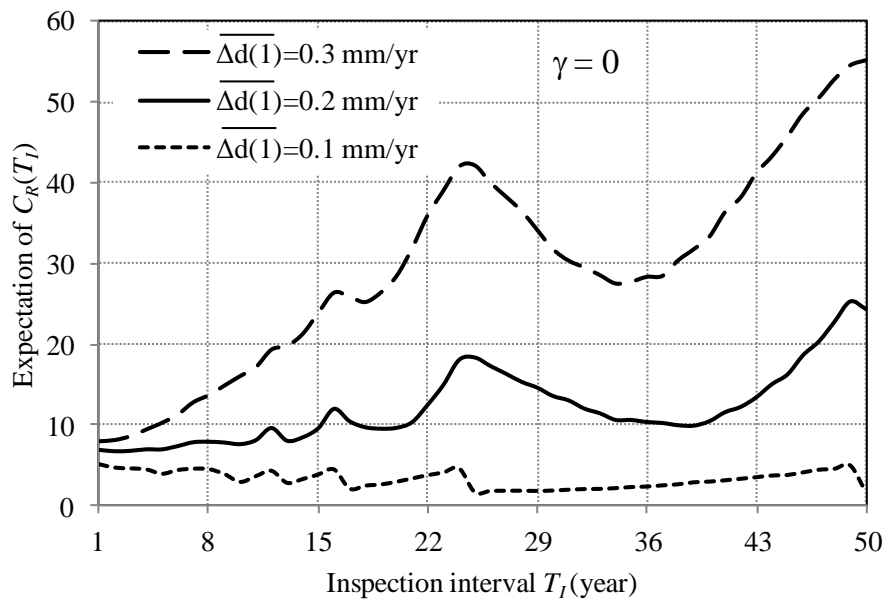
(b)



(c)

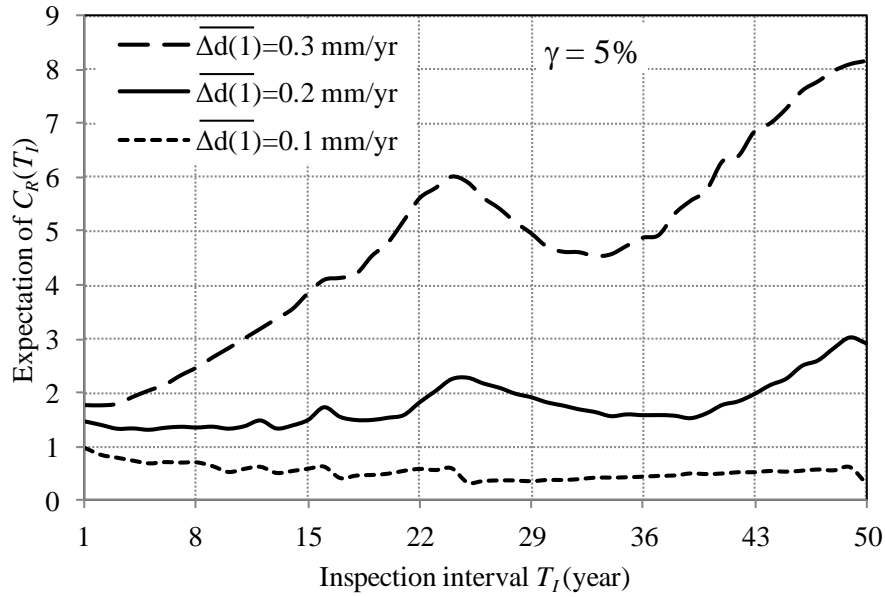
Figure 6.6 Expected cost rate vs the inspection interval  $T_I$  in term of the safety factors

The results shown in Fig. 6.7 illustrate the impact of the mean of the growth rate of the defect depth (denoted by  $\overline{\Delta d(1)}$ ) on  $E[C_R(T_I)]$  and  $T_{IO}$ . Three cases of  $\overline{\Delta d(1)}$  were considered, namely  $\overline{\Delta d(1)} = 0.1, 0.2$  and  $0.3$  mm/yr, respectively. The COV of  $\Delta d(1)$  was fixed at 50% for the three cases. As expected,  $E[C_R(T_I)]$  increases with  $\overline{\Delta d(1)}$  at a given inspection interval. The increase in  $E[C_R(T_I)]$  is particularly significant as  $\overline{\Delta d(1)}$  increases from 0.2 to 0.3 mm/yr, for  $T_I \geq 15$  years. Furthermore,  $T_{IO}$  decreases as  $\overline{\Delta d(1)}$  increases:  $T_{IO}$  equals 25, 2 and 1 year for  $\overline{\Delta d(1)} = 0.1, 0.2$  and  $0.3$  mm/yr, respectively, for  $\gamma = 0$ , and 50, 5 and 2 years, respectively, for  $\gamma = 5\%$ .



(a)

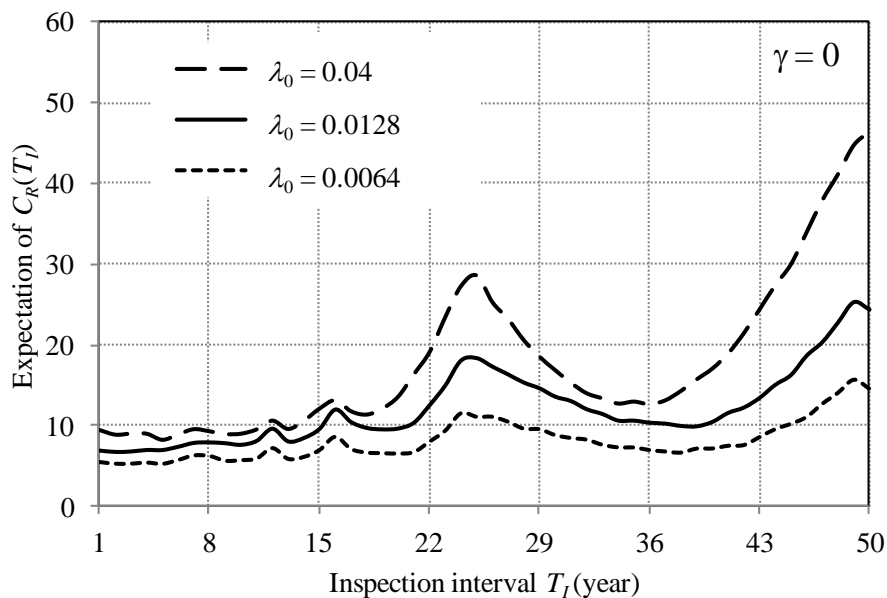




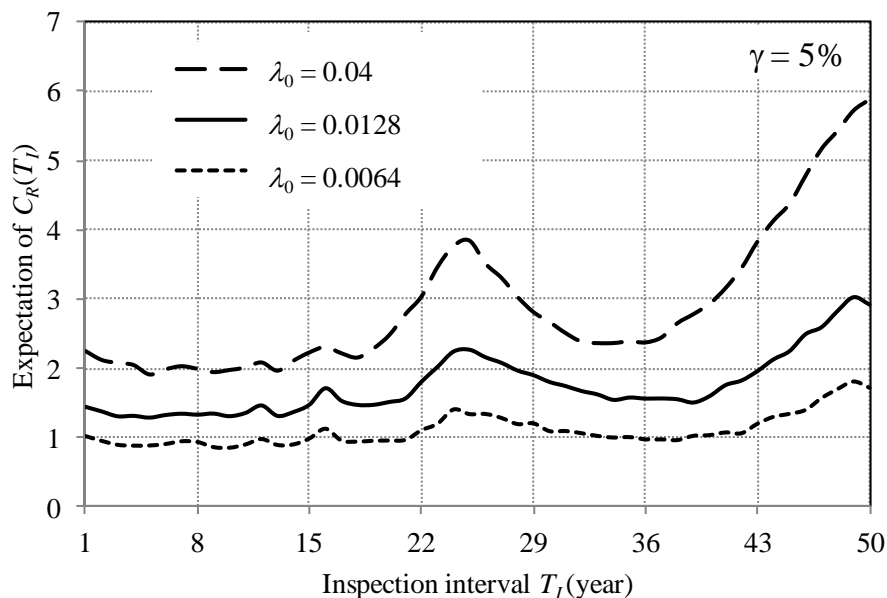
(b)

Figure 6.7 Expected cost rate vs the inspection interval  $T_I$  in term of mean of growth rate

The impact of the instantaneous generation rate in Eq. (6.1) on  $E[C_R(T_I)]$  and  $T_{IO}$  is illustrated in Fig. 6.8(a) for  $\gamma = 0$ , and Fig. 6.8(b) for  $\gamma = 5\%$ , respectively, where the proportional constant (i.e.  $\lambda_0$ ) in the instantaneous rate was assumed to equal 0.0064, 0.0128 or 0.04. Results shown in Fig. 6.8 indicate that a larger value of  $\lambda_0$ , as expected, leads to a higher value of  $E[C_R(T_I)]$  and  $T_{IO} = 5$  (10), 2 (5) and 5 (5) years for  $\lambda_0 = 0.0064$ , 0.0128 and 0.04, respectively, if  $\gamma = 0$  (5%).  $T_{IO}$  corresponding to  $\lambda_0 = 0.04$  (i.e. 5 years) is longer than that corresponding to  $\lambda_0 = 0.0064$  and 0.0128 (i.e. 5 and 2 years, respectively), which is attributed to the following three aspects. First,  $E[C_{R_M}(T_I)]$  governs  $E[C_R(T_I)]$ , for a range of inspection intervals (say,  $1 \leq T_I \leq 10$  years) for the three cases shown in Fig. 6.8. Second, the total expected number of defects corresponding to  $\lambda_0 = 0.04$  is higher than those corresponding to  $\lambda_0 = 0.0064$  and 0.0128; the former will trigger more excavation and repair than the latter given the same PoD,  $\xi_E(\xi_R)$  and  $\eta_E(\eta_R)$  and an inspection interval. Lastly, a longer inspection interval leads to a lower  $E[C_{R_M}(T_I)]$  especially for the case with a larger number of defects.



(a)



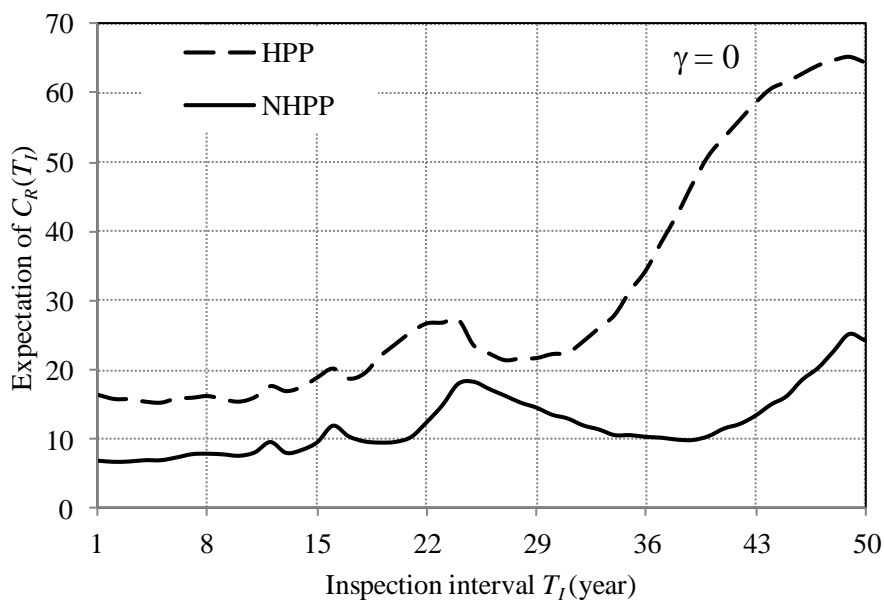
(b)

Figure 6.8 Expected cost rate vs the inspection interval  $T_I$  in term of  $\lambda_0$ 

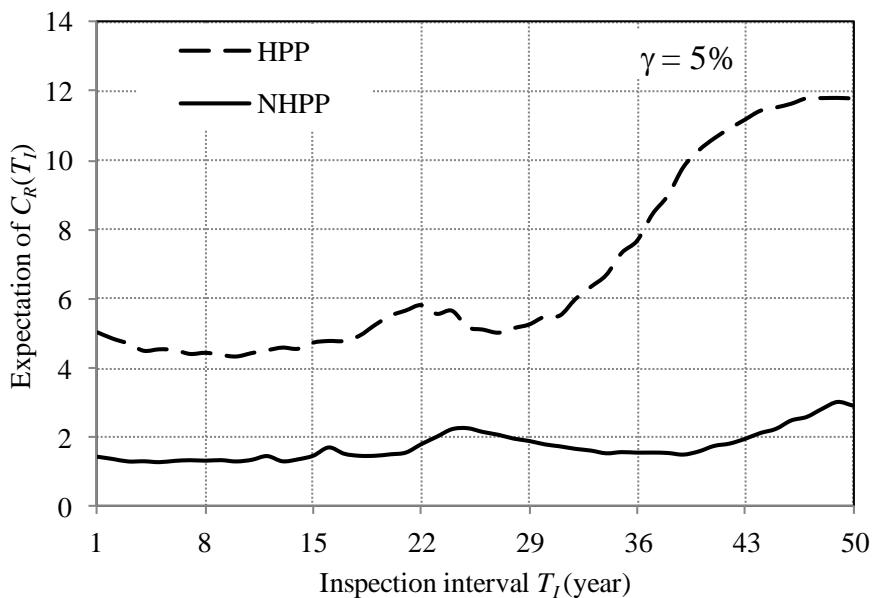
To investigate the impact of the defect generation model on the optimal inspection interval, the homogeneous Poisson process was further considered. To this end, an equivalent generation rate (denoted by  $\lambda$ ) for HPP was considered and evaluated by  $\lambda =$

$\Lambda(T)/T$ . It follows from  $T = 50$  years and  $\Lambda(t)$  corresponding to the baseline case presented in Section 6.5.1 that  $\lambda = 0.32$ . The corresponding results are given in Fig. 6.9.

Figure 6.9 indicates that the HPP model leads to a higher value of  $E[C_R(T_I)]$  than the NHPP model. This is mainly because the failure probabilities corresponding to the HPP model are higher than those corresponding to the NHPP model as indicated by Fig. 6.10, resulting in a higher expected cost of failure for the former model; on the other hand, the total maintenance cost (i.e.  $E[C_{R,M}(T_I)]$ ) corresponding to the former is higher than that corresponding to the latter for a wide range of inspection intervals (say,  $1 \leq T_I \leq 36$  years). Note that the results shown in Fig. 6.10 are further addressed in the following section. The optimal inspection interval corresponding to the HPP model (i.e.  $T_{IO} = 5$  (10) years) is longer than that corresponding to the NHPP model (i.e.  $T_{IO} = 2$  (5) years) for  $\gamma = 0$  (5%). This observation makes sense and can be explained by the same reason as stated for Fig. 6.8 because the total expected number of defects corresponding to the HPP model is always higher than that corresponding to the NHPP model (see Fig. 6.11) at a given inspection interval.



(a)

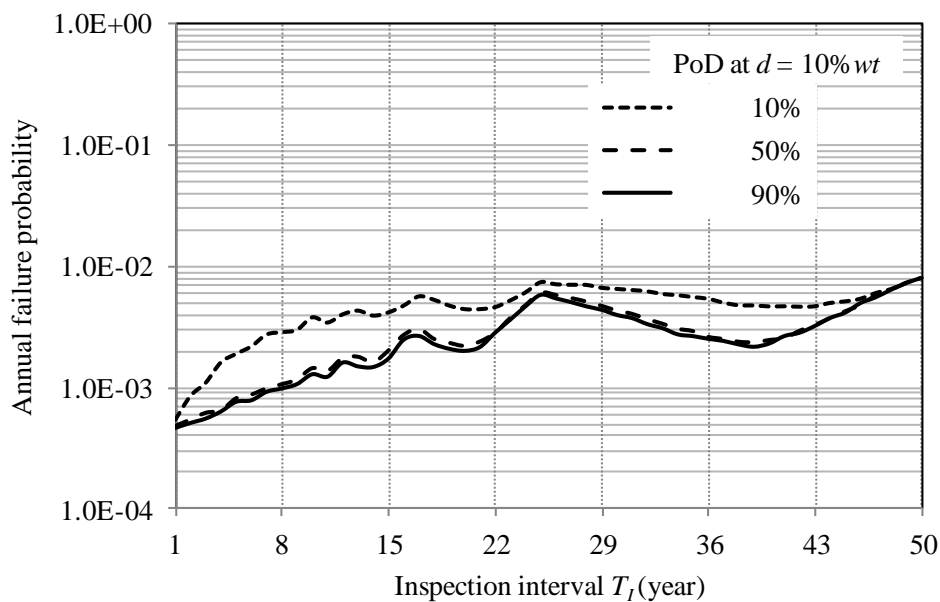


(b)

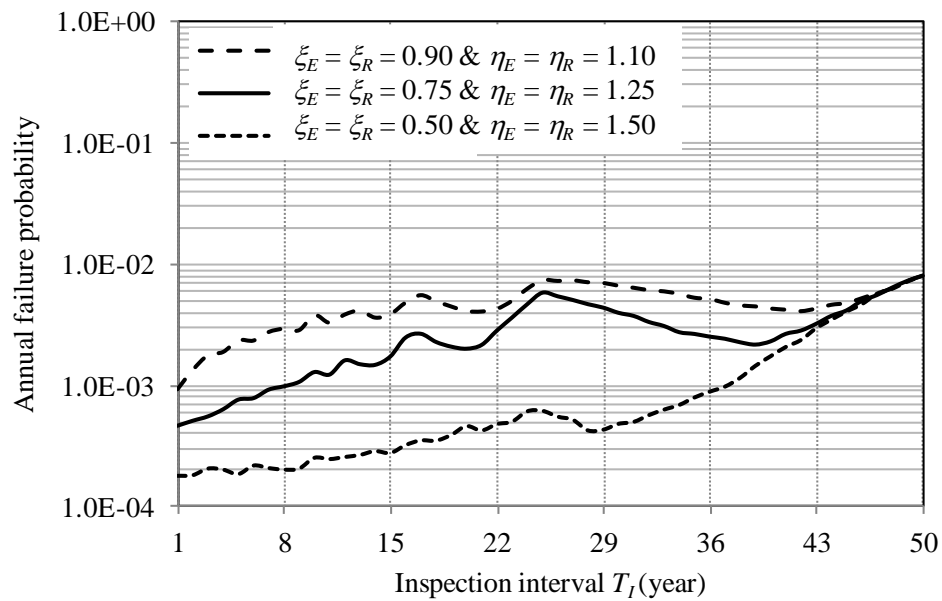
Figure 6.9 Expected cost rate vs the inspection interval  $T_I$  in term of the defect generation model

The annual failure probabilities (i.e.  $P_{af}$ ) corresponding to different scenarios of the parametric analysis are shown as a function of the inspection interval in Figs. 6.10(a) through 6.10(e). Figure 6.10 can be used to select  $T_{IO}$  by incorporating the reliability constraint. For example, if the allowable annual failure probability for a pipe joint is set equal to  $5.5 \times 10^{-4}$ , the reliability constraint-based  $T_{IO}$  equals 2 years for the baseline case as shown in Fig. 6.10. That multiple peaks and valleys exist on the annual failure probability curves suggests that the similar trend shown in Figs. 6.4 through 6.9 can be explained from Fig. 6.10. Without loss of generality, consider the curve for the baseline case (i.e. the solid line). Given a simulation trial, the total number of failures conditional on  $T_I = 50$  years is in general more than that conditional on  $T_I = 25$  years. This is shown in the annual failure probability given in Fig. 6.10; that is, the annual failure probability corresponding to  $T_I = 25$  years is lower than that corresponding to  $T_I = 50$  years. Furthermore, the local minima appearing on the curve of  $E[C_R(T_I)]$  (e.g. at  $T_I = 36$  years) are mainly because the inspection and repair carried out in the 36<sup>th</sup> year mitigate some of the critical defects that will likely cause failure of the pipe joint over the remaining 14 years of its service life. This implies that an inspection interval of 36 years is more

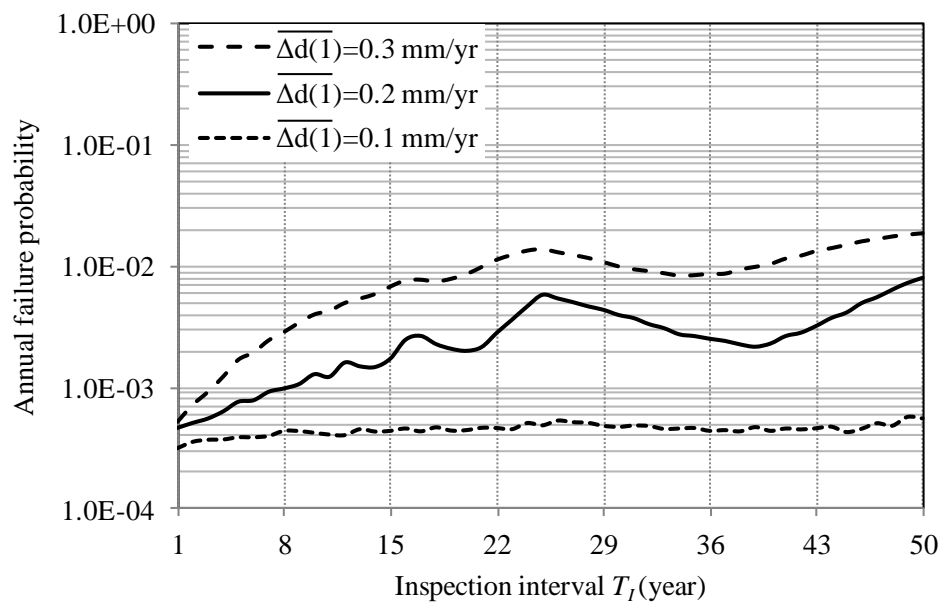
effective than an interval of 25 years for this particular case. Finally, the annual failure probabilities associated with the HPP model are higher than those associated with the NHPP model, as reflected in Fig. 6.10. This is attributed to the fact that the expected total number of defects generated within time  $[0, t]$ , denoted by  $E[N(t)]$  (i.e.  $\Lambda(t)$  in Eq. (6.1)), corresponding to the HPP model is always greater than that corresponding to the NHPP model except for  $t = 50$  years, as shown in Fig. 6.11; therefore, the failure probability of the pipe joint corresponding to the former is higher than that corresponding to the latter.



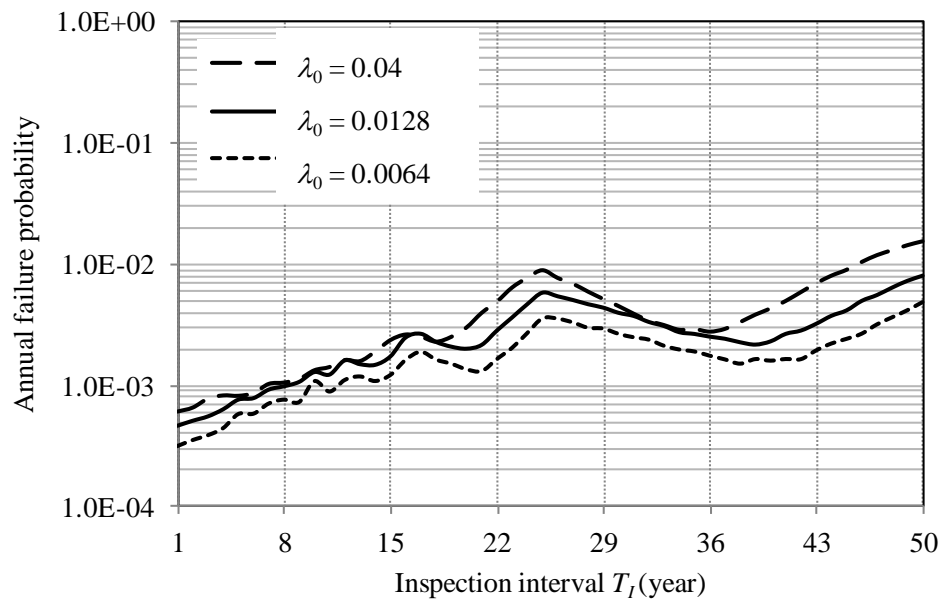
(a)



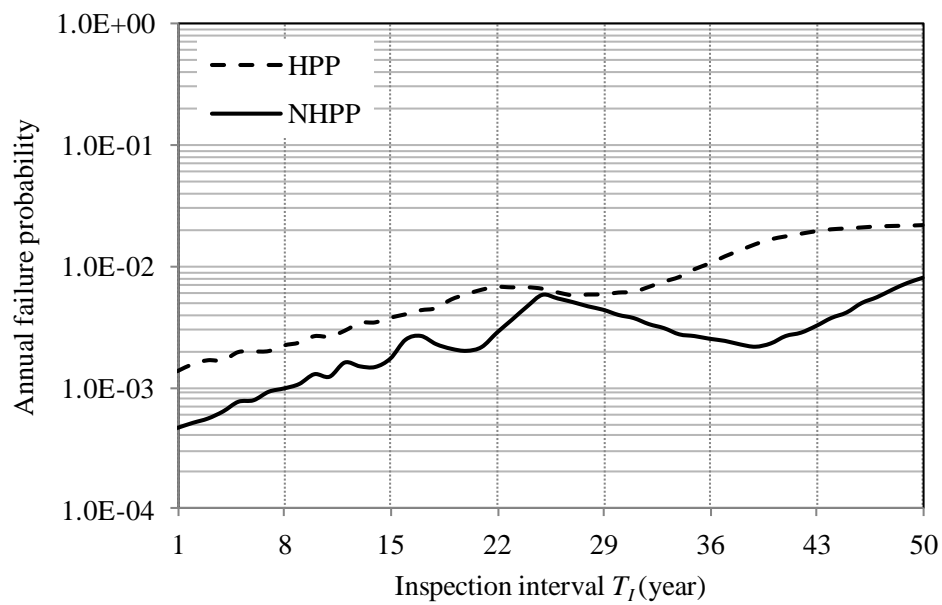
(b)



(c)



(d)



(e)

Figure 6.10 Annual failure probability vs the inspection interval  $T_I$

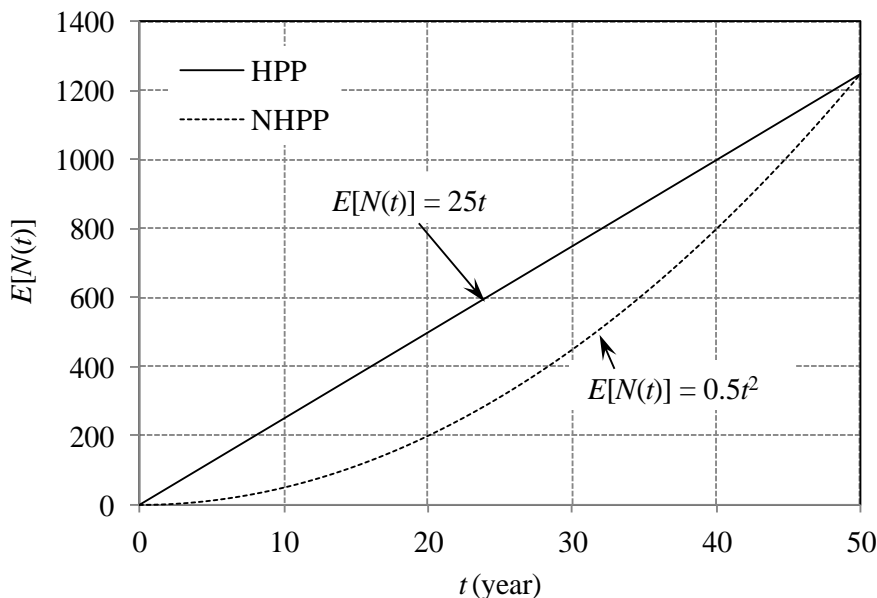


Figure 6.11 Comparison of the expectation of the HPP and NHPP

## 6.6 Conclusions

This chapter describes a probabilistic investigation aimed at determining the optimal inspection interval for onshore underground natural gas pipelines subjected to metal-loss corrosion considering the uncertainties in the number of corrosion defects on the pipeline and the sizes of the defects as well as the uncertainties associated with the ILI tools. The investigation is applicable to determining the optimal time to carry out the first inspection for newly-built pipelines. The non-homogenous Poisson process is used to characterize the generation of new defects over time. The homogeneous gamma process is used to model the growth of individual defects in the through pipe wall thickness direction (i.e. defect depth). The uncertainties associated with the ILI tools incorporated in the methodology include the probability of detection (PoD) and a general form of the measurement error (i.e. bias and random scattering error). For a given inspection interval, the total costs of corrosion inspection and repair over the service life of the pipeline for a reference pipe joint are formulated considering that the entire joint, as opposed to specific defects, is repaired by the maintenance action, which is consistent with the industry practice. The cost of failure corresponds to the burst of the corroded pipeline due to internal pressure, and includes both the direct and indirect costs. The



Monte Carlo simulation technique is adopted to evaluate the expected cost rate, i.e. the expected total costs of inspection, repair and failure per one year of the service life. The minimum expected cost rule is then employed to determine the optimal inspection interval.

The impact of model parameters on the optimal inspection interval is investigated through parametric analyses of an example pipeline. The following observations are obtained from the analysis results. First, the optimal inspection interval decreases as the failure cost and/or depth growth rate increases. Second, the instantaneous generation rate of the defect generation model and the PoD value have a marked impact on the expected cost rate and the optimal inspection interval. Third, the optimal inspection interval increases as the criteria for excavating and repairing corrosion defects become more stringent; the excavation and repair criteria commonly adopted by the industry is cost-effective for inspection intervals that range from 2 to 15 years. Finally, the homogeneous Poisson process-based defect generation model leads to a higher expected cost rate than the non-homogeneous Poisson process-based defect generation model, if the mean value of the total number of defects generated over the entire service life is the same for both models. The former model leads to a longer optimal inspection interval than the latter model if the discount rate equals zero and 5%. The algorithms for determining the optimal inspection interval considering uncertainties from different sources developed in this study will facilitate the reliability-based pipeline corrosion management.

## References

- Al-Amin, M., Zhou, W., Zhang, S., Kariyawasam, S. and Wang, H. (2012). Bayesian model for the calibration of ILI tools. Proceedings of IPC 2012; IPC2012-90491, ASME, Calgary.
- Ang, A. H. S. and Tang, W. H. (1975). Probability Concepts in Engineering Planning and Design, Volume I: Basic Principles. John and Wiley & sons, NY.
- Beichelt, F. E. and Fatti, L. P. (2002). Stochastic Process and Their Applications. Taylor and Francis, NY.

- Cheng, T. and Pandey, M. D. (2012). An accurate analysis of maintenance cost of structures experiencing stochastic degradation. *Structure and Infrastructure Engineering*, 8(4): 329-339.
- Cosham, A., Hopkins, P. and Macdonald, K. A. (2007). Best practice for the assessment of defects in pipelines—corrosion. *Engineering Failure Analysis*, 14: 1245-65.
- Cox, D.R. and Oakes, D. *Analysis of Survival Data*. London: Chapman & Hall, 1984.
- CSA. (2007). *Oil and gas pipeline systems, CSA standard Z662-07*. Mississauga, Ontario, Canada: Canadian Standard Association.
- Fuller, W. A. (1987). *Measurement Error Models*. John Wiley & Sons, Inc., NY.
- Gomes, W. J. S., Beck, A. T. and Haukaas, T. (2013). Optimal inspection planning for onshore pipelines subjected to external corrosion. *Reliability Engineering and System Safety*, 118: 18-27.
- Hong, H. P. (1999). Inspection and maintenance planning under external corrosion considering generation of new defects. *Structural Safety*, 21:203-222.
- Jaech, J. L. (1985). *Statistical Analysis of Measurement Errors*. John Wiley & Sons, Inc., NY.
- Jiao, G., Sotberg, T. and Igland, R. T. (1995). SUPERB 2M statistical data-basic uncertainty measures for reliability analysis of offshore pipelines. SUPERB project report.
- Johnson, R. A. (2000). *Probability and Statistics for Engineers (6th edition)*. Prentice-Hall Inc, US.
- Kariyawasam, S. (2012). Private communication.
- Kariyawasam, S. and Peterson, W. (2010). Effective improvements to reliability based corrosion management. *Proceedings of IPC 2010; IPC2010-31425*, ASME, Calgary.
- Kariyawasam, S., Yeung, P., Clouston, S. and Hurd, G. (2012). Overcoming technical limitations in identifying and Characterizing critical complex corrosion. *Proceedings of IPC 2012; IPC2012-90529*, ASME, Calgary.

- Kiefner, J. F. and Vieth, P. H. (1989). A modified criterion for evaluating the remaining strength of corroded pipe. Rep. PR 3-805, Pipeline Research Committee, American Gas Association, Columbus, OH.
- Kulkarni, V. G. (2010). Modeling and Analysis of Stochastic System (2nd edition). Chapman & Hall/CRC, UK.
- Kuniewski, S. P., van de Weide, J. A. M. and van Noortwijk, J. M. (2009). Sampling inspection for the evaluation of time-dependent reliability of deteriorating systems under imperfect defect detection. *Reliability Engineering and System Safety*, 94(9): 1480-1490.
- Morrison, T. B. and Worthingham, R. G. (1992). Reliability of high pressure line pipe under external corrosion. *ASME, OMAE, V-B*, 401-408.
- Nessim, M. and Zhou, W. (2005). Target Reliability Levels for the Design and Assessment of Onshore Natural Gas Pipelines. C-FER report, GRI-04/230, Gas Research Institute, Des Plaines, IL.
- Parzen, E. (1962). *Stochastic Process*. Holden-day, Inc., SF, US.
- Rodriguez III, E. S. and Provan, J. W. (1989). Part II: development of general failure control system for estimating the reliability of deteriorating structures. *Corrosion Science*, 45(3):193-206.
- Stephens, M. and Nessim, M. A. (2006). A comprehensive approach to corrosion management based on structural reliability method. *Proceedings of IPC 2006; IPC06-10458*, ASME, Calgary.
- Zhou, W. (2010). System reliability of corroding pipelines. *International Journal of Pressure Vessels and Piping*, 87: 587-95.
- Zhou, W. and Huang, G. X. (2012) Model error assessments of burst capacity models for corroded pipelines. *International Journal of Pressure Vessels and Piping*, 99-100: 1-8.
- Zhou, W. and Nessim, M. A. (2011). Optimal design of onshore natural gas pipelines. *Journal of Pressure Vessel Technology*, ASME, 133:031702.

## **Chapter 7 Summary, Conclusions and Recommendations for Future Study**

### **7.1 General**

The work reported in this thesis is focused on the reliability-based corrosion management of energy pipelines, including development of the probabilistic models for the growth of metal-loss corrosion defects on energy pipelines, and applications of these models in the context of time-dependent reliability assessment and optimal maintenance decision on the corroding pipelines. Conclusions obtained from the research and recommendations for future study are summarized as follows.

### **7.2 Development of Probabilistic Models for the Growth of Metal-loss Corrosion**

Four stochastic process-based models were developed to characterize the growth of depth of metal-loss corrosion defects on energy pipelines, namely the homogeneous and non-homogeneous gamma processes- (HGP- and NHGP-), inverse Gaussian process- (IGP-) and geometric Brownian motion- (GBM-) based models, which are described in Chapters 2, 3 and 4, respectively.

All these growth models were formulated in a hierarchical Bayesian framework, which allows consideration of the uncertainties from different sources, e.g. the uncertainties associated with the model parameters and ILI tools. The model parameters involved in each of the four models were assumed to be uncertain. The statistical inference of these model parameters were evaluated using the Markov Chain Monte Carlo (MCMC) simulation techniques based on the ILI data obtained from multiple ILI runs. A general form of the measurement error, including the biases and random scattering error as well as the correlation between the random scattering errors associated with different ILI tools were incorporated in the Bayesian updating.

The HGP-, NHGP- and IGP-based models are state-independent whereas the GBM-based model is state-dependent. The GBM-based model approximate the growth path as

a piecewise linear growth, and is more flexible than the GP- and IGP-based models because the latter two models involve a specific assumption about the mean growth path (e.g. linear or power-law function of time). Furthermore, these models are defect-specific as opposed to segment-specific models, which are favored by pipeline engineers in that they allow for identification of the critical defect. These models are suitable for pipelines for which multiple sets of ILI data have been collected from different ILIs with not long intervals. Finally, the spatial correlation of individual defects was ignored in the four growth models developed in this study.

The growth models were applied to a total of 62 external corrosion defects, for which the field-measured depths (i.e. actual depths) are known from excavation and multiple sets of ILI-reported depths were collected from the ILI runs carried out prior to excavation. The ILI data were used to carry out the Bayesian updating and make inference of the model parameters. Then the growth models were validated by a comparison of the predicted depths at the time of excavation with the corresponding field measurements.

The comparison suggests that the growth models can predict the actual depth of the defect reasonable well; for example, approximately 90% of the predicted depths fall within the bounds of actual depth  $\pm 10\%$ . The predictions suggest that the models by and large lead to a poor prediction if the ILI data incorporated in the Bayesian updating involves larger measurement errors. The mean squared error of prediction (MSEP) was employed to evaluate and compare the predictive qualities of a given model with different assumptions of predictive methods, and the predictive qualities of different models with a given predictive method. The MSEP values suggested that the predictive accuracies of the NHGP-, HGP- and IGP-based models are similar. Furthermore, the four Bayesian growth models are significantly better than the conventional linear growth model commonly used by the pipeline industry.

The proposed growth model will facilitate the application of defect-based pipeline corrosion management program by maintaining the structural integrity of the pipelines while achieving optimal allocation of the limited resources for maintenance.

### 7.3 Time-dependent System Reliability Analysis of a Corroding Pipeline

A simulation-based methodology was developed in Chapter 5 to evaluate the time-dependent failure probability of a pipe segment containing multiple active corrosion defects. This model incorporates the developed corrosion growth models and the Poisson square wave process-based internal pressure model. The time-dependent failure probability of the pipe segment was evaluated in terms of three distinctive failure modes, namely small leak, large leak and rupture. The proposed methodology was applied to two pipe segments, denoted as segments 1 and 2, respectively, selected from an in-service underground natural gas pipeline.

The time-dependent reliability of segment 1 containing 25 active external corrosion defects was evaluated using the HGP-based growth model. The internal pressure was assumed to be a PSWP, random variable or deterministic value. Three assumptions for the parameters involved in the HGP-based growth model were considered, namely uncertain and correlated, uncertain but independent, and deterministic. Sensitivity analysis results suggest that the internal pressure model has a negligible impact on the probability of small leak and a marked impact on the probability of large leak; on the other hand, the uncertainties and correlations of the model parameters have a marked impact on the probabilities of small leak and large leak. These observations highlight the importance of properly considering the uncertainty in the internal pressure in the reliability analysis as well as the importance of appropriately accounting for the uncertainties in the growth parameters as well as their correlations in the reliability analysis based on the HGP-based growth model.

The HGP-, NHGP-, IGP- and GBM-based growth models were employed to evaluate the time-dependent system reliability of Segment 2 to investigate the impact of the growth models on the time-dependent reliability of corroding pipeline. Segment 2 contains 10 active defects for which the predicted depths obtained from the four models agree well with the actual depths (e.g. the absolute deviations between the predicted and actual depths are less than 5 %wt). The small deviation allows comparing the failure probabilities corresponding to different growth models to be founded on a common basis.

The internal pressure was characterized by a random variable. Results of the comparative study suggest that the growth models have a significant impact on the probability of small leak, but insignificant impact on the probabilities of large leak and rupture.

#### **7.4 Optimal Maintenance Decisions on Corroding Energy Pipelines**

A probabilistic investigation was carried out to determine the optimal inspection interval for onshore underground natural gas pipelines subjected to metal-loss corrosion. This investigation accounts for the uncertainties in the number of corrosion defects on the pipeline and the sizes of the defects as well as the uncertainties associated with the ILI tools. The non-homogenous Poisson process (NHPP) was used to characterize the generation of new defects over time. The homogeneous gamma process (HGP) was used to model the growth of defect depth (i.e. in the through pipe wall thickness direction) of individual defects. The uncertainties associated with the ILI tools incorporated in the methodology include the probability of detection (PoD) and a general form of the measurement error (i.e. the biases and random scattering error). For a given inspection interval, the total costs of corrosion inspection and repair over the service life of the pipeline for a reference pipe joint were formulated considering that the entire joint, as opposed to specific defects, is repaired by the maintenance action, which is consistent with the industry practice. The Monte Carlo simulation technique was adopted to evaluate the expected cost rate, i.e. the expected total costs of inspection, repair and failure per one year of the service life. The minimum expected cost rule was then employed to determine the optimal inspection interval.

The investigation is illustrated by an example pipeline. The impact of model parameters (e.g. the cost of failure, the excavation and repair criteria, the mean of growth rate, PoD, the growth rate of the defect depth and defect generation model) on the optimal inspection interval was investigated through parametric analyses. The following observations are obtained from the analysis results. First, the optimal inspection interval decreases as the failure cost and/or depth growth rate increases. Second, PoD and PoF have a marked impact on the expected cost rate, but no impact on the optimal inspection interval. Third, the optimal inspection interval increases as the criteria for excavating and

repairing corrosion defects become more stringent. Finally, the HPP-based defect generation model leads to a higher expected cost rate than the NHPP-based defect generation model, if the mean value of the total number of defects generated over the entire service life is the same for both models. The former model leads to a shorter optimal inspection interval than the latter model if the discount rate equals zero; however, the two models lead to the same optimal inspection interval if the discount rate equals 5%. The proposed algorithms provides a framework for determining the optimal inspection interval for corroding pipelines considering uncertainties from different sources and will facilitate the reliability-based pipeline integrity management.

## **7.5 Recommendations for Future Study**

The recommended future investigations are described as follows.

First, the spatial correlation among the growth of different defects is a worthy topic. The spatial correlation can be quantified based on the inspection data and incorporated into the development of the defect growth model.

Second, the spatial variability of pipeline and environmental conditions surrounding the pipelines was implicitly considered in the developed models. Such local covariates as the pipe steel, coating and soil types, if available, can be explicitly taken into account in the growth model to further improve or refine the model.

Third, the defect population included in the multiple ILI data sets used in the Bayesian updating is fixed in the present study. The new defects generated between the different inspections should be incorporated in the updating of the growth models.

Fourth, the generation of new corrosion defects needs to be quantified based on the ILI data, and incorporated in the system reliability analysis and determination of the optimal re-inspection interval for corroding pipelines. Furthermore, the risk attitude models, e.g. the stochastic dominance rule and cumulative prospect theory, can be incorporated in the decision-making to properly consider the risk attitudes of the decision makers.



Finally, the multi-objective optimization approach can be used to develop optimal maintenance strategies for corroding pipelines because it is desirable for the decision makers to determine a maintenance plan that minimizes the maintenance cost and maximizes the reliability of the pipeline.

## Appendix A Full Conditional Posterior Distributions of Model Parameters (GP-based Model)

1. The posterior distribution of  $\Delta x_{ij}$  ( $i=1, 2, \dots, m; j=1, 2, \dots, n$ )

- Gamma prior distribution given by Eq. (2.5);
- Likelihood function given by Eq. (2.8);

The posterior distribution of  $\Delta x_{ij}$  is

$$\begin{aligned} p(\Delta x_{ij} | \mathbf{y}_i, \Delta A_{ij}, \beta_i, t_{i0}) &\propto L(\mathbf{y}_i | \Delta \mathbf{x}_i) \pi(\Delta x_{ij} | \Delta A_{ij}, \beta_i) \\ &\propto \exp \left( -\frac{1}{2} (\mathbf{y}_i - (\mathbf{a} + \mathbf{b} \mathbf{x}_i))' (\boldsymbol{\Sigma}_{E_i})^{-1} (\mathbf{y}_i - (\mathbf{a} + \mathbf{b} \mathbf{x}_i)) \right) (\Delta x_{ij})^{\Delta A_{ij} - 1} \exp(-\Delta x_{ij} \beta_i) \quad (\text{A.1a}) \end{aligned}$$

or

$$\begin{aligned} &\ln[p(\Delta x_{ij} | \mathbf{y}_i, \Delta A_{ij}, \beta_i, t_{i0})] \\ &\propto -\frac{1}{2} (\mathbf{y}_i - (\mathbf{a} + \mathbf{b} \mathbf{x}_i))' (\boldsymbol{\Sigma}_{E_i})^{-1} (\mathbf{y}_i - (\mathbf{a} + \mathbf{b} \mathbf{x}_i)) + (\Delta A_{ij} - 1) \ln(\Delta x_{ij}) - \Delta x_{ij} \beta_i \quad (\text{A.1b}) \end{aligned}$$

2. The posterior distribution of  $\alpha$

- Gamma prior distribution  $\pi(\alpha | p_1, q_1)$ ;
- Likelihood function given by Eq. (2.10b);

$$\begin{aligned} p(\alpha | \Delta \mathbf{x}, \boldsymbol{\kappa}, \boldsymbol{\beta}, \mathbf{t}_0, p_1, q_1) &\propto \prod_{i=1}^m \prod_{j=1}^n L(\Delta x_{ij} | \Delta A_{ij}, \beta_i) \pi(\alpha | p_1, q_1) \\ &\propto \prod_{i=1}^m \prod_{j=1}^n \left[ (\beta_i)^{\Delta A_{ij}} (\Delta x_{ij})^{\Delta A_{ij} - 1} / \Gamma(\Delta A_{ij}) \right] \alpha^{p_1 - 1} \exp(-\alpha q_1) \quad (\text{A.2a}) \end{aligned}$$

or

$$\begin{aligned} &\ln[p(\alpha | \Delta \mathbf{x}, \boldsymbol{\kappa}, \boldsymbol{\beta}, \mathbf{t}_0, p_1, q_1)] \\ &\propto \sum_{i=1}^m \sum_{j=1}^n \left( \Delta A_{ij} \ln(\beta_i) + (\Delta A_{ij} - 1) \ln(\Delta x_{ij}) - \ln(\Gamma(\Delta A_{ij})) \right) + (p_1 - 1) \ln \alpha - \alpha q_1 \quad (\text{A.2b}) \end{aligned}$$

3. The posterior distribution of  $\boldsymbol{\kappa}$

- Gamma prior distribution  $\pi(\boldsymbol{\kappa} | p_2, q_2)$ ;
- Likelihood function given by Eq. (2.10b);

$$\begin{aligned}
p(\kappa|\Delta\mathbf{x}, \alpha, \boldsymbol{\beta}, \mathbf{t}_0, p_2, q_2) &\propto \prod_{i=1}^m \prod_{j=1}^n L(\Delta x_{ij}|\Delta A_{ij}, \beta_i) \pi(\kappa|p_2, q_2) \\
&\propto \prod_{i=1}^m \prod_{j=1}^n \left( (\beta_i)^{\Delta A_{ij}} (\Delta x_{ij})^{\Delta A_{ij}-1} / \Gamma(\Delta A_{ij}) \right) \kappa^{p_2-1} \exp(-\kappa q_2)
\end{aligned} \tag{A.3a}$$

or

$$\begin{aligned}
&\ln[p(\kappa|\Delta\mathbf{x}, \alpha, \boldsymbol{\beta}, \mathbf{t}_0, p_2, q_2)] \\
&\propto \sum_{i=1}^m \sum_{j=1}^n \left( \Delta A_{ij} \ln(\beta_i) + (\Delta A_{ij} - 1) \ln(\Delta x_{ij}) - \ln(\Gamma(\Delta A_{ij})) \right) + (p_2 - 1) \ln \kappa - \kappa q_2
\end{aligned} \tag{A.3b}$$

4. The posterior distribution of  $t_{i0}$

- Uniform prior distribution  $\pi(t_{i0}|p_3, q_3)$ ;
- Likelihood function given by Eq. (2.10a);

$$\begin{aligned}
p(t_{i0}|\Delta\mathbf{x}_i, \Delta A_{ij}, \beta_i, p_3, q_3) &\propto \prod_{j=1}^n L(\Delta x_{ij}|\Delta A_{ij}, \beta_i) \pi(t_{i0}|p_3, q_3) \\
&\propto \prod_{j=1}^n \left( (\beta_i)^{\Delta A_{ij}} (\Delta x_{ij})^{\Delta A_{ij}-1} / \Gamma(\Delta A_{ij}) \right)
\end{aligned} \tag{A.4a}$$

or

$$\begin{aligned}
&\ln[p(t_{i0}|\Delta\mathbf{x}_i, \Delta A_{ij}, \beta_i, p_3, q_3)] \\
&\propto \sum_{j=1}^n \left( \Delta A_{ij} \ln(\beta_i) + (\Delta A_{ij} - 1) \ln(\Delta x_{ij}) - \ln(\Gamma(\Delta A_{ij})) \right)
\end{aligned} \tag{A.4b}$$

5. The posterior distribution of  $\beta_i$

- Gamma prior distribution  $\pi(\beta|p_4, q_4)$ ;
- Likelihood function given by Eq. (2.10a);

$$\begin{aligned}
p(\beta_i|\Delta\mathbf{x}_i, \Delta A_{ij}, t_{i0}, p_4, q_4) &\propto \prod_{j=1}^n L(\Delta x_{ij}|\Delta A_{ij}, \beta_i) \pi(\beta_i|p_4, q_4) \\
&\propto (\beta_i)^{\sum_{j=1}^n \Delta A_{ij} + p_4 - 1} \exp \left( - \left( \sum_{j=1}^n \Delta x_{ij} + q_4 \right) \beta_i \right) \\
&\propto (\beta_i)^{\alpha(t_{in} - t_{i0})^{\kappa} + p_4 - 1} \exp \left( - (\sum_{j=1}^n \Delta x_{ij} + q_4) \beta_i \right)
\end{aligned} \tag{A.5a}$$

$$\beta_i \sim f_G(\alpha(t_{in} - t_{i0})^{\kappa} + p_4, \sum_{j=1}^n \Delta x_{ij} + q_4) \tag{A.5b}$$

## Appendix B Procedure of the MCMC Simulation

Denote  $\mathbf{y}_i = (y_{i1}, y_{i2}, \dots, y_{ij}, \dots, y_{in})'$ ,  $\Delta \mathbf{x}_i = (\Delta x_{i1}, \Delta x_{i2}, \dots, \Delta x_{ij}, \dots, \Delta x_{in})$ ,  $\Delta \mathbf{x} = (\Delta \mathbf{x}_1, \Delta \mathbf{x}_2, \dots, \Delta \mathbf{x}_m)$ ,  $\boldsymbol{\beta} = (\beta_1, \beta_2, \dots, \beta_m)$  and  $\mathbf{t}_0 = (t_{10}, t_{20}, \dots, t_{m0})$ . A step-by-step procedure based on a hybrid of the M-H algorithm and Gibbs sampler to sequentially generate the random samples of the parameters in the growth model is described in the following.

1) Let  $s$  denote the counter of simulation trial, and set initial values:  $\Delta \mathbf{x}^{(0)}$ ,  $\alpha^{(0)}$ ,  $\kappa^{(0)}$ ,  $\mathbf{t}_0^{(0)}$  and  $\boldsymbol{\beta}^{(0)}$ ; start from  $s = 1$  and carry out the following:

2) Based on Eq. (A.1), for given  $i$ , start from  $j = 1$ ,

2.1) Generate  $\Delta x_{ij}^{(*)}$  from the proposal function;

2.2) Calculate

$$\phi = \frac{p(\Delta x_{i1}^{(s)}, \Delta x_{i2}^{(s)}, \dots, \Delta x_{i,j-1}^{(s)}, \Delta x_{ij}^{(*)}, \Delta x_{i,j+1}^{(s-1)}, \Delta x_{in}^{(s-1)} | \mathbf{y}_i, \alpha^{(s-1)}, \kappa^{(s-1)}, \mathbf{t}_{i0}^{(s-1)}, \boldsymbol{\beta}_i^{(s-1)})}{p(\Delta x_{i1}^{(s)}, \Delta x_{i2}^{(s)}, \dots, \Delta x_{i,j-1}^{(s)}, \Delta x_{ij}^{(s-1)}, \Delta x_{i,j+1}^{(s-1)}, \Delta x_{in}^{(s-1)} | \mathbf{y}_i, \alpha^{(s-1)}, \kappa^{(s-1)}, \mathbf{t}_{i0}^{(s-1)}, \boldsymbol{\beta}_i^{(s-1)})}$$

2.3) Generate a uniform random draw  $u$  from 0 to 1.

2.4) Set  $\Delta x_{ij}^{(s)} = \Delta x_{ij}^{(*)}$  if  $u \leq \min(\phi, 1)$ , and  $\Delta x_{ij}^{(s)} = \Delta x_{ij}^{(s-1)}$  otherwise;

2.5) Repeat 2.1) through 2.4) for  $mn$  times and obtain  $\Delta \mathbf{x}^{(s)}$ ;

3) Based on Eq. (A.2)

3.1) Generate  $\alpha^{(*)}$  from the proposal function;

3.2) Calculate

$$\phi = \frac{p(\alpha^{(*)} | \Delta \mathbf{x}^{(s)}, \kappa^{(s-1)}, \mathbf{t}_0^{(s-1)}, \boldsymbol{\beta}^{(s-1)}, p_1, q_1)}{p(\alpha^{(s-1)} | \Delta \mathbf{x}^{(s)}, \kappa^{(s-1)}, \mathbf{t}_0^{(s-1)}, \boldsymbol{\beta}^{(s-1)}, p_1, q_1)}$$

3.3) Generate a uniform random draw  $u$  from 0 to 1.

3.4) Set  $\alpha^{(s)} = \alpha^{(*)}$  if  $u \leq \min(\phi, 1)$ , and  $\alpha^{(s)} = \alpha^{(s-1)}$  otherwise;

4) Based on Eq. (A.3)

4.1) Generate  $\kappa^{(*)}$  from the proposal function;

4.2) Calculate

$$\phi = \frac{p(\kappa^{(*)} \mid \Delta \mathbf{x}^{(s)}, \alpha^{(s)}, \mathbf{t}_0^{(s-1)}, \boldsymbol{\beta}^{(s-1)}, p_2, q_2)}{p(\kappa^{(s-1)} \mid \Delta \mathbf{x}^{(s)}, \alpha^{(s)}, \mathbf{t}_0^{(s-1)}, \boldsymbol{\beta}^{(s-1)}, p_2, q_2)}$$

4.3) Generate a uniform random draw  $u$  from 0 to 1.

4.4) Set  $\kappa^{(s)} = \kappa^{(*)}$  if  $u \leq \min(\phi, 1)$ , and  $\kappa^{(s)} = \kappa^{(s-1)}$  otherwise;

5) Based on Eq.(A.4), start from  $i = 1$ :

5.1) Generate  $t_{i0}^{(*)}$  from the proposal function;

5.2) Calculate

$$\phi = \frac{p(t_{i0}^{(*)} \mid \Delta \mathbf{x}_i^{(s)}, \alpha^{(s)}, \kappa^{(s)}, \beta_i^{(s-1)}, p_3, q_3)}{p(t_{i0}^{(0)} \mid \Delta \mathbf{x}_i^{(s)}, \alpha^{(s)}, \kappa^{(s)}, \beta_i^{(s-1)}, p_3, q_3)}$$

5.3) Generate a uniform random draw  $u$  from 0 to 1.

5.4) Set  $t_{i0}^{(s)} = t_{i0}^{(*)}$ , if  $u \leq \min(\phi, 1)$ , and  $t_{i0}^{(s)} = t_{i0}^{(s-1)}$  otherwise;

5.5) Repeat Steps 5.1) through 5.4) for  $m$  times, then  $\mathbf{t}_0^{(s)}$  is obtained;

6) Based on Eq.(A.5b), sample  $\beta_i^{(s)}$  from  $f_G(\beta_i \mid \Delta \mathbf{x}_i^{(s)}, \alpha^{(s)}, \kappa^{(s)}, t_{i0}^{(s)}, p_4, q_4)$  using Gibbs sampler sequentially for  $i = 1, 2, \dots, m$ , and obtain  $\boldsymbol{\beta}^{(s)}$ ;

7) Repeat Steps 2) through 6) for  $N$  cycles until each of the chains of all parameters converge to a stationary process.

## Appendix C Full Conditional Posterior Distributions of Model Parameters (IGP-based Model)

Scenario I: defect-specific  $\alpha$  and  $t_0$  and common  $\xi$

1. The posterior distribution of  $\Delta x_{ij}$  ( $i=1, 2, \dots, m; j=1, 2, \dots, n$ )

- Inverse Gaussian prior distribution given by  $\pi(\Delta x_{ij}|\Delta\theta_{ij}, \xi(\Delta\theta_{ij})^2)$  with  $\Delta\theta_{ij}$  given by Eq. (3.3);
- Likelihood function given by Eq. (2.8);

The posterior distribution of  $\Delta x_{ij}$  is

$$\begin{aligned}
 p(\Delta x_{ij}|\mathbf{y}_i, \Delta\theta_{ij}, \xi, t_{i0}) &\propto L(\mathbf{y}_i|\Delta\mathbf{x}_i)\pi(\Delta x_{ij}|\Delta\theta_{ij}, \xi(\Delta\theta_{ij})^2) \\
 &\propto \\
 &\exp\left(-\frac{1}{2}(\mathbf{y}_i - (\mathbf{a} + \mathbf{b}\mathbf{x}_i))'(\boldsymbol{\Sigma}_{E_i})^{-1}(\mathbf{y}_i - (\mathbf{a} + \mathbf{b}\mathbf{x}_i))\right)(\Delta x_{ij})^{-3/2} \exp\left(-\frac{\xi(\Delta x_{ij} - \Delta\theta_{ij})^2}{2\Delta x_{ij}}\right)
 \end{aligned} \tag{C.I.1a}$$

or

$$\begin{aligned}
 &\ln[p(\Delta x_{ij}|\mathbf{y}_i, \Delta\theta_{ij}, \xi, t_{i0})] \\
 &\propto -\frac{1}{2}(\mathbf{y}_i - (\mathbf{a} + \mathbf{b}\mathbf{x}_i))'(\boldsymbol{\Sigma}_{E_i})^{-1}(\mathbf{y}_i - (\mathbf{a} + \mathbf{b}\mathbf{x}_i)) - \frac{3}{2}\ln(\Delta x_{ij}) - \frac{\xi(\Delta x_{ij} - \Delta\theta_{ij})^2}{2\Delta x_{ij}}
 \end{aligned} \tag{C.I.1b}$$

2. The posterior distribution of  $\alpha_i$

- Gamma prior distribution  $\pi(\alpha_i|p_1, q_1)$ ;
- Likelihood function given by Eq. (3.5a);

The posterior distribution of  $\alpha_i$  is

$$\begin{aligned}
 p(\alpha_i|\Delta\mathbf{x}_i, \xi, t_{i0}, p_1, q_1) &\propto L(\alpha_i|\Delta\mathbf{x}_i)\pi(\alpha_i|p_1, q_1) \\
 &\propto \prod_{j=1}^n \left( \Delta\theta_{ij} \exp\left(-\frac{\xi(\Delta x_{ij} - \Delta\theta_{ij})^2}{2\Delta x_{ij}}\right) \right) \alpha_i^{p_1-1} \exp(-\alpha_i q_1)
 \end{aligned} \tag{C.I.2a}$$

or

$$\begin{aligned} & \ln[p(\alpha_i|\Delta\mathbf{x}_i, \xi, t_{i0}, p_1, q_1)] \\ & \propto \sum_{j=1}^n \left( \ln(\Delta\theta_{ij}) - \frac{\xi(\Delta x_{ij} - \Delta\theta_{ij})^2}{2\Delta x_{ij}} \right) + (p_1 - 1)\ln\alpha_i - \alpha_i q_1 \end{aligned} \quad (\text{C.I.2b})$$

3. The posterior distribution of  $t_{i0}$

- Uniform prior distribution  $\pi(t_{i0}|p_2, q_2)$ ;
- Likelihood function given by Eq. (3.5a);

The posterior distribution of  $t_{i0}$  is

$$\begin{aligned} p(t_{i0}|\Delta\mathbf{x}_i, \alpha_i, \xi, p_2, q_2) & \propto L(t_{i0}|\Delta\mathbf{x}_i)\pi(t_{i0}|p_2, q_2) \\ & \propto \prod_{j=1}^n \Delta\theta_{ij} \exp\left(-\frac{\xi(\Delta x_{ij} - \Delta\theta_{ij})^2}{2\Delta x_{ij}}\right) \end{aligned} \quad (\text{C.I.3a})$$

or

$$\ln[p(t_{i0}|\Delta\mathbf{x}_i, \alpha_i, \xi, p_2, q_2)] \propto \sum_{j=1}^n \left( \ln(\Delta\theta_{ij}) - \frac{\xi(\Delta x_{ij} - \Delta\theta_{ij})^2}{2\Delta x_{ij}} \right) \quad (\text{C.I.3b})$$

4. The posterior distribution of  $\xi$

- Gamma prior distribution  $\pi(\xi|p_3, q_3)$ ;
- Likelihood function given by Eq. (3.5b);

The posterior distribution of  $\xi$  is

$$\begin{aligned} p(\xi|\Delta\mathbf{x}, \alpha_i, t_{i0}, p_3, q_3) & \propto L(\xi|\Delta\mathbf{x})\pi(\xi|p_3, q_3) \\ & \propto \exp\left(-\beta\left(\sum_{i=1}^m \sum_{j=1}^n \left(\frac{(\Delta x_{ij} - \Delta\theta_{ij})^2}{2\Delta x_{ij}}\right) + q_3\right)\right) \beta^{\frac{mn}{2} + p_3 - 1} \end{aligned} \quad (\text{C.I.4a})$$

$$\xi \sim f_G\left(\frac{mn}{2} + p_3, \sum_{i=1}^m \sum_{j=1}^n \left(\frac{(\Delta x_{ij} - \Delta\theta_{ij})^2}{2\Delta x_{ij}}\right) + q_3\right) \quad (\text{C.I.4b})$$

Scenario II: defect-specific  $\alpha$ ,  $t_0$  and  $\xi$

1. The posterior distribution of  $\Delta x_{ij}$  ( $i=1, 2, \dots, m; j=1, 2, \dots, n$ )

- Inverse Gaussian prior distribution given by  $\pi(\Delta x_{ij}|\Delta\theta_{ij}, \xi_i(\Delta\theta_{ij})^2)$ , with  $\Delta\theta_{ij}$  given by Eq. (3.3);

- Likelihood function given by Eq. (2.8);

The posterior distribution of  $\Delta x_{ij}$  is

$$\begin{aligned}
 p(\Delta x_{ij} | \mathbf{y}_i, \Delta \theta_{ij}, \xi_i, t_{i0}) &\propto L(\mathbf{y}_i | \Delta \mathbf{x}_i) \pi(\Delta x_{ij} | \Delta \theta_{ij}, \xi_i (\Delta \theta_{ij})^2) \\
 &\propto \\
 &\exp\left(-\frac{1}{2}(\mathbf{y}_i - (\mathbf{a} + \mathbf{b}\mathbf{x}_i))'(\boldsymbol{\Sigma}_{E_i})^{-1}(\mathbf{y}_i - (\mathbf{a} + \mathbf{b}\mathbf{x}_i))\right) (\Delta x_{ij})^{-3/2} \exp\left(-\frac{\xi_i(\Delta x_{ij} - \Delta \theta_{ij})^2}{2\Delta x_{ij}}\right)
 \end{aligned} \tag{C.II.1a}$$

or

$$\begin{aligned}
 &\ln[p(\Delta x_{ij} | \mathbf{y}_i, \Delta \theta_{ij}, \xi_i, t_{i0})] \\
 &\propto -\frac{1}{2}(\mathbf{y}_i - (\mathbf{a} + \mathbf{b}\mathbf{x}_i))'(\boldsymbol{\Sigma}_{E_i})^{-1}(\mathbf{y}_i - (\mathbf{a} + \mathbf{b}\mathbf{x}_i)) - \frac{3}{2}\ln(\Delta x_{ij}) - \frac{\xi_i(\Delta x_{ij} - \Delta \theta_{ij})^2}{2\Delta x_{ij}}
 \end{aligned} \tag{C.II.1b}$$

2. The posterior distribution of  $\alpha_i$

- Gamma prior distribution  $\pi(\alpha_i | p_1, q_1)$ ;
- Likelihood function given by Eq. (3.5a) with  $\xi$  being replaced by  $\xi_i$ ;

The posterior distribution of  $\alpha_i$  is

$$\begin{aligned}
 p(\alpha_i | \Delta \mathbf{x}_i, \xi_i, t_{i0}, p_1, q_1) &\propto L(\alpha_i | \Delta \mathbf{x}_i) \pi(\alpha_i | p_1, q_1) \\
 &\propto \prod_{j=1}^n \left( \Delta \theta_{ij} \exp\left(-\frac{\xi_i(\Delta x_{ij} - \Delta \theta_{ij})^2}{2\Delta x_{ij}}\right) \right) \alpha_i^{p_1-1} \exp(-\alpha_i q_1)
 \end{aligned} \tag{C.II.2a}$$

or

$$\begin{aligned}
 &\ln[p(\alpha_i | \Delta \mathbf{x}_i, \xi_i, t_{i0}, p_1, q_1)] \\
 &\propto \sum_{j=1}^n \left( \ln(\Delta \theta_{ij}) - \frac{\xi_i(\Delta x_{ij} - \Delta \theta_{ij})^2}{2\Delta x_{ij}} \right) + (p_1 - 1)\ln\alpha_i - \alpha_i q_1
 \end{aligned} \tag{C.II.2b}$$

3. The posterior distribution of  $t_{i0}$

- Uniform prior distribution  $\pi(t_{i0} | p_2, q_2)$ ;
- Likelihood function given by Eq. (3.5a) with  $\xi$  being replaced by  $\xi_i$ ;

The posterior distribution of  $t_{i0}$  is



$$\begin{aligned}
p(t_{i0}|\Delta\mathbf{x}_i, \alpha_i, \xi_i, p_2, q_2) &\propto L(t_{i0}|\Delta\mathbf{x}_i)\pi(t_{i0}|p_2, q_2) \\
&\propto \prod_{j=1}^n \left( \Delta\theta_{ij} \exp\left(-\frac{\xi_i(\Delta x_{ij}-\Delta\theta_{ij})^2}{2\Delta x_{ij}}\right) \right)
\end{aligned} \tag{C.II.3a}$$

or

$$\ln[p(t_{i0}|\Delta\mathbf{x}_i, \alpha_i, \xi_i, p_2, q_2)] \propto \sum_{j=1}^n \left( \ln(\Delta\theta_{ij}) - \frac{\xi_i(\Delta x_{ij}-\Delta\theta_{ij})^2}{2\Delta x_{ij}} \right) \tag{C.II.3b}$$

4. The posterior distribution of  $\xi_i$

- Gamma prior distribution  $\pi(\xi_i|p_3, q_3)$ ;
- Likelihood function  $\prod_{j=1}^n f_{\Delta x_{ij}}(\Delta x_{ij}|\Delta\theta_{ij}, \xi_i(\Delta\theta_{ij})^2)$ ;

The posterior distribution of  $\xi_i$  is

$$\begin{aligned}
p(\xi_i|\Delta\mathbf{x}_i, \alpha_i, t_{i0}, p_3, q_3) &\propto L(\xi_i|\Delta\mathbf{x}_i)\pi(\xi_i|p_3, q_3) \\
&\propto \exp\left(-\beta\left(\sum_{j=1}^n\left(\frac{(\Delta x_{ij}-\Delta\theta_{ij})^2}{2\Delta x_{ij}}\right) + q_3\right)\right)\beta^{\frac{n}{2}+p_3-1}
\end{aligned} \tag{C.II.4a}$$

$$\xi_i \sim f_G\left(\frac{n}{2} + p_3, \sum_{j=1}^n\left(\frac{(\Delta x_{ij}-\Delta\theta_{ij})^2}{2\Delta x_{ij}}\right) + q_3\right) \tag{C.II.4b}$$

Scenario III: defect-specific  $t_0$  and common  $\alpha$  and  $\xi$

1. The posterior distribution of  $\Delta x_{ij}$  ( $i=1, 2, \dots, m; j=1, 2, \dots, n$ )

- Inverse Gaussian prior distribution given by  $\pi(\Delta x_{ij}|\Delta\theta_{ij}, \xi(\Delta\theta_{ij})^2)$ , with  $\alpha_i$  in Eq. (3.3) being replaced by  $\alpha$ ;
- Likelihood function given by Eq. (2.8);

The posterior distribution of  $\Delta x_{ij}$  is

$$\begin{aligned}
p(\Delta x_{ij}|\mathbf{y}_i, \Delta\theta_{ij}, \xi, t_{i0}) &\propto L(\mathbf{y}_i|\Delta\mathbf{x}_i)\pi(\Delta x_{ij}|\Delta\theta_{ij}, \xi(\Delta\theta_{ij})^2) \\
&\propto \\
&\exp\left(-\frac{1}{2}(\mathbf{y}_i - (\mathbf{a} + \mathbf{b}\mathbf{x}_i))'(\boldsymbol{\Sigma}_{E_i})^{-1}(\mathbf{y}_i - (\mathbf{a} + \mathbf{b}\mathbf{x}_i))\right)(\Delta x_{ij})^{-3/2} \exp\left(-\frac{\xi(\Delta x_{ij}-\Delta\theta_{ij})^2}{2\Delta x_{ij}}\right)
\end{aligned}$$

(C.III.1a)

or

$$\begin{aligned} & \ln[p(\Delta \mathbf{x}_{ij} | \mathbf{y}_i, \Delta \theta_{ij}, \xi, t_{i0})] \\ & \propto -\frac{1}{2}(\mathbf{y}_i - (\mathbf{a} + \mathbf{b}\mathbf{x}_i))'(\boldsymbol{\Sigma}_{E_i})^{-1}(\mathbf{y}_i - (\mathbf{a} + \mathbf{b}\mathbf{x}_i)) - \frac{3}{2}\ln(\Delta x_{ij}) - \frac{\xi(\Delta x_{ij} - \Delta \theta_{ij})^2}{2\Delta x_{ij}} \end{aligned} \quad (\text{C.III.1b})$$

2. The posterior distribution of  $\alpha$ 

- Gamma prior distribution  $\pi(\alpha | p_1, q_1)$ ;
- Likelihood function  $\prod_{i=1}^m f_{\Delta \mathbf{x}_i}(\Delta \mathbf{x}_i | \Delta \theta_{ij}, \xi(\Delta \theta_{ij})^2)$ ;

The posterior distribution of  $\alpha$  is

$$\begin{aligned} p(\alpha | \Delta \mathbf{x}, \xi, t_{i0}, p_1, q_1) & \propto \prod_{i=1}^m L(\alpha | \Delta \mathbf{x}_i) \pi(\alpha | p_1, q_1) \\ & \propto \prod_{i=1}^m \prod_{j=1}^n \left( \Delta \theta_{ij} \exp\left(-\frac{\xi(\Delta x_{ij} - \Delta \theta_{ij})^2}{2\Delta x_{ij}}\right) \right) \alpha^{p_1-1} \exp(-\alpha q_1) \end{aligned} \quad (\text{C.III.2a})$$

or

$$\begin{aligned} & \ln[p(\alpha | \Delta \mathbf{x}, \xi, t_{i0}, p_1, q_1)] \\ & \propto \sum_{i=1}^m \sum_{j=1}^n \left( \ln(\Delta \theta_{ij}) - \frac{\xi(\Delta x_{ij} - \Delta \theta_{ij})^2}{2\Delta x_{ij}} \right) + (p_1 - 1)\ln\alpha - \alpha q_1 \end{aligned} \quad (\text{C.III.2b})$$

3. The posterior distribution of  $t_{i0}$ 

- Uniform prior distribution  $\pi(t_{i0} | p_2, q_2)$ ;
- Likelihood function given by Eq. (3.5a) with  $\alpha_i$  being replaced by  $\alpha$ ;

The posterior distribution of  $t_{i0}$  is

$$\begin{aligned} p(t_{i0} | \Delta \mathbf{x}_i, \alpha, \xi, p_2, q_2) & \propto L(t_{i0} | \Delta \mathbf{x}_i) \pi(t_{i0} | p_2, q_2) \\ & \propto \prod_{j=1}^n \left( \Delta \theta_{ij} \exp\left(-\frac{\xi(\Delta x_{ij} - \Delta \theta_{ij})^2}{2\Delta x_{ij}}\right) \right) \end{aligned} \quad (\text{C.III.3a})$$

or

$$\ln[p(t_{i0}|\Delta\mathbf{x}_i, \alpha, \xi, p_2, q_2)] \propto \sum_{j=1}^n \left( \ln(\Delta\theta_{ij}) - \frac{\xi(\Delta x_{ij} - \Delta\theta_{ij})^2}{2\Delta x_{ij}} \right) \quad (\text{C.III.3b})$$

4. The posterior distribution of  $\xi$

- Gamma prior distribution  $\pi(\xi|p_3, q_3)$ ;
- Likelihood function given by Eq. (3.5b) with  $\alpha_i$  being replaced by  $\alpha$ ;

The posterior distribution of  $\xi$  is

$$\begin{aligned} p(\xi|\Delta\mathbf{x}, \alpha, t_{i0}, p_3, q_3) &\propto L(\xi|\Delta\mathbf{x})\pi(\xi|p_3, q_3) \\ &\propto \exp\left(-\beta\left(\sum_{i=1}^m \sum_{j=1}^n \left(\frac{(\Delta x_{ij} - \Delta\theta_{ij})^2}{2\Delta x_{ij}}\right) + q_3\right)\right) \beta^{\frac{mn}{2} + p_3 - 1} \end{aligned} \quad (\text{C.III.4a})$$

$$\xi \sim f_G\left(\frac{mn}{2} + p_3, \sum_{i=1}^m \sum_{j=1}^n \left(\frac{(\Delta x_{ij} - \Delta\theta_{ij})^2}{2\Delta x_{ij}}\right) + q_3\right) \quad (\text{C.III.4b})$$

Scenario IV: defect-specific  $t_0$  and  $\xi$  and common  $\alpha$

1. The posterior distribution of  $\Delta x_{ij}$  ( $i=1, 2, \dots, m; j=1, 2, \dots, n$ )

- Inverse Gaussian prior distribution given by  $\pi(\Delta x_{ij}|\Delta\theta_{ij}, \xi_i(\Delta\theta_{ij})^2)$ , with  $\alpha_i$  in Eq. (3.3) being replaced by  $\alpha$ ;
- Likelihood function given by Eq. (2.8);

The posterior distribution of  $\Delta x_{ij}$  is

$$\begin{aligned} p(\Delta x_{ij}|\mathbf{y}_i, \Delta\theta_{ij}, \xi_i, t_{i0}) &\propto L(\mathbf{y}_i|\Delta\mathbf{x}_i)\pi(\Delta x_{ij}|\Delta\theta_{ij}, \xi_i(\Delta\theta_{ij})^2) \\ &\propto \\ &\exp\left(-\frac{1}{2}(\mathbf{y}_i - (\mathbf{a} + \mathbf{b}\mathbf{x}_i))'(\boldsymbol{\Sigma}_{E_i})^{-1}(\mathbf{y}_i - (\mathbf{a} + \mathbf{b}\mathbf{x}_i))\right) (\Delta x_{ij})^{-3/2} \exp\left(-\frac{\xi_i(\Delta x_{ij} - \Delta\theta_{ij})^2}{2\Delta x_{ij}}\right) \end{aligned} \quad (\text{C.IV.1a})$$

or

$$\begin{aligned} &\ln[p(\Delta x_{ij}|\mathbf{y}_i, \Delta\theta_{ij}, \xi_i, t_{i0})] \\ &\propto -\frac{1}{2}(\mathbf{y}_i - (\mathbf{a} + \mathbf{b}\mathbf{x}_i))'(\boldsymbol{\Sigma}_{E_i})^{-1}(\mathbf{y}_i - (\mathbf{a} + \mathbf{b}\mathbf{x}_i)) - \frac{3}{2}\ln(\Delta x_{ij}) - \frac{\xi_i(\Delta x_{ij} - \Delta\theta_{ij})^2}{2\Delta x_{ij}} \end{aligned} \quad (\text{C.IV.1b})$$

2. The posterior distribution of  $\alpha$

- Gamma prior distribution  $\pi(\alpha|p_1, q_1)$ ;
- Likelihood function  $\prod_{i=1}^m f_{\Delta x_i}(\Delta \mathbf{x}_i | \Delta \theta_{ij}, \xi_i (\Delta \theta_{ij})^2)$ ;

The posterior distribution of  $\alpha$  is

$$p(\alpha | \Delta \mathbf{x}, \xi_i, t_{i0}, p_1, q_1) \propto \prod_{i=1}^m L(\alpha | \Delta \mathbf{x}_i) \pi(\alpha | p_1, q_1)$$

$$\propto \prod_{i=1}^m \prod_{j=1}^n \left( \Delta \theta_{ij} \exp \left( -\frac{\xi_i (\Delta x_{ij} - \Delta \theta_{ij})^2}{2 \Delta x_{ij}} \right) \right) \alpha^{p_1 - 1} \exp(-\alpha q_1) \quad (\text{C.IV.2a})$$

or

$$\ln[p(\alpha | \Delta \mathbf{x}, \xi_i, t_{i0}, p_1, q_1)]$$

$$\propto \sum_{i=1}^m \sum_{j=1}^n \left( \ln(\Delta \theta_{ij}) - \frac{\xi_i (\Delta x_{ij} - \Delta \theta_{ij})^2}{2 \Delta x_{ij}} \right) + (p_1 - 1) \ln \alpha - \alpha q_1 \quad (\text{C.IV.2b})$$

3. The posterior distribution of  $t_{i0}$

- Uniform prior distribution  $\pi(t_{i0}|p_2, q_2)$ ;
- Likelihood function given by Eq. (3.5a) with  $\xi$  being replaced by  $\xi_i$ ;

The posterior distribution of  $t_{i0}$  is

$$p(t_{i0} | \Delta \mathbf{x}_i, \alpha, \xi_i, p_2, q_2) \propto L(t_{i0} | \Delta \mathbf{x}_i) \pi(t_{i0} | p_2, q_2)$$

$$\propto \prod_{j=1}^n \Delta \theta_{ij} \exp \left( -\frac{\xi_i (\Delta x_{ij} - \Delta \theta_{ij})^2}{2 \Delta x_{ij}} \right) \quad (\text{C.IV.3a})$$

or

$$\ln[p(t_{i0} | \Delta \mathbf{x}_i, \alpha, \xi_i, p_2, q_2)] \propto \sum_{j=1}^n \left( \ln(\Delta \theta_{ij}) - \frac{\xi_i (\Delta x_{ij} - \Delta \theta_{ij})^2}{2 \Delta x_{ij}} \right) \quad (\text{C.IV.3b})$$

4. The posterior distribution of  $\xi_i$

- Gamma prior distribution  $\pi(\xi_i|p_3, q_3)$ ;
- Likelihood function  $\prod_{j=1}^n f_{\Delta x_{ij}}(\Delta x_{ij} | \Delta \theta_{ij}, \xi_i (\Delta \theta_{ij})^2)$ ;

The posterior distribution of  $\xi_i$  is

$$\begin{aligned}
p(\xi_i|\Delta\mathbf{x}_i, \alpha, t_{i0}, p_3, q_3) &\propto L(\xi_i|\Delta\mathbf{x}_i)\pi(\xi_i|p_3, q_3) \\
&\propto \exp\left(-\beta\left(\sum_{j=1}^n\left(\frac{(\Delta x_{ij}-\Delta\theta_{ij})^2}{2\Delta x_{ij}}\right)+q_3\right)\right)\beta^{\frac{n}{2}+p_3-1}
\end{aligned} \tag{C.IV.4a}$$

$$\xi_i \sim f_G\left(\frac{n}{2}+p_3, \sum_{j=1}^n\left(\frac{(\Delta x_{ij}-\Delta\theta_{ij})^2}{2\Delta x_{ij}}\right)+q_3\right) \tag{C.IV.4b}$$

## Appendix D Full Conditional Posterior Distributions of Model Parameters (GBM-based Model)

1. The posterior distribution of  $t_{i0}$  ( $i = 1, 2, \dots, m$ )

- Uniform prior distribution,  $\pi(t_{i0}|p_1, q_1)$ ;
- Likelihood function given by Eq. (4.7);

$$\begin{aligned}
 p(t_{i0}|\mathbf{y}_i, r_{i0}, \boldsymbol{\eta}_i, p_1, q_1) &\propto L(\mathbf{y}_i|r_{i0}, \boldsymbol{\eta}_i, t_{i0}) \pi(t_{i0}|p_1, q_1) \\
 &\propto \exp\left(-\frac{1}{2}(\mathbf{y}_i - (\mathbf{a} + \mathbf{b}\mathbf{x}_i))'(\boldsymbol{\Sigma}_{E_i})^{-1}(\mathbf{y}_i - (\mathbf{a} + \mathbf{b}\mathbf{x}_i))\right)
 \end{aligned} \tag{D.1a}$$

Or

$$\ln[p(t_{i0}|\mathbf{y}_i, r_{i0}, \boldsymbol{\eta}_i, p_1, q_1)] \propto -\frac{1}{2}(\mathbf{y}_i - (\mathbf{a} + \mathbf{b}\mathbf{x}_i))'(\boldsymbol{\Sigma}_{E_i})^{-1}(\mathbf{y}_i - (\mathbf{a} + \mathbf{b}\mathbf{x}_i)) \tag{D.1b}$$

2. The posterior distribution of  $\beta$

- Gaussian prior distribution,  $\pi(\beta|p_2, q_2)$ , with  $p_2$  and  $q_2$  denoting the mean and precision (i.e. the inverse of variance) of  $\beta$ , respectively;
- Likelihood function given by Eq. (4.8);

$$\begin{aligned}
 p(\beta|\boldsymbol{\eta}, \sigma^2, t_{i0}, p_2, q_2) &\propto \prod_{i=1}^m \prod_{j=1}^{n-1} L(\eta_{ij}|\beta, \sigma^2, t_{i0}) \pi(\beta|p_2, q_2) \\
 &\propto \exp\left(-\sum_{i=1}^m \sum_{j=1}^{n-1} \left(\frac{(\eta_{ij} - \beta \Delta t_{i,j-1})^2}{2\sigma^2 \Delta t_{i,j-1}}\right) - \frac{q_2(\beta - p_2)^2}{2}\right)
 \end{aligned} \tag{D.2a}$$

Or

$$\ln[p(\beta|\boldsymbol{\eta}, \sigma^2, t_{i0}, p_2, q_2)] \propto -\sum_{i=1}^m \sum_{j=1}^{n-1} \left(\frac{(\eta_{ij} - \beta \Delta t_{i,j-1})^2}{2\sigma^2 \Delta t_{i,j-1}}\right) - \frac{q_2(\beta - p_2)^2}{2} \tag{D.2b}$$

3. The posterior distribution of  $\sigma^2$

- Gamma prior distribution,  $\pi(\sigma^2|p_3, q_3)$ ;
- Likelihood function given by Eq. (4.8);

$$\begin{aligned}
p(\sigma^2 | \boldsymbol{\eta}, \beta, t_{i0}, p_3, q_3) &\propto \prod_{i=1}^m \prod_{j=1}^{n-1} L(\eta_{ij} | \beta, \sigma^2, t_{i0}) \pi(\sigma^2 | p_3, q_3) \\
&\propto (\sigma^2)^{-\frac{m(n-1)}{2} + p_3 - 1} \exp\left(-\sum_{i=1}^m \sum_{j=1}^{n-1} \left(\frac{(\eta_{ij} - \beta \Delta t_{i,j-1})^2}{2\sigma^2 \Delta t_{i,j-1}}\right) - \sigma^2 q_3\right)
\end{aligned} \tag{D.3a}$$

Or

$$\begin{aligned}
&\ln[p(\sigma^2 | \boldsymbol{\eta}, \beta, t_{i0}, p_3, q_3)] \\
&\propto \left(-\frac{m(n-1)}{2} + p_3 - 1\right) \ln(\sigma^2) - \sum_{i=1}^m \sum_{j=1}^{n-1} \left(\frac{(\eta_{ij} - \beta \Delta t_{i,j-1})^2}{2\sigma^2 \Delta t_{i,j-1}}\right) - \sigma^2 q_3
\end{aligned} \tag{D.3b}$$

4. The posterior distribution of  $r_{i0}$  ( $i = 1, 2, \dots, m$ )

- Gamma prior distribution,  $\pi(r_{i0} | p_4, q_4)$ ;
- Likelihood function given by Eq. (4.7);

$$\begin{aligned}
p(r_{i0} | \mathbf{y}_i, \boldsymbol{\eta}_i, t_{i0}, p_4, q_4) &\propto L(\mathbf{y}_i | r_{i0}, \boldsymbol{\eta}_i, t_{i0}) \pi(r_{i0} | p_4, q_4) \\
&\propto \exp\left(-\frac{1}{2}(\mathbf{y}_i - (\mathbf{a} + \mathbf{b}\mathbf{x}_i))' (\boldsymbol{\Sigma}_{E_i})^{-1} (\mathbf{y}_i - (\mathbf{a} + \mathbf{b}\mathbf{x}_i)) - r_{i0} q_4\right) \cdot (r_{i0})^{p_4 - 1}
\end{aligned} \tag{D.4a}$$

Or

$$\begin{aligned}
&\ln(p(r_{i0} | \mathbf{y}_i, \boldsymbol{\eta}_i, t_{i0}, p_4, q_4)) \\
&\propto -\frac{1}{2}(\mathbf{y}_i - (\mathbf{a} + \mathbf{b}\mathbf{x}_i))' (\boldsymbol{\Sigma}_{E_i})^{-1} (\mathbf{y}_i - (\mathbf{a} + \mathbf{b}\mathbf{x}_i)) - r_{i0} q_4 + (p_4 - 1) \ln(r_{i0})
\end{aligned} \tag{D.4b}$$

5. The posterior distribution of  $\eta_{ij}$  ( $i = 1, 2, \dots, m; j = 1, \dots, n-1$ )

- Gaussian prior distribution,  $\pi(\eta_{ij} | \beta \Delta t_{i,j-1}, \sigma^2 \Delta t_{i,j-1})$  with  $\beta \Delta t_{i,j-1}$  and  $\sigma^2 \Delta t_{i,j-1}$  denoting the mean and variance of  $\eta_{ij}$ , respectively;
- Likelihood function given by Eq. (4.7);

$$\begin{aligned}
p(\eta_{ij} | \mathbf{y}_i, r_{i0}, t_{i0}, \beta, \sigma^2) &\propto L(\mathbf{y}_i | r_{i0}, \boldsymbol{\eta}_i, t_{i0}) \pi(\eta_{ij} | \beta \Delta t_{i,j-1}, \sigma^2 \Delta t_{i,j-1}) \\
&\propto \exp\left(-\frac{1}{2}(\mathbf{y}_i - (\mathbf{a} + \mathbf{b}\mathbf{x}_i))' (\boldsymbol{\Sigma}_{E_i})^{-1} (\mathbf{y}_i - (\mathbf{a} + \mathbf{b}\mathbf{x}_i)) - \frac{(\eta_{ij} - \beta \Delta t_{i,j-1})^2}{2\sigma^2 \Delta t_{i,j-1}}\right)
\end{aligned} \tag{D.5a}$$

Or

$$\begin{aligned} & \ln[p(\eta_{ij} | \mathbf{y}_i, r_{i0}, t_{i0}, \beta, \sigma^2)] \\ & \propto -\frac{1}{2}(\mathbf{y}_i - (\mathbf{a} + \mathbf{b}\mathbf{x}_i))'(\boldsymbol{\Sigma}_{E_i})^{-1}(\mathbf{y}_i - (\mathbf{a} + \mathbf{b}\mathbf{x}_i)) - \frac{(\eta_{ij} - \beta\Delta t_{i,j-1})^2}{2\sigma^2\Delta t_{i,j-1}} \end{aligned} \quad (\text{D.5b})$$



## Appendix E Copyright Permission

FW: ASME PUBLICATIONS PERMISSION REQUEST FORM SUBMISSION

Dear Mr. Zhang,

It has been confirmed that your paper was presented at the Conference, therefore, it is our pleasure to grant you permission to use the ASME paper “TIME-DEPENDENT CORROSION GROWTH MODELING USING MULTIPLE ILI DATA,” by S. Zhang, W. Zhou, M. Al-Amin, S. Kariyawasam and H. Wang, Proceedings of the 2012 9th International Pipeline Conference, Paper Number IPC2012-90502, as cited in your letter for inclusion in a Doctoral Thesis entitled Development of Probabilistic Corrosion Growth Models with Applications in Integrity Management of Pipelines to be published by Western University.

Permission is granted for the specific use as stated herein and does not permit further use of the materials without proper authorization. As is customary, we request that you ensure full acknowledgment of this material, the author(s), source and ASME as original publisher. Acknowledgment must be retained on all pages printed and distributed.

Many thanks for your interest in ASME publications.

Sincerely,

Permissions & Copyrights

## ELSEVIER LICENSE

This is a License Agreement between Shenwei Zhang ("You") and Elsevier ("Elsevier") provided by Copyright Clearance Center ("CCC"). The license consists of your order details, the terms and conditions provided by Elsevier, and the payment terms and conditions.

All payments must be made in full to CCC. For payment instructions, please see information listed at the bottom of this form.

Supplier	Elsevier Limited
Registered Company Number	1982084
Customer name	Shenwei Zhang
License number	3167140480965
License date	Jun 13, 2013
Licensed content publisher	Elsevier
Licensed content publication	Corrosion Science
Licensed content title	Inverse Gaussian process-based corrosion growth model for energy pipelines considering the sizing error in inspection data
Licensed content author	Shenwei Zhang,Wenxing Zhou,Hao Qin
Licensed content date	August 2013
Licensed content volume number	73
Licensed content issue number	None
Number of pages	12
Start Page	309
End Page	320
Type of Use	reuse in a thesis/dissertation
Intended publisher of new work	other
Portion	full article
Format	both print and electronic
Are you the author of this Elsevier article?	Yes
Will you be translating?	No

Title of your thesis/dissertation	Development of Probabilistic Corrosion Growth Models with Applications in Integrity Management of Pipelines
Expected completion date	Jul 2013
Estimated size (number of pages)	200
Elsevier VAT number	GB 494 6272 12

## ELSEVIER LICENSE

This is a License Agreement between Shenwei Zhang ("You") and Elsevier ("Elsevier") provided by Copyright Clearance Center ("CCC"). The license consists of your order details, the terms and conditions provided by Elsevier, and the payment terms and conditions.

All payments must be made in full to CCC. For payment instructions, please see information listed at the bottom of this form.

Supplier	Elsevier Limited
Registered Company Number	1982084
Customer name	Shenwei Zhang
License number	3290901101669
License date	Dec 16, 2013
Licensed content publisher	Elsevier
Licensed content publication and Piping	International Journal of Pressure Vessels and Piping
Licensed content title	System reliability of corroding pipelines considering stochastic process-based models for defect growth and internal pressure
Licensed content author	Shenwei Zhang, Wenxing Zhou
Licensed content date	November–December 2013
Licensed content volume number	111–112
Licensed content issue number	None
Number of pages	11
Start Page	120
End Page	130
Type of Use	reuse in a thesis/dissertation
Intended publisher of new work	other
Portion	full article
Format	both print and electronic
Are you the author of this Elsevier article?	Yes
Will you be translating?	No

Title of your thesis/dissertation	Development of Probabilistic Corrosion Growth Models with Applications in Integrity Management of Pipelines
Expected completion date	Dec 2013
Estimated size (number of pages)	200
Elsevier VAT number	GB 494 6272 12

## Terms and Conditions

### INTRODUCTION

1. The publisher for this copyrighted material is Elsevier. By clicking "accept" in connection with completing this licensing transaction, you agree that the following terms and conditions apply to this transaction (along with the Billing and Payment terms and conditions established by Copyright Clearance Center, Inc. ("CCC"), at the time that you opened your Rightslink account and that are available at any time at <http://myaccount.copyright.com>).

### GENERAL TERMS

2. Elsevier hereby grants you permission to reproduce the aforementioned material subject to the terms and conditions indicated.

3. Acknowledgement: If any part of the material to be used (for example, figures) has appeared in our publication with credit or acknowledgement to another source, permission must also be sought from that source. If such permission is not obtained then that material may not be included in your publication/copies. Suitable acknowledgement to the source must be made, either as a footnote or in a reference list at the end of your publication, as follows:

“Reprinted from Publication title, Vol /edition number, Author(s), Title of article / title of chapter, Pages No., Copyright (Year), with permission from Elsevier [OR APPLICABLE SOCIETY COPYRIGHT OWNER].” Also Lancet special credit - “Reprinted from The Lancet, Vol. number, Author(s), Title of article, Pages No., Copyright (Year), with permission from Elsevier.”

4. Reproduction of this material is confined to the purpose and/or media for which permission is hereby given.

5. Altering/Modifying Material: Not Permitted. However figures and illustrations may be altered/adapted minimally to serve your work. Any other abbreviations, additions, deletions and/or any other alterations shall be made only with prior written authorization of Elsevier Ltd. (Please contact Elsevier at [permissions@elsevier.com](mailto:permissions@elsevier.com))

6. If the permission fee for the requested use of our material is waived in this instance, please be advised that your future requests for Elsevier materials may attract a fee.

7. **Reservation of Rights:** Publisher reserves all rights not specifically granted in the combination of (i) the license details provided by you and accepted in the course of this licensing transaction, (ii) these terms and conditions and (iii) CCC's Billing and Payment terms and conditions.

8. **License Contingent Upon Payment:** While you may exercise the rights licensed immediately upon issuance of the license at the end of the licensing process for the transaction, provided that you have disclosed complete and accurate details of your proposed use, no license is finally effective unless and until full payment is received from you (either by publisher or by CCC) as provided in CCC's Billing and Payment terms and conditions. If full payment is not received on a timely basis, then any license preliminarily granted shall be deemed automatically revoked and shall be void as if never granted. Further, in the event that you breach any of these terms and conditions or any of CCC's Billing and Payment terms and conditions, the license is automatically revoked and shall be void as if never granted. Use of materials as described in a revoked license, as well as any use of the materials beyond the scope of an unrevoked license, may constitute copyright infringement and publisher reserves the right to take any and all action to protect its copyright in the materials.

9. **Warranties:** Publisher makes no representations or warranties with respect to the licensed material.

10. **Indemnity:** You hereby indemnify and agree to hold harmless publisher and CCC, and their respective officers, directors, employees and agents, from and against any and all claims arising out of your use of the licensed material other than as specifically authorized pursuant to this license.

11. **No Transfer of License:** This license is personal to you and may not be sublicensed, assigned, or transferred by you to any other person without publisher's written permission.

12. **No Amendment Except in Writing:** This license may not be amended except in a writing signed by both parties (or, in the case of publisher, by CCC on publisher's behalf).

13. **Objection to Contrary Terms:** Publisher hereby objects to any terms contained in any purchase order, acknowledgment, check endorsement or other writing prepared by

you, which terms are inconsistent with these terms and conditions or CCC's Billing and Payment terms and conditions. These terms and conditions, together with CCC's Billing and Payment terms and conditions (which are incorporated herein), comprise the entire agreement between you and publisher (and CCC) concerning this licensing transaction. In the event of any conflict between your obligations established by these terms and conditions and those established by CCC's Billing and Payment terms and conditions, these terms and conditions shall control.

14. Revocation: Elsevier or Copyright Clearance Center may deny the permissions described in this License at their sole discretion, for any reason or no reason, with a full refund payable to you. Notice of such denial will be made using the contact information provided by you. Failure to receive such notice will not alter or invalidate the denial. In no event will Elsevier or Copyright Clearance Center be responsible or liable for any costs, expenses or damage incurred by you as a result of a denial of your permission request, other than a refund of the amount(s) paid by you to Elsevier and/or Copyright Clearance Center for denied permissions.

#### LIMITED LICENSE

The following terms and conditions apply only to specific license types:

15. Translation: This permission is granted for non-exclusive world English rights only unless your license was granted for translation rights. If you licensed translation rights you may only translate this content into the languages you requested. A professional translator must perform all translations and reproduce the content word for word preserving the integrity of the article. If this license is to re-use 1 or 2 figures then permission is granted for non-exclusive world rights in all languages.

16. Website: The following terms and conditions apply to electronic reserve and author websites:

Electronic reserve: If licensed material is to be posted to website, the web site is to be password-protected and made available only to bona fide students registered on a relevant course if:

This license was made in connection with a course,

This permission is granted for 1 year only. You may obtain a license for future website posting,



All content posted to the web site must maintain the copyright information line on the bottom of each image,

A hyper-text must be included to the Homepage of the journal from which you are licensing at <http://www.sciencedirect.com/science/journal/xxxxx> or the Elsevier homepage for books at <http://www.elsevier.com>, and

Central Storage: This license does not include permission for a scanned version of the material to be stored in a central repository such as that provided by Heron/XanEdu.

17. Author website for journals with the following additional clauses:

All content posted to the web site must maintain the copyright information line on the bottom of each image, and the permission granted is limited to the personal version of your paper. You are not allowed to download and post the published electronic version of your article (whether PDF or HTML, proof or final version), nor may you scan the printed edition to create an electronic version. A hyper-text must be included to the Homepage of the journal from which you are licensing at <http://www.sciencedirect.com/science/journal/xxxxx>. As part of our normal production process, you will receive an e-mail notice when your article appears on Elsevier's online service ScienceDirect ([www.sciencedirect.com](http://www.sciencedirect.com)). That e-mail will include the article's Digital Object Identifier (DOI). This number provides the electronic link to the published article and should be included in the posting of your personal version. We ask that you wait until you receive this e-mail and have the DOI to do any posting.

Central Storage: This license does not include permission for a scanned version of the material to be stored in a central repository such as that provided by Heron/XanEdu.

18. Author website for books with the following additional clauses:

Authors are permitted to place a brief summary of their work online only.

A hyper-text must be included to the Elsevier homepage at <http://www.elsevier.com>. All content posted to the web site must maintain the copyright information line on the bottom of each image. You are not allowed to download and post the published electronic version of your chapter, nor may you scan the printed edition to create an electronic version.

Central Storage: This license does not include permission for a scanned version of the material to be stored in a central repository such as that provided by Heron/XanEdu.

19. Website (regular and for author): A hyper-text must be included to the Homepage of the journal from which you are licensing at <http://www.sciencedirect.com/science/journal/xxxxx>. or for books to the Elsevier homepage at <http://www.elsevier.com>

20. Thesis/Dissertation: If your license is for use in a thesis/dissertation your thesis may be submitted to your institution in either print or electronic form. Should your thesis be published commercially, please reapply for permission. These requirements include permission for the Library and Archives of Canada to supply single copies, on demand, of the complete thesis and include permission for UMI to supply single copies, on demand, of the complete thesis. Should your thesis be published commercially, please reapply for permission.

21. Other Conditions:

## Curriculum Vitae

- Name:** Shenwei Zhang
- Post-secondary Education and Degrees:**
- Shandong University  
Jinan, Shandong, China  
1997-2001 B.E.
- Shandong University  
Jinan, Shandong, China  
2001-2004 M.E.Sc
- Tongji University  
Shanghai, Shanghai, China  
2004-2007 Ph.D.
- The University of Western Ontario  
London, Ontario, Canada  
2010-2014 Ph.D.
- Honours and Awards:**
- Research and Teaching Assistants Scholarship  
The University of Western Ontario  
2010-2014
- Natural Sciences and Engineering Research Council (NSERC)  
CGS D2  
The University of Western Ontario  
2012-2014
- Related Work Experience**
- Assistant professor  
Shandong University  
Jinan, Shandong, China  
2007-2010
- Research and Teaching Assistants  
The University of Western Ontario  
2010-2014
- Publications:**
1. **Zhang, S.**, Zhou, W. and Qin, H. (2013) Inverse Gaussian process-based corrosion growth model for energy pipelines considering sizing error in inspection data. *Corrosion Science*, 73: 309-320.

2. **Zhang, S.** and Zhou, W. (2013) System reliability assessment of 3D steel frame designed per AISC LRFD specification. *International Journal of Advanced Steel Constructions*, 9(1): 77-89.
3. **Zhang, S.** and Zhou, W. (2013) System reliability of corroding pipelines considering stochastic process-based models for defect growth and internal pressure. *International Journal of Pressure Vessels and Piping*, 111-112: 120-130.
4. **Zhang, S.** and Zhou, W. (2014) An efficient methodology for the reliability analysis of corroding pipelines. *Journal of Pressure Vessel Technology*, DOI: 10.1115/1.4026797.
5. **Zhang, S.**, Zhou, W. and Al-Amin, M., Kariyawasam, S. and Wang, H. (2014) Time-dependent corrosion growth modeling using multiple ILI data. *Journal of Pressure Vessel Technology*, DOI: 10.1115/1.4026798.
6. **Zhang, S.** and Zhou, W. (2013) Probabilistic characterization of metal-loss corrosion growth on underground pipelines based on geometric Brownian motion process. *Structure and Infrastructure Engineering*, DOI:10.1080/15732479.2013.875045.
7. **Zhang, S.** and Zhou, W. (2014) Bayesian dynamic linear model for growth of corrosion defects on energy pipelines. *Reliability Engineering and System Safety* (accepted in April, 2014).
8. **Zhang, S.** and Zhou, W. (2014) Cost-based optimal maintenance decisions for corroding natural gas pipelines based on stochastic degradation models. *Engineering Structures* (revision submitted in February, 2014).
9. Qin, H., **Zhang, S.** and Zhou, W. (2013) Inverse Gaussian process-based corrosion growth modeling and its application in the reliability analysis for energy pipelines. *Frontiers of Structural and Civil Engineering*, 7(3): 276-287.
10. Zhou, W., Hong, H. and **Zhang, S.** (2012) Effect of correlated defect growth on system reliability of corroding pipelines. *International Journal of Pressure Vessels and Piping*, 96-97: 68-77.
11. Hong, H., Zhou, W., **Zhang, S.** and Ye, W. (2014) Optimal condition-based maintenance decisions for systems with dependent stochastic degradation of components. *Reliability Engineering and System Safety*, 121: 276-288.
12. Al-Amin, M., Zhou, W., **Zhang, S.**, Kariyawasam, S. and Wang, H. (2014) Hierarchical Bayesian corrosion growth model based on in-line inspection data. *Journal of Pressure Vessel Technology*, DOI: 10.1115/1.4026579.